



















1976-1995 Atwood Boehm Chang Chen Choi Christensen Chuang Coleman Crandall Dong Gregonis Herron Ives Janatova Jhon Kessler L

View Arrange By Action Share Edit Tags

Name	^	Date Modified	Size	Kind
 Chang Herron 1995 Acid Antibody Adsorption Lin.pdf		Oct 10, 2006, 9:12 PM	4 MB	PDF Doc
 Chang Herron Lin 1995 Antibody Immunoassays-compressed.pdf		Yesterday, 6:09 PM	3.6 MB	PDF Doc
 Chen 1976 Pharmacokinetic Models.pdf		Oct 10, 2006, 8:22 PM	2.7 MB	PDF Doc
 Chen 1978 Salicylate Pharmacokinetic Model Coleman Temple.pdf		Oct 10, 2006, 8:15 PM	2.7 MB	PDF Doc
 Chen 1982 Dong Lysozyme Adsorption Methylation.pdf		Oct 10, 2006, 8:06 PM	879 KB	PDF Doc
 Chen 1985 Hemoglobin Adsorption van Wagenen.pdf		Oct 10, 2006, 8:02 PM	1.8 MB	PDF Doc
 Chen 1986 PolySulfoalkyl Surfaces.pdf		Oct 10, 2006, 7:54 PM	1.9 MB	PDF Doc
 Chen Boehm 1989 Thermal Mo...lation Antibodies Christensen.pdf		Oct 10, 2006, 7:44 PM	1 MB	PDF Doc
 Choi Jhon 1977 Water in Gels III.pdf		Oct 10, 2006, 7:41 PM	1.8 MB	PDF Doc
 Christensen 1989 SPIE Fluoresc...anescent Wang Ives Yoshida.pdf		Oct 10, 2006, 7:33 PM	1.3 MB	PDF Doc
 Chuang 1985 prothrombin adsorption.pdf		Oct 10, 2006, 7:25 PM	2.7 MB	PDF Doc
 Coleman 1974 Foreign Body Reaction Expt King.pdf		Oct 10, 2006, 7:07 PM	1.9 MB	PDF Doc
 Coleman 1974 Foreign Body Reaction Review King.pdf		Oct 10, 2006, 7:14 PM	2.2 MB	PDF Doc
 Coleman 1976 Platelets Albuminated Atwood.pdf		Sep 16, 2010, 7:03 PM	678 KB	PDF Doc
 Coleman 1978 SEM Microscopy Artificial Hearts Lawson.pdf		Aug 17, 2006, 2:21 PM	2.7 MB	PDF Doc
 Coleman 1981 Calcification TASAIO Lim Kessler.pdf		Oct 10, 2006, 6:24 PM	2.6 MB	PDF Doc
 Coleman 1982 Blood-Materials Hypotheses gregonis.pdf		Aug 17, 2006, 9:39 PM	3.6 MB	PDF Doc
 Crandall 1981 Albumin Labeling iodination Janatova.pdf		Aug 14, 2006, 9:25 PM	3.5 MB	PDF Doc

Adsorption Mechanism of Acid Pretreated Antibodies on Dichlorodimethylsilane-Treated Silica Surfaces

I-NAN CHANG,* JINN-NAN LIN,^{†1} JOSEPH D. ANDRADE,*[†] AND JAMES N. HERRON^{†‡2}

Departments of *Material Science & Engineering, [†]Bioengineering, and [‡]Pharmaceutics, University of Utah, Salt Lake City, Utah 84112

Received March 15, 1994; accepted January 31, 1995

Previously, Lin *et al.* (*J. Immunol. Methods* 125, 67, 1989; *J. Chromatogr.* 542, 41, 1991) showed that acid pretreated antibodies (Abs) exhibited a twofold higher antigen-binding capacity than native Abs when immobilized to solid surfaces that have strong nonspecific protein adsorption properties (e.g., polystyrene and silica). In the present article several experiments were conducted in order to elucidate the adsorption mechanism of acid pretreated antibodies. It was found that acid pretreatment time could be used to control the packing efficiency and orientation of Abs adsorbed to silica surfaces hydrophobized with dichlorodimethylsilane (DDS). Further, our results suggest that acid pretreatment leads to an increased exposure of hydrophobic regions in the constant fragment of the immunoglobulin. Selective adsorption of these regions produces a preferential orientation in which the antigen-binding fragments are accessible to bulk solution. This results in a higher antigen-binding capacity than observed when native Abs (no acid pretreatment) are immobilized on DDS-treated silica surfaces. © 1995 Academic Press, Inc.

INTRODUCTION

Immobilized antibodies (Abs) have been used widely in applications such as clinical diagnostic assays and separations (1, 2). In particular, immobilization of Abs to silica surfaces has become a subject of considerable interest because of recent progress in the areas of optical immunosensors (3, 4) and high performance affinity chromatography (5–7). One of the most commonly used immobilization methods is physical adsorption of Abs onto silica surfaces. Although this method is relatively simple and convenient, it suffers from low antigen-binding capacity (AgBC). In 1989 our group showed that a 2-fold improvement in AgBC could be achieved by a brief exposure of Abs to a low pH environment prior to immobilization (6). Several other conclusions were drawn from this study including: (a) acid

pretreated Abs exhibited a 2.5-fold higher packing efficiency on surfaces than untreated Abs; (b) the net increase in AgBC was due to a combination of factors including the activity of Ab before immobilization, the Ab surface concentration, and the orientation of immobilized Abs; and (c) enhancement of AgBC was dependent on acid pretreatment time, with optimum activity being observed for pretreatment times of 20 min. Similar observations have been reported by Ishikawa *et al.* (7) and Conradie *et al.* (8).

In 1991 our group showed that both the enhanced AgBC and the higher packing efficiency observed on silica surfaces were surface-induced phenomena, especially for those surfaces which exhibited strong nonspecific protein adsorption properties (9). In such cases the orientation of the Ab on the surface was almost completely controlled by physical adsorption, even when site-specific immobilization chemistry was used. In 1992, a similar conclusion was reached using monoclonal Abs and polystyrene beads as a substrate (10). Since then, few if any studies have addressed these issues from the perspective of protein adsorption. Thus, the objective of the present study is to gain insight into acid pretreatment effects by analyzing them in terms of protein adsorption theory.

In addition to higher packing efficiency and better orientation control, two additional factors may affect the AgBC of immobilized acid pretreated Abs. First, acid pretreatment may cause aggregation of Abs in solution, which could lead to higher packing efficiency—especially if the oligomeric form exhibits a higher affinity for silica surfaces than the monomeric form does (11). Second, acid pretreated Abs may form multilayers on the surface, which may result in a higher surface concentration of Ab (12). The relative importance of both of these issues will also be addressed in this article. Finally, an explanation will be offered for the reduced Ab surface concentration and lower AgBC that are typically observed at long acid pretreatment times (6, 9).

MATERIALS AND METHODS

Antibody Systems and Concentration Measurements

Polyclonal goat anti-human serum albumin (anti-HSA) was used as a model antibody. Specifically, the immunoglob-

¹ Present address: Boehringer-Mannheim Corp., Research and Development, 9115 Hague Road, Indianapolis, IN 46256.

² To whom correspondence should be addressed at Department of Pharmaceutics & Pharmaceutical Chemistry, 301 Skaggs Hall, University of Utah, Salt Lake City, UT 84112.

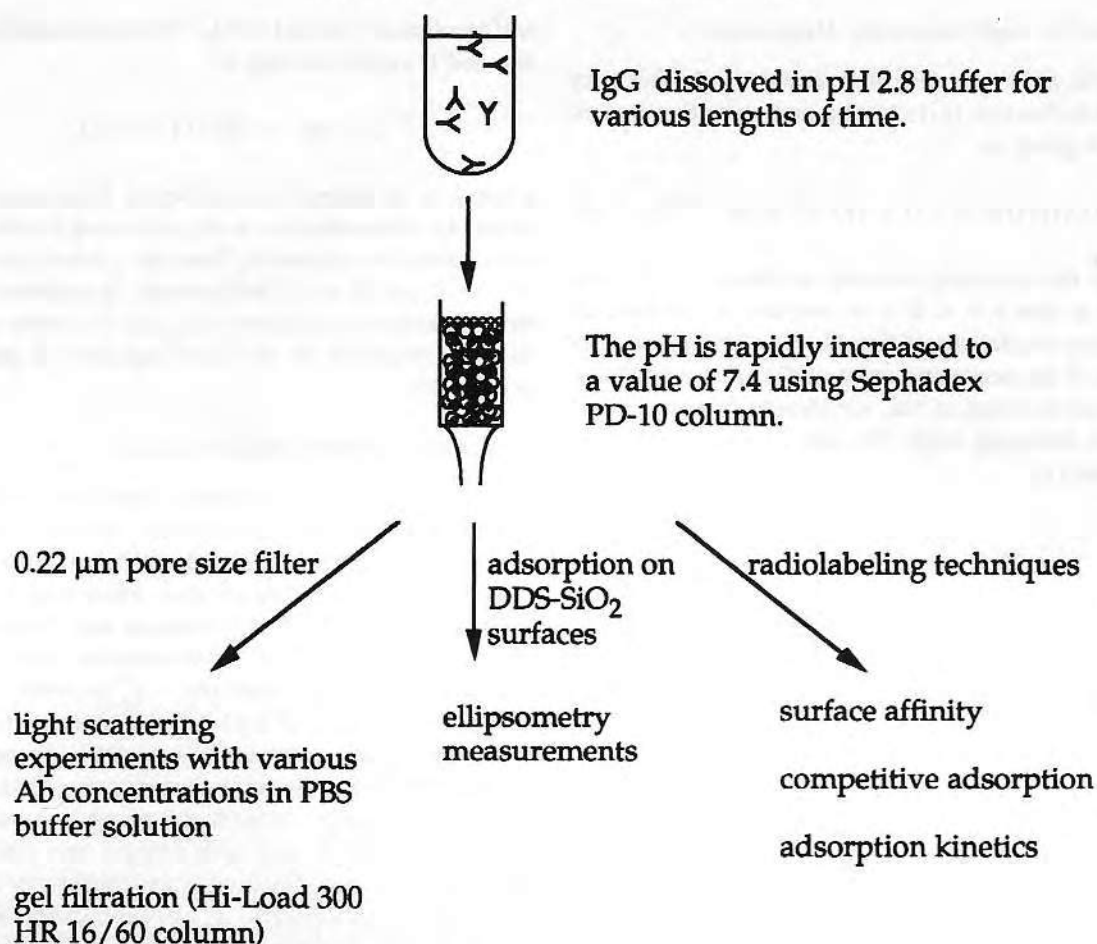


FIG. 1. Schematic representation of acid pretreatment procedures and experimental outline.

ulin G (IgG) fraction was purchased from Cappel Laboratories and used without further purification. Antibody concentrations were determined by absorbance at 280 nm using a UV-visible spectrophotometer (Beckman, Model 35). Values of $1.35 \text{ ml mg}^{-1} \text{ cm}^{-1}$ and 150,000 were used for the extinction coefficient ($\epsilon_{280 \text{ nm}}^{0.1\%}$) and molecular weight (MW) of anti-HSA, respectively.

Preparation of Acid Pretreated Abs

Approximately 8 mg of anti-HSA Ab was dissolved in 0.5 ml of 0.1 M citric acid/sodium phosphate buffer solution (pH 2.7) and incubated for various lengths of time (1, 20, 60, and 300 min) (see Fig. 1). Solutions were then neutralized by passage through a PD-10 column (Pharmacia) which had been equilibrated in phosphate-buffered saline, pH 7.4 (PBS).

Light Scattering Measurements

Light scattering measurements were used to characterize the solution properties of native Abs and acid pretreated Abs (13, 14). The experiments were performed using a Brookha-

ven Instruments spectrometer system, equipped with a BI 2030 AT digital correlator. A He-Ne laser (Melles Griot) operating at 633 nm was used as a light source. Sample solutions were filtered with a 0.22- μm pore size filter (Millipore) before measurements were performed. Several different concentrations of protein solutions (native and acid pretreated) were measured in these experiments.

Two kinds of light scattering experiments were performed. The first was dynamic (quasielastic) light scattering measurements. With this method, scattered light was detected by a photo-multiplier tube in the spectrometer system and a digital correlator was used to measure the intensity autocorrelation function (see below), from which the hydrodynamic radius (r) of Abs in different experimental conditions could be obtained (14, 15).

The second type of experiments involved static light scattering measurements. The intensity of the scattering light was detected by the photomultiplier tube at different scattering angles (30, 60, and 90°). The refractive index increment $\partial n/\partial c$ (n , refractive index; c , concentration) was measured by using a Model RF-600 differential refractometer (C. N. Wood MFG. Co., Newtown, PA) (16).

Data Analysis for Light Scattering Measurements

For dynamic light scattering measurements, the intensity autocorrelation function ($G(\tau)$) of a noninteracting system of particles is given as

$$G(\tau) = \langle I(t)I(t + \tau) \rangle = \langle I \rangle^2 (1 + Be^{-K^2 D_0 \tau}), \quad [1]$$

where $I(t)$ is the scattering intensity at time t , $I(t + \tau)$ is the intensity at time $t + \tau$, B is an instrument constant, D_0 is the diffusion coefficient of the Ab in solution, and K is the modulus of the scattering vector (17). The modulus K can be defined in terms of the wavelength of the incident light (λ), the scattering angle (θ), and the refractive index of the solution (n):

$$K = \frac{4\pi n}{\lambda} \sin\left(\frac{\theta}{2}\right). \quad [2]$$

For a given correlation function, a value of $\tau_c = 1/(D_0 K^2)$ can be found in the decay curve and D_0 will be solved. The relationship between hydrodynamic radius and diffusion coefficient is given by the Stokes-Einstein equation:

$$\frac{D_0}{6\pi\eta r_0} = \frac{kT}{3\pi\eta R_0}. \quad [3]$$

Here, k is the Boltzmann constant, T is the temperature, η is the solvent shear viscosity, r_0 is the radius of Ab in solution, and R_0 is the diameter of Ab in solution.

For an interacting system, Eqs. [1] and [3] can still be used to get a collective diffusion coefficient D and an apparent diameter R , which is concentration dependent. The relationship between them can be written as

$$R = R_0(1 + k_R C) \quad [4]$$

$$D = D_0(1 + k_D C), \quad [5]$$

where k_R and k_D are the interaction coefficients and C is the solution concentration of Ab. The values of θ , T , η , and n used in this experiment were 90° , 25°C , 0.904 cP , and 1.334 , respectively.

A similar approach can be applied to static light scattering data. The average scattered light intensity of a solution of small noninteracting particles is

$$I = ACM_0, \quad [6]$$

where A is a calibration constant related to the refractive index increment ($\partial n/\partial C$), C is the Ab concentration in solution, and M_0 is the molecular weight of the Ab (13, 18). For an interacting system, an apparent molecular weight M

will be obtained instead of M_0 . The relationship between M , M_0 , and C can be written as

$$M^{-1} = M_0^{-1}(1 + k_1 C), \quad [7]$$

where k_1 is the interaction coefficient. Experiments with different Ab concentrations were performed in order to determine values for M_0 and D_0 from the y-intercepts of plots of M^{-1} vs C and D vs C , respectively. In addition, values for the interaction coefficients (k_D and k_1) were determined from the slopes of the M^{-1} vs C and D vs C plots, respectively (19).

Preparation of DDS-Silica Surfaces

Silica samples were silanized and characterized as described previously by Lin *et al.* (6). In brief, sample chips were cut from $2.5 \times 2.5 \times 0.1\text{ cm}$ fused silica slides (CO grade, ESCO) and the edges were finely polished. Finished chips were $1.1 \times 0.95 \times 0.1\text{ cm}$ in size. For silanization, chips were fit into $13 \times 75\text{ mm}$ culture tubes (Fisher) in which all experiments took place. Chips were first cleaned in chromic acid at 80°C (6) and then allowed to react with 10% (v/v) dichlorodimethylsilane (DDS, Petrarch) in dry toluene for 30 min at room temperature. Next, they were rinsed with absolute ethanol and cured in a vacuum oven (which had been flushed with nitrogen gas three times) at $120\text{--}130^\circ\text{C}$ for 1 h. The quality and uniformity of the DDS layer were characterized by contact angle measurements using the Wilhelmy plate apparatus and ESCA analysis. Typically, DDS-silica surfaces prepared in this manner exhibited advancing and receding contact angles of 89 and 65° , respectively.

Radiolabeling of Abs

Native and acid pretreated anti-HSA Abs were labeled with carrier-free Na^{125}I (100 mCi/ml, Amersham) by the chloramine-T method as described by Chuang *et al.* (20) and Lin *et al.* (6). The labeling procedure was as follows: $500\text{ }\mu\text{l}$ of Ab solution (2 mg/ml) was gently mixed with $3\text{ }\mu\text{l}$ of Na^{125}I and $50\text{ }\mu\text{l}$ of freshly made chloramine-T solution (Kodak, 4 mg/ml in PBS buffer) for 1 min. The reaction was terminated by adding $50\text{ }\mu\text{l}$ of sodium metabisulfite solution (Fisher Scientific Co., 4.8 mg/ml in PBS buffer) for 2–3 min. Unreacted iodide was removed using a Sephadex G-25 (coarse, Pharmacia) column.

The labeling efficiency of each preparation was determined by precipitating a small portion of the labeled Ab with 20% trichloroacetic acid (TCA, Sigma) in the presence of bovine serum albumin (BSA) as carrier protein. The radioactivity of the ^{125}I -labeled Ab was determined by subtracting the radioactivity of the supernatant from that of the original solution (before adding TCA). Radioactivity measurements were made using a gamma counter (Beckman

Model 170 M). Preparations with labeling efficiency values greater than 0.97 were used in subsequent experiments. The specific activity of each such preparation was determined by measuring both the radioactivity and concentration (using A_{280} measurements as described above) of the ^{125}I -labeled Abs.

Adsorption Isotherms of Abs on DDS-Silica Surfaces

Hydrophobic DDS-silica surfaces were exposed to solutions of either native or acid-pretreated Abs for 3 h at room temperature (20°C) without stirring or agitation. After adsorption, the chips were rinsed five times with PBS buffer. The radioactivity of each chip was then determined. Adsorption isotherms were determined by varying the Ab concentration and measuring the surface concentration of adsorbed Ab for each concentration. Isotherms were determined for native Abs and for Abs pretreated with acid for 1, 20, 60, and 300 min. Control experiments were also performed, in which ^{125}I -labeled Abs were mixed with unlabeled antibodies and adsorption isotherms determined for several different molar ratios of labeled to unlabeled antibodies. These studies were described elsewhere (21, 22) and did not reveal any significant differences (with respect to adsorption behavior) between the unlabeled and labeled Abs.

Analysis of Adsorption Data

The classical Langmuir theory of gas adsorption can be applied to proteins in solution provided that (a) the solution is sufficiently dilute, (b) only one type of adsorption site is present, (c) there are no lateral interactions between adsorbed proteins, and (d) adsorption is reversible (23). In such cases the surface concentration of adsorbed antibody (Γ) is given by

$$\Gamma = \frac{\Gamma_{\max} KC}{1 + KC}, \quad [8]$$

where Γ_{\max} is the surface concentration of Ab at full monolayer coverage, K is the affinity constant, and C is the free Ab concentration in bulk solution. The affinity constant K is defined as the reciprocal of the free Ab concentration when $\Gamma = \Gamma_{\max}/2$. Although this relation can be used to determine the affinity directly from a binding isotherm, it is more common to use Scatchard and/or Hill plots (23). Both of these plots are linear and can be analyzed by ordinary least-squares to yield values for the affinity constant (24). Although Scatchard and Hill plots are more commonly used for analyzing protein-ligand binding equilibrium, one of us (J.D.A.) showed previously that they are equally applicable for reversible protein adsorption from dilute solutions (23). The Scatchard and Hill equations are given, respectively, by

$$\frac{\Gamma}{C} = K_s \Gamma_{\max} - K_s \Gamma \quad [9]$$

$$\log\left(\frac{\Gamma}{\Gamma_{\max} - \Gamma}\right) = a \cdot \log(K_h) + a \cdot \log(C), \quad [10]$$

where K_s and K_h are affinity constants determined from the Scatchard and Hill methods, respectively. The slope (a) of the Hill plot is defined as the Hill coefficient. A value of 1.0 is indicative of one class of adsorption sites with no lateral interactions between adsorbed protein molecules, as would be the case with true Langmuir adsorption (i.e., cases in which the second and third assumptions are satisfied). Values greater than one are indicative of positive cooperativity (lateral interactions which improve adsorption at high surface coverages), while values less than one are indicative of negative cooperativity (lateral interactions which decrease the probability of adsorption) or more than one type of adsorption site (heterogeneous adsorption). Finally, some mention should be made of the above assumption of reversibility. Previous studies have shown that immunoglobulins adsorb initially to silica surfaces in a quasi-reversible fashion, but eventually undergo conformational changes that lead to almost irreversible binding (25). Although the 3-h adsorption time used in these studies is thought to fall within the quasi-reversible regime, adsorption constants cited in this article should be viewed more as tools for evaluating empirical adsorption data than as rigorous measures of surface activity.

Gel Filtration

A commercial gel permeation chromatography column (Pharmacia, Hi-Load 300 HR 16/60 preparative grade) was used to characterize acid-pretreated and native Abs and to separate monomeric and polymeric Ab fractions. An acid pretreatment time of 60 min was used for this experiment. The pH of the acid pretreated Ab solution was increased from 2.8 to 7.4 by passing the low pH solution through a PD-10 column pre-equilibrated in PBS, and its concentration (typically about 16 mg/ml) was measured at pH 7.4. This solution was then applied to the gel filtration column (Fig. 1) and eluted with PBS at pH 7.4. Different fractions were collected and used for competitive adsorption experiments.

Competitive Adsorption between Acid Pretreated and Native Abs

Three different competitive adsorption experiments were performed in which the following mixtures were allowed to adsorb to DDS-silica surfaces: (a) equal amounts of native and monomeric acid pretreated Abs, (b) equal amounts of native and polymeric acid pretreated Abs, and (c) equal amounts of native and unfractionated acid pretreated Abs

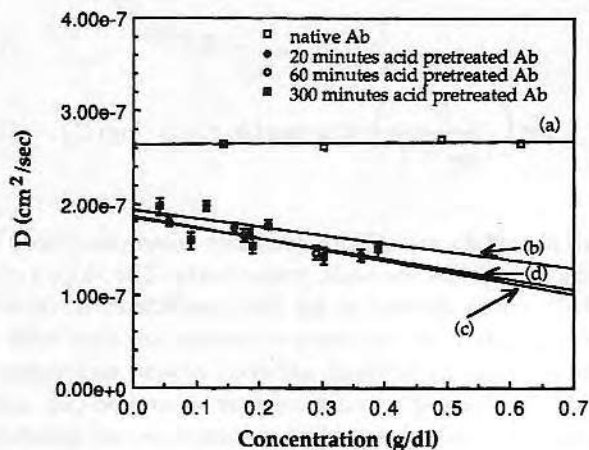


FIG. 2. Collective diffusion coefficient (D) plotted as a function of the Ab concentration at 25°C. (a) Native Ab, (b) 20-min acid pretreated Ab, (c) 60-min acid pretreated Ab, and (d) 300-min acid pretreated Ab. Experimental points and error bars represent the mean and standard error of three independent measurements, while solid lines represent a regression model based on Eq. [5].

(including monomeric and polymeric Abs). An acid pretreatment time of 60 min and an adsorption time of 3 h were used in each case. The total concentration of Ab in each mixture was 0.8 mg/ml. Surface concentrations of Abs in each mixture were determined separately by radiolabeling one of the Abs at a time.

Adsorption Kinetics of Native and Acid Pretreated Abs

Adsorption kinetics of native and acid pretreated Abs were monitored by using radiolabeled tracer Abs. Experiments were performed at several different bulk Ab concentrations. These included 0.46, 0.79, and 0.91 mg/ml for native Ab, and 0.14, 0.41, and 0.88 mg/ml for acid pretreated Ab. An acid pretreatment time of 60 min was used in each case. At each bulk concentration, chips were immersed in the Ab solution for various lengths of time (1, 2, 5, 30, 50, and 180 min) and then rinsed five times in PBS buffer. The amount of adsorbed Ab was then determined using a gamma counter.

Adsorption kinetics data were analyzed using three different methods. First, surface concentration was plotted versus time^{1/2} in order to determine whether or not adsorption was diffusion-limited. Second, kinetic data were analyzed using a method suggested by Sevastianov *et al.* (26, 27), in which surface concentration is plotted on a logarithmic time scale. Such plots are useful for analyzing heterogeneous adsorption, especially in cases where a reorientation step occurs immediately after the initial adsorption event. Third, data were analyzed using the saturation kinetics model proposed by Jennissen (28–30), in which adsorption rate is plotted versus bulk Ab concentration. In this model, the adsorption rate is expected to reach a plateau value at high Ab concentration if a rate-limiting reorientation (or nucleation) event is requisite for adsorption, as shown in

$$V_{on} = \frac{V_{max}C_0}{K_d + C_0}, \quad [11]$$

where V_{on} is the experimental initial adsorption rate, V_{max} is the maximum on-rate, K_d is the apparent dissociation constant, and C_0 is the initial concentration of free Ab.

Ellipsometry Measurements

Ellipsometry has been widely used in studying the thickness of adsorbed protein films on surfaces (31, 32). In this study, a silicon (Si) wafer with an artificial oxidized silicon dioxide film (SiO_2) was used instead of the fused silica surfaces used in the other protein adsorption experiments. The surface chemistry of this Si– SiO_2 wafer was the same as that of the clean silica surfaces (33) and the thickness of the SiO_2 film was 1350 Å, which enabled sensitive protein adsorption measurements (34). The SiO_2 layer was first derivatized with DDS and then exposed partially to a native or acid pretreated Ab solution for 3 h. An acid pretreatment time of 60 min was used. Concentrations of 1 mg/ml were used for both native and acid pretreated Abs. The section of the surface containing adsorbed Abs was rinsed with PBS buffer and then with deionized water. The sample was air dried and the thickness of the Ab layer was measured by ellipsometry in air. The area without adsorbed Abs was used as a reference. Measurements were taken with a Model AR 2000 ellipsometer (Rudolf Research Co., U.S.A.). The thickness and index of refraction of the adsorbed protein layer were determined from ellipsometer data using a computer program written by McCrackin (35) based on the pseudorefractive index model (36, 37).

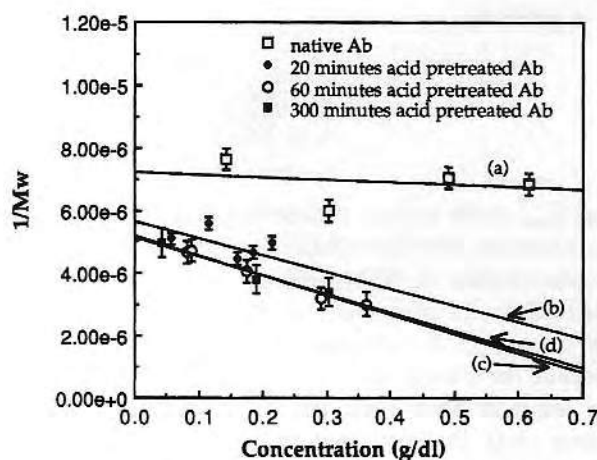


FIG. 3. Reciprocal of the apparent molecular weight of Abs plotted as a function of Ab concentration at 25°C. (a) Native Ab, (b) 20-min acid pretreated Ab, (c) 60-min acid pretreated Ab, and (d) 300-min acid pretreated Ab. Experimental points and error bars represent the mean and standard error of three independent measurements, while solid lines represent a regression model based on Eq. [7].

TABLE 1

Summary of Apparent Molecular Weight (M_0), Collective Diffusion Coefficient (D_0), and Interaction Coefficient (k_1 , k_D) Values of Native and Acid Pretreated Abs from Light Scattering Experiments

Acid pretreatment time (min)	M_0 (KDa)	k_1 (dl/g)	D_0 ($\times 10^{-7}$ cm ² /s)	k_D (dl/g)
0 ^a	139	-0.11	2.64	+0.016
20	177	-0.95	1.87	-0.52
60	193	-1.21	1.85	-0.65
300	195	-1.17	1.84	-0.61

^a Native Ab.

RESULTS

Light Scattering

Static light scattering experiments showed that the corrected scattering intensity of both native and acid pretreated Abs was independent of scattering angle. This suggested that a small, hard sphere model was appropriate for both types of Abs (13–17). Figure 2 shows the collective diffusion coefficient (D) as a function of bulk Ab concentration, for several different acid pretreatment times. These data were fitted using Eq. [5] to determine the diffusion coefficient (D_0) and interaction coefficient (k_D). Data were also analyzed by plotting apparent molecular weight (M) as a function of Ab concentration, as shown in Fig. 3. Values for M_0 and k_1 were then determined using Eq. [7]. Calculated values for D_0 , k_D , M_0 , and k_1 are listed in Tables 1 and 2.

These analyses showed that acid pretreated Abs exhibited a higher molecular weight than native Abs. Acid pretreated Abs also exhibited smaller diffusion coefficients, which indicated that the hydrodynamic radii of such Abs were probably greater than those of native Abs. Taken together, these findings suggest that acid pretreatment promotes aggregation—a hypothesis which is consistent with the negative values observed for the interaction coefficients (k_D and k_1) of acid pretreated Abs. Such negative values are usually indicative of strong attractive interactions between solute molecules (18, 19). In contrast, interaction coefficients values for native Abs were much smaller and differed in sign—negative for k_1 , and positive for k_D . This suggested that interactions between native Ab molecules were almost nonexistent (18, 19). Finally, the magnitudes of k_D and k_1 were very similar at different acid pretreatment times, which indicated that the interactions between Ab molecules at different acid treatment times were also similar.

From the above results, it is possible to calculate the association constant (K) between Ab molecules in solution for both the native and acid pretreated preparations. The association process is given as



where P_1 is the monomer, P_2 is the dimer, P_3 is the trimer, and so on. Assuming that the association constant is independent of Ab concentration, the relationship between association constant and apparent molecular weight can be expressed as

$$K_2 = \frac{[P_2]}{[P_1]^2} = -\lim_{C \rightarrow 0} \left[\frac{M_1/M - 1}{C} \right], \quad [13]$$

where K_2 is the association constant for the dimer in buffer solution, M is the apparent molecular weight obtained from light scattering data, M_1 is the molecular weight of monomeric native Ab (150 KDa), and C is the Ab concentration (38). By plotting $((M_1/M) - 1)/C$ vs C and extrapolating to $C = 0$, K_2 can be determined. The results are presented in Table 2 and show that acid pretreated Abs exhibited significantly higher K_2 values than native Abs. However, similar K_2 values were obtained at all three pretreatment times (20, 60, and 300 min). This suggests that events leading to aggregation probably occur in the first 20 min of acid pretreatment and that longer exposure does not induce any additional aggregation mechanisms, although the number of aggregates formed probably does increase with exposure time.

Adsorption Isotherms of Abs on DDS-Silica Surfaces

Figure 4 shows adsorption isotherms for native and acid pretreated Abs on DDS-silica surfaces. Initially, these data were analyzed using the Langmuir, Scatchard, and Hill equations (Eqs. [8], [9], and [10], respectively). However, biphasic Scatchard plots were observed for both native and acid pretreated Abs. Such plots are usually indicative of two classes of adsorption sites with different affinities, which invalidates the use of the Langmuir and Scatchard equations in this instance. This is because both equations are based on the assumption of one class of noninteracting binding sites (in contrast, the Hill equation is appropriate because it assumes more than one class of sites). This problem was resolved by modifying Eq. [8] to contain terms for both high and low affinity adsorption sites,

TABLE 2

The Dimer Association Constant K_2 of Native and Acid Pretreated Abs in Solution, Calculated from Light Scattering Data

Acid pretreatment time (min)	Dimer association constant ($\times 10^4$ M ⁻¹)
0 ^a	1 \pm 0.06
20	8 \pm 1
60	7 \pm 1
300	10 \pm 2

^a Native Ab.

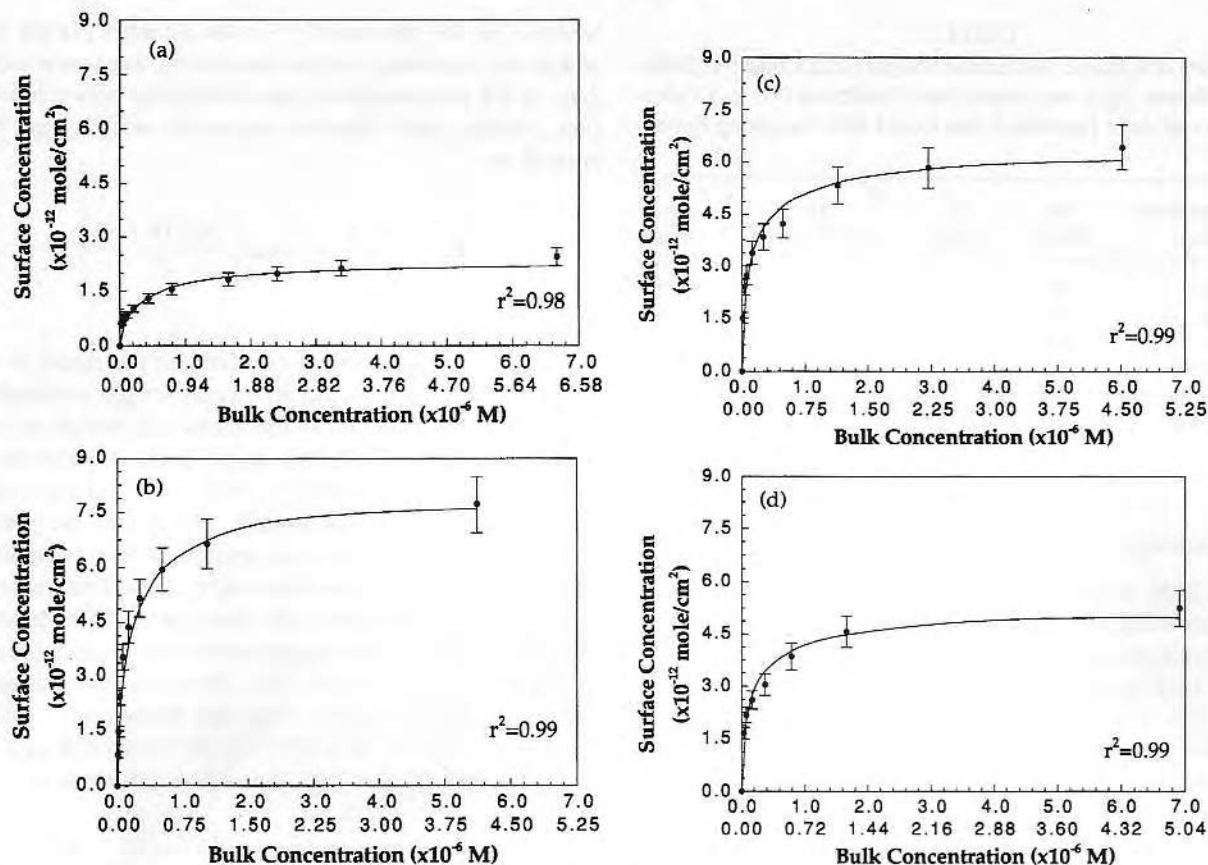


FIG. 4. Surface concentration of adsorbed Ab plotted as a function of free bulk Ab concentration at 25°C. (a) Native Ab, (b) 20-min acid pretreated Ab, (c) 60-min acid pretreated Ab, and (d) 300-min acid pretreated Ab. Experimental points and error bars represent the mean and standard error of either three or four independent measurements ($n = 3$ for native Ab, and $n = 4$ for acid pretreated Ab). Solid lines are the results of a multivariate analysis which was used to model adsorption data (see Discussion). The goodness of fit (r^2) of the experimental data to this model is indicated on each figure. The upper x-axis scale is the concentration of total (monomer + oligomer) Ab in bulk solution, while the lower x-axis scale is the concentration of monomeric Ab (calculated from light scattering data).

$$\Gamma = \frac{\Gamma_1 K_1 C}{K_1 + C} + \frac{\Gamma_2 K_2 C}{K_2 + C}, \quad [14]$$

where K_1 and Γ_1 are the affinity constant and maximum surface concentration, respectively, of the high affinity class of adsorption sites, and K_2 and Γ_2 are the affinity constant and maximum surface concentration, respectively, of the low affinity class of adsorption sites. In addition, the Hill affinity constant (K_h , Eq. [10]) can be viewed as a weighted average of K_1 and K_2 . Values for adsorption parameters determined from Eqs. [8], [10], and [14] are presented in Table 3. Although values determined for the Langmuir constant (K , Eq. [8]) are not very accurate because two classes of adsorption sites are present, values for the maximum surface concentration (Γ_{\max}) are much more reliable because they are derived from the plateau region of the adsorption isotherm.

Hill analysis (Eq. [10]) showed that values for the average affinity constant (K_h) did not differ significantly for the native and acid pretreated Abs, in contrast to the maximum surface concentration (Γ_{\max}), which was significantly higher

for acid pretreated Abs. This suggested that changes in adsorption affinity were not the primary reason for the higher surface concentrations observed for acid pretreated Abs. Further, Hill coefficients were less than one in all cases. It is difficult for us to distinguish whether this phenomenon is due to negative cooperativity (39, 28) or heterogeneity (28) of polyclonal Ab on DDS-silica surfaces, although negative cooperativity of IgG adsorption on silica surfaces has been reported by Sevastianov and Asanov (40). It is interesting to note that the Hill coefficient approaches one with increasing acid pretreatment time. This suggests that acid pretreated Abs are more homogeneously adsorbed on DDS-silica surface than native Abs.

As mentioned above, adsorption data for both native and acid pretreated Abs were fit to a two-component adsorption model. The high affinity component exhibited K_1 values in the range of 10^7 to $10^8 M^{-1}$. Interestingly, the maximum K_1 value was observed for native Ab, while the minimum value was observed for 20-min acid pretreated Ab. In contrast, the maximum surface concentration of this component

TABLE 3
The Effect of Acid Pretreatment Time on Adsorption Affinity to DDS-Silica Surfaces by Three Different Analysis Methods

Ab acid pretreatment time (min)	One-component Langmuir		Two-component Langmuir				Hill	
	K ($\times 10^6 M^{-1}$)	Γ_{\max} ($\times 10^{-12} \text{ mol/cm}^2$)	Γ_1 ($\times 10^{-12} \text{ mol/cm}^2$)	K_1 ($\times 10^7 M^{-1}$)	Γ_2 ($\times 10^{-12} \text{ mol/cm}^2$)	K_2 ($\times 10^6 M^{-1}$)	K_h ($\times 10^6 M^{-1}$)	a
0 ^a	3 \pm 1	2.5 \pm 0.1	0.9 \pm 0.2	12 \pm 2	2.0 \pm 0.4	0.9 \pm 0.2	7 \pm 1	0.7
20	8 \pm 1	7.8 \pm 0.3	6.0 \pm 0.6	1.6 \pm 0.2	2.0 \pm 0.3	3.2 \pm 0.4	9 \pm 1	0.8
60	7 \pm 1	6.5 \pm 0.4	2.7 \pm 0.3	7.4 \pm 0.8	3.0 \pm 0.4	2.5 \pm 0.3	9 \pm 1	0.9
300	6 \pm 1	5.4 \pm 0.2	3.8 \pm 0.6	3.2 \pm 0.5	2.9 \pm 0.4	3.4 \pm 0.5	6 \pm 1	0.9

^a Native Ab.

(Γ_1) was greatest for 20-min acid pretreated Ab, but decreased at longer pretreatment times. The low affinity component exhibited K_2 values between $1 \times 10^6 M^{-1}$ and $3 \times 10^6 M^{-1}$ and its maximum surface concentration ($\Gamma_2 \approx 2.5 \times 10^{-12} \text{ mol/cm}^2$) was relatively constant with acid pretreatment time. These data were somewhat perplexing considering that no clear trends emerged between the model parameters and surface concentration. This suggested that additional factors were involved, as will be examined in greater detail under Discussion.

Gel Filtration

Both native and acid pretreated Abs were subjected to gel filtration chromatography in order to examine the relative fractions of monomeric and oligomeric Abs. These results are shown in Fig. 5. The native Ab solution exhibited only a small fraction (<5%) of dimer at an Ab concentration of 1 mg/ml, while the acid pretreated Ab contained about a 21% fraction of dimer. At an Ab concentration of 10 mg/ml, the dimer fraction increased to about 33%, and a 20% fraction of oligomeric Abs was also observed (see Fig. 5c). These results were consistent with the Ab dimerization constant determined from light scattering experiments in solution. The light scattering experiments suggested that the fractions of dimer were 6 and 25% for 1 mg/ml solutions of native and acid pretreated Ab (60 min), respectively. Data obtained for 10 mg/ml acid pretreated Ab cannot be fit to this model due to the large fraction of polymeric Ab. Monomer and dimer fractions were collected for competitive adsorption experiments.

Competitive Adsorption of Monomeric or Oligomeric Ab from Acid Pretreated and Native Abs

Competitive adsorption experiments were performed with the following equimolar antibody mixtures: (a) native Ab and monomeric acid pretreated Ab, (b) native Ab and polymeric acid pretreated Ab, and (c) native Ab and unfractionated acid pretreated Ab (including both monomeric and polymeric fractions). Results are presented in Table 4 and

show that in all three cases the surface concentration of acid pretreated Ab is significantly higher than that of the native Ab. This suggests that acid pretreated Ab molecules are significantly (>3.5-fold) more surface active than their native counterparts. Further, the monomeric species appears to be considerably more surface active than the polymeric species as evidenced by the 1.8-fold higher surface concentra-

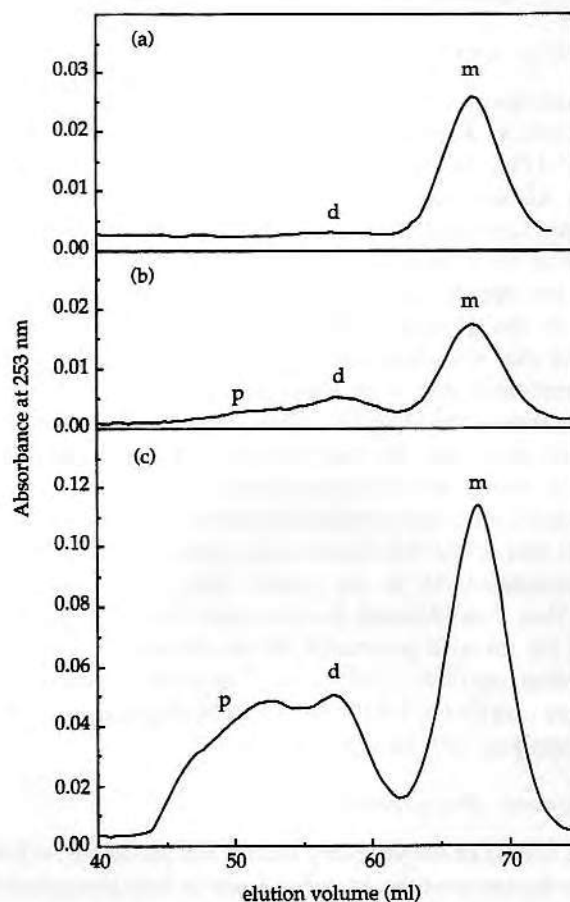


FIG. 5. Gel filtration chromatography of native and acid pretreated Ab at 25°C. (a) Native Ab, 1 mg/ml, (b) 60-min acid pretreated Ab, 1 mg/ml, and (c) 60-min acid pretreated Ab, 10 mg/ml. Samples were eluted in PBS buffer, pH 7.4.

TABLE 4
Competitive Adsorption of Native and Acid Pretreated Abs on
DDS-Silica Surfaces

	Surface concentration of native Ab ($\mu\text{g}/\text{cm}^2$)	Surface concentration of acid pretreated Ab ($\mu\text{g}/\text{cm}^2$)
Native Ab + unfractionated acid pretreated Ab	0.11 ± 0.00	0.81 ± 0.02
Native Ab + monomeric acid pretreated Ab ^a	0.12 ± 0.01	0.75 ± 0.06
Native Ab + polymeric acid pretreated Ab ^a	0.12 ± 0.02	0.42 ± 0.05

Note. An acid pretreatment time of 60 min was used.

^a The acid pretreated Ab was separated by gel filtration techniques.

tion of the former. Finally, the surface concentration of unfractionated acid pretreated Ab was not statistically different from that of the monomeric species, which implies that the monomeric species probably dominates the adsorption process.

Adsorption Kinetics of Native and Acid Pretreated Abs

Adsorption kinetics of native and acid pretreated Abs are shown in Fig. 6. Plots of surface concentration versus $\text{time}^{1/2}$ (Fig. 6a) indicated that neither adsorption of the native Ab nor that of the 60-min acid pretreated Ab was diffusion-limited at times greater than 1 min (23). We were unable to measure adsorption times of less than 1 min due to the low specific activity of the ^{125}I -IgG and the detection limit of the gamma counter. Sevastianov analysis (26) showed that the adsorption kinetics of native and 60-min acid pretreated Abs were linear when plotted using a logarithmic time scale (Fig. 6b). This suggests that both native and acid pretreated Abs may undergo conformational reorientation during the adsorption process. This postulate was examined further using saturation kinetics experiments (28–30). It was found that kinetic data obtained for the 60-min acid pretreated Ab fit the model (Eq. [11]) significantly better than data obtained for the native Ab. The results obtained for the acid pretreated Ab are shown in Fig. 7. The V_{max} value was $(5.6 \pm 0.9) \times 10^{-12} \text{ mol cm}^{-2} \text{ min}^{-1}$ and the K_d value was $(3.4 \pm 0.8) \times 10^{-6} \text{ M}$. The physical meaning of these analyses will be discussed later.

Ellipsometry Measurements

The results of ellipsometry studies are presented in Table 5. The thickness of the adsorbed layer of acid pretreated Ab was only 1.6-fold greater than that of an adsorbed layer of native Ab. This difference is small when one considers that the surface concentration of adsorbed acid pretreated Ab is 2.5-fold higher than that of the adsorbed native Ab on a

DDS-silica surface (6). Further, both thicknesses are well within the range expected for an Ab monolayer (33), and the refractive indices are similar, which is reasonable for adsorbed protein layers (32).

DISCUSSION

Previous studies in our laboratory showed that optimal surface concentration and AgBC were obtained when anti-HSA Abs were pretreated with acid for 20 min before immobilization to DDS-silica surfaces (6, 9). In this article we investigated four possible explanations for this phenomenon. These included: (a) acid pretreated Abs aggregate in solution, and the aggregates exhibit higher surface affinity than monomeric Abs; (b) multilayers of Ab form on surfaces; (c) there is a higher packing efficiency of Ab on surfaces; and (d) the orientation is more efficiently controlled. The validity of each explanation is discussed below.

Conformational changes in Abs at low pH have been demonstrated by a number of techniques including infrared spec-

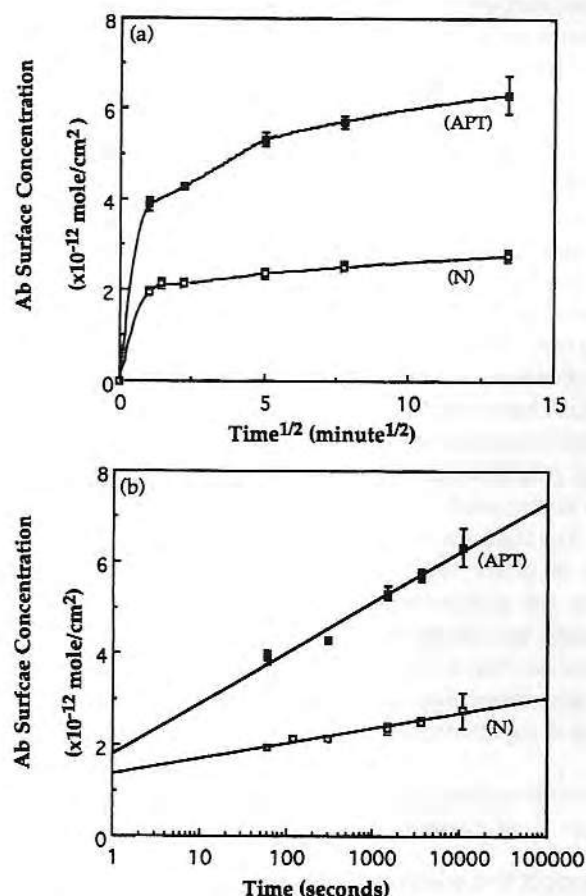


FIG. 6. Adsorption kinetics of native and acid pretreated Abs on DDS-silica surfaces at 25°C. The surface concentration of Ab is given as a function of (a) $\text{time}^{1/2}$ and (b) $\log_{10}(\text{time})$. Experimental points and error bars represent the mean and standard error of four independent measurements. APT denotes 60-min acid pretreated Ab and N denotes native Ab.

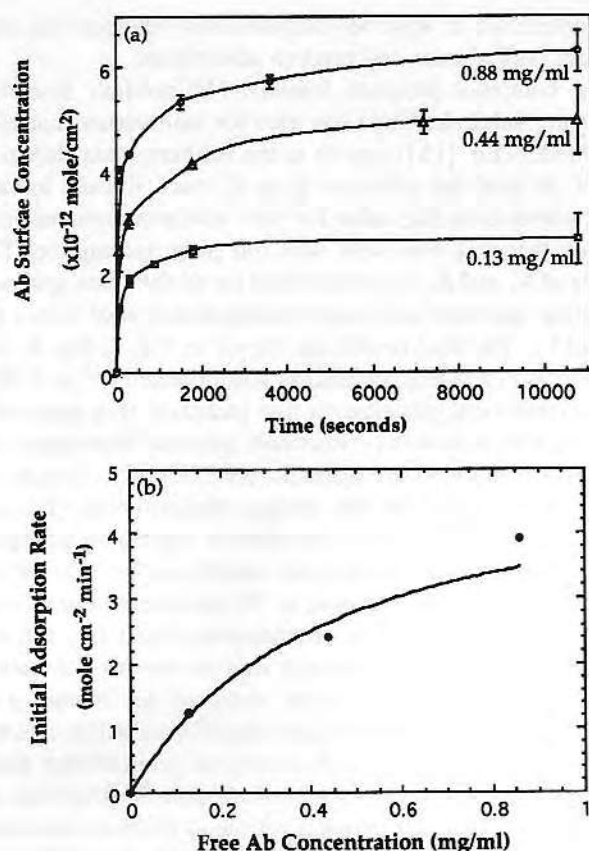


FIG. 7. Initial adsorption rate of 60-min acid pretreated Ab on DDS-silica surfaces as a function of bulk Ab concentration. (a) Adsorption kinetics at different initial free Ab concentrations and (b) initial adsorption rate as a function of initial bulk Ab concentration. Experimental points and error bars represent the mean and standard error of four independent measurements.

troscopy (41), circular dichroism (42), and fluorescence spectroscopy studies (6). Further, a hydrophobic probe study suggested that acid treatment caused increasing exposure of hydrophobic regions at the surface of the Ab with increasing acid treatment time (9), which led to destabilization and aggregation of the Ab. This hypothesis was proven by light scattering experiments (Tables 1 and 2). When Abs were acid pretreated for 60 min, 28% of Abs in a 1 mg/ml solution was in the form of aggregates (dimer). This cannot be ignored when studying the adsorption properties of acid pretreated Abs. However, competitive adsorption studies of native Ab with monomeric or polymeric acid pretreated Abs (shown in Table 4) indicated that the polymeric acid pretreated Abs did not exhibit higher surface affinity than monomeric acid pretreated Abs. These results suggest that the hydrophobically induced aggregation of the polymeric acid pretreated Abs cannot lead to a higher affinity on DDS-silica surfaces. One possible explanation is that when Abs aggregate by hydrophobic interactions, the hydrophobic regions on the acid pretreated Ab are buried inside the aggre-

gate and thus are unavailable for surface interactions. Another reason may be that aggregated Abs occupy more surface area than an equivalent amount of monomeric Ab and hence would exhibit lower surface concentration.

Multilayer adsorption of Abs has been reported in many articles (12, 42). In most such cases, adsorption was not saturable at low bulk Ab concentrations (~ 2 mg/ml). In our experiments, however, adsorption isotherms reached saturation at bulk concentrations of 1–2 mg/ml; also curves were smooth and devoid of inflection points (Fig. 4). These observations suggest that a multilayer adsorption mechanism is not operable in our case. Ellipsometry measurements also support this conclusion (Table 5). The adsorbed layer of acid pretreated Ab is only 50% thicker than that of native Ab (68 Å vs 45 Å). Further, both of these values are well within the range expected for a monolayer of IgG.

Analysis of adsorption isotherms suggested that at least two different adsorption components were present. There are two possible explanations for this observation. First, certain subpopulations of this polyclonal Ab system (anti-HSA) may be less conformationally stable and hence more easily affected by the low pH environment. If the fraction affected increases with increasing acid pretreatment time, then a gradual increase in surface affinity with pretreatment time is expected. If this hypothesis is correct, then the surface concentration and AgBC should increase with increasing acid pretreatment time and gradually reach a plateau value. Because such behavior was not observed in our experiments, however, this hypothesis is unlikely to be the main source of the observed adsorption heterogeneity.

The second explanation is based on the different susceptibilities of the antigen-binding fragment (Fab) and constant fragment (Fc) regions of the immunoglobulin molecule to acid-induced conformational changes. Previous studies of Abs in solution and at air/water or water/solid interfaces have shown that the Fc exhibits lower conformational stability than the Fab (43–45). We postulate that brief exposure to a low pH environment produces conformational changes principally in the Fc region. Previously, we showed that such conformational changes probably involved increased

TABLE 5
Ellipsometry Measurements of Native and Acid Pretreated Abs on DDS-SiO₂ Surfaces

	Native Ab	Acid pretreated Ab
d (Å)	43 \pm 3	68 \pm 7
n	1.52 \pm 0.05	1.55 \pm 0.02

Note. A pseudorefractive index model was used to analyze ellipsometry data, where d and n are the thickness and refractive index, respectively, of an Ab layer adsorbed to a DDS-SiO₂ surface. An acid pretreatment time of 60 min was used. Values represent the mean and standard error of sixteen independent determinations.

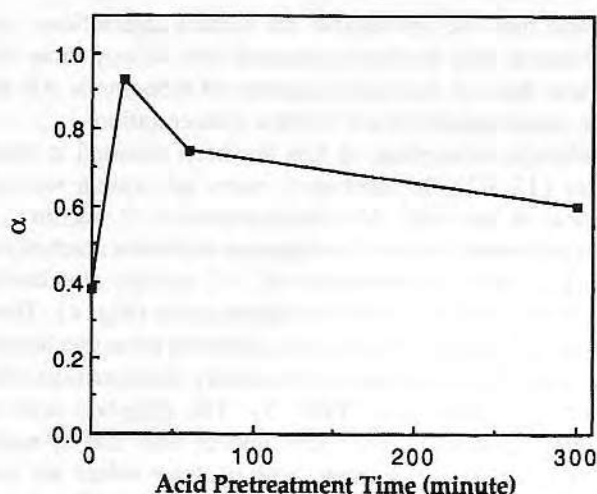


FIG. 8. Orientalional factor (α) plotted as a function of acid pretreatment time. Determined from multivariate analysis of data shown in Figs. 4a–4d.

exposure of hydrophobic regions to solvent (9). Because these regions exhibit higher affinity for hydrophobic surfaces than the native Ab, the acid treated antibody will adsorb with a preferential orientation; i.e., the Fc region adsorbs, leaving the Fab free to bind to antigen in bulk solution. However, upon longer acid pretreatment time, hydrophobic regions also arise in the Fab. Since they adsorb with equal affinity to the hydrophobic regions in the Fc, preferential orientation and AgBC decrease with longer acid pretreatment time.

To investigate this hypothesis, we added an additional parameter (α) to the two-component Langmuir equation (Eq. [14]) that accounts for the orientation of the Ab on the surface:

$$\Gamma = \frac{\alpha\Gamma_1 K_1 C}{1 + K_1 C} + \frac{\alpha\Gamma_2 K_2 C}{1 + K_2 C} \quad [15]$$

In this model, the affinities (K_1 , K_2) of the two types of adsorption sites are independent of acid pretreatment time, while the maximum concentrations of such sites (Γ_1 , Γ_2) and the orientation (α) of the adsorbed Ab molecules are allowed to vary with pretreatment time. The orientational parameter α is related to the density of each adsorbed Ab molecule. A value close to 1 represents the highest possible packing density. Presumably, such a value is obtained when the Fc region of Ab adsorbs on surfaces, leaving the Fab free to bind to antigen in bulk solution. Lower values of α reflect lower packing densities, presumably caused by more random orientations of adsorbed Abs that occupy greater surface area per Ab molecule. It was impossible to predict a minimum value for α , a priori. A value of 0 represents an infinite adsorbed surface area per Ab molecule, clearly a physical impossibility. In practice, a minimum value of ca. 0.3 was obtained (see Fig. 8), which suggests about a three-

fold difference in adsorbed surfaces area between the most densely packed case and random adsorption.

The computer program *Scientist* (MicroMath Scientific Software, Salt Lake City) was used for multivariate analysis. The model (Eq. [15]) was fit to the isotherm data shown in Fig. 4. At first, the values of K_1 or K_2 were allowed to vary and came to a similar value for each acid pretreatment time, a result that was consistent with our prior assumption. The values of K_1 and K_2 were then fixed for further data analysis. A similar approach was used for determination of values for Γ_1 and Γ_2 . The final results are shown in Fig. 4, Fig. 8, and Table 6; an excellent correlation was obtained ($r^2 > 0.98$). The orientational parameter α first increased to a maximum value of 0.93 at 20 min pretreatment time and then decreased with increasing acid pretreatment time (Fig. 8). This result is consistent with both the surface concentration (Γ) and AgBC of adsorbed Ab as a function of increasing acid pretreatment time. Interestingly, the model predicts that the increased surface concentration at 20 min pretreatment time is due to a combination of orientational effects (α) and the number of high affinity binding sites in the Ab population (Γ_1). In Table 6, the Γ_1 value observed for 20-min acid pretreated Ab was twofold higher than that of native Ab, but did not increase further with additional pretreatment time. In a previous study (9), we showed that the exposure of hydrophobic regions increased with acid pretreatment time. The reason for this disparity may be due to steric effects—the area of the hydrophobic probe is much smaller than the adsorption sites on DDS surfaces—so Γ_1 may be sterically limited by the number of IgG molecules that can fit into a monolayer on the DDS surface. This same limitation would not apply to a hydrophobic probe in solution.

Although the above model explains a number of our observations about the surface concentration and AgBC of immobilized Abs, it does not provide a physical interpretation of the orientational factor α . In particular, we do not know whether the orientation of an adsorbed Ab molecule is the result of a competitive adsorption process, analogous to the “Vroman effect” (46), or if it is due to a conformational

TABLE 6
Multivariate Analysis of Native and Acid Pretreated Abs on DDS–Silica Surfaces

Parameter	Acid pretreatment time (min)			
	0 ^a	20	60	300
Γ_1 ($\times 10^{-12}$ mol/cm ²)	2.4 \pm 0.2	5.0 \pm 0.9	5.0 \pm 0.9	5.0 \pm 0.9
K_1 ($\times 10^7$ M ⁻¹)	2.0 \pm 0.6	2.0 \pm 0.6	2.0 \pm 0.6	2.0 \pm 0.6
Γ_2 ($\times 10^{-12}$ mol/cm ²)	3.7 \pm 0.8	3.7 \pm 0.8	3.7 \pm 0.8	3.7 \pm 0.8
K_2 ($\times 10^6$ M ⁻¹)	1.6 \pm 0.2	1.6 \pm 0.2	1.6 \pm 0.2	1.6 \pm 0.2
α	0.38	0.93	0.74	0.60
r^2	0.98	0.99	0.99	0.99

^a Native Ab.

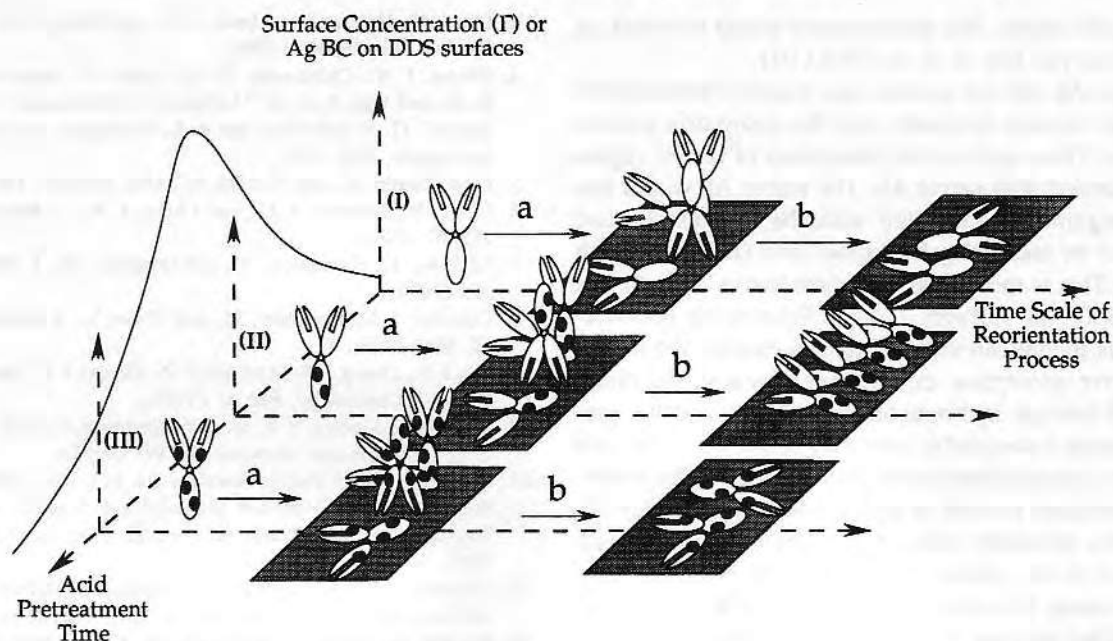


FIG. 9. Proposed mechanism for acid pretreatment effects on the orientation and antigen-binding capacity of adsorbed antibodies. (I) Native Ab. (II) Abs pretreated for a short period (ca. 20 min). Limited exposure to acidic conditions results in an increased number of hydrophobic regions (dark patches) occurring mainly in the Fc region. (III) Abs pretreated for longer times (>20 min). Longer exposure to acidic conditions results in appearance of hydrophobic regions throughout the entire Ab molecule. The initial adsorption step is denoted by "a," and the reorientation step is denoted by "b."

shift (or rearrangement) between the two classes of adsorption sites (K_1 and K_2) within the adsorbed Ab molecule. Fortunately, our adsorption kinetic experiments provided some insight into these issues. Sevastianov *et al.* (26) proposed a model for heterogeneous adsorption of IgG to quartz surfaces, in which IgG molecules were allowed to significantly change their "effective adsorption area" by undergoing a reorientation event on the surface. Further, this model predicts that adsorption kinetic curves will exhibit a strong logarithmic dependency with respect to time. Such a logarithmic dependency was observed for both native and 60-min acid pretreated Abs in our experiments (see Fig. 6b), which suggests that the adsorption mechanism of both types of Abs involves a reorientation step (27). In addition, when surface concentrations were extrapolated to early adsorption times (1 s) using Sevastianov's model, surface concentration values of 1.4×10^{-12} and 1.8×10^{-12} mol/cm² were predicted for native and acid pretreated Abs, respectively. Both of these values are similar to those found in Sevastianov's experiments, which gives us confidence that his model is applicable to our system. Finally, saturation kinetics experiments (Fig. 7) indicated that the initial adsorption rate of 60-min acid pretreated Abs was saturable with increasing bulk Ab concentration. This suggests that the adsorption of such Abs involves a nucleation or growth-limited step (28–30).

In summary, a model which combines two adsorption sites in one Ab molecule with reorientation of the Ab on the surface is used to explain the behavior of acid pretreated Ab

on surfaces. Figure 9 shows a schematic representation of this model. There are three axes in this figure—the Ab adsorption time scale, the acid pretreatment time, and the AgBC of Abs on surfaces (or Ab surface concentration). The "Y"-shaped figures represent the Abs. The black spots represent the exposed hydrophobic areas in Ab after acid pretreatment. There are three stages (I, II, and III) with different areas of hydrophobic exposure. The initial adsorption step is labeled "a," and the reorientation step is labeled "b." Our experimental results suggest that, in the case of shorter acid pretreatment times, the area of hydrophobic exposure most likely occurred in the Fc region (due to the reduced temperature stability of the C_{H2}–C_{H2} domain dimer). Upon exposure of this region, the hydrophobic interaction increased between the Fc and the hydrophobicized silica surface. This resulted in the reorientation of acid pretreated Ab on the surface and a smaller overall "footprint" for adsorbed Ab molecules. This smaller footprint led to a higher packing efficiency (high α value) and preferential adsorption of the Fc region. An increase in both adsorbed Ab (Γ) and AgBC resulted from this mechanism. In the case of longer acid pretreatment times, exposed hydrophobic areas appeared in both Fab and Fc regions of Abs, and preferential adsorption of the Fc region decreased. The footprint of Ab on the surface thus increased. This caused both a lower packing efficiency (lower α value) and less exposure of the Fab, and led to a reduction in both amount of adsorbed Ab and AgBC. From the above, it is easy to conclude that the Fc region of the Ab plays an important role in this hypothesis.

Without the Fc region, this phenomenon would not exist, as was shown by van Erp *et al.* in 1992 (10).

The native Ab did not possess any exposed hydrophobic areas caused by acid treatment, and the adsorption process was random. Thus, preferential adsorption of the Fc region was not observed with native Ab. The native Ab would like to have a maximum interaction with the hydrophobicized silica surface by increasing its contact area (footprint) with the surface. This is the reason why most native Abs attempt to "lie down" on surfaces (from ellipsometry measurements). This model can also be used to explain the results of competitive adsorption experiments. Because the dimer was formed through hydrophobic interactions and the previously exposed hydrophobic area may be buried in the core of the dimer, the adsorbed dimer does not exhibit the preferential reorientation process or higher packing efficiency observed for the monomer. Also, this model is consistent with the two-binding-site model presented in the Scatchard isotherm calculation. It is easy for us to consider that the higher affinity binding constant is due to exposed hydrophobic regions in the acid pretreated Ab and that the lower affinity binding constant is due to random adsorption sites that occur to some degree in almost all proteins.

CONCLUSION

These studies showed that an increased exposure of high affinity adsorption sites is the most important factor affecting the surface concentration and AgBC of acid pretreated Ab adsorbed to DDS-silica surfaces. Furthermore, these changes probably result from an increase in the hydrophobic interaction between Ab and hydrophobic DDS-silica surfaces. With short acid pretreatment time (Fig. 7), these changes mostly occur in the Fc region of the Ab. This leads to preferential adsorption of the Fc, higher packing efficiency on the surface, and a higher AgBC. For longer treatment times, hydrophobic regions are exposed throughout the whole IgG molecule, which leads to lower packing efficiency and AgBC. It is hoped that increasing our understanding of the adsorption properties of Abs will lead to more effective immobilization strategies.

ACKNOWLEDGMENTS

This work has been supported in part by the Center for Biopolymers at Interfaces, University of Utah, and AKZO Corporate Research America, Inc. We thank Mr. J. Y. Wang for help with the ellipsometry measurements and Mr. Y. K. Chuang for help with the light scattering experiments.

REFERENCES

1. Taylor, R. F., "Protein Immobilization: Fundamentals and Applications," p. 263. Dekker, New York, 1991.
2. Mohr, P., and Pommerening, K., "Affinity Chromatography: Practical and Theoretical Aspects." Dekker, New York, 1985.
3. Lin, J. N., Herron, J., Andrade, J. D., and Brizgys, M., *IEEE Trans. Biomed. Eng.* **35**, 466 (1988).
4. Herron, J. N., Christensen, D. A., Hlady, V., Janatova, V., Wang, H.-K., and Wei, A.-P., in "Advances in Fluorescence Sensing Technology" (J. R. Lakowicz and R. B. Thompson, Eds.), p. 28. SPIE, Bellingham, WA, 1993.
5. Ernst-Cabrera, K., and Wilchek, M., *Anal. Biochem.* **159**, 267 (1986).
6. Lin, J. N., Andrade, J. D., and Chang, I. N., *J. Immunol. Methods* **125**, 67 (1989).
7. Ishikawa, E., Hamahuchi, Y., and Imagawa, M., *J. Immunoassay* **1**, 385 (1980).
8. Conradie, J. D., Govender, M., and Visser, L., *J. Immunol. Methods* **59**, 289 (1983).
9. Lin, J. N., Chang, I. N., Andrade, J. D., Herron, J. N., and Christensen, D. A., *J. Chromatogr.* **542**, 41 (1991).
10. van Erp, R., Linders, Y. E. M., van Sommeren, A. P. G., and Gribnau, T. C. J., *J. Immunol. Methods* **152**, 191 (1992).
11. Zsom, R. L. J., *J. Colloid Interface Sci.* **111**, 434 (1986).
12. Silberberg, A., in "Surface and Interfacial Aspects of Biomedical Polymers" (J. D. Andrade, Ed.), p. 321. Plenum Press, New York, 1985.
13. Tonnelat, J., and Guinand, S., in "Experimental Methods in Biophysical Chemistry" (C. Nicolau, Ed.), p. 135. Wiley, New York, 1973.
14. Jøssang, T., Feder, J., and Rosenqvist, E., *J. Chem. Phys.* **82**, 574 (1985).
15. Rosenqvist, E., Jøssang, T., and Feder, J., *Mol. Immunol.* **24**, 495 (1987).
16. Brice, B. A., and Halwer, M., *J. Opt. Soc. Am.* **41**, 1033 (1951).
17. Cummins, H. Z., in "Photon Correlation and Light Beating Spectroscopy" (H. Z. Cummins and E. R. Pike, Eds.), p. 285. Plenum Press, New York, 1975.
18. Corti, M., and Degiorgio, V., *J. Phys. Chem.* **85**, 711 (1981).
19. Petsev, D. N., and Denkov, N. D., *J. Colloid Interface Sci.* **149**, 329 (1992).
20. Chuang, H. Y. K., King, W. F., and Mason, R. G., *J. Lab. Clin. Med.* **92**, 483 (1983).
21. Lin, J. N., Ph. D. thesis, University of Utah, Salt Lake City, 1988.
22. Chang, I. N., Ph. D. thesis, University of Utah, Salt Lake City, 1994.
23. Andrade, J. D., in "Surface and Interfacial Aspects of Biomedical Polymers" (J. D. Andrade, Ed.), p. 1. Plenum Press, New York, 1985.
24. Cantor, C. R., and Schimmel, P. R., "Biophysical Chemistry," p. 843. Freeman, New York, 1980.
25. Hlady, V., Van Wagenen, R. A., and Andrade, J. D., in "Surface and Interfacial Aspects of Biomedical Polymers" (J. D. Andrade, Ed.), p. 81. Plenum Press, New York, 1985.
26. Sevastianov, V. I., Kulik, E. A., and Kalinin, I. D., *J. Colloid Interface Sci.* **145**, 191 (1991).
27. Sevastianov, V. I., *CRC Crit. Rev. Biocompat.* **4**(2), 109 (1988).
28. Jennissen, H. P., *Biochemistry* **15**, 5683 (1976).
29. Jennissen, H. P., *J. Solid Phase Biochem.* **4**, 151 (1979).
30. Jennissen, H. P., *J. Colloid Interface Sci.* **111**, 570 (1986).
31. Ma, S. M., Coleman, D. L., and Andrade, J. D., *Surf. Sci.* **56**, 117 (1976).
32. Arwin, H., *Applied Spectrosc.* **40**, 313 (1986).
33. Lin, Y. S., Ph. D. thesis, University of Utah, Salt Lake City, 1993.
34. Wang, J. Y., Stroup, E., Wang, X. F., and Andrade, J. D., in "SPIE International Conference on Thin Film Physics and Applications," Vol. 1519, p. 835. SPIE, Bellingham, WA, 1991.
35. McCrackin, F. L., "A Fortran program for analysis of ellipsometer measurements," U.S. Government Printing Office, 1969.
36. Vasicek, A., "Optics of Thin Films." North-Holland, Amsterdam, 1960.
37. McCrackin, F. L., Passaglia, E., Stromberg, R. R., and Steinberg, H. L., *J. Res. Nat. Bur. Stand.* **67A**, 363 (1963).

38. Adams, E. T., and Filmer, D. L., *Biochemistry* **5**, 2971 (1966).
39. Levitzki, A., and Koshland, D. E., Jr., *Curr. Top. Cell Regul.* **10**, 1 (1976).
40. Sevastianov, V. I., and Asanov, A. N., in "Transactions, 3rd World Biomaterials Congress," Business Center for Academic Societies, p. 91. Japan, Tokyo, 1988.
41. Abaturov, L. V., Nezlin, R. S., Vengerova, T. I., and Varshavsky, J. M., *Biochim. Biophys. Acta* **194**, 386 (1969).
42. Young, B. R., Pitt, W. G., and Cooper, S. L., *J. Colloid Interface Sci.* **125**, 246 (1988).
43. Lavrentev, V. V., Chasovnikova, L., and Sorokin, Ju., in "Adhesion and Adsorption of Polymers, Part B" (Lieng-Huang Lee, Ed.), p. 847. Plenum Press, New York, 1980.
44. Tijssen, P., "Practice and Theory of Enzyme Immunoassays: Laboratory Techniques in Biochemistry and Molecular Biology." Elsevier, Amsterdam, 1985.
45. Huber, R., *Klin. Wochenschr.* **58**, 1217 (1980).
46. Brash, J. L., and Uniyal, S., *J. Polym. Sci. Polym. Symp.* **66**, 377 (1979).

Photoaffinity Labeling of Antibodies for Applications in Homogeneous Fluoroimmunoassays

I-Nan Chang,[†] Jinn-Nan Lin,[‡] Joseph D. Andrade,^{†,‡} and James N. Herron^{*,†,§}

Departments of Material Science and Engineering, Bioengineering, and Pharmaceutics, University of Utah, Salt Lake City, Utah 84112

A homogeneous noncompetitive immunoassay based on photoaffinity labeling techniques is described. Using this method, a fluorophore (reporter) can be specifically attached to an antibody in the vicinity of its antigen-combining sites. Upon antigen binding, changes in the fluorescence spectrum of the reporter molecule are often observed. Two fluorophores, pyrene and dansyl, were evaluated for this purpose. Also, this technology is ideal for fluorescence energy-transfer immunoassays that require labeling of the antibody with either a donor or acceptor fluorophore. In such cases, a fluorescent dye can be specifically attached near the antigen-combining site, where it can participate in high-efficiency energy transfer with its complementary fluorophore attached to the antigen.

The fluoroimmunoassay has become a common clinical chemistry procedure for the analysis of a wide range of analytes, such as drugs, hormones, and proteins (see reviews by Dito¹ and by Painter²). Such immunoassays are divided into two categories—heterogeneous assays, which involve physical separation of the assay mixture before detection, and homogeneous assays, in which no separation steps are required. The majority of existing fluoroimmunoassays are heterogeneous. Furthermore, they are often competitive assays, in which a fluorescently labeled antigen (or antibody) competes for binding with an unlabeled antigen (or antibody).^{3,4} In such assays, the fluorescently labeled species is referred to as the “tracer” and the unlabeled species as the “analyte”. Depending on the assay being performed, the analyte can be either an antigen (Ag) or an antibody (Ab). After removal of unbound analyte and tracer, the signal intensity from the bound tracer is found to be inversely proportional to the analyte concentration in the original solution. The separation step always complicates the design of these immunoassays and can degrade their overall performance.⁵

By eliminating the separation step, homogeneous immunoassays can lessen or eliminate most of the above disadvantages.⁵ A

homogeneous immunoassay based on spectral changes of a fluorescently labeled antibody upon binding of unlabeled Ag was first reported by Liburdy in 1979.⁶ In this study, an anti-human immunoglobulin G (IgG) Ab was randomly labeled with *N*-(3-pyrene)maleimide (PM), a fluorophore that is highly sensitive to local polarity changes.⁷ The PM-labeled Ab exhibited an enhanced fluorescence intensity in the presence of the Ag. Furthermore, results of control experiments indicated that the increase in fluorescence intensity was Ag specific. However, a high degree of labeling of (degree of labeling 17 pyrene molecules/1 Ab molecule) was reported, which caused a high level of fluorescence background and precipitation of labeled Ab upon storage. In solving these problems, the degree labeling must be decreased, and if possible, the fluorophores should be conjugated only to positions in the proximity of the antigen-combining sites.

In 1989, Pollack et al. used a so called “affinity labeling” technique to achieve the above goals.⁸ In their study, anti-dinitrophenol (DNP) antigen-binding fragments (Fab) were modified with cleavable affinity labels. These labels consisted of DNP groups (antigen) linked to electrophilic or α -bromo ketone groups through cleavable disulfide or thiophenyl linkages. The affinity labels were covalently attached to Fab fragments, followed by the cleavage of the label with dithiothreitol (DTT). These thiol-derivatized Fab fragments can specifically react with fluorophores through a thiol chemistry. The results indicated that the labeled fluorophores were attached in the vicinity of the antigen-combining sites and that the degree labeling of was ~ 1 . Fluorescence binding experiments showed that the addition of the antigen (DNP-glycine) to the fluorescein-labeled, thiol-derivatized Fab fragment resulted in a decrease in fluorescence intensity, providing a direct assay of ligand binding.

On the basis of the effectiveness of this affinity labeling technique, we investigated the use of a photoaffinity labeling technique to specifically attach highly sensitive fluorophores in the vicinity of antigen-combining sites. In our studies, a photoactive azide group was used instead of the thermal reactive group, which was used by Pollack.⁸ Specifically, nitrophenyl azide was chosen as the photoactive group. Its optimal photolysis occurs at a longer wavelength (320–350 nm) than observed for aryl azide groups (265–275 nm).⁹ This limits damage to the protein caused

[†] Department of Material Science and Engineering.

[‡] Department of Bioengineering.

[§] Department of Pharmaceutics.

(1) Dito, W. R. *Clin. Chem.* **1981**, (Oct), 10–18.

(2) Painter, P. *Diagn. Clin. Test.* **1990**, 28, 40–42.

(3) Anderson, F. P.; Miller, W. G. *Clin. Chem.* **1988**, 34, 1417–1421.

(4) Ishikawa, E.; Kawai, T.; Miyat, K. *Enzyme Immunoassay*; Igaku-Shoin: New York, 1981; Chapter 1.

(5) Zuk, R. F.; Rowley, G. L.; Ullman, E. F. *Clin. Chem.* **1979**, 25, 1554–1560.

(6) Liburdy, R. P. *J. Immunol. Methods* **1979**, 28, 233–242.

(7) Kalyanasundaram, K.; Thomas, J. K. *J. Am. Chem. Soc.* **1977**, 99, 2039–2044.

(8) Pollack, S. J.; Nakayama, G. R.; Schultz, P. G. *Methods Enzymol.* **1989**, 178, 551–568.

(9) Ji, T. H. *Biochim. Biophys. Acta* **1979**, 559, 39–69.

label is a disulfide bond, which can be reduced to a thiol group using DTT. After the photoaffinity labeling process, a free thiol group is introduced in the vicinity of the antigen-combining sites, and a fluorophore can be specifically attached using thio-reactive chemistry. The maleimide-thiol and thiol-thiol exchange reactions were used in this report.¹⁰

Different fluorophores were used to test this technique. Pyrene and dansyl were chosen for immunoassays based on spectral changes, and the tetramethylrhodamine-fluorescein pair was chosen for an energy-transfer immunoassay. The reason for choosing pyrene and dansyl was that these fluorophores are especially sensitive to environmental changes and have commonly been used as fluorescence probes in several applications. Dansyl fluoresces only weakly in water, with an emission maximum at ~580 nm and a quantum yield of less than 0.1. However, in a solvent of low dielectric constant, the emission maximum shifts toward the blue and the quantum yield increases markedly (up to 0.7).¹¹ Dansyl also has a very large Stoke shift, resulting in a low background of scattered light, which is ideal for homogeneous assay applications. Pyrene exhibits similar properties and has been used as a homogeneous assay reporter for years.⁶ The tetramethylrhodamine-fluorescein pair was chosen because of the large overlap of the emission spectrum of the donor (fluorescein) with the absorption spectrum of the acceptor (tetramethylrhodamine).¹²

EXPERIMENTAL SECTION

Ab-Ag System and Concentration Measurements. Polyclonal goat anti-biotin Ab (anti-B) IgG fraction (Sigma Chemical Co.) was used as a model Ab. Antibody concentrations were determined by absorbance at 280 nm using a UV-visible spectrophotometer (Beckman, Model 35). Values of 1.35 and 150 000 were used for the absorption extinction coefficient ($E_{280\text{nm}}^{0.1\%}$) and molecular weight of anti-B Ab, respectively. Biotin (Pierce Co.) concentration was determined directly by dry weight.

Preparation of Photoaffinity Label. The photoaffinity label consisted of a terminal photoactive group and a disulfide bridge and was prepared by following procedure (Figure 1). The antigen *N*-(2-aminoethyl)biotinamide (biotin ethylenediamine) with a primary amine group was purchased from the Molecular Probes Co. (Eugene, OR). Ten milligrams of this compound was dissolved in 2 mL of *N,N*-dimethylformamide solvent (DMF; Aldrich) (predried by molecular sieves and CaCl_2). The solution was then mixed with 20 mg of a heterobifunctional reagent, sulfosuccinimidyl 2-(*m*-azido-*o*-nitrobenzamido)-1,3'-dithiopropionate (SAND; Pierce Co.) and 4 μL of triethylamine (Aldrich). This mixture was allowed to react for 24 h at 20 °C in the dark, followed by separation on a silica gel (200–400 mesh, Aldrich) column equilibrated in a methanol-acetone solution (1:1 volume ratio). The products were analyzed by thin-layer chromatography (TLC) using silica gel plates with fluorescent indicator (Merck) and a methanol-acetone (50:50) solvent system. The product (biotin-AND) migrated as a single spot on TLC, with an R_f value of 0.81. The IR spectrum of biotin-AND (dissolved in CHCl_3)

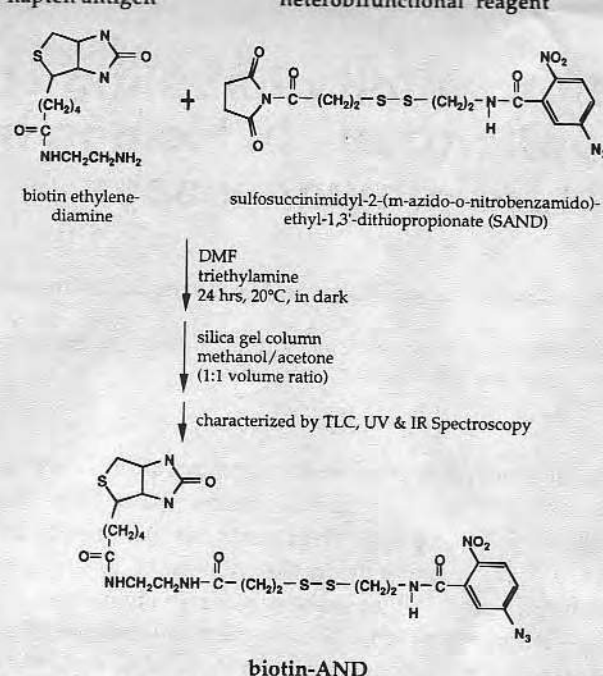


Figure 1. Schematic representation of the preparation of photoaffinity label.

exhibited a characteristic N_3 stretch at 2150 cm^{-1} .¹³ The characteristic ester stretch at 1700 cm^{-1} was not observed in biotin-AND, but a stronger characteristic amide stretch at 1650 cm^{-1} was found in comparison with the IR spectrum of SAND. Comparison of the UV-visible spectra of biotin-AND in phosphate buffer saline (PBS pH 7.4) before and after UV irradiation showed that, after irradiation, biotin-AND exhibited the characteristic absorption spectra of the photolysis products of nitrophenyl azide (data not shown).¹³ Taken together these results suggested that the photoaffinity label (biotin-AND) had been successfully prepared.

Antibody Modification. Affinity Labeling. Experimental procedures for photoaffinity labeling are outlined in Figure 2. Anti-B Abs were photoaffinity labeled in 0.15 M PBS (pH 7.4) at a protein concentration of 6 mg/mL (0.04 mM) with a 4-fold molar excess of biotin-AND reagent (0.16 mM). The concentration of biotin-AND was determined by UV absorption at 320 nm, using an extinction coefficient of $9 \times 10^3\text{ M}^{-1}\text{ cm}^{-1}$.¹³ This reaction mixture was incubated for 1 h at room temperature in the dark to allow the photoaffinity label to bind to the antibody. The reaction mixture was irradiated for 6 min with a 750 W mercury lamp (Schoeffel Instrument Co.) through a 320 nm band-pass filter (Oriol Co.). The reaction vessel was placed 20 cm from the light source. Unreacted biotin-AND was removed by gel permeation chromatography with a PD-10 column (Pharmacia) equilibrated in PBS.

Cleavage of Affinity Label (Biotin-AND). The pH of the photoaffinity labeled antibody preparation was adjusted from 7.4 to 8.0 using 0.2 M carbonate-bicarbonate buffer, pH 9.2 (CBB), and its concentration was adjusted to 2 mg/mL by addition of 0.1 M sodium phosphate buffer (pH 8.0). Next, DTT was added to reduce the disulfide bond in the affinity label. Specifically, 0.2 mL of a 500 mM solution of DTT in 0.1 M sodium phosphate

(10) Brinkly, M. *Bioconjugate Chem.* **1992**, 3, 2–13.

(11) Chen, R. F. *Arch. Biochem. Biophys.* **1967**, 120, 609–620.

(12) Meadows, D.; Schultz, J. S. *Talanta* **1988**, 35, 145–150.

(13) Lewis, R. V.; Roberts, M. F.; Dennis, E. A.; Allison, W. S. *Biochemistry* **1977**, 16, 5650–5654.

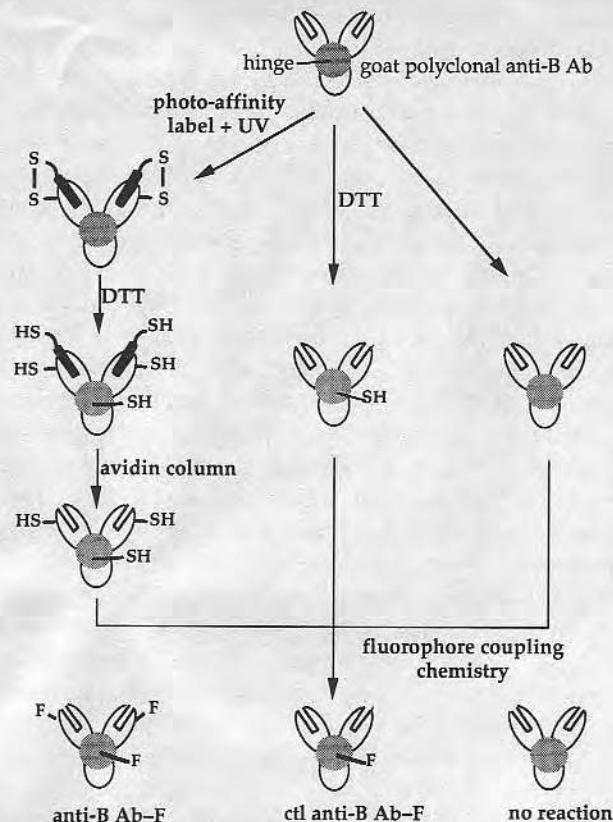


Figure 2. Schematic representation of photoaffinity labeling procedures and an outline of the control experiments.

buffer (pH 8.0) and 0.2 mL of a 20 mM solution of EDTA (in the same buffer) were added to 2 mL of the above Ab solution. This mixture was allowed to react for 16 h at 37 °C. Following the reaction, a 50-fold molar excess of biotin (compared to the Ab concentration) was added to the Ab solution to displace the cleaved affinity label (biotin-SH) from the antigen-combining sites. Unbound biotin and biotin-SH were removed by gel permeation chromatography using a PD-10 column equilibrated in PBS. Anti-biotin Abs with a free thiol group (anti-B Ab-SH) near the antigen-combining site were successfully prepared in this manner.

Efficiency of Photoaffinity Label. Since biotin does not absorb light in the visible or near-UV ranges of the spectrum, we used a biotin-fluorescein conjugate (biotin-Fl; Molecular Probes) to indirectly determine the efficiency of the photoaffinity labeling process. An excess amount of biotin-Fl was added to saturate the antigen-combining sites of anti-B Abs, and then unbound biotin-Fl was separated with a PD-10 column. Since fluorescein exhibits strong absorbance at 495 nm ($E_{495\text{nm}}^{\text{M}} = 75\,000\text{ M}^{-1}\text{ cm}^{-1}$), the concentration of bound biotin-Fl was determined by measuring the absorbance at 495 nm. The Ab concentration was determined by measuring the absorbance at 280 nm. However, since fluorescein also absorbed at 280 nm, a correction factor was applied ($A_{280}(\text{total}) = A_{280}(\text{Ab}) + A_{280}(\text{Fl})$; $A_{280}(\text{Fl}) = 0.28A_{495}(\text{Fl})$). The activity of the anti-B Ab was determined by taking the ratio of bound biotin-Fl to total antigen-combining sites. The same procedures were used to determine the activity of photoaffinity labeled anti-B Ab without disulfide bond cleavage and with disulfide bond cleavage. By comparing the activities of

these three Ab preparations, the efficiency of the photoaffinity labeling procedure can be determined. Another control experiment was performed in which goat anti-human serum albumin (anti-HSA) was photoaffinity labeled instead of the anti-B Ab. In this case, fluorescein-AND (Fl-AND) was used as the photoaffinity label. It was prepared as described above except that fluoresceinamine was used as the starting material. Photo-affinity labeling, disulfide cleavage, and characterization of labeling efficiency were performed as described above.

Derivatization with Fluorophores. Thiol-derivatized anti-biotin antibodies prepared by the above procedures still contained biotin in their antigen-combining sites. Bound biotin was removed by passing the Ab solution through an avidin column (Pierce). Approximately 80% of the bound biotin could be removed by this method (Figure 2).

In the next step, one of three different fluorophores (pyrene, dansyl, or tetramethylrhodamine) was conjugated to the free thiol group. In the case of pyrene, *N*-(1-pyrene)maleimide (Molecular Probes) was predissolved in dry DMSO and then added to anti-B Ab-SH, which had been dialyzed into 0.2 M acetate buffer (pH 6.0). This mixture was allowed to react for 6 h at 4 °C. The molar ratio of pyrenemaleimide to Ab was 4:1. The volume of the DMSO solution should not exceed 5% of that of the Ab solution in order to avoid precipitation of the Ab. Alternately, PM adsorbed to Celite (PM-C; Molecular Probes¹⁵) could be used instead of PM dissolved in DMSO. The same reaction conditions were used in this case except that the molar ratio of PM to Ab was 20:1.

For labeling Abs with dansyl, didansyl-L-cystine (DC; Molecular Probes) was dissolved in 0.2 M phosphate buffer (pH 8.5) and added to anti-B Ab-SH that had been dialyzed into the same buffer. This mixture was incubated for 4 h at 25 °C. The molar ratio of DC to Ab was 10:1, and the volume ratio of the DC solution to the Ab solution was 0.1:1. In the case of tetramethylrhodamine, 5-(and 6)-maleimidotetramethylrhodamine (TRM; Molecular Probes) was dissolved in DMSO and added to anti-B Ab-SH that had been dialyzed into 0.2 M acetate buffer (pH 6.0). The mixture was allowed to react for 4 h at 4 °C. The molar ratio of TRM to Ab was 4:1. All these fluorophore-Ab conjugates were purified using a PD-10 column equilibrated in PBS.

Labeled Abs for Control Experiments. In addition to attaching fluorophores to photoaffinity-labeled Abs, conjugation reactions were also performed on the following two Ab preparations as controls—native Abs (no affinity label or DTT treatment) and DTT-treated Abs (no affinity label, but treated with DTT as described above for affinity-labeled Abs). Since native Abs usually do not possess free thiol groups, little if any labeling of these Abs is expected. However, when native Abs are treated with DTT, free thiol groups are produced in the hinge region, which can be labeled with fluorophores. Thus, photoaffinity-labeled Abs should contain fluorophores in both the hinge region and the vicinity of the antigen-combining site, whereas DTT-treated Abs should be labeled only in the hinge region.

For Abs labeled with tetramethylrhodamine, an additional conjugate was prepared as a control. Specifically, native Abs were dialyzed into CBB and allowed to react with tetramethylrhodamine-5-(and 6)-isothiocyanate (TRITC; Molecular Probes) for 1, 2, 4, and 6 h at 4 °C. The molar ratio of TRITC to Abs was 10:1. The conjugate was purified with a PD-10 column equilibrated in PBS.

(14) Haugland, R. P. *Handbook of Fluorescence Probes and Research Chemicals*; Molecular Probes, Inc.: Eugene, OR, 1992; Part I-III.

(15) Rinderknecht, H. *Experientia* 1960, 16, 430-431.

Since TRITC is an amine-reactive probe, fluorophores are primarily attached to lysine residues that are randomly distributed throughout the surface of the Ab.

Degree of Labeling. The degree of labeling is defined as the number of fluorescent dye molecules conjugated to each antibody molecule. It was determined by measuring the absorbance of both the dye and the antibody at their respective absorption maxima. In the case of pyrene, a wavelength of 343 nm was used, and 325 nm was used for dansyl and 540 nm for tetramethylrhodamine.¹⁴ The absorbance of the antibody was measured at 280 nm. Because most dyes exhibit some absorption at 280 nm, the observed $A_{280\text{nm}}$ value was corrected for the contribution of the dye. Correction factors have been reported in the literature for all three^{10,16,17,22} dyes. Once an absorbance value has been obtained for the dye (A_{dye}), and a corrected A_{280} value obtained for the antibody, the following formula was used to compute the degree of labeling:

$$\text{degree of labeling} = \left(\frac{E_{\text{Ab}}^{\text{IM}}}{E_{\text{dye}}^{\text{IM}}} \right) \left(\frac{\text{Abs}_{\text{dye}}}{\text{corrected } A_{280}} \right) \quad (1)$$

Antigen Binding Assay Based on Spectral Changes.

Because photoaffinity-labeled Abs were derivatized with fluorophores at or near the antigen-combining site, it was probable that antigen binding would alter the local environment of the fluorophore.²⁰ For this reason, anti-B Abs were photoaffinity labeled with either pyrene or dansyl, both of which are sensitive to environmental changes. A set of parallel experiments were performed with each conjugate. In brief, labeled Abs were titrated with antigen, and a fluorescence emission spectrum was recorded after each addition of antigen. Two kinds of antigens were used to characterize the spectral behavior of fluorophores conjugated to anti-B Abs. The first was biotin conjugated to goat IgG (biotin-IgG), which was used as a protein antigen analog. Biotin-IgG was prepared by adding sulfosuccinimidyl-6-(biotinamido) hexanoate (NHS-LC-biotin; Pierce) to goat IgG dissolved in CBB buffer and allowing the mixture to react for 3 h at 25 °C. The molar ratio of NHS-LC-biotin to IgG was 4:1. Biotin-IgG was purified using a PD-10 column. A degree of labeling value of ~3 (biotin molecules per IgG) was determined using the HABA reagent (Pierce).¹⁸ Underivatized biotin (Molecular Probes) was used as the second kind of antigen.

Fluorescence spectra were measured with a PC-1 photon counting spectrofluorometer (ISS, Champaign, IL). Pyrene fluorescence was excited at 340 nm (dispersion 16 nm fwhm), and emission spectra were recorded between 360 and 600 nm (dispersion 8 nm fwhm). Dansyl fluorescence was excited at 320 nm (dispersion 16 nm fwhm), and emission spectra were recorded between 480 and 580 nm (dispersion 8 nm fwhm). In each experiment, a 2×10^{-7} M concentration of the labeled anti-B Ab dissolved in PBS was titrated with aliquots of a 7×10^{-6} M solution

of biotin-IgG. Over the course of the titration, the concentration of biotin-IgG was varied between 0 and 8×10^{-7} M. The maximum concentration of biotin-IgG was 4 times greater than the anti-B Ab concentration, resulting in a 6:1 molar ratio of biotin to antigen-combining sites (on the average, each antigen molecule possessed three biotin groups). A control experiment was performed by titrating the labeled anti-B Ab with the same concentration of nonspecific goat IgG. A similar titration experiment was performed using underivatized biotin as the antigen. In this case, the concentration of biotin was varied over a range of $(0-2) \times 10^{-6}$ M. At the highest concentration, there was a 5:1 ratio of biotin to antigen-combining sites. All titrations were performed at 25 °C. After each addition of antigen, the reactants were allowed to incubate for 30 min before spectra were recorded.

Energy Transfer Immunoassay. In a typical energy-transfer immunoassay, a fluorescent "donor" molecule is conjugated to the antigen and a fluorescent "acceptor" molecule is coupled to the antibody. When an antigen-antibody complex forms, the donor and acceptor molecules may be brought close enough together (≤ 50 Å) for energy transfer to occur.²¹ Because photoaffinity labeling can be used to specifically couple fluorophores in the vicinity of the antigen-combining site, it should be an ideal method for optimizing the distance between the donor and acceptor molecules. Fluorescein and tetramethylrhodamine comprise a good energy-transfer pair. In this study, fluorescein was attached to the antigen (biotin) and tetramethylrhodamine to the antibody.

In each experiment, a 2×10^{-7} M concentration of biotin-Fl solution was titrated with aliquots of either TRM-labeled anti-B Ab (7×10^{-6} M) or TRITC-labeled anti-B Ab (7×10^{-6} M). Antibody concentration was varied over a range of $(0-2) \times 10^{-6}$ M. Control experiments were performed by using a 2×10^{-7} M concentration of fluorescein instead of the biotin-Fl conjugate. At the highest concentration of Ab, there was a 10:1 molar ratio of Ab to biotin-Fl. In energy-transfer experiments, the donor fluorophore (fluorescein) was excited directly at 480 nm (dispersion 8 nm fwhm), and emission was recorded over a range of 490–600 nm (dispersion 4 nm fwhm). Reactants were allowed to equilibrate for 30 min before spectra were recorded.

RESULTS AND DISCUSSION

Efficiency of Photoaffinity Label. The efficiency of the photoaffinity labeling technique at attaching free thiol groups in the vicinity of the antigen-combining site was evaluated using an indirect method. In brief, three different Ab preparations (see below) were exposed to a saturating amount of antigen (biotin-fluorescein), and the excess antigen was removed by gel filtration. At this point, any remaining antigen was probably bound to the antibody. The ratio of bound antigen per antibody was determined spectrophotometrically. This procedure was performed for the following three Ab preparations: (1) native anti-B Ab; (2) anti-B Ab, photoaffinity labeled with biotin-AND but not reduced with DTT; (3) anti-B Ab, photoaffinity labeled and reduced with DTT. The results of these experiments are shown in Table 1.

The antigen binding activity of the native anti-B Ab is only ~45% (each Ab has two binding sites for antigen), which is normal for chromatographically purified polyclonal Ab. When the anti-B Ab is photoaffinity labeled and the disulfide bond is cleaved by DTT, the cleavage product (biotin-thiol) should be exchangeable by an excess amount of biotin-Fl. The antigen binding activity of

(16) Kinoshita, T.; Iinuma, F.; Tsuji, A. *Anal. Biochem.* **1974**, *61*, 632–637.

(17) Wang, K.; Feramisco, J. R.; Ash, J. F. *Methods Enzymol.* **1982**, *85*, 514–562.

(18) Green, N. M. *Methods Enzymol.* **1970**, *18A*, 418.

(19) Char, K.; Gast, A. P.; Frank, C. W. *Langmuir* **1988**, *4*, 989–998.

(20) Dixon, F. J. *Advances in Immunology*; Academic Press: New York, 1988; Vol. 43, pp 99–133.

(21) Brynda, E.; Hlady, V.; Andrade, J. D. *J. Colloid Interface Sci.* **1990**, *139*, 374–380.

(22) Knopp, J. A.; Weber, G. *J. Biol. Chem.* **1969**, *244*, 6309–6315.

Table 1. Efficiency of Photoaffinity Labeling of Anti-Biotin Antibodies

parameter	label		
	native	PAL ^a + DTT	PAL ^a
photoaffinity label	—	+	+
DTT reduction	—	+	—
[bound biotin-Fl]/[IgG]	0.9 ± 0.1	0.9 ± 0.1	0.50 ± 0.05
antigen binding activity (%)	45 ± 5	45 ± 5	25 ± 2.5
labeling efficiency ^b	nd ^c	nd ^c	44 ± 6

^a PAL, Anti-B Ab was photoaffinity labeled with biotin-AND. ^b Labeling efficiency (LE) was determined using the following formula: $LE = (R_{\text{native}} - R_{\text{PAL}})/R_{\text{native}}$, where R is the ratio of bound biotin-Fl molecules per antibody. ^c nd, not determined.

DTT-treated, photoaffinity-labeled anti-B Ab is the same as that of the native anti-B Ab. This suggests that the UV irradiation and DTT reduction steps do not reduce the biotin-binding activity of the Ab or produce any cross-linking between the combining site and the antigen.

In the case of the photoaffinity-labeled antibody that was not reduced with DTT, an antigen binding activity of ~25% was observed. Since reduction with DTT is required to release the biotin-SH portion of the photoaffinity label, these results suggest that the photoaffinity labeling process was 44% effective (see Table 1). In other words, the photoaffinity label was successfully conjugated to only ~44% of the sites that could bind biotin. Because the biotin-SH portion of the label was not released, it remained bound in the antigen-combining site and prevented them from binding biotin-Fl. The other 56% of the sites that did bind biotin-Fl probably did not receive a photoaffinity label.

A control photoaffinity labeling study was performed with a heterologous (nonreactive) antigen-antibody pair. In this study, the photoaffinity label was synthesized using (Fl-AND instead of biotin and polyclonal goat anti-HSA were used instead of anti-biotin. The photoaffinity label was conjugated to anti-HSA using the same procedures described for biotin-AND and anti-B Abs, but in this case, only ~3% of the antibodies were labeled. Thus, nonspecific labeling of Abs by this procedure is very low.

Location of Extrinsic Fluorophores. In a control experiment, none of the fluorophores—pyrenemaleimide, tetramethylrhodamine, and didansylcystine—were observed to react with unmodified anti-B antibodies. Conjugation occurred only in the following two circumstances: (1) Abs were reduced with DTT or (2) Abs were photoaffinity labeled and then reduced. This indicates that these fluorophores can only be attached to reduced disulfide bonds in the hinge region (obtained through DTT reduction) or to sulfhydryl groups introduced in the vicinity of the antigen-combining sites via photoaffinity labeling (Figure 2).

Antigen-Binding Assays. *Pyrene Conjugated anti-B Ab.* Degree of labeling values of 2 and 0.4 were determined for anti-B Abs photoaffinity labeled with PM and PM-C, respectively. Furthermore, when PM was conjugated to DTT-treated anti-B Abs (without photoaffinity labeling), a degree of labeling of ~2 was observed. The fluorescence spectra of these three pyrene-labeled Abs are shown in Figure 3a–c. Very similar emission spectra were obtained for the two PM conjugates (photoaffinity labeled and DTT treated). Both spectra exhibited an emission maximum at 460 nm, which is due to the excimer peak of pyrene.¹⁸ This means that, in these conjugates, two or more pyrene groups were attached in close proximity to each other. This is because the

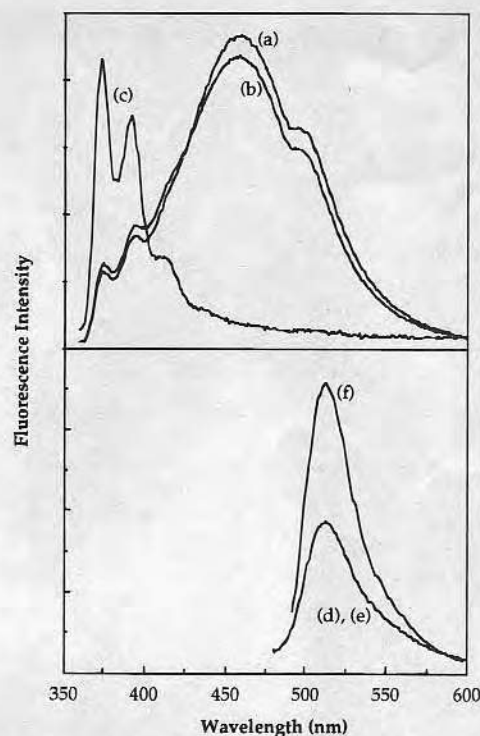


Figure 3. Fluorescence spectra of (a) PM-conjugated photoaffinity-labeled Ab, (b) PM-conjugated DTT-treated Ab, (c) PM-C-conjugated photoaffinity-labeled Ab, (d) dansylated photoaffinity-labeled Ab, (e) dansylated DTT-treated Ab, and (f) biotin-Fl. An excitation wavelength of 340 nm was used for (a–c), 320 nm was used for (d and e), and 480 nm was used for (f).

excimer peak is only observed when pyrenes are located within 4–5 Å of each other.¹⁹ In contrast, an emission maximum of 375 nm was observed for anti-B Abs photoaffinity labeled with PM-C. The observed spectrum is characteristic of the pyrene monomer.

The results of antigen binding experiments are shown in Table 2. Fluorescence intensity values for each fluorophore-anti-biotin conjugate were normalized to the value obtained in the absence of antigen. Two different kinds of antigen were investigated—free biotin and biotin₃-IgG. The former was a good model for a haptenic (low molecular weight) antigen, while the latter was analogous to a protein antigen.

Since pyrene is very sensitive to local polarity⁷ and has been used as a hydrophobic probe,¹⁴ it is important to select the right control for specific binding. Arguably, this is best accomplished by comparing the fluorescence intensity obtained for the photoaffinity-labeled antibody (labeled both near the active site and in the hinge region) with that obtained for the DTT-treated antibody (labeled only in the hinge). Making this comparison for the pyrene conjugate with the higher degree of labeling, we find that the fluorescence intensity decreased by >45% for biotin, ~31% for nonspecific IgG, and ~11% for biotin₃-IgG. Of these, probably only the decrease observed for biotin is significant, especially since the shape of the emission spectrum changed (see Figure 4).

Furthermore, a larger decrease was observed for nonspecific IgG than for biotin₃-IgG, which suggested that pyrene's fluorescence was affected by the nonspecific IgG rather than by the biotin₃-IgG. In fact, in five of the six pyrene-anti-B conjugates, an increase in fluorescence intensity was observed in the presence of nonspecific IgG (relative to that obtained in the absence of antigen). Taken together, these results suggest that pyrene groups attached to anti-B Abs can bind (probably nonspecifically)

Table 2. Normalized Fluorescence Intensity of Reporter Fluorophores Attached to Anti-Biotin Antibodies

fluorescent label location degree of labeling	pyrene maleimide hinge + active site 2	Labeling Parameters		dansyl hinge + active site 1.4	dansyl hinge 1
		pyrene maleimide hinge 2	pyrene maleimide (on Celite) hinge + active site 0.4		
antigen		normalized fluorescence intensity ^a			
none	1	1	1	1	1
biotin (10-fold excess) ^b	<0.5 ^c	0.91	0.92	0.82	0.99
nonspecific IgG (4-fold excess) ^d	0.95	1.38	1.2	1.07	1.0
biotin ₃ -IgG (4-fold excess) ^d	1.16	1.31	1.2	1.36	1.0

^a All fluorescence intensity values were normalized to those obtained for anti-biotin Abs in the absence of antigen. ^b A molar ratio of biotin to anti-biotin Ab of 10:1 was used. ^c The shape of the emission spectra changed significantly. See Figure 4. ^d A molar ratio of nonspecific IgG to anti-biotin Ab of 4:1 was used.

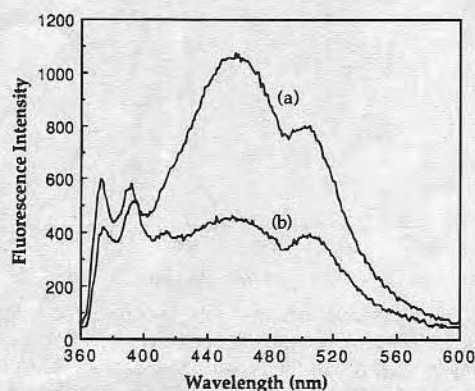


Figure 4. Fluorescence spectra of (a) PM-conjugated photoaffinity-labeled Ab without any antigen, (b) PM-conjugated photoaffinity-labeled Ab with a 10-fold molar excess of the biotin hapten.

with the goat IgG used in the antigen-binding studies. This is not surprising, considering pyrene's hydrophobic nature, but it probably means that pyrene is a poor choice for a reporter molecule.

Dansylated Anti-B Abs. Fluorescence spectra of dansylated anti-B Abs (both DTT-treated and photoaffinity labeled) are shown in Figure 3. The emission maximum was observed at 520 nm in both cases. The degree of labeling was 1.4 for photoaffinity-labeled Abs and ~1 for the DTT-treated Abs. As with pyrene-labeled Abs, binding studies were performed with free biotin, nonspecific IgG, and biotin₃-IgG. Intensity values were normalized to those obtained in the absence of antigen. The results are listed in Table 2. The fluorescence intensity of Abs photoaffinity labeled with dansyl increased by 36% when saturated with biotin₃-IgG, but decreased by 18% when saturated with biotin hapten. The fluorescence intensity in control experiments (nonspecific IgG) also increased by 7%. These results indicate that, upon binding of antigen, environmental changes occur in the vicinity of the antigen-combining site,²⁰ which lead to changes in the fluorescence spectrum of the fluorophore. In the case of biotin binding, the dansyl group experiences a more polar environment and its fluorescence is quenched. In contrast, upon binding of biotin₃-IgG, the environment becomes less polar and the fluorescence of the probe is enhanced. The difference between the two cases is probably due to the IgG molecule that is conjugated to the biotin in the second case. Upon binding of biotin₃-IgG, the reporter is buried between two proteins and experiences an environment not unlike the interior of the protein. For Abs labeled by DTT treatment alone, these antigen-induced environmental changes probably have little influence on dansyl groups coupled

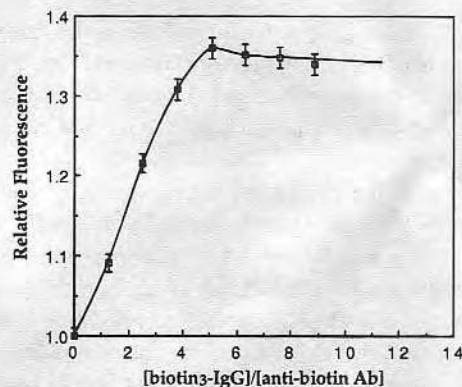


Figure 5. Normalized fluorescence intensity of dansylated photoaffinity-labeled Ab as a function of increasing concentration of biotin₃-IgG. An Ab concentration of 2×10^{-7} M was used.

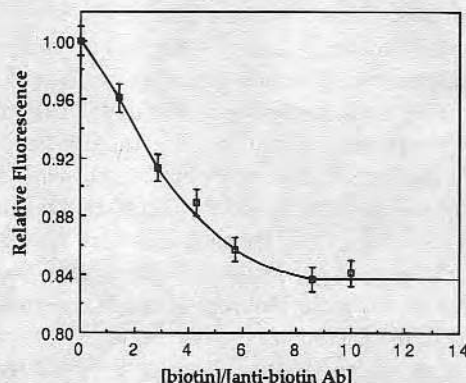


Figure 6. Normalized fluorescence intensity of dansylated photoaffinity-labeled Ab as a function of increasing concentration of the biotin hapten. An Ab concentration of 2×10^{-7} M was used.

to the hinge region, and very little perturbation of the emission spectra occurs upon binding. Figures 5 and 6 show the results of titration experiments for biotin₃-IgG and biotin, respectively. Unlike pyrene, the fluorescence spectrum of dansyl is much simpler (from Figure 3), and secondary effects such as intramolecular aminolysis²³ and excimer formation do not occur. The sensitivity of dansyl to antigen-induced environmental effects is also superior to that of pyrene. Thus, we believe that dansyl has excellent potential as a reporter molecule in direct homogeneous fluoroimmunoassays.

Tetramethylrhodamine-Conjugated Abs for Energy-Transfer Assay. Because the quantum yield of tetramethylrhodamine (TR) is

(23) Wu, C. W.; Yarbroogh, L. R.; Wu, F. Y. H. *Biochemistry* **1976**, *15*, 2863-2868.

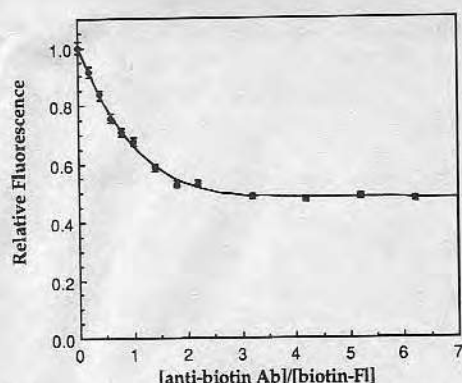


Figure 7. Normalized fluorescence intensity of biotin-Fl as a function of increasing concentration of anti-B Ab photoaffinity labeled with TRM. A biotin-Fl concentration of 2×10^{-7} M was used.

Table 3. Maximum Energy-Transfer Efficiency for Different Conjugation Methods

fluorophore	conjugation method	position of fluorophore	degree of labeling ^a	Q_{\max}^b (%)
TRM	photoaffinity	antigen-combining site + hinge	0.4	48
TRM	DTT treatment	hinge	0.5	36
TRITC	primary amine	random	0.2	30
TRITC	primary amine	random	0.7	38
TRITC	primary amine	random	0.9	39
TRITC	primary amine	random	3.7	42

^a Degree of labeling, number of dye molecules conjugated to each anti-biotin antibody. ^b Q_{\max} , maximum quenching of fluorescence observed when antigen (biotin-fluorescein) was completely saturated with anti-B antibodies. Since tetramethylrhodamine is a dark acceptor in these studies, Q_{\max} is equivalent to the maximum energy-transfer efficiency.

relatively low when conjugated to anti-B Abs, TR should really be considered a "dark acceptor" or quencher¹⁴ in this energy-transfer study. The degree of labeling of TRM when conjugated by photoaffinity labeling was ~ 0.4 , while a value of ~ 0.5 was observed for TRM coupled only by DTT treatment. For Abs randomly labeled with TRITC, degree of labeling values of 0.2, 0.7, 0.9, and 3.7 were observed for 1, 2, 4, and 6 h reaction times, respectively. Biotin-Fl was used as a fluorescence energy-transfer donor, and its fluorescence spectrum is shown in Figure 3. In this particular energy-transfer immunoassay, biotin-Fl is strongly fluorescent when free in solution, but upon binding to anti-B Ab, its excited state energy is transferred to TRM or TRITC groups attached to the Ab. Since these groups are dark acceptors, a net decrease in the fluorescence of biotin-Fl is observed upon binding. All fluorescence measurements were normalized to the intensity of free biotin-Fl. A typical quenching curve is shown in Figure 7. In this case, TRM was conjugated to the Ab by photoaffinity labeling, and a maximum of $\sim 48\%$ quenching (48% energy-transfer efficiency) was observed when biotin-Fl was saturated with anti-B Ab. This maximum quenching value (Q_{\max}) will determine the precision of the assay and should be highest for Abs labeled by the photoaffinity labeling technique. Values for Q_{\max} obtained for the different conjugation methods and degree of labeling are shown in Table 3. As expected, the highest Q_{\max} value (48%) was observed for photoaffinity labeling, while a value of 36% was observed for Abs labeled in the hinge region by the DTT treatment. For Abs randomly labeled with TRITC, Q_{\max} varied from 30% to 42% with increasing degree of labeling. Thus,

photoaffinity labeling is an effective method for optimal placement of fluorescent probes in energy-transfer studies.

It is known that the efficiency of fluorescence energy transfer is proportional to r^{-6} , where r is the distance between the donor and acceptor.²¹ If the energy-transfer acceptor (tetramethylrhodamine) is located in the vicinity of the bound antigen (biotin-Fl), the efficiency should be high (close to 100%). However, even with photoaffinity labeling, less than 50% energy-transfer efficiency was observed. This suggests that less than half of the antigen-combining sites were labeled with tetramethylrhodamine. Moreover, when anti-B Abs were labeled randomly with TRITC, most of the labels were located at sites distant from the antigen-combining site. This is why a much higher degree of labeling is required for TRITC to exhibit an energy-transfer efficiency roughly equivalent to that photoaffinity-labeled TRM (see Table 3). The same explanation can be applied to TRM attached to Abs using the DTT treatment. The fluorophore is conjugated to the hinge region, which is located at least 70 Å from the antigen-combining sites.²⁰

CONCLUSIONS

Two different fluorophores (pyrene and dansyl) were evaluated as reporter molecules in a direct homogeneous immunoassay based on anti-biotin antibodies. Although pyrene was suitable for the detection of the biotin hapten, it failed to discriminate between biotin₃-IgG (used as a model of protein antigens) and nonspecific IgG. Thus, pyrene is probably not a good candidate for a reporter molecule. Because of its hydrophobic nature, it has a tendency to bind nonspecifically to proteins.

Much better results were obtained when dansyl was used as a reporter molecule. Specific changes in its emission spectrum were observed for both the biotin hapten and biotin₃-IgG. Interestingly, its fluorescence intensity decreased by 16% upon binding the biotin hapten, but increased by 35% upon binding biotin₃-IgG. This indicates that the environment of the reporter becomes more polar upon binding the low molecular weight biotin hapten and less polar after binding the protein analog. Although this result seems contradictory at first, it can be explained by assuming that dansyl competes with biotin for the antigen-combining site. Upon binding the biotin hapten, the reporter is displaced into the surrounding media, which is more polar than the active site. However, when the reporter is displaced by biotin₃-IgG, it remains trapped at the interface of two protein molecules—an environment that probably has a low dielectric constant (and hence less solvent relaxation and fluorescence quenching of the fluorophore).

Arguably, the most effective use of the photoaffinity labeling technique was in an energy-transfer immunoassay, in which fluorescein and tetramethylrhodamine were used as the respective energy-transfer donor and acceptor molecules. In this case, fluorescein was conjugated to the biotin hapten and tetramethylrhodamine was attached to anti-biotin antibodies using photoaffinity labeling. An energy-transfer efficiency of almost 50% was observed upon binding of biotin-Fl, which indicates that the photoaffinity labeling technique attached close to half of the TRM groups at positions within energy-transfer distance (~ 54 Å, see ref 24) from the antigen-combining site. Presumably, the other 50% of the TRM groups were attached to the hinge region, which is outside of energy-transfer distance. Finally, we believe that the

(24) Zheng, T.-S. M.S. Thesis, University of Utah, Salt Lake City, UT, 1994.

concentration of the DTT (used to reduce the disulfide bond in the photoaffinity label) could be optimized to give fewer free thiol groups in the hinge region. This would increase the number of reporter groups (or energy-transfer acceptors) in the vicinity of the antigen-combining sites and improve the sensitivity of the immunoassay.

ACKNOWLEDGMENT

This work was supported in part by the Center for Biopolymers at Interfaces, University of Utah, and by AKZO Corporate

Research America, Inc. This paper is submitted by I.N.C. in partial fulfillment of the Ph.D. degree, Department of Material Science & Engineering, University of Utah.

Received for review March 15, 1994. Accepted December 19, 1994.*

AC9402539

* Abstract published in *Advance ACS Abstracts*, February 1, 1995.

Pharmacokinetic Model for Simultaneous Determination of Drug Levels in Organs and Tissues

C. N. CHEN and J. D. ANDRADE *

Abstract □ An extension of the Bischoff-Dedrick pharmacokinetic model is presented. This model is derived from basic considerations of drug distribution with physiological and anatomical meaning. The Bischoff-Dedrick model can simultaneously predict drug distribution with time in blood, organs, and tissues of pharmacological interest. The parameters are applied to a 15-kg standard dog. The experimental kinetic data of thiopental in brain, plasma, liver, lean tissue, and adipose tissue in a dog are used to demonstrate the feasibility of the model. Allowable variations in the parameters are determined. In general, the kinetics of drug distribution in blood, organs, and tissues depend on the drug dosage, lipid solubility, partition coefficients, metabolism rate, excretion rate, protein binding, route of administration, sizes of organs and tissues, and blood flow rates through organs and tissues. These factors enter the kinetic model separately and explicitly so their effects on the kinetics of drug distribution can be studied to provide valuable information for optimal therapy.

Keyphrases □ Pharmacokinetic model—proposed for simultaneous determination of drug distribution with time in blood, organs, and tissues, demonstrated with thiopental in dogs □ Distribution, drug—simultaneous determination in blood, organs, and tissues, pharmacokinetic model, demonstrated with thiopental in dogs □ Thiopental—distribution in blood, organs, and tissues, pharmacokinetic model for simultaneous determination proposed, dogs

Drug concentration in blood is measured clinically because this procedure is easier and more convenient than the sampling of other tissues or fluids. Therefore, it has been used as an index of dose scheduling for therapeutics. Conventional pharmacokinetic models (1) correlate kinetic data of drug concentration in blood by using one or several exponential terms. Each exponential term in the conventional model represents a compartment; single or multiple compartments are used to curve fit the experimental kinetic data. The coefficients and rate constants in the pharmacokinetic equations are then determined from the curve-fit parameters.

Drug concentrations in blood with time depend on the drug dosage, lipid solubility, partition coefficients, metabolism rate, excretion rate, protein binding, and route of administration. Common pharmacokinetic models put all these factors into the rate constants and coefficients of the curve-fit equations. Unless the rate constants and coefficients can be expressed as explicit functions of related factors, they cannot be predicted without experimental kinetic data.

Some cardiac drugs, *e.g.*, digitalis, or ultrashort-acting barbiturates, *e.g.*, thiopental, have rather narrow margins of safety. Their kinetic distribution in blood may not provide sufficient information for adequate therapy. Digitalis kinetics in heart muscle and thiopental kinetics in brain can provide much better information for optimal therapy than the drug levels present in blood (2-4). Furthermore, knowledge of

the drug distribution in blood, organs, and tissues may be necessary for providing optimal treatment. Conventional pharmacokinetic models cannot provide such information.

An entirely different approach to pharmacokinetic modeling was developed by Bischoff, Dedrick, and their coworkers (5-13), beginning in 1966. Their pharmacokinetic model simultaneously predicts the kinetics of drug distribution in blood, organs, and tissues of pharmacological interest. They successfully applied it to predict pharmacokinetics of thiopental (8), methotrexate (9, 12), and cytarabine (13). Bischoff and Dedrick (8) used the physiological parameters of a 70-kg standard male and a four-compartment model (blood, viscera, lean tissue, and adipose tissue) to simulate experimental kinetic data (2) of thiopental distribution in plasma, liver, lean tissue, and adipose tissue of the dog. They combined brain, heart, kidneys, liver, *etc.*, as a viscera compartment (8).

Since thiopental kinetics in the brain may provide valuable information for optimal therapy, an attempt was made to predict thiopental kinetics in the brain and, simultaneously, to predict thiopental kinetics in plasma, liver, lean tissue, and adipose tissue based on the physiological parameters of a 15-kg standard dog by using the Bischoff-Dedrick approach. The model can also be applied to study the pharmacokinetics of other drugs.

THEORETICAL

The data of Brodie *et al.* (2, 3) (Figs. 1 and 2), showing thiopental kinetics in plasma, liver, lean tissue, adipose tissue, and brain of the dog, were used to demonstrate the feasibility of the model. At least five body regions are defined: brain, liver, lean tissue, adipose tissue, and blood pool (blood volume in the capillary bed of any body region is included in that body region while the remaining blood is grouped together as another body region, called the blood pool). In mammals, blood from the GI area perfuses the liver. Thus, the GI tissues were added as another body region. Since there was little interest in the kinetics of thiopental in kidneys or heart, these and other organs were considered as another body region called viscera.

A diagram of blood circulation in the seven body regions is shown in Fig. 3. As blood flow carries the drug to the capillary bed where the drug diffuses into the tissue, each body region except the blood pool in Fig. 3 is further divided into two portions: the blood volume in the capillary bed and the tissue volume without blood. The physiological parameters of the model for a 15-kg standard dog are also shown in Fig. 3. A detailed discussion of the derivation of these parameters is presented in *Appendix I*.

Protein binding plays an important role in pharmacological effects and pharmacokinetics, since most drugs are bound to plasma proteins, especially to albumin and various tissue components (11). It is well recognized that not all macromolecules in blood or tissue are responsible for binding with the drug. Shen and Gibaldi (14) showed that the predicted thiopental concentrations in plasma and lean tissue, based on the total macromolecule content in organs and tissues, were substantially overestimated by the Bischoff-

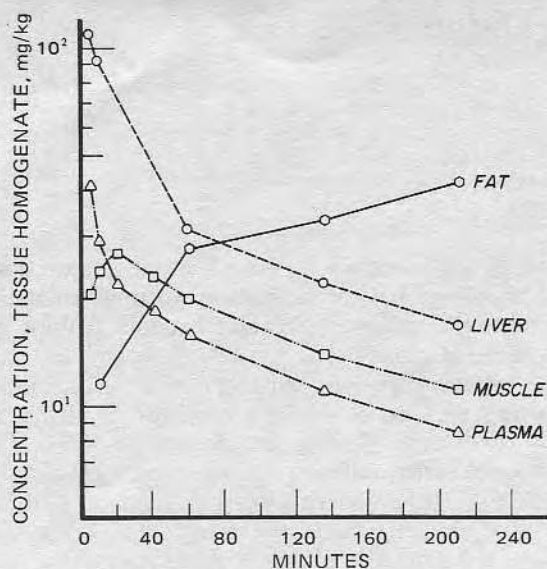


Figure 1—Experimental thiopental concentrations in various tissues of a dog after 25 mg/kg iv (redrawn from Ref. 2).

Dedrick model. Bischoff and Dedrick (7, 8) proposed the concept of effective protein fraction and applied it to their model for thiopental pharmacokinetics. In the addendum to Shen and Gibaldi's article (14), Bischoff and Dedrick favored the use of effective protein concentration rather than effective protein fraction utilizing:

$$C_T = F_W C + C_M X \quad (\text{Eq. 1})$$

where the total drug concentration (C_T) in blood or tissue is defined in terms of the volume fraction of water (F_W), free drug concentration (C), effective binding macromolecule concentration (C_M), and bound drug "concentration" (X , the amount of bound drug per unit of effective binding macromolecules). This approach obviates assuming unit densities, and there is no need for the two coefficients to be fractions that add up to unity.

Volume fractions of water in blood, organs, and tissues are available in the literature and in biological data handbooks. Table I lists calculated and reported values for volume fractions of water in organs and tissues of the dog. The volume fraction of water in the tissue portion of any body region can be calculated by:

$$V_{YzB} F_{W,B} + V_{YzT} F_{W,YzT} = (V_{YzB} + V_{YzT}) F_{W,Yz} \quad (\text{Eq. 2})$$

where:

- $F_{W,B}$ = volume fraction of water in blood
- $F_{W,YzT}$ = volume fraction of water in tissue portion of Yz body region
- $F_{W,Yz}$ = volume fraction of water in Yz body region
- V_{YzB} = blood volume in Yz body region
- V_{YzT} = tissue volume in Yz body region

The effective binding macromolecule concentration (C_M) in blood or tissue can be determined in terms of the fraction of bound drug (F) and the equilibrium relation between free and bound drug in blood or tissue. A detailed discussion of how effective binding macromolecule concentrations in blood and tissues were derived is presented in Appendix II.

The physical picture of dynamic drug distribution at any instant in any body region is as follows. The inflow drug (free and bound) mixes with the drug in the capillary bed and the mixed drug (free drug only) in the capillary bed then diffuses into the tissue. Both the changing free drug concentrations in blood water and tissue water disturb and then reestablish the equilibrium relations between free and bound drug in the capillary bed and the tissue. When a well-mixed state in the capillary bed is assumed, the outflow drug concentration (free and bound) from the body region is the same as that reestablished in the capillary bed.

For highly lipid-soluble drugs, the rate of mass transfer between blood in the capillary bed and tissue is so fast that, at any instant, the free drug concentration in tissue water effectively equals that

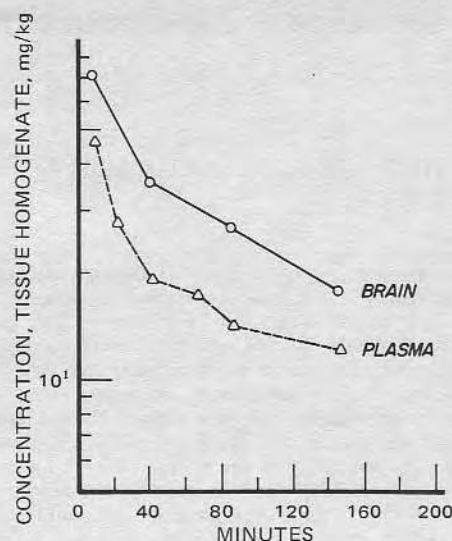


Figure 2—Experimental thiopental concentrations in plasma and brain of a dog after 40 mg/kg iv (redrawn from Ref. 3).

in blood water. This condition was called the "flow-limiting condition" by Dedrick and Bischoff (7), who discussed mathematical details of the condition and found that highly lipid-soluble compounds, such as thiopental and aniline, approximate the condition.

The transient mass balance for any body region can be expressed as:

$$\left[\begin{array}{l} \text{accumulation rate of free} \\ \text{drug and bound drug in} \\ \text{both capillary bed and} \\ \text{tissue portion} \end{array} \right] = \left[\begin{array}{l} \text{inflow rate of free drug} \\ \text{and bound drug from} \\ \text{blood pool and/or other} \\ \text{body regions} \end{array} \right] + [\text{drug injection rate, if any}] - [\text{outflow rate of free drug and bound drug from body region}] - [\text{metabolism rate and/or excretion rate of drug, if any}] \quad (\text{Eq. 3})$$

The mathematical equation of transient mass balance for body region Y (Fig. 4) is:

$$(F_{W,B} V_{YB} + F_{W,YT} V_{YT}) \frac{dC_Y}{dt} + (C_{M,B} V_{YB}) \frac{dX_{YB}}{dt} + (C_{M,YT} V_{YT}) \frac{dX_{YT}}{dt} = Q_Y (F_{W,B} C_B + C_{M,B} X_B) - Q_Y (F_{W,B} C_Y + C_{M,B} X_{YB}) \quad (\text{Eq. 4})$$

where:

$$C_{M,B} = F_{Pl,B} C_{M,Pl} + (1 - F_{Pl,B}) C_{M,RBC}$$

and:

- C_B = free drug concentration in blood water from the blood pool (micromoles per liter)
- C_Y = free drug concentration in blood water or tissue water of body region Y (micromoles per liter)
- $C_{M,B}$ = effective binding macromolecule concentration in blood (kilograms per liter)
- $C_{M,Pl}$ = effective binding macromolecule concentration in plasma (kilograms per liter)
- $C_{M,RBC}$ = effective binding macromolecule concentration in red blood cells (kilograms per liter)
- $C_{M,YT}$ = effective binding macromolecule concentration in tissue portion of body region Y (kilograms per liter)
- $F_{W,B}$ = volume fraction of water in blood
- $F_{W,YT}$ = volume fraction of water in tissue portion of body region Y

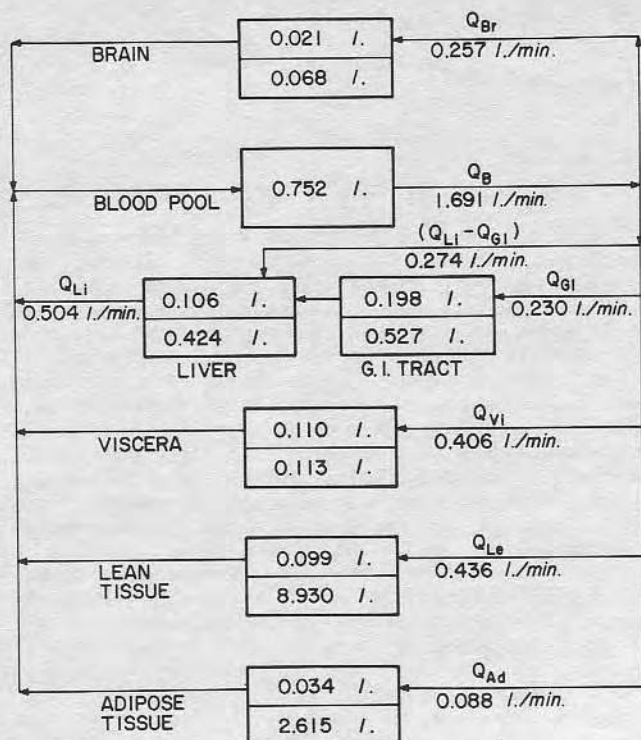


Figure 3—Body regions and blood flow of a 15-kg dog.

- $F_{Pl,B}$ = volume fraction of plasma in blood
 Q_Y = volumetric blood flow rate from body region Y (liters per minute)
 t = time (minutes)
 V_{YB} = blood volume in capillary bed of body region Y (liters)
 V_{YT} = volume of tissue portion of body region Y (liters)
 X_B = bound drug concentration (amount of bound drug per unit of effective binding macromolecules) from the blood pool (micromoles per kilogram)
 X_{YB} = bound drug concentration in capillary bed of body region Y (micromoles per kilogram)
 X_{YT} = bound drug concentration in tissue portion of body region Y (micromoles per kilogram)

The first term on the left-hand side of Eq. 4 represents the accumulation rate of free drug in both blood water and tissue water. The second and third terms indicate accumulation rates of bound drug in the capillary bed and in the tissue portion, respectively. The first term on the right-hand side of Eq. 4 represents the inflow rate of free drug and bound drug from the blood pool, and the sec-

Table I—Calculated and Reported Values for Volume Fractions of Water in Organs and Tissues of the Dog

Tissue (Yz)	$F_{W,Yz}^a$	$F_{W,YzT}^b$
Whole blood	0.800 ^c	—
Plasma	0.930 ^c	—
Red blood cells	0.640 ^c	—
Whole brain	0.795 ^c	0.794
Liver	0.746 ^c	0.733
Intestines	0.757 ^c	0.741
Heart	0.783 ^c	0.775
Kidneys	0.802 ^c	0.807
Viscera	0.791 ^d	0.782
Lean tissue	0.776 ^c	0.776
Adipose tissue	0.200 ^e	0.192

^a Reported values for volume fractions of water in various tissues.
^b Calculated values for volume fractions of water in tissue portions of various tissues. ^c P. L. Altman and D. S. Dittmer, "Biology Data Book," vol. 1, 2nd ed., Federation of American Societies for Experimental Biology, Bethesda, Md., 1972, pp. 19, 393, 394. ^d The value for volume fraction of water in viscera was calculated from heart and kidneys. ^e C. H. Best and N. B. Taylor, "The Living Body," 4th ed., Holt, Rinehart and Winston, New York, N.Y., 1966, p. 55.

ond term indicates the outflow rate of free drug and bound drug from body region Y (Fig. 4).

Similarly, the transient mass balance was applied for each body region shown in Fig. 3. The goal was to predict thiopental kinetics in plasma. The blood was divided into plasma and red blood cells, using a hematocrit value of 45% (volume). The concept of effective binding macromolecule concentration in blood and various tissues (Appendix II) and the flow-limiting condition are applied to the following mathematical model.

For the blood pool:

$$F_{Pl,B} = 0.55 \quad (\text{Eq. 5})$$

$$C_{M,B} = F_{Pl,B}C_{M,Pl} + (1 - F_{Pl,B})C_{M,RBC} \quad (\text{Eq. 6})$$

The transient mass balance for the blood pool (Figs. 3 and 4) is:

$$\begin{aligned} & (F_{W,B}V_B) \frac{dC_B}{dt} + (C_{M,B}V_B) \frac{dX_B}{dt} \\ & \left[\text{accumulation rate of free drug in blood pool} \right] + \left[\text{accumulation rate of bound drug in blood pool} \right] \\ & = Q_{Br}(F_{W,B}C_{Br} + C_{M,B}X_{Br}) + Q_{Li}(F_{W,B}C_{Li} + C_{M,B}X_{LiB}) \\ & + Q_{Vi}(F_{W,B}C_{Vi} + C_{M,B}X_{ViB}) + Q_{Le}(F_{W,B}C_{Le} + C_{M,B}X_{LeB}) \\ & + Q_{Ad}(F_{W,B}C_{Ad} + C_{M,B}X_{AdB}) + Mg(t) \\ & \left[\text{summation of inflow rates of free and bound drug from five body regions} \right] + \left[\text{injection term} \right] \\ & - Q_B(F_{W,B}C_B + C_{M,B}X_B) \\ & \left[\text{outflow rate of free and bound drug from blood pool} \right] \end{aligned} \quad (\text{Eq. 7})$$

The particular symbols are defined under *Notation*.

The term $Mg(t)$ is the injection term, where M is the total amount of the drug injected and $g(t)$ is a normalized injection function (7, 8):

$$g(t) = 30\lambda(\lambda t)^2(1 - \lambda t)^2 \quad (\text{Eq. 8})$$

where λ is the reciprocal of the injection duration. The term $Mg(t)$ simulates a smooth injection and is convenient for computation (7, 8). Note that:

$$\int_0^{1/\lambda} g(t) dt = 1 \quad (\text{Eq. 9})$$

A similar mass balance for the liver (Li) gives:

$$\begin{aligned} & (F_{W,B}V_{LiB} + F_{W,LiT}V_{LiT}) \frac{dC_{Li}}{dt} + \\ & \left[\text{accumulation rates of free drug in capillary bed and tissue portion of liver} \right] \\ & (C_{M,B}V_{LiB}) \frac{dX_{LiB}}{dt} + C_{M,LiT}V_{LiT} \frac{dX_{LiT}}{dt} \\ & \left[\text{accumulation rates of bound drug in capillary bed and tissue portion of liver} \right] \\ & = (Q_{Li} - Q_{GI})(F_{W,B}C_B + C_{M,B}X_B) + Q_{GI}(F_{W,B}C_{GI} + C_{M,B}X_{GIB}) \\ & \left[\text{inflow rates of free and bound drug from blood pool} \right] + \left[\text{inflow rates of free and bound drug from GI area} \right] \\ & - Q_{Li}(F_{W,B}C_{Li} + C_{M,B}X_{LiB}) - R_{Li}(C_{Li}) \\ & \left[\text{outflow rate of free and bound drug from liver} \right] + \left[\text{metabolism rate of drug} \right] \end{aligned} \quad (\text{Eq. 10})$$

The metabolism rate (7, 8) is written in the simple Michaelis-Menten form:

$$R_{Li}(C_{Li}) = \frac{k_{Li}C_{Li}}{k_{M,Li} + C_{Li}} \quad (\text{Eq. 11})$$

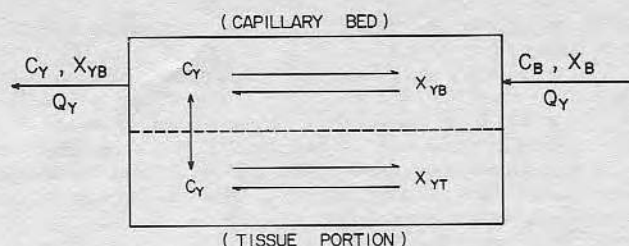


Figure 4—Diagram of transient mass balance for the body region Y under the assumptions of a well-mixed state in the capillary bed and flow-limiting condition for highly lipid-soluble drugs.

Since the metabolism mainly occurs in the liver, all metabolism of thiopental is assumed to occur in the liver. In general, similar terms could be added to other body regions if necessary. Mark (15) reported a value for the overall metabolism rate of thiopental as 15%/hr. The parameters (k_{Li} and $k_{M,Li}$) in Eq. 11 were empirically adjusted to provide values of $k_{Li} = 5.68$ μ moles/min and $k_{M,Li} = 4.0$ μ moles/liter for a 15-kg standard dog. The remaining mass balances have similar forms.

For the brain (Br) region:

$$(F_{W,B}V_{BrB} + F_{W,BrT}V_{BrT})\frac{dC_{Br}}{dt} + (C_{M,B}V_{BrB})\frac{dX_{BrB}}{dt} + (C_{M,BrT}V_{BrT})\frac{dX_{BrT}}{dt} = Q_{Br}(F_{W,B}C_B + C_{M,B}X_B - F_{W,Br}C_{Br} - C_{M,B}X_{BrB}) \quad (\text{Eq. 12})$$

For the viscera (Vi) region:

$$(F_{W,B}V_{ViB} + F_{W,ViT}V_{ViT})\frac{dC_{Vi}}{dt} + (C_{M,B}V_{ViB})\frac{dX_{ViB}}{dt} + (C_{M,ViT}V_{ViT})\frac{dX_{ViT}}{dt} = Q_{Vi}(F_{W,B}C_B + C_{M,B}X_B - F_{W,Vi}C_{Vi} - C_{M,B}X_{ViB}) \quad (\text{Eq. 13})$$

For the GI (GI) tissue region:

$$(F_{W,B}V_{GIB} + F_{W,GIT}V_{GIT})\frac{dC_{GI}}{dt} + (C_{M,B}V_{GIB})\frac{dX_{GIB}}{dt} + (C_{M,GIT}V_{GIT})\frac{dX_{GIT}}{dt} = Q_{GI}(F_{W,B}C_B + C_{M,B}X_B - F_{W,GI}C_{GI} - C_{M,B}X_{GIB}) \quad (\text{Eq. 14})$$

For the lean tissue (Le) region:

$$(F_{W,B}V_{LeB} + F_{W,LeT}V_{LeT})\frac{dC_{Le}}{dt} + (C_{M,B}V_{LeB})\frac{dX_{LeB}}{dt} + (C_{M,LeT}V_{LeT})\frac{dX_{LeT}}{dt} = Q_{Le}(F_{W,B}C_B + C_{M,B}X_B - F_{W,Le}C_{Le} - C_{M,B}X_{LeB}) \quad (\text{Eq. 15})$$

For the adipose tissue (Ad) region:

$$(F_{W,B}V_{AdB} + F_{W,AdT}V_{AdT})\frac{dC_{Ad}}{dt} + (C_{M,B}V_{AdB})\frac{dX_{AdB}}{dt} + (C_{M,AdT}V_{AdT})\frac{dX_{AdT}}{dt} = Q_{Ad}(F_{W,B}C_B + C_{M,B}X_B - F_{W,Ad}C_{Ad} - C_{M,B}X_{AdB}) \quad (\text{Eq. 16})$$

Adipose tissue must be handled somewhat differently (Appendix II). It is worth noting that free drug concentrations and bound drug concentrations in all body regions (Fig. 3) are involved in Eq. 7, while the free drug concentration and bound drug concentration in the blood pool appear in all equations. Thus, each equation is not independent but interrelated to the others, constituting a set of simultaneous differential equations. There are 20 unknown variables (seven free drug concentrations in blood water or tissue water of the seven body regions and 13 bound drug concentrations in the capillary beds and tissue portions of the seven body regions) in Eqs. 7, 10, and 12–16. Seven equations can serve to solve only seven variables. Therefore, to solve the seven simultaneous equations, 13 remaining variables should be correlated to the seven selected variables by certain relationships.

Equilibrium relationships between free drug concentrations and bound drug concentrations in blood, organs, and tissues can be determined experimentally and provide the 13 relationships to solve the seven simultaneous differential equations. Actually, the equilibrium relationships between free and bound drug in the capillary beds of all body regions are the same. Hence, only seven equilibrium relations (one in the blood and six in the tissue portions of six body regions) are required.

Any equilibrium relation between free and bound drug in blood and various tissues can be determined by a general form of Langmuir adsorption (16, 17):

$$r = \sum_{i=1}^n \frac{N_i K_i C}{1 + K_i C} \quad (\text{Eq. 17})$$

where:

- r = moles of bound drug per mole of binding macromolecule (moles per mole)
- C = free drug concentration (micromoles per liter)
- N_i = average number of type i binding sites per molecule of binding macromolecule (moles per mole)
- K_i = intrinsic association constant of type i binding site (liters per micromole)

Goldbaum and Smith (18) measured the binding of several barbiturates in 1% bovine serum albumin at drug levels of pharmacological interest. They correlated the observed data with the form of Langmuir adsorption for two types of binding sites:

$$r = \frac{N_1 K_1 C}{1 + K_1 C} + \frac{N_2 K_2 C}{1 + K_2 C} \quad (\text{Eq. 18})$$

Bound drug concentration (X , micromoles of bound drug per kilogram of effective binding macromolecule) can be related to r , to be

Table II—Parameter Values for Kinetic Model of Thiopental in a 15-kg Dog

Parameter	Numerical Values
Effective binding macromolecule concentration ^a , kg/liter	$C_{M,Pl} = 0.0146$, $C_{M,RBC} = 0.0152$, $C_{M,B} = 0.0149$, $C_{M,BrT} = 0.0233$, $C_{M,LiT} = 0.0408$, $C_{M,GIT} = 0.0331$, $C_{M,ViT} = 0.0409$, $C_{M,LeT} = 0.0222$, $C_{M,AdT} = 0.8700$
Binding site constants (7, 8), μ moles/kg	$B_1 = 18,400$, $B_2 = 305,000$
Intrinsic association constant (7, 8), liters/ μ mole	$K_1 = 0.060$, $K_2 = 0.000625$
Lipid solubility constant (7, 8)	$B_A = 100$
Injection parameter ^b	$M = 1420.45$ μ moles, $\lambda = 0.20$ min ⁻¹
Metabolism constant ^b	$k_{Li} = 5.68$ μ moles/min, $k_{M,Li} = 4.0$ μ moles/liter

^a For detailed calculation, see Appendix II. ^b The values were modified from Refs. 7 and 8 to suit the condition of 25 mg of thiopental/kg for a 15-kg dog.

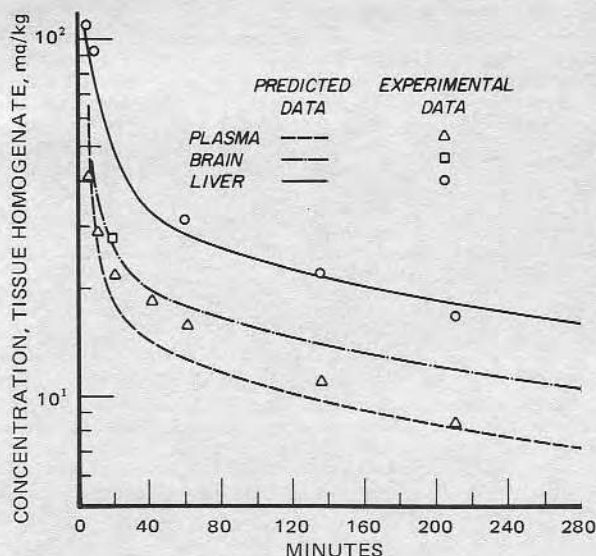


Figure 5—Predicted and experimental thiopental concentrations in plasma, brain, and liver following 25 mg/kg iv.

defined in terms of free drug concentration (C):

$$X = \frac{10^9}{M_P}(r) = \frac{B_1 K_1 C}{1 + K_1 C} + \frac{B_2 K_2 C}{1 + K_2 C} \quad (\text{Eq. 19})$$

where:

$$Bi = \frac{10^9}{M_P}(Ni)$$

where M_P = molecular weight of binding macromolecule; 68,000 was assumed for the albumin to calculate constant Bi shown in Table II.

Since no other equilibrium relationships are available, Eq. 19 with the constants in Table II was assumed to represent the equilibrium relation in blood, organs, and tissues as an approximation and was used to solve the simultaneous Eqs. 7, 10, and 12-16. This approximation is reasonable if the equilibrium relationships between free drug concentrations and bound drug concentrations in blood and various tissues of the dog have similar curve shapes to those measured in 1% bovine serum albumin by Goldbaum and Smith (18). It is assumed that the fractions of bound drug (thiopental) in blood, organs, and tissues of the dog are similar to those of the rabbit, which are available (18) and are used to calculate effective binding macromolecule concentrations (Appendix II). How close must they be for a reasonable approximation will be discussed later.

One may wonder whether the equilibria between free and bound drug in the body regions can be established so quickly that the equilibrium relationships can be applied to the equations of transient mass balances for the various body regions. Colowick and Womack (19), in their studies on binding of diffusible molecules by macromolecules, pointed out that the usual chemical equilibrium for the binding reaction can be reached quickly, suggesting that the equilibrium relationships between free and bound drug in blood and tissues can be applied to the equations of transient mass balances.

The term for the excretion rate is included in the general treatment (20). Since the excretion of unchanged thiopental is negligible (21), the term is omitted in this treatment.

RESULTS AND DISCUSSION

Analytical solutions of the simultaneous differential equations were not feasible because of nonlinearities caused by the binding terms. Therefore, Eqs. 7, 10, and 12-16 were solved by numerical methods (20). The numerical results for the dosage of 25 mg of thiopental/kg are presented in Figs. 5 and 6. The predicted kinetics in plasma and several organs and tissues of interest agree well with the experimental data (2).

The same mathematical model used to develop Eqs. 7, 10, and

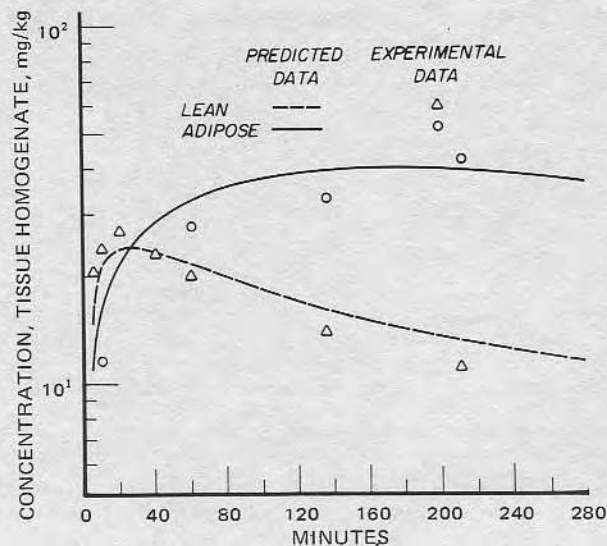


Figure 6—Predicted and experimental thiopental concentrations in lean and adipose tissues following 25 mg/kg iv.

12-16 was applied to predict the thiopental distribution in plasma and brain (3) shown in Fig. 2 by modifying some of the parameters in Table II to meet the new conditions. Because 40 mg of thiopental/kg was intravenously injected, the total amount of thiopental injected to a 15-kg dog was 2272.72 instead of 1420.45 μ moles and the injection duration was 8 min so that $\lambda = 0.125 \text{ min}^{-1}$. The predicted kinetics in plasma and brain also agree well with the experimental data (Fig. 7).

Mathematical Model Testing—This mathematical model involves many parameters that must be known to certain degrees of accuracy. If the model is stable enough, some reasonable variations of the parameters should not appreciably change the results. Physiological parameters in Table I and Fig. 3 are statistical average values, which may be close to true values. Biochemical parameters in Table II are determined from experiment and are expected to deviate from true values. Because the true values for all parameters are unknown, the values for all parameters in Tables I and II and Fig. 3 were assumed to be standard values. The stability of the model was tested by comparing the numerical results from standard values for all parameters with those from a variation of $\pm 10\%$ of standard value for each of the following parameters:

1. $\pm 10\%$ variation of the volume of any body region
2. $\pm 10\%$ variation of the volume and the blood flow rate of any body region

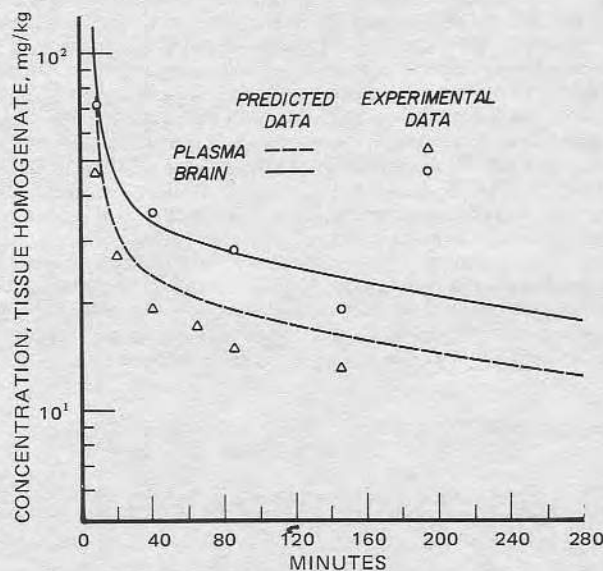


Figure 7—Predicted and experimental thiopental concentrations in plasma and brain following 40 mg/kg iv.

Table III—Volumes and Blood Supplies of Different Body Regions for a 15-kg Standard Dog

Tissue	Total Tissue Volume (Including Blood), liters	Tissue Volume (Excluding Blood ^a), liters	Blood Volume in Capillary Bed, liters	Blood Flow Rate, liters/min
Brain	0.089 ^b	0.068	0.021 ^c	0.257 ^d
Liver	0.530 ^b	0.424	0.106 ^e	0.504 ^f
Adrenals	0.002 ^b	0.001	0.001 ^c	0.034 ^d
Kidneys	0.090 ^b	0.025	0.065 ^c	0.264 ^f
Thyroid	0.003 ^b	0.001	0.002 ^c	0.027 ^d
Heart	0.128 ^b	0.086	0.042 ^c	0.081 ^d
GI	0.725 ^b	0.527	0.198 ^e	0.230 ^g
Lean tissue	9.029 ^h	8.930	0.099 ^f	0.436 ^d
Fatty marrow	0.480 ⁱ	0.472	0.008 ^c	0.020 ^d
Fat	2.169 ⁱ	2.143	0.026 ^c	0.068 ^d

^a Calculated from total tissue volume minus blood volume in the capillary bed. ^b W. S. Spector, "Handbook of Biological Data," Saunders, Philadelphia, Pa., 1956, pp. 163, 283. ^c Calculated under the assumption that dogs and humans have the same ratio of blood volume in capillary bed to tissue volume without blood. ^d Calculated under the assumption that blood flow rate in certain tissues or organs have the same percentages of blood flow rate from the blood pool as that of standard man. ^e E. E. Selkurt, "Physiology," 2nd ed., Little, Brown, Boston, Mass., 1966, pp. 391–393. ^f D. S. Dittmer and R. M. Grebe, "Handbook of Circulation," Saunders, Philadelphia, Pa., 1959, pp. 71, 127, 129. ^g J. P. Delaney and J. Custer, *Circ. Res.*, 17, 394(1965). ^h Calculated under the assumption of 60.2% of body weight. ⁱ Calculated under the assumption that dogs and humans have the same percentage of body weight for the corresponding tissues.

3. $\pm 10\%$ variation of the value for each volume fraction of water in any body region

4. $\pm 10\%$ variation of the lipid solubility constant, B_A

5. $\pm 10\%$ variation of the metabolism constant, k_{Li}

6. $\pm 10\%$ variation of the binding site constants, B_i

7. $\pm 10\%$ and $\pm 5\%$ variation of the fractional data of bound drug in various tissues

The data (20) show that $\pm 10\%$ variation in each parameter, except fractional data of bound drug in various tissues, can be tolerated without significantly affecting the results. This finding verifies that the model is quite stable, allowing at least $\pm 10\%$ variations in all parameters but fractional data of bound drug where a $\pm 5\%$ variation is acceptable. This indicates that the values for fractions of bound drug in blood, organs, and tissues are more sensitive parameters than the others in the model and, therefore, must be determined more accurately.

Conclusions—Thiopental kinetics in brain are very important for anesthetic studies. The model not only predicts thiopental distribution in blood but also simultaneously provides thiopental kinetics in brain and other organs. Conventional pharmacokinetic models can never achieve this feature. One important feature of the model is that each equation is not independent but interrelated to the others.

One potential application is that if the model can be verified for a given drug in a species pharmacokinetically similar to humans, it can then be applied to predict human pharmacokinetics by making certain modifications in physiological and biochemical parameters. The experimentally observed drug distribution in plasma or blood can be used to compare with the corresponding kinetics predicted by the model. If they agree well, the predicted drug distribution in the other body regions that are difficult to sample may be expected to follow corresponding kinetic courses with confidence, even if they cannot be verified experimentally. Therefore, the model can provide valuable information for optimal therapeutic regimens.

Another potential application of the model is that the pharmacokinetics of some critical substances such as uric acid, creatinine, and urea in patients suffering from renal failure or of exogenous poisons in acutely intoxicated patients can be analyzed with respect to extracorporeal device treatments. In such cases, the extracorporeal device adds one more equation to the model system, and certain physiological parameters such as blood flow rates through organs and tissues must be modified. This type of analysis could lead to more optimal extracorporeal device treatment (20).

APPENDIX I: DETAILS OF PHYSIOLOGICAL PARAMETERS

The viscera body region shown in Fig. 3 includes kidneys, thyroid, heart, and adrenals; the adipose tissue body region contains fatty marrow and fat. The blood volume of the blood pool is from total blood volume (1.320 liters) minus the sum of the blood volumes of the other six body regions shown in Fig. 3. The blood flow rate from the blood pool is the sum of the blood flow rates from the

other five body regions (excluding blood flow rate from the GI area) (Table III).

APPENDIX II

The effective binding macromolecule concentrations¹ (7, 14) in various tissues can be derived as follows. If there are D μ moles of drug contained in tissue homogenate of Yz body region with W liters of water (tissue water and blood water in the tissue homogenate) and P kg effective binding macromolecules out of total macromolecules in the tissue, the following relation can be established:

$$D = WC + PX \quad (\text{Eq. A1})$$

where C is free drug concentration in blood water or tissue water (micromoles per liter), and X is bound drug concentration (the amount of bound drug per unit of effective binding macromolecules) in the tissue (micromoles per kilogram). The fraction of bound drug in the tissue homogenate, F , is defined as $F = PX/D$. Substituting this into Eq. A1 gives:

$$D = (1 - F)D + PX \quad (\text{Eq. A2})$$

When Eq. A2 is divided by the total volume of the tissue homogenate, it becomes:

$$C_T = (1 - F)C_T + C_{M,Yz}X \quad (\text{Eq. A3})$$

where C_T is the total drug concentration, and $C_{M,Yz}$ is the effective binding macromolecule concentration of Yz tissue homogenate. This relationship can be further simplified:

$$C_{M,Yz} = \frac{FC_T}{X} \quad (\text{Eq. A4})$$

Substituting Eq. 19 into Eq. A4 gives:

$$C_{M,Yz} = FC_T \left(\frac{B_1 K_1 C}{1 + K_1 C} + \frac{B_2 K_2 C}{1 + K_2 C} \right) \quad (\text{Eq. A5})$$

The effective binding macromolecule concentration in any tissue homogenate (Table IV) can be calculated by using Eq. A5 if the fraction of bound drug (F) in a certain total drug concentration (C_T) and the equilibrium relationship between the free drug concentration and bound drug concentration in the tissue homogenate are known.

The effective binding macromolecule concentration in the tissue portion (Table IV) can be calculated by the following equations,

¹ K. B. Bischoff, School of Chemical Engineering, Cornell University, Ithaca, NY 14850, and R. L. Dedrick, Biomedical Engineering and Instrumentation Branch, National Institutes of Health, Bethesda, MD 20014, personal communication

Table IV—Binding Parameters of Thiopental in Various Organs and Tissues of the Rabbit

Parameter	Liver	Heart	Kidneys	Brain	Lean Tissue	Red Blood Cells	Plasma, Undiluted	Viscera ^a	GI Tissue ^a
F^b	0.66	0.62	0.53	0.50	0.45	0.40	0.85	0.58	—
$C_{M,Yz}^c$	0.0356	0.0313	0.0235	0.0213	0.0221	0.0152	0.0146	0.0281	0.0281
$C_{M,YzT}^c$	0.0408	0.0393	0.0459	0.0233	0.0222	—	—	0.0409	0.0331

^aData shown were calculated by the method discussed in Appendix II. ^bFractions of bound drug in organs and tissues except plasma were determined from tissue homogenate diluted to five volumes (18). ^c $C_{M,Yz}$ and $C_{M,YzT}$ are the effective binding macromolecule concentrations, which have been multiplied by five (dilution factor), in tissue homogenate and in the tissue portion, respectively. The values shown were calculated by the method discussed in Appendix II.

taking the liver as an example:

$$C_{M,B} = F_{Pl,B} C_{M,Pl} + (1 - F_{Pl,B}) C_{M,RBC} \quad (\text{Eq. A6})$$

$$\frac{V_{LiB}}{V_{LiB} + V_{LiT}} C_{M,B} + \frac{V_{LiT}}{V_{LiB} + V_{LiT}} C_{M,LiT} = C_{M,Li} \quad (\text{Eq. A7})$$

The viscera body region consists of kidneys, heart, thyroid, and adrenals. Since the volume fraction of the thyroid and adrenals in the viscera is negligible and their fractional bound thiopental data are not available, effective binding macromolecule concentrations in kidneys (Ki) and heart (He) (Table IV) were used to calculate the effective binding macromolecule concentration in the viscera by the following equation:

$$C_{M,Vi} = \frac{V_{Ki} C_{M,Ki} + V_{He} C_{M,He}}{V_{Ki} + V_{He}} \quad (\text{Eq. A8})$$

Fractional bound drug data are not available for GI tissue, so its effective binding macromolecule concentration was not calculated. Therefore, the value of the effective binding macromolecule concentration in the viscera was assigned to the GI tissue. The effective binding macromolecule concentration in the GI tissue portion was then determined.

The tissue binding in adipose tissue¹ is somewhat different from that in other tissues and must be handled differently. The equilibrium relationship between free and bound drug in the capillary bed of adipose tissue is the same as Eq. 19:

$$X_{AdB} = C_{Ad} \left(\frac{B_1 K_1}{1 + K_1 C_{Ad}} + \frac{B_2 K_2}{1 + K_2 C_{Ad}} \right) \quad (\text{Eq. A9})$$

Total drug concentration in the capillary bed of adipose tissue, $C_{T,AdB}$, is defined as:

$$C_{T,AdB} = F_{W,B} C_{Ad} + C_{M,B} X_{AdB} \quad (\text{Eq. A10})$$

Substituting Eq. A9 into Eq. A10 gives:

$$C_{T,AdB} = C_{Ad} \left[F_{W,B} + C_{M,B} \left(\frac{B_1 K_1}{1 + K_1 C_{Ad}} + \frac{B_2 K_2}{1 + K_2 C_{Ad}} \right) \right] \quad (\text{Eq. A11})$$

The tissue "binding" by adipose tissue is primarily the lipid solubility for which a simple linear Henry's law solubility relationship can be used (7, 8). Thus, drug concentration in adipose tissue (X_{AdT}) is proportional to free drug concentration (C_{Ad}) in tissue water:

$$X_{AdT} = B_A C_{Ad} \quad (\text{Eq. A12})$$

Total drug concentration in adipose tissue portion ($C_{T,AdT}$) is defined as:

$$C_{T,AdT} = F_{W,AdT} C_{Ad} + C_{M,AdT} X_{AdT} \quad (\text{Eq. A13})$$

When Eq. A12 is substituted into Eq. A13, Eq. A13 becomes:

$$C_{T,AdT} = C_{Ad} (F_{W,AdT} + C_{M,AdT} B_A) \quad (\text{Eq. A14})$$

The partition coefficient of adipose tissue (K_{Ad}) is defined as the ratio of total drug concentration in adipose tissue to that in its blood:

$$K_{Ad} = \frac{C_{T,AdT}}{C_{T,AdB}} = \frac{F_{W,AdT} + C_{M,AdT} B_A}{F_{W,B} + C_{M,B} \left(\frac{B_1 K_1}{1 + K_1 C_{Ad}} + \frac{B_2 K_2}{1 + K_2 C_{Ad}} \right)} \quad (\text{Eq. A15})$$

Since¹ $K_{Ad} = 15$ and $B_A = 100$, at $C_{Ad} = 100$ ($\mu\text{moles/liter}$), $C_{M,AdT}$, which can be solved by Eq. A15, is 0.870.

NOTATION

- C_{Yz} = free drug concentration in tissue water or blood water of Yz body region (micromoles per liter)
 $C_{M,Yz}$ = effective binding macromolecule concentration in Yz body region (kilograms per liter)
 $C_{M,YzT}$ = effective binding macromolecule concentration in tissue portion of Yz body region (kilograms per liter)
 $F_{W,B}$ = volume fraction of water in blood
 $F_{W,YzT}$ = volume fraction of water in tissue portion of Yz body region
 Q_B = blood flow rate from blood pool (liters per minute)
 Q_{Yz} = blood flow rate from Yz body region (liters per minute)
 V_{YzB} = blood volume within capillary bed of Yz body region (liters)
 V_{YzT} = volume of tissue portion of Yz body region (liters)
 X_{YzB} = bound drug concentration (amount of bound drug per unit of effective binding macromolecules) in capillary bed of Yz body region (micromoles per kilogram)
 X_{YzT} = bound drug concentration (amount of bound drug per unit of effective binding macromolecules) in tissue portion of Yz body region (micromoles per kilogram)
Yz = various body regions and tissues

REFERENCES

- (1) A. Rescigno and G. Segre, "Drug and Tracer Kinetics," 1st American ed., Blaisdell, Lexington, Mass., 1966.
- (2) B. B. Brodie, E. Bernstein, and L. C. Mark, *J. Pharmacol. Exp. Ther.*, **105**, 421(1952).
- (3) B. B. Brodie and C. A. M. Hogben, *J. Pharm. Pharmacol.*, **9**, 345(1957).
- (4) "The Pharmacological Basis of Therapeutics," 4th ed., L. S. Goodman and A. Gilman, Eds., Macmillan, New York, N.Y., 1970.
- (5) K. B. Bischoff and R. G. Brown, *Chem. Eng. Progr. Symp. Ser. No. 66*, **62**, 33(1966).
- (6) K. B. Bischoff, in "Chemical Engineering in Medicine and Biology," D. Hershey, Ed., Plenum, New York, N.Y., 1967, p. 417.
- (7) R. L. Dedrick and K. B. Bischoff, *Chem. Eng. Progr. Symp. Ser. No. 84*, **64**, 32(1968).
- (8) K. B. Bischoff and R. L. Dedrick, *J. Pharm. Sci.*, **57**, 1346(1968).
- (9) D. S. Zaharko, R. L. Dedrick, K. B. Bischoff, J. A. Longstreth, and V. T. Oliverio, *J. Nat. Cancer Inst.*, **46**, 775(1971).
- (10) K. B. Bischoff, K. J. Himmelstein, R. L. Dedrick, and D. S. Zaharko, in "Chemical Engineering in Medicine," R. F. Gould, Ed., American Chemical Society, Washington, D.C., 1973, p. 47.
- (11) R. L. Dedrick, D. D. Ferrester, and D. H. W. Ho, *Biochem. Pharmacol.*, **21**, 1(1972).
- (12) R. L. Dedrick, D. S. Zaharko, and R. J. Lutz, *J. Pharm. Sci.*, **62**, 882(1973).
- (13) R. L. Dedrick, D. D. Ferrester, T. N. Cannon, S. M. El Dar-eer, and L. B. Mellett, *Biochem. Pharmacol.*, **22**, 2405(1973).
- (14) D. Shen and M. Gibaldi, *J. Pharm. Sci.*, **63**, 1698(1974).
- (15) L. C. Mark, *Clin. Pharmacol. Ther.*, **4**, 504(1963).
- (16) F. Karush, *J. Amer. Chem. Soc.*, **72**, 2705(1950).
- (17) J. D. Teresi and J. M. Luck, *J. Biol. Chem.*, **194**, 823(1952).
- (18) L. R. Goldbaum and P. K. Smith, *J. Pharmacol. Exp. Ther.*, **111**, 197(1954).

(19) S. P. Colowick and F. C. Womack, *J. Biol. Chem.*, **224**, 774(1969).

(20) C. N. Chen, Ph.D. dissertation, University of Utah, Salt Lake City, Utah, 1976.

(21) G. M. C. Masson and E. Beland, *Anesthesiology*, **6**, 483(1945).

ACKNOWLEDGMENTS AND ADDRESSES

Received May 1, 1975, from the College of Engineering, College of Pharmacy, and the Institute for Biomedical Engineering, University of Utah, Salt Lake City, UT 84112.

Accepted for publication July 21, 1975.

The authors thank Dr. Sen-Maw Fang and Dr. David Gough for many helpful suggestions. They are particularly grateful to Dr. Kenneth B. Bischoff and Dr. Robert L. Dedrick for providing invaluable advice and information.

Supported in part by National Science Foundation Grant GH38996X and National Institutes of Health-Food and Drug Administration Grant FD 00480-01.

* To whom inquiries should be directed.

Pharmacokinetic Model for Salicylate in Cerebrospinal Fluid, Blood, Organs, and Tissues

C. N. CHEN, D. L. COLEMAN, J. D. ANDRADE^{*}, and
A. R. TEMPLE

Received May 10, 1976, from the College of Engineering and College of Pharmacy, University of Utah, Salt Lake City, UT 84112.
Accepted for publication April 6, 1977.

Abstract □ The developed pharmacokinetic model, an extension of the Bischoff-Dedrick model, simultaneously predicts the kinetic behavior of salicylate in cerebrospinal fluid, blood, organs, and tissues. The model, which is entirely different from conventional compartment models, is derived from basic considerations of drug distribution with biochemical and physiological meaning. The dog was studied at three different dosages of salicylate: therapeutic, moderate intoxication, and severe intoxication. The predicted kinetics of salicylate in cerebrospinal fluid, blood, plasma, liver, muscle, and adipose tissue by the model agreed well with the experimental data. The effectiveness of hemoperfusion treatment for the severely intoxicated dog by albumin-coated activated carbon and its effect on the kinetic behavior of salicylate in cerebrospinal fluid, blood, organs, and tissues were studied. The model was also applied to predict the kinetic changes of salicylate in the body during and after the extracorporeal treatment. The predicted results also agreed with the experimental data.

Keyphrases □ Models, pharmacokinetic—developed to predict behavior of salicylate in cerebrospinal fluid, blood, organs, and tissues, compared to experimental data with dogs □ Pharmacokinetic models—developed to predict behavior of salicylate in cerebrospinal fluid, blood, organs, and tissues, compared to experimental data with dogs □ Salicylate—pharmacokinetic model developed to predict behavior in cerebrospinal fluid, blood, organs, and tissues, compared to experimental data with dogs

Blood or plasma drug levels have been used as an index of dose scheduling for therapeutics under the assumption that the drug level in blood or plasma corresponds to the pharmacological effect of the drug. Conventional pharmacokinetic models have been widely applied to simulate the kinetic behavior of drug levels in blood or plasma. However, the knowledge of drug levels in blood or plasma with time may not provide sufficient information for adequate therapy. The kinetic information of drug levels in brain, cerebrospinal fluid, blood, organs, and tissues of pharmacological interest may be necessary for the development of more appropriate dosage regimens.

The model developed and used in this study is an extension of the Bischoff-Dedrick model (1, 2). This model is derived from basic considerations of drug distribution

with biochemical and physiological meaning. The model has been applied successfully to predict the pharmacokinetics of thiopental (2, 3), methotrexate (1, 4, 5), and cytarabine (6).

Previously, an extended version of the Bischoff-Dedrick model was used to predict thiopental kinetics in the dog (2). In this paper, the model previously presented (2) is modified and applied to salicylate in the dog. The model also is modified to consider the effects of activated carbon hemoperfusion on the pharmacokinetics of salicylate in the dog. Since drug-protein binding plays an important role in pharmacological effect and pharmacokinetics, the model also is applied to predict the pharmacokinetics of free (unbound) salicylate levels in plasma water, which is more related to the pharmacological effect of the drug.

THEORETICAL

A diagram of blood circulation through various body regions is shown in Scheme I. The blood pool is the blood volume excluding the blood contained in the capillary beds of organs and tissues in the body.

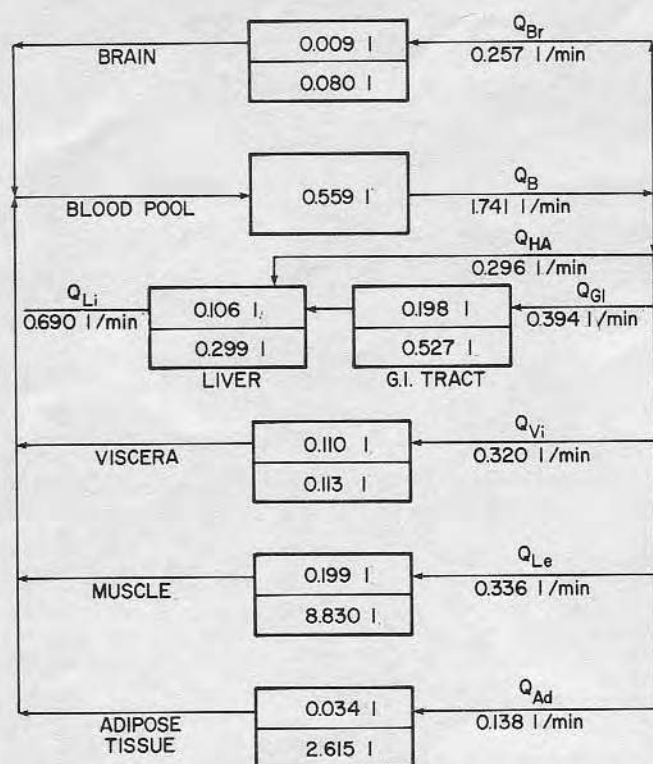
The transient mass balance for any organ or body region can be expressed as (2):

$$\left[\begin{array}{l} \text{drug accumulation rate} \\ \text{in both capillary bed and} \\ \text{tissue portion} \end{array} \right] = \left[\begin{array}{l} \text{drug inflow rate from} \\ \text{blood pool and/or} \\ \text{other body regions} \end{array} \right] + [\text{drug ingestion rate, if any}] - \left[\begin{array}{l} \text{drug outflow rate} \\ \text{from body region} \end{array} \right] - \left[\begin{array}{l} \text{drug metabolism rate and/or} \\ \text{excretion rate, if any} \end{array} \right] \quad (\text{Eq. 1})$$

The mathematical equation of the transient mass balance for any body region (Y_z) is:

$$\frac{d(V_{YzB}C_{T,YzB})}{dt} + \frac{d(V_{YzT}C_{T,YzT})}{dt} = Q_{Yz}(C_{T,B} - C_{T,YzB}) \quad (\text{Eq. 2})$$

where the subscripts mean the following: B , blood; T , total or tissue; and Y_z , a body region such as Ad (adipose), Br (brain), GI (gastrointestinal), Li (liver), Mu (muscle), and Vi (viscera); and where $C_{T,B}$ is the total



Scheme I—Body regions and blood flows for a 15-kg (average) dog. Key: l = liters.

(bound and unbound) drug concentration in blood from the blood pool, $C_{T,YzB}$ is the total drug concentration in the capillary bed (blood portion) of the body region (Yz), $C_{T,YzT}$ is the total drug concentration in the tissue portion of the body region (Yz), Q_{Yz} is the blood flow rate from the body region (Yz), t is time, V_{YzB} is the blood volume in the capillary bed of the body region (Yz), and V_{YzT} is the tissue volume in the tissue portion of the body region (Yz).

Most drugs can be bound to plasma proteins, especially to albumin, and to various tissue components (7). The free (unbound) drug level in the target organ(s) is more related to the pharmacological effect of the drug. The model considers this factor by correlating the total drug concentration with the free drug concentration in blood, organs, and tissues. The relationship between the total drug concentration, $C_{T,B}$, and the free drug concentration, $C_{F,B}$, in blood can be determined *in vitro*. Thus:

$$C_{T,B} = f_B(C_{F,B}) \quad (\text{Eq. 3})$$

where $f_B(C_{F,B})$ is a mathematical expression of the total drug concentration in terms of the free drug concentration in blood.

The mathematical relation between the total drug concentration, $C_{T,YzB}$, and the free drug concentration, $C_{F,YzB}$, in the blood of any organ capillary bed, YzB , is the same as that in Eq. 3:

$$C_{T,YzB} = f_B(C_{F,YzB}) \quad (\text{Eq. 4})$$

Similarly, the total drug concentration, $C_{T,YzT}$, in the tissue portion of the body region, Yz , can be expressed in terms of the corresponding free drug concentration, $C_{F,YzT}$, by another function, $f_{YzT}(C_{F,YzT})$:

$$C_{T,YzT} = f_{YzT}(C_{F,YzT}) \quad (\text{Eq. 5})$$

After Eqs. 3–5 are substituted into Eq. 2, Eq. 2 becomes:

$$\frac{d[V_{YzB}f_B(C_{F,YzB})]}{dt} + \frac{d[V_{YzT}f_{YzT}(C_{F,YzT})]}{dt} = Q_{Yz}[f_B(C_{F,B}) - f_B(C_{F,YzB})] \quad (\text{Eq. 6})$$

Equation 6 can be developed to the following equation:

$$V_{YzB}f_B'(C_{F,YzB})\frac{dC_{F,YzB}}{dt} + f_B(C_{F,YzB})\frac{dV_{YzB}}{dt} + V_{YzT}f_{YzT}'(C_{F,YzT})\frac{dC_{F,YzT}}{dt} + f_{YzT}(C_{F,YzT})\frac{dV_{YzT}}{dt} = Q_{Yz}[f_B(C_{F,B}) - f_B(C_{F,YzB})] \quad (\text{Eq. 7})$$

where $f_B'(C_{F,YzB}) = df_B(C_{F,YzB})/dC_{F,YzB}$ and $f_{YzT}'(C_{F,YzT}) = df_{YzT}(C_{F,YzT})/dC_{F,YzT}$.

Capillaries in organs and tissues differ widely in their permeability characteristics. There are two types of mass transfer between the capillaries and the surrounding tissue. One type is the nearly instantaneous establishment of an equilibrium free drug concentration between the capillaries and the tissue. The capillaries of the liver permit the passage of substances quite readily (8). The equilibrium free drug concentration between the liver capillaries and the surrounding tissue can be established rapidly. In this case, the free drug concentration, $C_{F,YzT}$, in the tissue effectively equals the free drug concentration, $C_{F,YzB}$, in the capillaries. That is:

$$C_{F,YzT} = C_{F,YzB} \quad (\text{Eq. 8})$$

Substitution of Eq. 8 into Eq. 5 gives:

$$C_{T,YzT} = f_{YzT}(C_{F,YzB}) \quad (\text{Eq. 9})$$

Equations 8 and 9 are substituted into Eq. 7, rearranged, and simplified to:

$$[V_{YzB}f_B'(C_{F,YzB}) + V_{YzT}f_{YzT}'(C_{F,YzB})]\frac{dC_{F,YzB}}{dt} + f_B(C_{F,YzB})\frac{dV_{YzB}}{dt} + f_{YzT}(C_{F,YzB})\frac{dV_{YzT}}{dt} = Q_{Yz}[f_B(C_{F,B}) - f_B(C_{F,YzB})] \quad (\text{Eq. 10})$$

The second type of mass transport through the capillary wall is the restricted passage between the capillaries and the tissue. For instance, the capillary wall in muscle is composed of an interlocking mosaic of endothelial cells with slits (junctions) between them that could function as the postulated pores and could account for the restricted passage of water-soluble compounds (9). The restricted transport of salicylate through the muscle capillary wall does not allow the instantaneous establishment of the equilibrium free salicylate concentration between the capillaries and the muscle tissue.

The restricted transport of drugs between the capillaries and the tissue may be described in terms of Fick's law. The changing rate of the free drug concentration, $C_{F,YzT}$, in the tissue is proportional to the free concentration difference between the capillaries and the tissue, which gives:

$$\frac{dC_{F,YzT}}{dt} = P_{Yz}(C_{F,YzB} - C_{F,YzT}) \quad (\text{Eq. 11})$$

where P_{Yz} is a proportionality constant called the permeability constant and $C_{F,YzB}$ and $C_{F,YzT}$ are the free drug concentrations in the capillaries and the tissue of the body region, Yz .

Substituting Eq. 11 into Eq. 7 gives:

$$V_{YzB}f_B'(C_{F,YzB})\frac{dC_{F,YzB}}{dt} + f_B(C_{F,YzB})\frac{dV_{YzB}}{dt} + V_{YzT}f_{YzT}'(C_{F,YzT})P_{Yz} \times (C_{F,YzB} - C_{F,YzT}) + f_{YzT}(C_{F,YzT})\frac{dV_{YzT}}{dt} = Q_{Yz}[f_B(C_{F,B}) - f_B(C_{F,YzB})] \quad (\text{Eq. 12})$$

MODEL

This study attempted to apply the model to predict the kinetic behavior of salicylate in cerebrospinal fluid, blood, liver, muscle, and adipose tissue because experimental kinetic data of salicylate in these body regions are available (10). At least five body regions may be defined: brain, liver, muscle, adipose tissue, and the blood pool (the blood volume excluding those blood volumes in the capillary beds of body regions). In mammals, blood from the GI area perfuses the liver. Thus, GI tissues are added as another body region. Since there is little interest in the kinetics of salicylate in the kidneys or heart, these two organs may be included in the body region called viscera.

A diagram of blood circulation in the seven body regions with physiological data of blood volumes, tissue volumes, and blood flows for a 15-kg (average) dog is shown in Scheme I. Some physiological data are revised and different from those given previously (2). These revised data represent the actually measured statistical data (11–18).

The transient mass balance for the blood pool can be expressed as:

$$\frac{d(V_{B,t}C_{T,B})}{dt} = (Q_{Br}C_{T,BrB} + Q_{Li}C_{T,LiB} + Q_{Vi}C_{T,ViB} + Q_{Mu}C_{T,MuB} + Q_{Ad}C_{T,AdB}) + Mg(t) - Q_B C_{T,B} \quad (\text{Eq. 13a})$$

Table I—Parameters and Constants for the Model^a

	Blood Pool	Brain	Liver	Viscera	GI Area	Muscle	Adipose Tissue
$F_{V,YzB}^b$	0.460	0.007	0.087	0.091	0.163	0.164	0.028
$F_{W,YzT}^c$	—	0.7936	0.7326	0.7824	0.7410	0.7757	0.1922

^a A (mg/liter) = 72.6645, M = 1.1571, B (mg/liter) = 175.1879, N = 1.2441, P_{CSF} (21, 22) (min^{-1}) = 0.0040, P_{Mu} (8, 23) (min^{-1}) = 4.5550, Q_{BL} (liter/min) = 0.001, Q_{ET} (liter/min) = 0.065, Q_{SE} (liter/min) = 0.00167, Q_{CSF} (8, 23) (ml/min) = 0.08, and V_{CSF} (ml) (8, 23) = 32 for a 15-kg (average) dog. ^b Fraction of the blood volume in organ capillaries to the total blood volume in the body. ^c Taken from Table 1 of Ref. 2.

or:

$$\left[\begin{array}{l} \text{drug accumulation} \\ \text{rate in blood pool} \end{array} \right] = \left[\begin{array}{l} \text{summation of drug inflow rates} \\ \text{from five body regions} \end{array} \right] + [\text{ingestion rate}] - [\text{drug outflow rate from blood pool}] \quad (\text{Eq. 13b})$$

Plasma protein binding of salicylate was studied by the equilibrium dialysis technique (19). A linear relation was found between the total salicylate concentration, C_{TP} , and the free concentration, C_{FP} , in plasma in the range of salicylate levels investigated (10):

$$C_{TP} = f_P(C_{FP}) = B + NC_{FP} \quad (\text{Eq. 14})$$

where B and N are constants (10) given in Table I.

The relationship between the total salicylate concentration and the free concentration in whole blood may be determined indirectly. Since the free (unbound) drug in plasma water is in equilibrium with the bound drug in both plasma and blood, simultaneous determination of both total salicylate concentrations in blood and plasma from the same samples makes it possible to find the free concentration corresponding to both total concentrations in plasma and blood from Eq. 14. The relation thus constructed between the total salicylate concentration, C_{TB0} , in original (nondiluted) blood and the free concentration, C_{FB} , in blood water is also linear (10):

$$C_{TB0} = f_B(C_{FB}) = A + MC_{FB} \quad (\text{Eq. 15})$$

The values for A and M are also listed in Table I.

The experimental salicylate distribution data were obtained during a 6-hr experiment (10) in which blood loss occurred due to the surgical trauma from taking tissue samples. Normal saline was given continuously to maintain adequate blood pressure and blood volume. Therefore, the blood in the body was gradually diluted during the experiment. The fraction of whole (nondiluted) blood at time t in the continuously diluted blood, $F_B(t)$, can be calculated from the solution to a differential equation of the mass balance for the whole (nondiluted) blood. The rate of change of the total whole (nondiluted) blood volume in the body is equal to the loss rate of the whole blood, $Q_{BL}F_B(t)$, due to bleeding. It gives:

$$\frac{d[V_{TB,t}F_B(t)]}{dt} = -Q_{BL}F_B(t) \quad (\text{Eq. 16})$$

where:

$$V_{TB,t} = V_{TB,0} + (Q_{SE} - Q_{BL})t \quad (\text{Eq. 17})$$

and $F_B(t)$ is the fraction of whole (nondiluted) blood in the continuously diluted blood at time t , Q_{BL} is the blood loss rate due to bleeding from tissues, Q_{SE} is the saline-entering rate to the vein, $V_{TB,0}$ is the total blood volume in the body at time zero, and $V_{TB,t}$ is the total blood volume (diluted blood) in the body at time t .

In this study, the normal saline infusion rate was kept constant while the bleeding rate of blood loss from tissues was assumed to be constant (Table I). After Eq. 17 is substituted into Eq. 16, the solution to Eq. 16, under the conditions of both Q_{SE} and Q_{BL} being constants, gives:

$$F_B(t) = F_B(0) \left[1 + \frac{(Q_{SE} - Q_{BL})t}{V_{TB,0}} \right]^{-[Q_{SE}/(Q_{SE} - Q_{BL})]} \quad (\text{Eq. 18})$$

Since time zero is the time just prior to blood dilution from saline infusion (10), the fraction of whole (nondiluted) blood at time zero, $F_B(0)$, is one.

The amount of salicylate in the diluted blood equals the amount of salicylate in the whole blood fraction plus that of salicylate in the water fraction of the diluted blood. Thus, it gives:

$$V_{TB,t}C_{TB} = [V_{TB,t}F_B(t)]C_{TB0} + [V_{TB,t}[1 - F_B(t)]]C_{FB} \quad (\text{Eq. 19})$$

Equation 19 may be simplified to:

$$C_{TB} = F_B(t)C_{TB0} + [1 - F_B(t)]C_{FB} \quad (\text{Eq. 20})$$

Substituting Eq. 15 into Eq. 20 and rearranging give:

$$C_{TB} = F_B(t)A + H_m(t)C_{FB} \quad (\text{Eq. 21})$$

where $H_m(t) = 1 + (M - 1)F_B(t)$, A and M are constants in Eq. 15 and their values are shown in Table I, C_{FB} is the free salicylate concentration in blood water, C_{TB0} is the total salicylate concentration in whole (undiluted) blood, and C_{TB} is the total salicylate concentration in the diluted blood at time t .

Similarly, the total salicylate concentration in the blood of the capillary bed of any body region, Yz , can be expressed as:

$$C_{T,YzB} = F_B(t)A + H_m(t)C_{F,YzB} \quad (\text{Eq. 22})$$

where $C_{F,YzB}$ is the free salicylate concentration in the capillary blood of any body region, Yz , and $C_{T,YzB}$ is the total salicylate concentration in the capillary blood of any body region, Yz . The blood volume of the blood pool, $V_{B,t}$, at time t can be calculated by:

$$V_{B,t} = V_{B,0} + (Q_{SE} - Q_{BL})tF_{V,B} \quad (\text{Eq. 23})$$

where $F_{V,B}$ is the fraction of the blood volume of the blood pool in the total blood volume, $V_{B,0}$ is the blood volume of the blood pool at time zero, and $V_{B,t}$ is the blood volume of the blood pool at time t . Substituting Eqs. 21–23 into Eq. 13 and rearranging result in:

$$\begin{aligned} \frac{dC_{F,B}}{dt} = & (Q_{Br}C_{F,BrB} + Q_{Li}C_{F,LiB} + Q_{Vi}C_{F,ViB} + Q_{Mu}C_{F,MuB} \\ & + Q_{Ad}C_{F,AdB})/V_{B,t} + Mg(t)/[V_{B,t}H_m(t)] \\ & - J_B(t)C_{F,B} - G_B(t) \end{aligned} \quad (\text{Eq. 24})$$

where:

$$G_B(t) = A[F_B'(t)/H_m(t) + (Q_{SE} - Q_{BL})F_{V,B}F_B(t)/[V_{B,t}H_m(t)]] \quad (\text{Eq. 25a})$$

and:

$$J_B(t) = [H_m'(t)/H_m(t) + (Q_{SE} - Q_{BL})F_{V,B}/V_{B,t} + Q_B/V_B] \quad (\text{Eq. 25b})$$

where $F_B'(t) = dF_B(t)/dt$; $H_m'(t) = dH_m(t)/dt$; $C_{F,B}$ is the free salicylate concentration in the blood pool; $C_{F,YzB}$ is the free salicylate concentration in the capillary bed of any body region, Yz ; Q_{Yz} is the blood flow rate from the body region, Yz ; and $V_{B,t}$ is the blood volume of the blood pool at time t .

An infusion pump was used to infuse the drug solution at a constant rate over 5 min (10). Thus, the ingestion term, $Mg(t)$, in Eq. 24 is equal to the dose divided by 5.

Liver—The transient mass balance for the liver (Li) is:

$$\begin{aligned} \frac{d(V_{LiB,t}C_{T,LiB})}{dt} + \frac{d(V_{LiT}C_{T,LiT})}{dt} = & (Q_{HA}C_{T,B} + Q_{GI}C_{T,GIB}) \\ & - Q_{Li}C_{T,LiB} - R_m \end{aligned} \quad (\text{Eq. 26a})$$

or:

$$\left[\begin{array}{l} \text{drug accumulation rate} \\ \text{in capillary bed and} \\ \text{tissue portion of liver} \end{array} \right] = \left[\begin{array}{l} \text{drug inflow rates from} \\ \text{blood pool (hepatic artery) and} \\ \text{GI tissue (portal vein)} \end{array} \right] - \left[\begin{array}{l} \text{drug outflow} \\ \text{rate from liver} \end{array} \right] - [\text{metabolism rate}] \quad (\text{Eq. 26b})$$

Salicylate did not bind with the tissue components of the liver (10), which suggests that the amount of salicylate in the liver tissue equals the free salicylate concentration, $C_{F,LiT}$, multiplied by the volume of liver tissue water, $V_{LiT}F_{w,LiT}$:

$$V_{LiT}C_{T,LiT} = (V_{LiT}F_{w,LiT})C_{F,LiT} \quad (\text{Eq. 27})$$

where $C_{F,LiT}$ and $C_{T,LiT}$ are the free and total salicylate concentrations

in the tissue portion of the liver, respectively; $F_{w,LiT}$ is the volume fraction of water in the tissue portion of the liver; and V_{LiT} is the volume of the tissue portion of the liver. Since the liver capillaries are highly permeable to salicylate, the equilibrium salicylate concentration (unbound concentration) between the capillaries and the liver tissue may be established nearly instantaneously:

$$C_{F,LiT} = C_{F,LiB} \quad (\text{Eq. 28})$$

Substitution of Eq. 28 into Eq. 27 yields:

$$V_{LiT}C_{T,LiT} = (V_{LiT}F_{w,LiT})C_{F,LiB} \quad (\text{Eq. 29})$$

The total salicylate concentration, $C_{T,LiB}$, and the blood volume, $V_{LiB,t}$, in the liver capillaries at time t have similar formulas as those in Eqs. 22 and 23:

$$C_{T,LiB} = F_B(t)A + H_m(t)C_{F,LiB} \quad (\text{Eq. 30})$$

and:

$$V_{LiB,t} = V_{LiB,0} + (Q_{SE} - Q_{BL})tF_{V,LiB} \quad (\text{Eq. 31})$$

where $F_{V,LiB}$ is the fraction of the blood volume of the liver capillary bed in the total blood volume, and $V_{LiB,0}$ and $V_{LiB,t}$ are the blood volumes of the liver capillary bed at time zero and t , respectively.

Substituting Eqs. 29–31 into Eq. 26a and rearranging yield:

$$\frac{dC_{F,LiB}}{dt} = (Q_{HA}C_{F,B} + Q_{GI}C_{F,GIB})H_m(t)/L_{Li}(t) - J_{Li}(t)C_{F,LiB} - R_m/L_{Li}(t) - G_{Li}(t) \quad (\text{Eq. 32})$$

where:

$$L_{Li}(t) = V_{LiB,t}H_m(t) + V_{LiT}F_{w,LiT}$$

$$G_{Li}(t) = A[V_{LiB,t}F_B'(t) + (Q_{SE} - Q_{BL})F_{V,LiB}F_B(t)]/L_{Li}(t)$$

$$J_{Li}(t) = [V_{LiB,t}H_m'(t) + (Q_{SE} - Q_{BL})F_{V,LiB}H_m(t) + Q_{Li}H_m(t)]/L_{Li}(t)$$

Q_{HA} = blood flow rate of the hepatic artery

Q_{GI} = blood flow rate from the GI body region

The metabolism rate, R_m , can generally be described in terms of the simple Michaelis-Menten form:

$$R_m = \frac{K_{Li}C_{F,LiT}}{K_{M,Li} + C_{F,LiT}} \quad (\text{Eq. 33})$$

There are two special cases: (a) if $C_{F,LiT} \gg K_{M,Li}$, then $R_m = K_{Li}$ (zero order), and (b) if $C_{F,LiT} \ll K_{M,Li}$, then $R_m = (K_{Li}/K_{M,Li})C_{F,LiT}$ (first order).

Since the metabolism mainly occurs in the liver, it was assumed that all salicylate metabolism occurs in the liver. In general, similar terms could be added to the other body regions if necessary. It was found previously (10) that the total excretion rate of unchanged salicylate and its metabolites (salicylurate, salicylglucuronide, and gentisate) was zero order and was 1.70 mg/min for the three dosages studied. Davis and Westfall (20) found that the amount of unchanged salicylate excreted in dog urine was 38% while that of its metabolites was 62% of the total amount excreted. The salicylate metabolism rate, which was assumed to be 62% of the total excretion rate, was 1.05 mg/min for the three dosages investigated.

Viscera—The transient mass balance for the viscera body region (V_i) is:

$$\frac{d(V_{ViB,t}C_{T,ViB})}{dt} + \frac{d(V_{ViT}C_{T,ViT})}{dt} = Q_{Vi}(C_{T,B} - C_{T,ViB}) - R_r \quad (\text{Eq. 34})$$

The renal excretion rate, R_r , of unchanged salicylate was 0.65 mg/min for the three dosages studied (10). The total salicylate concentration, $C_{T,ViB}$, and blood volume, $V_{ViB,t}$, in the viscera capillaries at time t may be written in a form similar to that for the liver capillaries. The permeability of the visceral (kidneys and heart) capillaries is assumed to be similar to that of the liver capillaries. Salicylate does not bind with the tissue components of the viscera either. Thus:

$$V_{ViT}C_{T,ViT} = (F_{w,ViT}V_{ViT})C_{F,ViT} = (F_{w,ViT}V_{ViT})C_{F,ViB} \quad (\text{Eq. 35})$$

$$C_{T,ViB} = F_B(t)A + H_m(t)C_{F,ViB} \quad (\text{Eq. 36})$$

and:

$$V_{ViB,t} = V_{ViB,0} + (Q_{SE} - Q_{BL})tF_{V,ViB} \quad (\text{Eq. 37})$$

Substituting Eqs. 35–37 into Eq. 34 and rearranging yield:

$$\frac{dC_{F,ViB}}{dt} = [Q_{Vi}H_m(t)/L_{Vi}(t)]C_{F,B} - J_{Vi}(t)C_{F,ViB} - G_{Vi}(t) - R_r/L_{Vi}(t) \quad (\text{Eq. 38})$$

where:

$$L_{Vi}(t) = V_{ViB,t}H_m(t) + V_{ViT}F_{w,ViT}$$

$$G_{Vi}(t) = A[V_{ViB,t}F_B'(t) + (Q_{SE} - Q_{BL})F_{V,ViB}F_B(t)]/L_{Vi}(t)$$

$$J_{Vi}(t) = [V_{ViB,t}H_m'(t) + (Q_{SE} - Q_{BL})F_{V,ViB}H_m(t) + Q_{Vi}H_m(t)]/L_{Vi}(t)$$

R_r = renal excretion rate of unchanged salicylate

GI Region—The transit mass balance for the GI region (GI) is:

$$\frac{d(V_{GIB,t}C_{T,GIB})}{dt} + \frac{d(V_{GIT}C_{T,GIT})}{dt} = Q_{GI}(C_{T,B} - C_{T,GIB}) \quad (\text{Eq. 39})$$

where:

$$V_{GIT}C_{T,GIT} = (V_{GIT}F_{w,GIT})C_{F,GIT} = (V_{GIT}F_{w,GIT})C_{F,GIB} \quad (\text{Eq. 40})$$

$$C_{T,GIB} = F_B(t)A + H_m(t)C_{F,GIB} \quad (\text{Eq. 41})$$

and:

$$V_{GIB,t} = V_{GIB,0} + (Q_{SE} - Q_{BL})tF_{V,GIB} \quad (\text{Eq. 42})$$

The following equation results from the substitution of Eqs. 40–42 into Eq. 39:

$$\frac{dC_{F,GIB}}{dt} = [Q_{GI}H_m(t)/L_{GI}(t)]C_{F,B} - J_{GI}(t)C_{F,GIB} - G_{GI}(t) \quad (\text{Eq. 43})$$

where:

$$L_{GI}(t) = V_{GIB,t}H_m(t) + V_{GIT}F_{w,GIT}$$

$$G_{GI}(t) = A[V_{GIB,t}F_B'(t) + (Q_{SE} - Q_{BL})F_{V,GIB}F_B(t)]/L_{GI}(t)$$

$$J_{GI}(t) = [V_{GIB,t}H_m'(t) + (Q_{SE} - Q_{BL})F_{V,GIB}H_m(t) + Q_{GI}H_m(t)]/L_{GI}(t)$$

Adipose Tissue—The transit mass balance for the adipose tissue region (Ad) is:

$$\frac{d(V_{AdB,t}C_{T,AdB})}{dt} + \frac{d(V_{AdT}C_{T,AdT})}{dt} = Q_{Ad}(C_{T,B} - C_{T,AdB}) \quad (\text{Eq. 44})$$

The tissue “binding” in adipose tissue is primarily due to the lipid solubility of the drug. Salicylate that is ionized at physiological pH is not lipid soluble. Salicylate in the small portion (about 19%) of water in adipose tissue accounts for the total amount of salicylate in the tissue portion, giving:

$$V_{AdT}C_{T,AdT} = (V_{AdT}F_{w,AdT})C_{F,AdT} = (V_{AdT}F_{w,AdT})C_{F,AdB} \quad (\text{Eq. 45})$$

Also:

$$C_{T,AdB} = F_B(t)A + H_m(t)C_{F,AdB} \quad (\text{Eq. 46})$$

and:

$$V_{AdB,t} = V_{AdB,0} + (Q_{SE} - Q_{BL})tF_{V,AdB} \quad (\text{Eq. 47})$$

Substituting Eqs. 45–47 into Eq. 44 and rearranging yield:

$$\frac{dC_{F,AdB}}{dt} = [Q_{Ad}H_m(t)/L_{Ad}(t)]C_{F,B} - J_{Ad}(t)C_{F,AdB} - G_{Ad}(t) \quad (\text{Eq. 48})$$

where:

$$L_{Ad}(t) = V_{AdB,t}H_m(t) + V_{AdT}F_{w,AdT}$$

$$G_{Ad}(t) = A[V_{AdB,t}F_B'(t) + (Q_{SE} - Q_{BL})F_{V,AdB}F_B(t)]/L_{Ad}(t)$$

$$J_{Ad}(t) = [V_{AdB,t}H_m'(t) + (Q_{SE} - Q_{BL})F_{V,AdB}H_m(t) + Q_{Ad}H_m(t)]/L_{Ad}(t)$$

Muscle—The transit mass balance for the muscle body region (Mu) is:

$$\frac{d(V_{MuB,t}C_{T,MuB})}{dt} + \frac{d(V_{MuT}C_{T,MuT})}{dt} = Q_{Mu}(C_{T,B} - C_{T,MuB}) \quad (\text{Eq. 49})$$

Salicylate does not bind with the tissue components of muscle. Hence:

$$V_{MuT}C_{T,MuT} = (V_{MuT}F_{w,MuT})C_{F,MuT} \quad (\text{Eq. 50})$$

$$C_{T,MuB} = F_B(t)A + H_m(t)C_{F,MuB} \quad (\text{Eq. 51})$$

and:

$$V_{MuB,t} = V_{MuB,0} + (Q_{SE} - Q_{BL})tF_{V,MuB} \quad (\text{Eq. 52})$$

It has been stated that the passage of water-soluble compounds such as salicylate through the muscle capillaries is restricted. The restricted drug transport can be described by:

$$\frac{dC_{F,MuT}}{dt} = P_{Mu}(C_{F,MuB} - C_{F,MuT}) \quad (\text{Eq. 53})$$

Substituting Eqs. 50–53 into Eq. 49 and rearranging give:

$$\frac{dC_{F,MuB}}{dt} = (Q_{Mu}/V_{MuB,t})C_{F,B} - I_{Mu}(t)C_{F,MuB} + \{P_{Mu}V_{MuT}F_{w,MuT}/[V_{MuB,t}H_m(t)]\}C_{F,MuT} - S_{Mu}(t) \quad (\text{Eq. 54})$$

where:

$$I_{Mu}(t) = [V_{MuB,t}H_m'(t) + (Q_{SE} - Q_{BL})F_{V,MuB}H_m(t) + P_{Mu}V_{MuT}F_{w,MuT} + Q_{Mu}H_m(t)]/[V_{MuB,t}H_m(t)]$$

$$S_{Mu}(t) = A\{F_B'(t)/H_m(t) + (Q_{SE} - Q_{BL})F_{V,MuB}F_B(t)/[V_{MuB,t}H_m(t)]\}$$

Brain—The transit mass balance for the brain region (Br) is

$$\frac{d(V_{BrB,t}C_{T,BrB})}{dt} + \frac{d(V_{BrT}C_{T,BrT})}{dt} = Q_{Br}(C_{T,B} - C_{T,BrB}) \quad (\text{Eq. 55})$$

No binding between salicylate and the brain tissue was found (10). Hence:

$$V_{BrT}C_{T,BrT} = (V_{BrT}F_{w,BrT})C_{F,BrT} \quad (\text{Eq. 56})$$

$$C_{T,BrB} = F_B(t)A + H_m(t)C_{F,BrB} \quad (\text{Eq. 57})$$

and:

$$V_{BrB,t} = V_{BrB,0} + (Q_{SE} - Q_{BL})tF_{V,BrB} \quad (\text{Eq. 58})$$

In the brain, the capillaries are much less permeable to water-soluble substances, perhaps because the endothelium of brain capillaries appears to be a continuous sheet of the glial connective tissue cells without visible pores (8). The cellular sheath of the brain capillaries highly impedes the passage of water-soluble compounds and accounts for the blood–brain barrier. The kinetics of salicylate penetration into cerebrospinal fluid and brain were studied previously (21, 22). The permeability constant, P_{CSF} , for salicylate penetration into cerebrospinal fluid (21, 22) is in the 0.0026–0.006-min⁻¹ range. Materials diffuse relatively freely in either direction between the cerebrospinal fluid and extracellular fluid deep into brain tissue (23). Therefore, the value of the permeability constant for the blood–cerebrospinal fluid barrier may be adopted as that for the passage of the drug between the brain capillaries and the brain tissue, i.e., $P_{Br} = P_{CSF}$.

The highly restricted transport of the drug in the brain can be written in terms of the free concentration difference between the capillaries and the brain tissue:

$$\frac{dC_{F,BrT}}{dt} = P_{Br}(C_{F,BrB} - C_{F,BrT}) \quad (\text{Eq. 59})$$

Substituting Eqs. 56–59 into Eq. 55 and rearranging give:

$$\frac{dC_{F,BrB}}{dt} = (Q_{Br}/V_{BrB,t})C_{F,B} - I_{Br}(t)C_{F,BrB} + \{P_{Br}V_{BrT}F_{w,BrT}/[V_{BrB,t}H_m(t)]\}C_{F,BrT} - S_{Br}(t) \quad (\text{Eq. 60})$$

where:

$$I_{Br}(t) = [V_{BrB,t}H_m'(t) + (Q_{SE} - Q_{BL})F_{V,BrB}H_m(t) + P_{Br}V_{BrT}F_{w,BrT} + Q_{Br}H_m(t)]/[V_{BrB,t}H_m(t)]$$

$$S_{Br}(t) = A\{F_B'(t)/H_m(t) + (Q_{SE} - Q_{BL})F_{V,BrB}F_B(t)/[V_{BrB,t}H_m(t)]\}$$

Kinetics of Salicylate Penetration into Cerebrospinal Fluid—In humans, the production rate of cerebrospinal fluid is in the 0.3–0.5 ml/min range with a total volume of about 120–200 ml (8, 23). The cerebrospinal fluid moves by bulk flow out of the ventricular system into the subarachnoid space and eventually returns to the bloodstream. The drug in the cerebrospinal fluid is removed as it returns to the general circulation.

The drug accumulation rate in the cerebrospinal fluid equals the drug penetration rate from the brain capillaries to the cerebrospinal fluid minus the drug removal rate due to the cerebrospinal fluid returning to the bloodstream. Thus:

$$\frac{d(V_{CSF}C_{CSF})}{dt} = V_{CSF}P_{CSF}(C_{F,BrB} - C_{CSF}) - Q_{CSF}C_{CSF} \quad (\text{Eq. 61})$$

Equation 61 may be simplified to:

$$\frac{dC_{CSF}}{dt} = P_{CSF}(C_{F,BrB} - C_{CSF}) - (Q_{CSF}/V_{CSF})C_{CSF} \quad (\text{Eq. 62})$$

where $C_{F,BrB}$ and C_{CSF} are the free concentrations in the brain capillaries and in the cerebrospinal fluid, respectively; P_{CSF} is the permeability constant for drug passage into the cerebrospinal fluid; Q_{CSF} is the production or removal rate of the cerebrospinal fluid; and V_{CSF} is the total cerebrospinal fluid volume.

There are 10 unknown variables (seven free concentrations in the blood pool and in the capillaries of the other six body regions plus three free concentrations in the cerebrospinal fluid and in the tissue portions of brain and muscle) in a system of 10 simultaneous equations (Eqs. 24, 32, 38, 43, 48, 53, 54, 59, 60, and 62). Ten equations can serve to solve 10 variables. Therefore, a system of the 10 simultaneous first-order ordinary differential equations can be solved numerically. In this study, the Runge-Kutta fourth-order method (10, 24) for solution of ordinary differential equations was employed to solve the 10 simultaneous equations. The solution gives simultaneously the kinetics of the 10 variables (free salicylate concentrations in this case).

Since the total salicylate concentration, $C_{T,B}$, in the blood pool and both the total salicylate concentration, $C_{T,YzB}$, in the capillary blood and the total salicylate concentration, $C_{T,YzT}$, in the tissue portion of any body region, Yz , can be correlated with their corresponding free salicylate concentrations by Eqs. 21, 22, 29, 35, 40, 45, 50, and 56, all kinetics of total salicylate concentrations in the blood pool and in both the capillary blood and tissue portions of various body regions can also be determined by the model. Model feasibility can be demonstrated by comparing the experimental kinetic data with the model-predicted results. Since the experimentally determined salicylate concentration in any organ, Yz , represents the total salicylate concentration, $C_{T,Yz}$, in that organ, which can be calculated in terms of the total salicylate concentration, $C_{T,YzB}$, in the capillary blood and the total salicylate concentration $C_{T,YzT}$, in the tissue portion of the body region by the following equation:

$$C_{T,Yz}(V_{YzB} + V_{YzT}) = C_{T,YzB}V_{YzB} + C_{T,YzT}V_{YzT} \quad (\text{Eq. 63})$$

the pharmacokinetics of total salicylate levels in various organs and tissues can be predicted by the model.

During the 6-hr experiment, blood loss occurred due to the bleeding from taking various tissue samples to obtain experimental kinetic data. Normal saline was continuously supplied to maintain adequate blood pressure and blood volume. The factors accounting for the blood dilution and the drug loss accompanying blood loss were considered in constructing the pharmacokinetic model. However, the kinetic behavior of salicylate distribution in the body of an intact dog in which tissue samples are not taken is expected to be a little different from that in the dog from which various tissue samples are taken. When tissue samples are not taken, neither blood loss nor blood dilution occurs. The fraction of whole (nondiluted) blood, $F_B(t)$, is always one, and the rates of saline supply and blood loss are zero. The solution to a system of the 10 simultaneous differential equations will give slightly higher salicylate levels in the body because there is no drug loss accompanying blood loss.

Effect of Hemoperfusion on Salicylate Kinetics—The effectiveness of hemoperfusion using albumin-coated activated carbon for acute, severely intoxicated cases was evaluated in terms of its effect on the salicylate body distribution (10). It was also attempted to apply the model to predict the salicylate pharmacokinetics in the body due to the extracorporeal treatment. A blood pump was used to shunt part of the femoral arterial blood through the extracorporeal device, and the “clean” blood out of the device was conducted into the femoral vein during the treatment. Thus:

$$Q_{Mu,ET} = Q_{Mu} - Q_{ET} \quad (\text{Eq. 64})$$

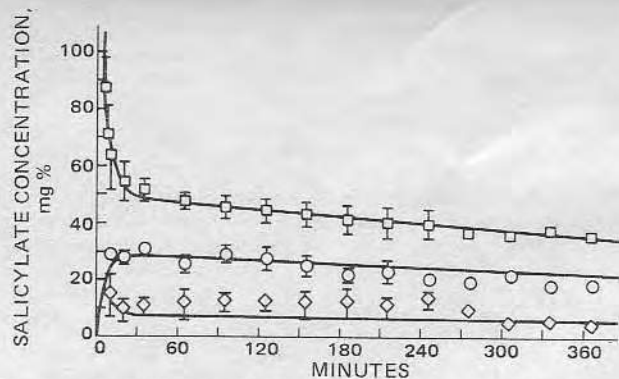


Figure 1—Predicted (solid lines) and experimental salicylate concentrations in blood (\square), muscle (\circ), and adipose tissue (\diamond) at a dose of 285 mg/kg (sodium salicylate).

where $Q_{Mu,ET}$ is the blood flow rate through the muscle during the extracorporeal treatment, Q_{ET} is the blood perfusion rate shunted through the extracorporeal device, and Q_{Mu} is the blood flow rate through the muscle without shunting blood through the device.

The salicylate removal rate by the extracorporeal treatment, R_{ET} , can be calculated by:

$$R_{ET} = Q_{ET}(C_{T,B} - C_{T,B,out}) \quad (\text{Eq. 65})$$

where $C_{T,B}$ is the total drug concentration from the blood pool entering the extracorporeal device and $C_{T,B,out}$ is the total drug concentration in the outflow blood from the device.

During extracorporeal treatment, Eqs. 13 and 49 of transient mass balance for the blood pool and for the muscle region should be modified to:

$$\begin{aligned} \frac{d(V_{B,t}C_{T,B})}{dt} = & (Q_{Br}C_{T,BrB} + Q_{Li}C_{T,LiB} + Q_{Vi}C_{T,ViB} \\ & + Q_{Mu,ET}C_{T,MuB} + Q_{ET}C_{T,B,out} + Q_{Ad}C_{T,AdB}) + Mg(t) \\ & - Q_B C_{T,B} \quad (\text{Eq. 66}) \end{aligned}$$

and:

$$\frac{d(V_{MuB,t}C_{T,MuB})}{dt} + \frac{d(V_{MuT}C_{T,MuT})}{dt} = Q_{Mu,ET}(C_{T,B} - C_{T,MuB}) \quad (\text{Eq. 67})$$

The right-hand side of Eq. 66 can also be written in terms of the salicylate removal rate by the extracorporeal treatment, R_{ET} , from Eq. 65 and becomes:

$$\begin{aligned} \frac{d(V_{B,t}C_{T,B})}{dt} = & (Q_{Br}C_{T,BrB} + Q_{Li}C_{T,LiB} + Q_{Vi}C_{T,ViB} \\ & + Q_{Mu,ET}C_{T,MuB} + Q_{Ad}C_{T,AdB}) + Mg(t) \\ & - (Q_B - Q_{ET})C_{T,B} - R_{ET} \quad (\text{Eq. 68}) \end{aligned}$$

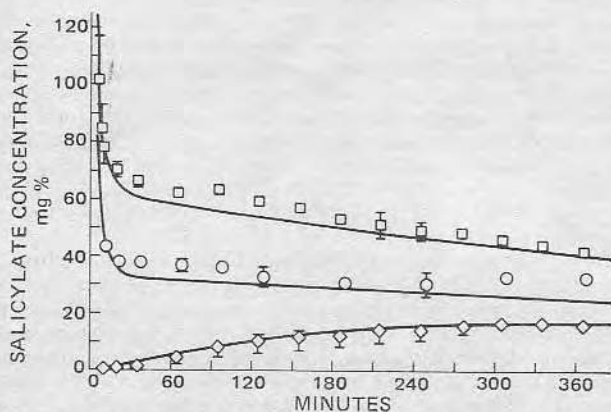


Figure 2—Predicted (solid lines) and experimental salicylate concentrations in plasma (\square), liver (\circ), and cerebrospinal fluid (\diamond) at a dose of 285 mg/kg (sodium salicylate).

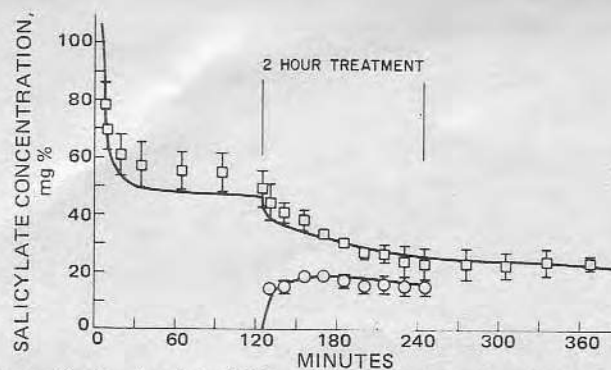


Figure 3—Predicted (solid lines) and experimental salicylate concentrations in blood under the influence of 2-hr hemoperfusion treatment at a dose of 285 mg/kg. Key: \square , inflow blood; and \circ , outflow blood.

Therefore, the pharmacokinetic behavior of salicylate in the body during the extracorporeal treatment also can be predicted by solving a system of 10 simultaneous equations.

RESULTS AND DISCUSSION

The values of parameters and constants necessary for solving the system of 10 simultaneous differential equations are shown in Table I and Scheme I.

Three different dosages of sodium salicylate were used: 135 mg/kg (therapeutic), 210 mg/kg (moderate intoxication), and 285 mg/kg (severe intoxication). Only the 285-mg/kg data are given here; data for the other dosages are available, however (10). Three or four mongrel dogs (15–25 kg) were evaluated with each dosage. An infusion pump was employed to infuse each dose at a constant rate over 5 min. A detailed description of the experimental method for quantitative studies on salicylate kinetics in cerebrospinal fluid, blood, plasma, liver, muscle, and adipose tissue is available (10).

The mean values ($\pm SD$) of the experimentally determined salicylate concentrations with time and the predicted pharmacokinetics (solid lines) by the model are shown in Figs. 1 and 2 for the 285-mg/kg dose. If a calculated standard deviation is within the size of a symbol representing a mean value, then the standard deviation is not shown in the figures. Time zero in the figures is the time just prior to infusing a dose. The good agreement between predicted kinetics and experimental data demonstrates model feasibility.

In an experiment with hemoperfusion treatment, a severely intoxicating dose (285 mg/kg) of sodium salicylate was administered intravenously to dogs (19–26 kg, average 23 kg) at a constant rate for 5 min. Two hours later, the poisoned dog was treated by an extracorporeal device containing 250 g (wet weight) of albumin-coated activated carbon¹ for 2 hr (10). The arterial blood from the femoral artery was shunted through the extracorporeal cartridge; salicylate in the blood was adsorbed by the carbon, and the outflow "clean" blood returned to the femoral vein.

The salicylate removal rate by hemoperfusion was calculated, as stated previously, in terms of the blood perfusion rate and the concentration difference between inflow and outflow blood samples (Fig. 3). The blood perfusion rate shunted from the femoral artery of a 23-kg (average) dog in the experiment (10) was kept at 100 ml/min by a blood pump. However, the physiological parameters employed in the pharmacokinetic modeling are based on a 15-kg (average) dog. Hence, the blood perfusion rate used in this model was adjusted to that for a 15-kg dog and gave 65 ml/min as the result of multiplying a ratio of the two body weights.

Figures 4–6 show the experimental kinetic data of salicylate levels (mean value $\pm SD$) in blood, plasma, muscle, adipose tissue, and cerebrospinal fluid and the predicted kinetics (solid lines) by the model under the effect of the 2-hr treatment. The kinetic changes of salicylate levels in the body during and after the hemoperfusion are also well predicted by the model with certain modifications in blood flows and in equations as expressed in the previous section.

The pharmacological effect of a drug is generally reflected better by the free (unbound) drug levels in blood or target organ(s). The relationships between free and total drug concentrations in blood and various

¹ Witco 517, Witco Chemical Co.

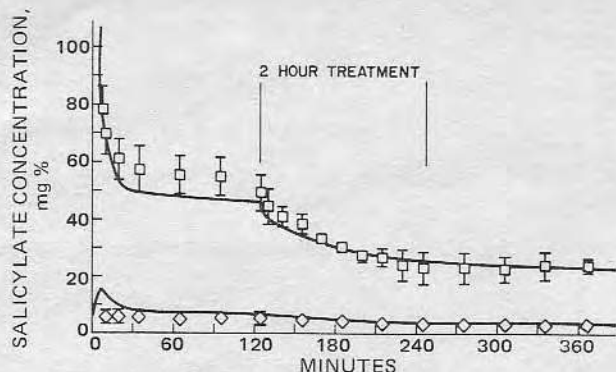


Figure 4—Predicted (solid lines) and experimental salicylate concentrations in blood (□) and adipose tissue (◇) under the influence of 2-hr hemoperfusion treatment at a dose of 285 mg/kg.

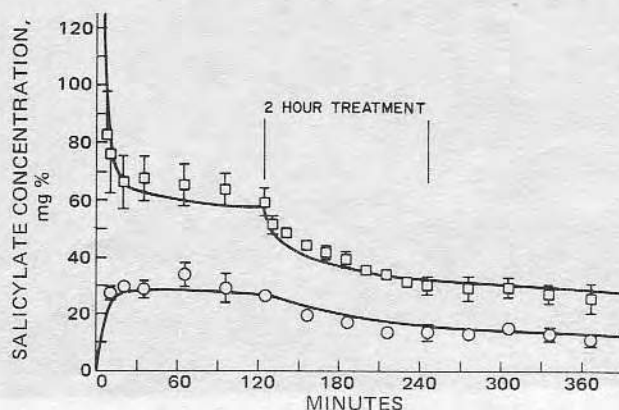


Figure 5—Predicted (solid lines) and experimental salicylate concentrations in plasma (□) and muscle (○) under the influence of 2-hr hemoperfusion treatment at a dose of 285 mg/kg.

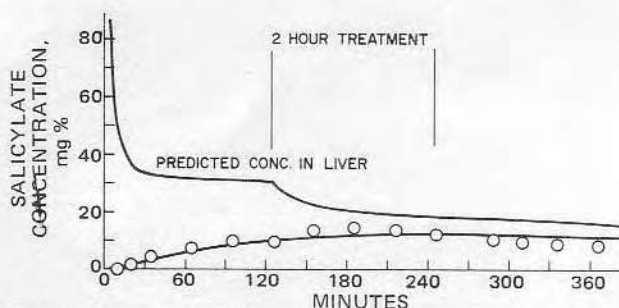


Figure 6—Predicted (solid lines) and experimental salicylate concentrations in cerebrospinal fluid (○) and liver under the influence of 2-hr hemoperfusion treatment at a dose of 285 mg/kg. No experimental data were obtained for liver as a result of heparin therapy being applied to the dog with the hemoperfusion treatment (10).

tissues were considered in constructing the equations for the model. Figures 7 and 8 show experimental (mean value \pm SD) and predicted (solid lines) kinetics of free and total salicylate levels in plasma with and without the hemoperfusion treatment. The results predicted by the model agree with the experimental data.

Curves and data comparable to those reported in Figs. 1-8 are also available for the 135- and 210-mg/kg doses (10).

CONCLUSIONS

Since knowledge of the kinetic behavior of a drug in blood or plasma may not provide sufficient information for appropriate therapy, kinetic information of drug levels in brain, cerebrospinal fluid, blood, organs, and tissues of pharmacological interest may be necessary for the development of improved dosage regimens. The pharmacokinetic model

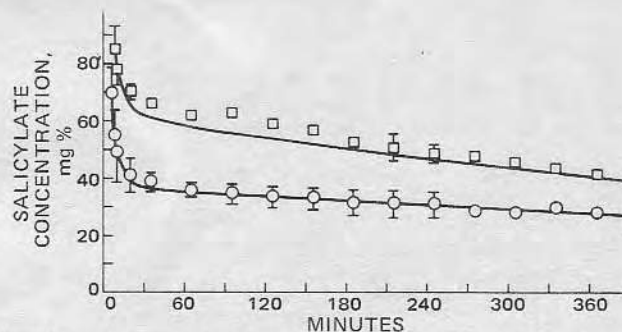


Figure 7—Predicted (solid lines) and experimental free salicylate concentration (○) and total salicylate concentration (□) in plasma at a dose of 285 mg/kg (sodium salicylate).

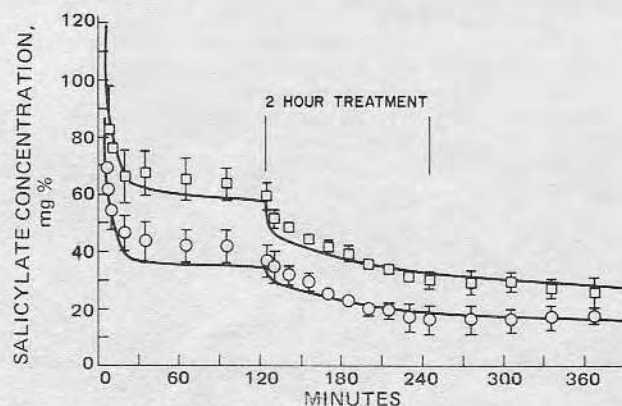


Figure 8—Predicted (solid lines) and experimental free salicylate concentration (○) and total salicylate concentration (□) in plasma under the influence of 2-hr hemoperfusion treatment at a dose of 285 mg/kg.

presented in this study can predict salicylate levels not only in blood or plasma but also in cerebrospinal fluid, liver, and other tissues. Conventional compartment models are unable to do so.

Free drug concentrations (variables to be solved) in all body regions (Scheme 1) are involved in Eq. 24 while the free drug concentration in the blood pool appears in the equation for each body region. Thus, each equation in a system of simultaneous differential equations is not independent but interrelated to the others. This feature of the model has an important application in clinical pharmacokinetics. If the model for a given drug can be verified in a species pharmacokinetically similar to humans, then it can be applied to predict pharmacokinetics of the drug in human blood, organs, and tissues of pharmacological importance by using the physiological and biochemical parameters of humans.

The experimentally observed kinetics of drug levels in blood or plasma may be used to compare with the corresponding kinetics predicted by the model. If they agree well, the model-predicted kinetics of drug distribution in the other body regions that are difficult to sample may be expected to represent closely the actual kinetic courses because of the interrelated characteristics of the equations. Therefore, the model can furnish more complete and valuable information for optimal therapeutic regimens. The model has been successfully applied to predict the pharmacokinetics of salicylate in the dog with and without extracorporeal activated carbon treatment.

REFERENCES

- (1) R. J. Lutz, R. L. Dedrick, J. A. Straw, M. M. Hart, P. Klubes, and D. S. Zaharko, *J. Pharmacokinet. Biopharm.*, **3**, 77 (1975).
- (2) C. N. Chen and J. D. Andrade, *J. Pharm. Sci.*, **65**, 717 (1976).
- (3) K. B. Bischoff and R. L. Dedrick, *ibid.*, **57**, 1346 (1968).
- (4) D. S. Zaharko, R. L. Dedrick, K. B. Bischoff, J. A. Longstreth, and V. T. Oliverio, *J. Natl. Cancer Inst.*, **46**, 775 (1971).
- (5) R. L. Dedrick, S. C. Zaharko, and R. J. Lutz, *J. Pharm. Sci.*, **62**, 882 (1973).
- (6) R. L. Dedrick, D. D. Forrester, J. N. Cannon, S. M. El Dareer, and L. B. Mellett, *Biochem. Pharmacol.*, **22**, 2405 (1973).

- (7) R. L. Dedrick, D. D. Forrester, and D. H. W. Ho, *ibid.*, **21**, 1 (1972).
- (8) A. Goldstein, L. Aronow, and S. W. Kalman, "Principles of Drug Action," 2nd ed., Wiley, New York, N.Y., 1974, p. 167.
- (9) J. G. Luft, in "The Inflammatory Process," B. W. Zweifach, L. Grant, and R. T. McCluskey, Eds., Academic, New York, N.Y., 1965, p. 121.
- (10) C. N. Chen, Ph.D. dissertation, University of Utah, Salt Lake City, Utah, 1976.
- (11) S. A. Duwe, G. L. DeNardo, M. A. Helikson, K. S. Watanabe, and L. G. Crowley, *Surg. Forum*, **21**, 376 (1970).
- (12) J. G. Gibson, A. M. Seligman, W. C. Peacock, J. C. Aub, J. Fine, and R. D. Evans, *J. Clin. Invest.*, **25**, 848 (1946).
- (13) V. A. Levin and D. D. Gilboe, *Stroke*, **1**, 270 (1970).
- (14) M. T. Velasquez, A. V. Notargioacomo, and J. N. Cohn, *Am. J. Physiol.*, **224**, 322 (1973).
- (15) E. G. Ohlsson, R. B. Rutherford, M. M. P. Haalebos, H. N. Wagner, and G. D. Zuidema, *J. Surg. Res.*, **10**, 201 (1970).
- (16) W. J. Kane and E. Grim, *J. Bone Joint Surg.*, **51**, 309 (1969).
- (17) P. A. Nielsen and N. J. Secher, *Life Sci.*, **9**, 75 (1970).
- (18) U. Finsterer, P. Pruchsunand, and H. Brechtelsbauer, *Pfluegers Arch. Eur. J. Physiol.*, **341**, 63 (1973).
- (19) C. Davison and P. K. Smith, *J. Pharmacol. Exp. Ther.*, **133**, 161 (1961).
- (20) L. E. Davis and B. A. Westfall, *Am. J. Vet. Res.*, **33**, 1253 (1972).
- (21) S. Mayer, R. P. Maickel, and B. B. Brodie, *J. Pharmacol. Exp. Ther.*, **127**, 205 (1959).
- (22) B. B. Brodie, H. Kurz, and L. S. Schanker, *ibid.*, **130**, 20 (1960).
- (23) D. P. Rall, in "Fundamentals of Drug Metabolism and Drug Disposition," B. N. LaDu, H. G. Mandel, and E. L. Way, Eds., Williams & Wilkins, Baltimore, Md., 1971, p. 76.
- (24) B. Carnahan, H. A. Luther, and J. O. Wilkes, "Applied Numerical Methods," Wiley, New York, N.Y., 1969, p. 361.

ACKNOWLEDGMENTS

Supported by National Institutes of Health Grant FD 00480-03 and National Science Foundation Grant GH 38996X.

The assistance of Dr. S. M. Fang, C. M. Chen, and A. Atwood is gratefully acknowledged.

Effect of Reductive Methylation on the Adsorption of Hen Lysozyme

Labeled proteins are commonly used to study active sites, binding interactions, protein adsorption, and interactions at interfaces. Two commonly used protein radiolabeling techniques are iodination and reductive alkylation. Radioiodination results in the formation of iodotyrosine and iodotryptophan groups (1). Reductive methylation results in the labeling of epsilon amino and terminal amine groups with tritiated methyl groups (1, 2). Recently several reports have pointed out that iodination may affect ligand binding, adsorption to solid surfaces, and chromatographic behavior (3-6).

We report a change in the adsorption of lysozyme dependent on the degree of reductive methylation. The enzymatic activity was unaffected by the labeling procedure.

Crystallized hen egg white lysozyme (Cal Biochem), tritiated formaldehyde (100 mCi/mole, New England Nuclear), *Micrococcus lysodeikticus* cell walls (Sigma Chemical), and Sephadex G-25 (Pharmacia Fine Chemicals) were used as received. Sodium cyanoborohydride (NaCNBH_3 , Aldrich Chemicals) was recrystallized as described by Jentoff and Dearborn (2). Borosilicate glass coverslips were purchased from Gold Seal. Preparation of clean glass coverslips followed a cleaning protocol consisting of: (1) scrubbing in Micro detergent

(International Product Corp.); (2) a 20-min soak in 70°C dichromate-sulfuric acid bath; (3) four separate 5-min rinses in double-distilled filtered water; (4) two 5-min rinses in absolute ethanol; (5) followed by vapor degreasing in trifluorochloroethanol (freon) vapor for 10 mins. The ultraclean glass coverslips were then given a 2-min radiofrequency glow discharge (RFGD) in an oxygen plasma at 35 W tuned radiofrequency power using 200 μm Hg oxygen pressure in a commercial RFGD unit (Tegal Scientific) followed by a 10-min purge in oxygen (99.999%). All cleaning was performed in a clean room. The cleaned coverslips were hydrophilic as determined by contact angle measurements (7). The coverslips were used directly or coated with *n*-pentyl triethoxy silane (NPS, Petrarch System) for use as a hydrophobic surface.

Hydrophobic glass surfaces were prepared by vapor silanization using NPS. A round bottom flask containing 10 ml NPS, 300 ml of *p*-xylene, 3 ml of lutidine, and a stirring bar was encircled by a heating mantle. The top of the vapor chamber had a lid and condensor attached. The reaction was allowed to reflux for 16 hr followed by another 16-hr reflux with 300 ml of toluene. The Wilhelmy plate technique was applied for contact angle measurement (7, 8); light microscopy was used

TABLE I
Degree of Labeling Effects on Adsorption and Enzymatic Activity of Hen Egg White Lysozyme^a

Labeling level	Unlabeled	Low	Medium	High
Degree of labeling (# of tritiated methyl groups/lysozyme)	0	0.0073 \pm 0.0003	0.107 \pm 0.002	1.37 \pm 0.02
Specific activity (dpm/ μg)	0	115 \pm 5	1710 \pm 30	27,700 \pm 300
Amount adsorbed ^b dpm/cm ²				
Hydrophilic	—	22 \pm 1	272 \pm 5	2915 \pm 65
Hydrophobic	—	32 \pm 3	366 \pm 5	4537 \pm 284
$\mu\text{g}/\text{cm}^2$				
Hydrophilic	—	0.19 \pm 0.01	0.16 \pm 0.01	0.13 \pm 0.01
Hydrophobic	—	0.28 \pm 0.02	0.21 \pm 0.01	0.21 \pm 0.01
Specific enzyme activity ^c ($\mu\text{g}/\text{min}/\text{mg}$)	1600 \pm 100	1650 \pm 150	1700 \pm 100	1650 \pm 100

^a Values are the average of three replicates \pm 1 standard deviation.

^b Amount adsorbed at 100 minutes in micrograms/cm² = (dpm/cm²)/specific activity (dpm/ μg).

^c In micrograms cell walls catalyzed/minute/milligram lysozyme.

to check for surface defects and particulates; X-ray photoelectron spectroscopy (XPS) was used to analyze the surfaces (9).

The surface of the glass coverslips examined by optical stereomicroscopy showed no gross defects. Contact angle measurement for NPS-coated coverslips had a receding angle of 58° and an advancing angle of 76° assuming the surface tension of water to be 72.6 dynes/cm (11). XPS data confirmed that the NPS-coated coverslips were silanized (11).

Radiolabeled lysozyme was prepared by reductive methylation (10) with slight modifications. Hen egg lysozyme in phosphate-buffered saline (PBS, 1.14 g $\text{Na}_2\text{HPO}_4 + 0.22 \text{ g } \text{KH}_2\text{PO}_4 + 8.5 \text{ g } \text{NaCl}$ to 1 liter), at a concentration of 3 mg/ml, was reacted with tritiated formaldehyde ($[^3\text{H}]\text{CHO}$) at concentrations of 3.32×10^{-6} , 3.27×10^{-5} , and $3.64 \times 10^{-4} \text{ mM}$ for low, medium, and high labeling, respectively. Sodium-CNBH₃ was added prior to addition of formaldehyde as a concentrated solution in PBS to give a final concentration of 20 mM. The mixture was allowed to react for 24 hr at 4°C with mild stirring. The reaction was then stopped

by passage through a Sephadex G-25 column pre-equilibrated with PBS buffer. A fraction collector was used in collecting 3.5-ml fractions of the elutant. A 25- μl aliquot of each fraction was then added to 10 ml of Aquasol II (New England Nuclear) and counted on a Beckman LS-9000 liquid scintillation counter (10 min or 2τ error, 53% efficiency). An unquenched tritiated standard in toluene was used as a calibration for window settings. The elution profile of $[^3\text{H}]\text{lysozyme}$ was plotted and $[^3\text{H}]\text{lysozyme}$ fractions were pooled. After dilution of the $[^3\text{H}]\text{lysozyme}$ solution to the desired concentrations with PBS, an aliquot was counted to determine its specific activity. The $[^3\text{H}]\text{lysozyme}$ concentrations were determined by absorbance measurements at 280 nm using a Beckman model 35 UV-visible spectrophotometer with PBS as reference. The molar extinction coefficient was determined as $3.1 \times 10^4 \text{ M}^{-1}$. The molecular weight used for the calculations was $1.39 \times 10^4 \text{ g/mole}$. The specific activity was expressed as dpm/ μg of labeled lysozyme (dpm, disintegrations/minute). The degree of labeling was expressed as number of tritiated methyl groups per molecule of lysozyme (Table I).

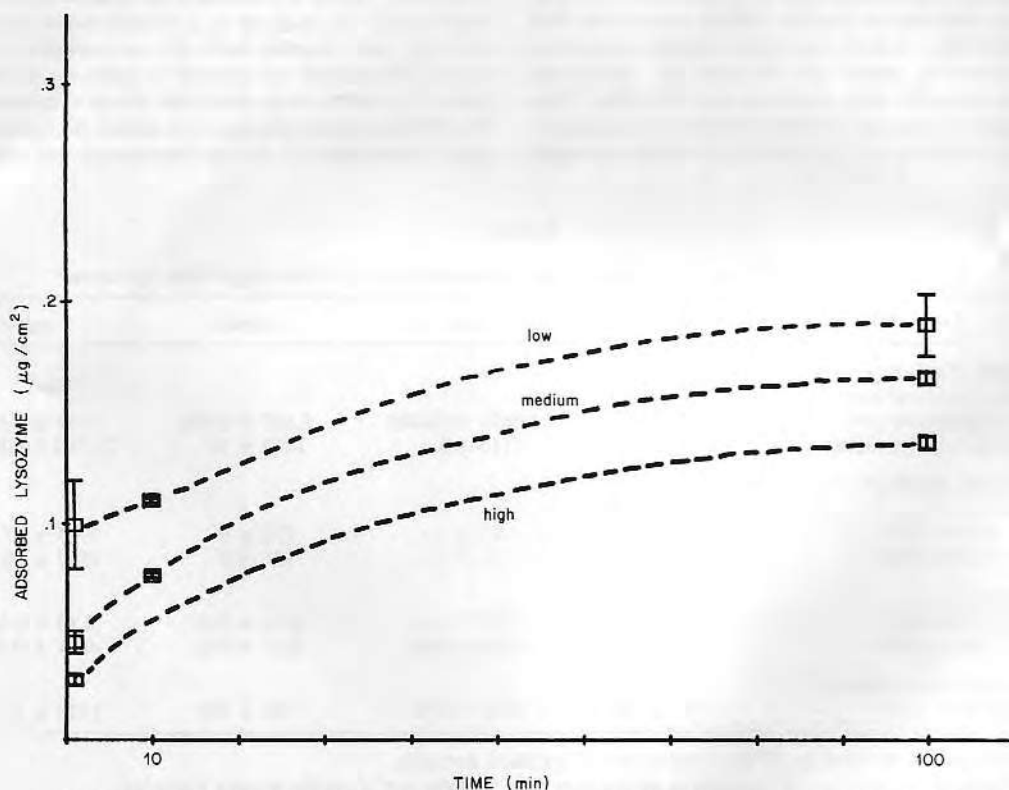


FIG. 1. Effect of degree of labeling (Table I) on the adsorption of $[^3\text{H}]\text{lysozyme}$ onto hydrophilic glass surfaces at 1, 10, and 100 min. Solution: 1.5 mg/ml lysozyme in PBS, pH 7.4. The values are the average of three replicates—error bars represent one standard deviation. Note that increasing the degree of labeling results in apparent adsorption, which is interpreted as the labeled protein adsorbing preferential to the unlabeled protein (5).

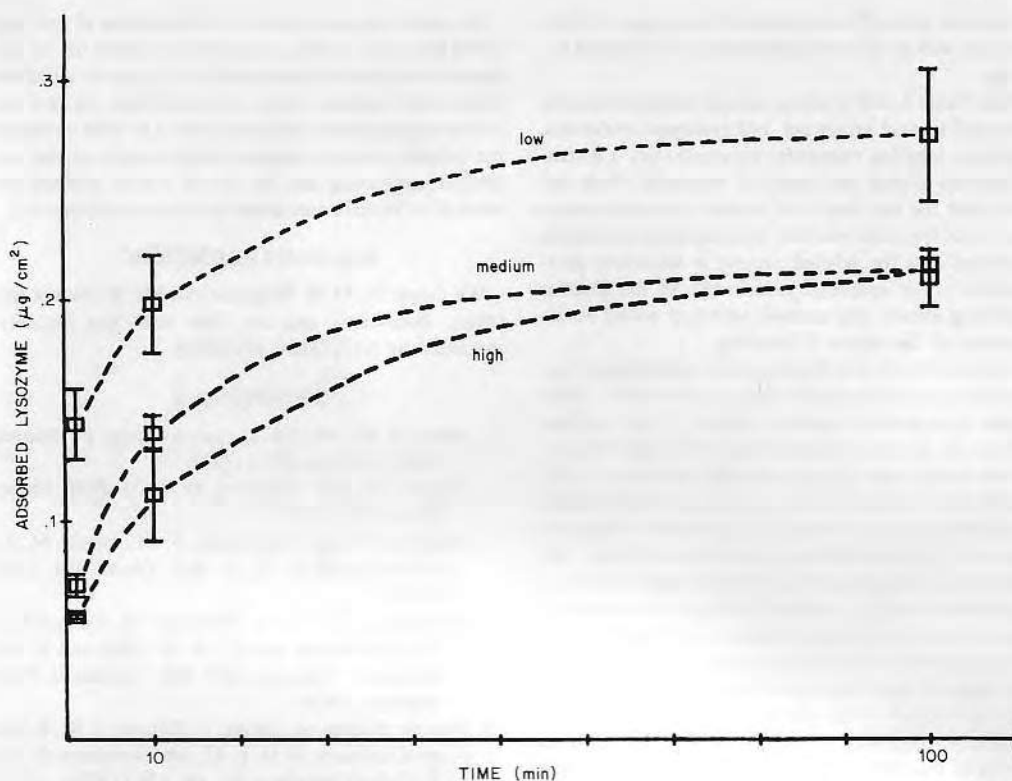


FIG. 2. Effect of degree of labeling (Table I) on the adsorption of $[^3\text{H}]$ lysozyme onto hydrophobic glass surfaces at 1, 10, and 100 min adsorption. The values are the average of three replicates—error bars represent one standard deviation. See legend to Fig. 1.

Labeled lysozyme (0.75 mg/ml) in PBS was characterized by taking the UV absorption spectrum of lysozyme between 350 to 250 nm with PBS buffer as reference. Circular dichroic (CD) spectra were obtained using a Jasco J-40A at room temperature with PBS buffer used for baseline adjustment (path length 1 cm; concentration 0.1 mg/ml; sensitivity 0.2 m°/cm; time constant 64 sec; scale 5 nm/cm; chart speed 0.5 cm/min; slit width 1 dm). The CD spectra was obtained from 250 to 210 nm. Emission fluorescence spectra (0.1 mg/ml) were obtained using an Aminco Bowman spectrophotofluorometer at room temperature with PBS buffer as reference. Emission spectra were recorded from 300 to 800 nm with the excitation wavelength set at 280 nm. No observable conformational changes were detected by UV, fluorescence, or CD methods.

The enzymatic activity of labeled and unlabeled lysozyme was measured at room temperature in 3-ml cuvettes containing 2.5 ml of *Micrococcus lysodeikticus* cell wall suspension (100 μg/ml in PBS). The reaction was allowed to proceed by adding 15 μg of lysozyme to the substrate suspension followed by rapid mixing. The specific enzymatic activity was determined by a turbidity measurement at 320 nm and reported as μg substrate catalyzed/min/mg lysozyme (Table I).

The adsorption experiments were performed at 20°C using the prepared glass surfaces and appropriately diluted labeled lysozyme solutions. All glass coverslips were hydrated in PBS buffer for 12 hr prior to the experiment. The adsorption was performed in 24-well disposable polystyrene tissue culture dishes (Falcon #3008). Each well contained 1.5 ml of labeled lysozyme in PBS. One glass coverslip was placed in each well. After the appropriate adsorption time, the glass coverslip was advanced to each of six different wells containing 1.75 ml PBS for rinsing of the excess bulk adsorbed protein; each "rinse" lasted 5 min. When the final rinse was completed, the glass sample was placed in a scintillation vial containing 10 ml of Aquasol fluor and the radioactivity counted. The amount of adsorbed lysozyme was calculated as μg of protein deposited per cm² surface area of glass coverslip. Since the glass coverslips consisted of highly smooth surfaces, only the geometric or apparent area was used for the calculation of total surface area.

The adsorption studies were performed using a matrix consisting of three different degrees of lysozyme labeling, three different adsorption time periods, and two different glass surfaces. The results are shown in Fig. 1 for hydrophilic glass and in Fig. 2 for NPS silanized

hydrophobic glass. The values are the average of three replicates with error bars representing one standard deviation.

From Table I, low labeling represents approximately 1 tritiated methyl group per 140 lysozyme molecules, while high labeling represents approximately 1.4 tritiated methyl groups per lysozyme molecule. From the above data the low degree of labeled lysozyme results in a greater apparent adsorbed amount on both surfaces, suggesting that the labeled protein is adsorbing preferentially to the unlabeled protein (5). In the absence of labeling effects, the amount adsorbed would be independent of the degree of labeling.

Lysozyme is a highly basic protein containing six epsilon amino groups exposed at the protein surface. There is some hydrophobic character evident at the surface, however, as demonstrated by Klotz (12). Since the reductive methylation reaction results in mono- or dimethylation of epsilon amino groups, one might expect some change in ionic interactions and some change in the overall hydrophobic character of the molecule. The hydrophobic change must occur in the near vicinity of the positively charged groups. Since reductive methylation adds a methyl group but does not change the overall charge of the epsilon amino groups, this suggests that there might be some ionic-hydrophobic interaction synergism as a result of the methylation process. This has been discussed briefly by Warshel in his discussion of the role of hydrophobic environments in ionic interactions in enzyme active sites (13). The fact that the experimental results show that the labeled protein adsorbs preferentially on a hydrophilic negatively charged glass surface suggests that the methylation reaction may actually increase the ionic interaction between lysozyme and the negative glass surface, perhaps via the Warshel mechanism (13). Based on hydrophobic considerations alone, one would expect that the methylated protein would adsorb to a greater extent than the native lysozyme on the hydrophobic surface; and this is in fact what is seen.

The overall higher amount of adsorption on the hydrophobic surface is also of considerable interest. Since the lysozyme surface has some nonpolar character, this may indicate the involvement of the polar glass substrate showing through the silane-treated glass surface. If the glass surface was not fully covered with the silane, if there are some bare glass patches on a microscopic scale, this could result in a synergistic interaction, coupling hydrophobic and ionic interactions which could result in an increased overall adsorption. All of this is speculative at this point.

The degree of labeling appears to have no significant effect on the biological enzymatic activity (Table I), confirming that the methylation is occurring largely on the surface of the protein through the surface epsilon amino groups and not in the active site or in the vicinity of the active site.

In conclusion, the reductive methylation of hen egg white lysozyme results in significant effects on its adsorption behavior on hydrophilic and *n*-pentyl silanized hydrophobic surfaces when adsorbed from purified solutions in phosphate-buffered saline. On both surfaces, the labeled material adsorbs preferentially to the unlabeled, suggesting that the use of labeled proteins for adsorption experiments must be treated with caution.

ACKNOWLEDGMENTS

We thank Dr. D. E. Gregonis and Mr. R. Stoker for advice, discussions, and aid. This work was partially supported by NIH Grant HL18519.

REFERENCES

1. Koch, G. K., Heertje, I., and van Stijn, F., *Radiochim. Acta* **24**, 215 (1977).
2. Jentoft, N., and Dearborn, D. G., *J. Biol. Chem.* **254**, 4359 (1979).
3. Koshland, M. E., Englberger, F. M., Erwin, M. J., and Gaddone, S. M., *J. Biol. Chem.* **238**, 1343 (1963).
4. Greenwood, F. C., in "Principle of Competitive Protein Binding Assay" (W. D. Odell and W. H. Daughady, Eds.), pp. 288-296. Lippincott, Philadelphia, 1971.
5. Van der Scheer, A., Feijen, J., Elhorst, J. K., Krugers-Dagneaux, P. G. L. C., and Smolders, C. A., *J. Colloid Interface Sci.* **66**, 136 (1978).
6. Crandall, R. E., Janatova, J., and Andrade, J. D., *Prep. Biochem.* **11**, 111 (1981).
7. Smith, L., Doyle, C., Gregonis, D. E., and Andrade, J. D., *J. Appl. Polym. Sci.* **26**, 1269 (1982).
8. Johnson, R. E., Jr., and Dettre, R. H., *Surface Colloid Sci.* **2**, 85 (1969).
9. Clark, D. T., and Feast, W. J., *J. Macromol. Sci.-Rev.* **C12**, 191 (1975).
10. Jentoft, J. E., Jentoft, N., Gerken, T. A., and Dearborn, D. G., *J. Biol. Chem.* **254**, 4366 (1979).
11. Stoker, R., Master Thesis, University of Utah, Salt Lake City (1981).
12. Klotz, I. M., *Arch. Biochem. Biophys.* **138**, 704 (1970).
13. Warshel, A., *Proc. Nat. Acad. Sci. USA* **75**, 5250 (1978).

J. CHEN
D. E. DONG
J. D. ANDRADE¹

Department of Bioengineering
University of Utah
Salt Lake City, Utah 84112

Received December 10, 1981; accepted January 22, 1982

¹ To whom correspondence and reprint request should be addressed.

Oxy- and deoxyhaemoglobin adsorption onto glass and polymer surfaces

Jie Chen*, J.D. Andrade[†] and R.A. VanWagenen

Department of Bioengineering, College of Engineering, University of Utah, Salt Lake City, Utah 84112, USA
(Received 9 July 1984; revised 29 October 1984)

The adsorption of deoxyhaemoglobin (deoxyHb) and oxyhaemoglobin (oxyHb) was determined on clean glass, *n*-pentyl triethoxysilane (NPS)-treated glass, polystyrene (PS), and a polyetherurethane (PEU). The adsorbed amounts range from 0.1 to 0.6 $\mu\text{g}/\text{cm}^2$ for oxyHb and from 0.3 to 0.7 $\mu\text{g}/\text{cm}^2$ for deoxyHb. DeoxyHb adsorbs onto all these surfaces more than oxyHb. The more hydrophobic the surface, the more adsorption of both deoxy and oxyHb forms.

These results suggest the oxyHb and deoxyHb interact differently with the surfaces studied. It is likely that the surface hydrophobicity of Hb plays a major role in Hb adsorption onto surfaces; the deoxyHb surface is more hydrophobic than the oxyHb surface. The binding sites for Hb adsorption may include the clefts between α_1 , β_1 . A surface-induced dimerization mechanism is proposed to explain the adsorption of oxyHb.

Keywords: Adsorption, deoxyHb, oxyHb, glass surface, polymer surface, haemoglobin

Horbett has reported¹ that Hb readily adsorbs on apolar surfaces and that this is totally out of proportion to its solution concentration. Surface enhancements range from 10 to 100-fold that of other plasma proteins. Later, Pierce² studied the adsorption of various ligand forms of Hb on partially hydrophobic alkyl agarose substrates and found that the adsorption of Hb is dependent on the ligand state of the molecule.

Recently Coleman and others in the Artificial Heart Group at Utah observed significant surface discolouration in retrieved artificial heart implants, which appeared to correlate with regions of turbulence, and perhaps local haemolysis, and with actual pumping diaphragm abrasion, resulting in local haemolysis³. They suggest that the colouration may be due to heme by-products.

It is generally accepted that implants in the arterial and venous systems behave differently, perhaps due to pO_2 , pH, pressure, and/or flow differences, but perhaps also due to different ligand forms of the Hb which may be present.

It is clear that blood contact with foreign surfaces, even under mild flow conditions, results in local haemolysis, in large part dependent on specific surface interactions⁴. Thus Hb may be present in sufficient concentration at local regions where sublethal haemolysis occurs, even though the systemic concentration of the protein may be very low.

The **haemoglobin hypothesis** is formulated as follows: If there exist regions of local turbulence or other trauma which can result in local Hb release, released Hb

may adsorb onto foreign surfaces in concentrations orders of magnitude greater than one would expect based on the solution concentration. Hb released on the venous side (in the deoxy form) may adsorb significantly differently from Hb released on the arterial side (in the oxy form). This behaviour, if it occurs *in vivo*, may be in part responsible for the different blood compatibility of implants in the venous and arterial system.

If surfaces containing oxy or deoxyHb, haptoglobin (Hp) or the oxyHb-Hp complex show different blood interactions, then surfaces designed for arterial compatibility may require different properties from those destined for venous application. It may also be that in a complex cardiovascular device where there are regions of local blood turbulence, the surface properties in local regions of blood trauma may even need to be different from the surface properties in other regions of the device.

We present here preliminary data on the adsorption of oxy and deoxyHb to a set of surfaces.

HAEMOGLOBIN

Ferrous Hb can exist in oxy and deoxy forms. The oxyHb has four oxygen molecules bound to the four oxygen binding sites. The binding sites of deoxyHb are empty. For a detailed description of the oxygenation mechanism and the various forms of Hb, see Reference 5.

The dimensions of Hb are approx. $64 \times 55 \times 50 \text{ \AA}$. All ionizable groups are in the aqueous environment and the hydrophobic groups are generally in the interior⁶. Hydrophobic clefts are exposed to the aqueous environment and, in view of the dynamics of protein structures, these clefts can instantaneously produce a hydrophobic

*Submitted in partial fulfilment of the requirements of the MSc degree in Bioengineering, University of Utah.

[†]To whom all correspondence and reprint requests should be directed.

surface patch. Polar groups within the protein are involved in stabilizing the structure through hydrogen bonds and salt bridges⁵.

The contacts between dissimilar chains ($\alpha_1\beta_2$, $\alpha_1\beta_1$, $\alpha_2\beta_1$, $\alpha_2\beta_2$) are hydrophobic in nature while contacts between similar chains ($\alpha_1\alpha_2$, $\beta_1\beta_2$) are more polar in nature. Upon oxygenation, the β chains rotate apart by about 7 Å, exposing polar contacts between similar chains ($\alpha_1\alpha_2$, $\beta_1\beta_2$)⁵. Upon oxygenation, 8 salt bridges are ruptured; the carboxyl terminus of both α and β are then free to rotate; they are not rotationally free in deoxyHb. These freely rotating carboxyl terminal amino acids now have different pKa's as a result of the different micro-environments and are associated with the Bohr effect — the release of protons upon oxygenation. The ligand binding affinity of partially oxygenated Hb increases owing to the rotations of the carboxyl terminal ends of the polypeptides, thereby reducing the steric hindrance present for the approach of subsequent binding ligands to the remaining unbound heme groups. This accounts for the allosteric cooperativity of Hb. The iso-ionic points of oxyHb and deoxyHb at 20°C are reported to be between 6.7 and 6.9⁷.

The surface hydrophobicity of deoxyHb is higher than that of oxyHb because: (i) Upon deoxygenation, the β chains rotate together by 7 Å, burying many polar contacts; (ii) DeoxyHb has 8 salt linkages which reduce the surface hydrophilicity by decreasing surface polar groups which would otherwise interact with the polar environment; (iii) DeoxyHb has a larger internal cavity than does oxyHb⁹. DeoxyHb is taut or tensed on the surface because of the salt linkages; this tends to 'squeeze' more hydrophobic clefts to the surface to form hydrophobic patches.

The deoxy form has a larger central cavity and an increased surface hydrophobicity. Although the dimer forms are not normally present (the dimer-tetramer equilibrium results in the tetramer form under most practical solution conditions), solid surface-induced dimerization may occur. Based on proton exchange studies of adsorbed oxyHb, Hallaway¹⁰ proposed that in order to optimize polar interactions with hydrophilic surfaces, the molecule may distort, resulting in surface dimers, which can then re-accommodate and even desorb. This probably only occurs with oxyHb on a charged, hydrophilic surface. The surface hydrophobicity of deoxyHb, coupled with the 8 internal salt bridges, make such a process unlikely. The $\alpha_1\alpha_2$ and $\beta_1\beta_2$ contacts in oxyHb are polar. Polar interactions with the surface reduce $\alpha_1\alpha_2$ and $\beta_1\beta_2$ interactions, promoting the surface dimerization.

In this preliminary study, oxyHb and deoxyHb were adsorbed onto four different surfaces, using a radiolabelling technique. The results suggest deoxyHb and oxyHb interact differently with the surfaces studied.

MATERIALS AND METHODS

Sodium cyanoborohydride (NaCNBH_3) (Aldrich Chemicals) was recrystallized as described by Jentoff and Dearborn¹¹; tritiated formaldehyde (100 mCi/mol) was obtained from New England Nuclear. Other materials included: borosilicate glass coverslips and glass vials (Kimble), *n*-pentyl triethoxysilane (NPS, Petrach Systems); polystyrene (PS, Scientific Products, Inc., Webster, NY); polyether-urethane (PU, Biomer, Ethicon, New Jersey); and Sephadex G-25 (Pharmacia Fine Chemicals).

OxyHb was prepared by a modification of the method of Antonini *et al.*¹². Blood was collected into a flask containing 2% sodium citrate and then diluted 1:5 with 1% NaCl. After centrifuging at 10°C for 15 min at 750 g, the supernatant was discarded and the red cells resuspended in 1% NaCl. This process was repeated 2–4 times. The cells were then lysed by adding to cold distilled H_2O and stirred mildly in the cold for 30 min. After centrifuging at 4°C for 30 min, at 20 000 g, the supernatant was collected. EDTA 10^{-5} M (final concentration) was added. The purified material is more than 95% Hb, the impurities being primarily red cell enzymes¹².

Radiolabelled oxyHb was prepared by reductive methylation¹³. The oxyHb solution was diluted to 3 mg/ml and then reacted with tritiated formaldehyde. NaCNBH_3 (3.27×10^{-5} mM) was added prior to the addition of 20 mM formaldehyde as a concentrated solution in PBS. The mixture was allowed to react for 24 h at 4°C with mild stirring. The reaction was then stopped by passage through a Sephadex G-25 column pre-equilibrated with PBS buffer and the Hb-containing fractions were collected. After dilution of the haemoglobin solution to the desired concentrations with PBS, a 25 μl aliquot of each fraction was added to 10 ml of Aquasol II (New England Nuclear) and counted on a Beckman LS-9000 liquid scintillation counter to determine the specific activity (10 min or 2% error; 53% efficiency). An unquenched tritiated standard in toluene was used as a calibration for window settings and efficiency determination.

DeoxyHb was prepared by equilibrating a solution of 1 mg oxyHb/ml PBS with N_2 gas for 30 min in a glove bag. Then 3 μg of $\text{Na}_2\text{S}_2\text{O}_4$ were added and mixed well, resulting in 100% deoxygenation of oxyHb. This was the stock deoxyHb solution.

Protein concentration was determined by absorbance measurements at 576 nm for oxyHb (molar extinction coefficient = $1.58 \times 10^{-4} \text{ cm}^{-1} \text{ M}^{-1}$)¹². The molecular weight used for the Beer's Law calculation was 16 000 g/mol.

Hb was characterized by taking the u.v.-visible absorption spectrum between 300 and 600 nm with PBS buffer as reference. Circular dichroic spectra were obtained using a Jasco J-40A, at room temperature, with PBS buffer used for baseline adjustment (path length 0.1 cm; conc. 1 mg/ml; sensitivity 5 m^0/cm ; time constant 4 s; wavelength expansion 10 nm/cm; chart speed 0.5 cm/min; slit width 1 dm). The CD spectra were obtained from 250 to 210 nm to determine mean residue ellipticities and secondary structure. The mean residue weight used was 114 g.

Regular and SDS polyacrylamide gel electrophoresis followed a discontinuous gel procedure described by Laemmli¹⁴. In this study, the following conditions were used: 3.7% upper gels; 7.5% lower gels; 3 μg oxyHb/well; Coomassie Brilliant Blue dye R-250 as a staining dye; 30 ma/40 V/60 min for stacking, 40 ma/170 V for running condition.

Glass coverslips were cleaned by scrubbing in Micro Detergent (International Product Corp.), followed by a 20 min soak at 70°C in a dichromate sulphuric acid. Four separate 5 min rinses in filtered double-distilled water

were followed by two 5 min rinses in absolute ethanol. The samples were then vapour degreased in trifluoro-chloroethanol (freon) vapour for 10 min followed by a 2 min radiofrequency glow discharge (RFGD) in an oxygen plasma at 35 W tuned radiofrequency power using 200 μ m Hg oxygen pressure in a commercial RFGD unit (Tegal Scientific), followed by a 10 min purge in oxygen (99.999%). All cleaning was performed in a restricted access clean room.

Hydrophobic glass surfaces were prepared by vapour silanization using NPS. A round bottomed flask containing 10 ml NPS, 300 ml of *p*-xylene, 3 ml of lutadine, and a stirring bar was encircled by a heating mantle. The top of the vapour chamber had a lid and condenser attached. The reaction was allowed to reflux for 16 h followed by another 16 h reflux with 300 ml of toluene.

Polymer surfaces were prepared by spin coating. Two drops of PS solution (3 wt% in toluene) were placed in the centre of the clean glass coverslip, which was mounted on a spin casting apparatus (Model EC101, Headway Research, Inc., Garland, TX). The sample was spun at 4000 rpm for 15 s to provide a smooth spin cast film. The polyether urethane (Biomer, Ethicon) was dip-coated from a 3% solution in *N,N*-dimethyl acetamide (DMAC). A dipping rate of 1 in/min was used.

After preparation, the samples were stored in a vacuum desiccator.

Surface characterization included the Wilhelmy plate advancing and receding contact angle technique for surface wetting characteristics¹⁵. A disc shaped glass coverslip was directly measured and the receding or advancing angle was calculated at its diameter¹⁹. Light microscopy was used to check for surface defects and particulate contamination. X-ray photoelectron spectroscopy was used for general surface analysis¹⁶.

The deoxyHb adsorption experiments were run at 20°C in a glove bag filled with N₂ gas using the prepared surfaces and appropriately diluted deoxyHb solutions.

All the samples were hydrated in phosphate-buffered saline (PBS) for 12 h before running the experiment¹⁹. The experiments were performed in disposable glass vials. The sample was placed in a vial containing 0.5 ml of PBS with one glass bead underneath the sample to prevent contact with the bottom of the vial. Hb solution was added to the 0.5 ml PBS in the vial to give the desired final concentration in a total volume of 2 ml.

After the appropriate adsorption time at 20°C, the 9 vials were connected to a nine-channel rinser¹⁹, and rinsed with 45 ml PBS per vial for 30 s. The sample was then picked up by a pair of tweezers and put in a scintillation vial which was filled with counting medium and the radioactivity measured¹⁹.

The amount of adsorbed Hb was calculated as nanograms (ng) of protein deposited per cm² surface area.

RESULTS AND DISCUSSION

Preparation and characterization of Hb and surfaces

Hb was characterized by u.v.-vis absorption spectroscopy. The addition of 3 μ g Na₂S₂O₄ to 1 mg oxyHb/ml PBS modifies the bimodal spectrum (maximum absorption peaks at 540 and 575 nm) to peak with a maximum

absorption of 565 nm, representing 100% deoxygenation¹². Some researchers¹⁷ deoxygenate by degassing or by N₂ equilibration. Unfortunately, both methods result in partially deoxygenated Hb and the degree of deoxygenation is not easy to control. The Na₂S₂O₄ method has been widely used¹² because of its ease, speed, and reproducibility; however, after deoxygenation the Na₂S₂O₄ will form a peroxide product (H₂O₂), presenting the danger of side reactions and damage to the haemoglobin molecule. A good policy is to remove most of the oxygen prior to the addition of Na₂S₂O₄ and to use dithionite only in slight molar excess [a general guideline is less than 0.1% (w/v)]¹². Dithionite is well tolerated in the visible region of the spectrum, but may cause disturbances below 400 nm¹². In this study, the u.v.-vis spectra did not show any detectable absorption by Na₂S₂O₄ due to the very low Na₂S₂O₄ concentrations used. Circular dichroic (CD) spectra (200–245 nm) showed no significant differences between labelled and unlabelled Hb. OxyHb has a different spectrum from deoxyHb. Electrophoresis was done using regular polyacrylamide gel and reduced SDS gels. No other protein bands were detected.

Water contact angles, obtained by the Wilhelmy plate technique, of the four different surfaces (clean glass, NPS, PS, and PU, are given in Table 1). The PS is very hydrophobic, while the clean glass coverslip is very hydrophilic. PU shows some hydrophobic and hydrophilic characters, NPS shows hydrophobic character, which is less than the PS surface.

The contact angles are measured after 1 h of equilibration in PBS buffer. All surfaces showed some degree of hysteresis, especially PS. The advancing and receding angles for PS become closer after 1 h soaking. The reason could relate to the imperfection of the PS film or permeation of water into the film. X-ray photoelectron spectroscopy (XPS) was used for surface composition analysis. C, N, Si, and O ratios indicated that all surfaces had the expected surface chemistry¹⁹.

Adsorption of Hb

Tritium labelling is a very sensitive method for quantitating protein adsorption. One of the problems of protein adsorption is the reproducible handling of the samples: whether they have been treated under the same conditions, e.g. incubation and rinsing conditions. Do they pick up denatured protein at the air/water interfaces? How efficiently can the samples be handled in order to allow several replicates, treatments, and controls to be done at the same time?

In this study, a multi-channel automatic rinsing system was developed to fulfil these requirements¹⁹. This device is calibratable, does not need a power supply, is easy to use and cheap to create. The rinsing is dropwise, gentle, and equal in each vial. Nine channels were easily handled. The device is useful for handling radioactive or biohazard materials.

Table 1 Summary of water contact angle data measured by the Wilhelmy plate method. All the surfaces were soaked in PBS buffer for 1 h before the measurements. The data are the average of three surfaces. The water had a measured surface tension of 72.4 dynes/cm.

Surface water angle	Clean glass	PU	NPS	PS
Advancing	15 \pm 5	75 \pm 10	75 \pm 10	88 \pm 5
Receding	2 \pm 5	30 \pm 10	62 \pm 10	70 \pm 5

The results of tritium labelled Hb (0.25 mg/ml in PBS) adsorbed onto the four different surfaces are shown in Figures 1–5 and summarized in Table 2. There are four general trends:

- 1 DeoxyHb adsorbs more than oxyHb onto all four surfaces studied.
- 2 The hydrophobic surfaces adsorb more Hb than the hydrophilic glass and PU.
- 3 OxyHb adsorbs relatively slowly onto the hydrophobic surface (up to 10 min) while deoxyHb adsorbs more rapidly during the first minute).

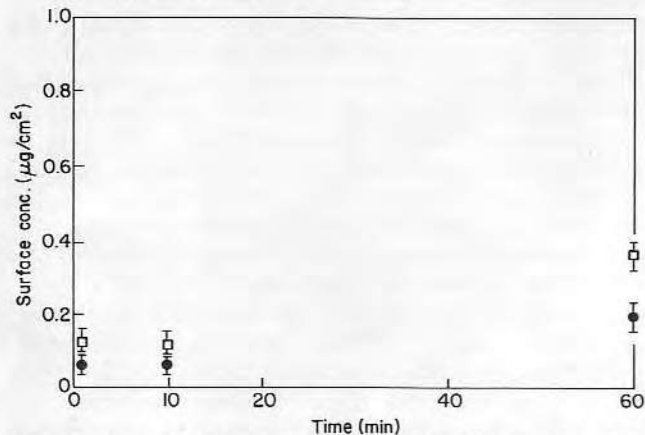


Figure 1 Adsorption of oxyHb (●) and deoxyHb (□) onto clean glass coverslips. The data were from three replicates of one experiment. The vertical bars indicate the standard deviation. The time span of 1, 10, or 60 min was the incubation time before rinsing with PBS buffer. The Hb concentration was 0.25 mg/ml in PBS at 20°C. (See text and Reference 19 for further details).

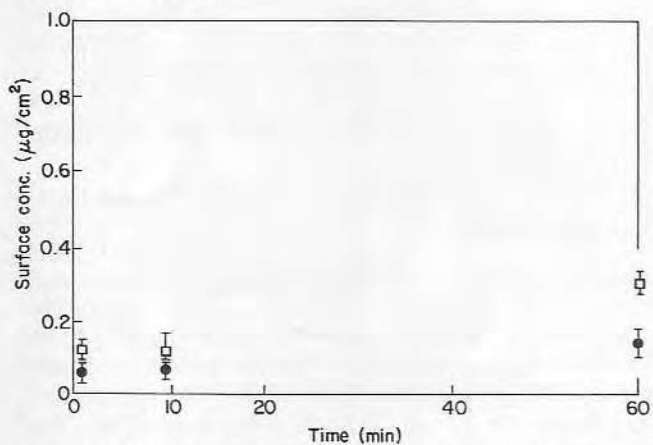


Figure 2 Adsorption of oxyHb (●) and deoxyHb (□) onto a PU coated surface. (See legend Figure 1 for further details).

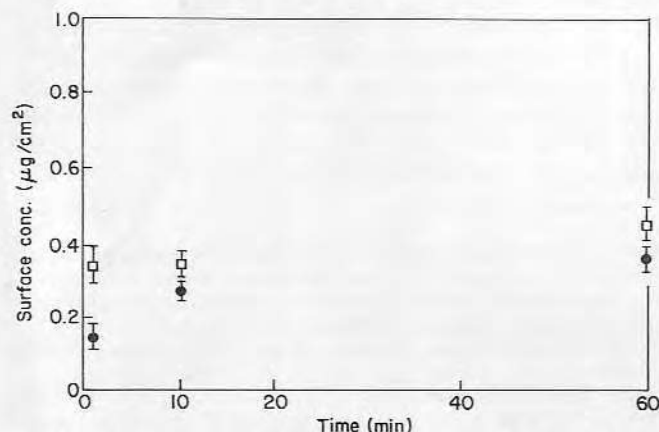


Figure 3 Adsorption of oxyHb (●) and deoxyHb (□) onto a NPS coated surface. (See legend Figure 1 for further details).

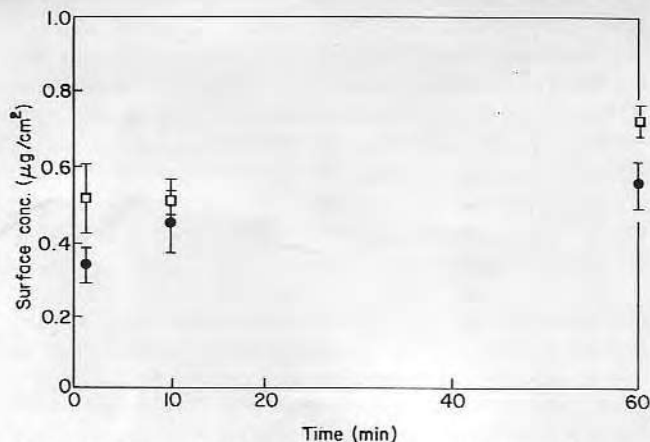


Figure 4 Adsorption of oxyHb (●) and deoxyHb (□) onto a PS coated surface. (See legend Figure 1 for further details).

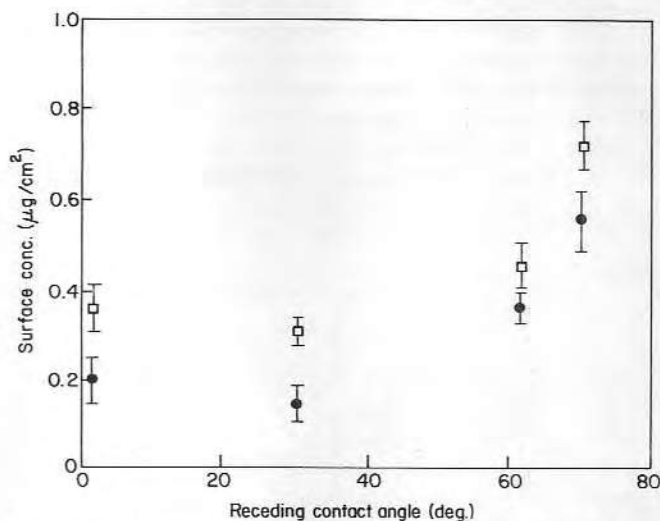


Figure 5 The correlation between the receding water contact angle and the amount of Hb adsorbed ($\mu\text{g}/\text{cm}^2$) at 60 min of exposure to a 0.25 mg/ml³ H-Hb in PBS (pH 7.4) at 20°C.

- 4 Both oxy and deoxyHb adsorb at similar rates onto the hydrophilic surfaces.

These trends will now be discussed:

- (a) DeoxyHb adsorbs more than oxyHb on hydrophobic surfaces. This confirms previous reports that surface hydrophobicity plays a major role in Hb adsorption¹⁸;
- (b) DeoxyHb adsorbs more than oxyHb on the hydrophilic surfaces. When oxyHb contacts a hydrophilic surface, the hydrophilic and charged amino acids located on the surface of the tetramer probably interact with the hydrophilic solid surface. One hypothesis is that

Table 2 Summary of radiolabelling study. Hb adsorbed ($\mu\text{g}/\text{cm}^2$) at 1, 10 and 60 min of exposure to a 0.25 mg/ml³ H-Hb in PBS (pH 7.4) at 20°C (standard deviation $\sim \pm 0.1 \mu\text{g}/\text{cm}^2$).

Protein	Incubation time (min)	Surface conc. ($\mu\text{g}/\text{cm}^2$)			
		Clean glass	PU	NPS	PS
DeoxyHb	1	0.13	0.12	0.37	0.45
	10	0.12	0.11	0.38	0.45
	60	0.37	0.31	0.47	0.72
OxyHb	1	0.03	0.03	0.17	0.37
	10	0.04	0.04	0.24	0.42
	60	0.21	0.14	0.36	0.56

surface-induced dimerization occurs^{10,11}. The oxyHb dimer is more hydrophobic than the corresponding deoxyHb tetramer, perhaps explaining why deoxyHb adsorbs more than oxyHb, even on hydrophilic surfaces; deoxyHb has a very low dimerization constant in solution (1×10^{-12}), probably because it is a taut structure (8 salt linkages hold it together). OxyHb is a relaxed structure which has a dimerization constant of 2×10^{-6} . Although there is no significant dimerization in 0.25 mg/ml solution, interaction with the surface may disturb the equilibrium and cause dimerization. Since oxyHb has a hydrophilic surface, it may not interact with hydrophobic surfaces strongly enough to cause the dimerization to occur.

- (c) *The more hydrophobic the surface, the more adsorption of deoxyHb.* The hydrophobic interaction appears to be the major mechanism for Hb adsorption¹⁸. Surface-induced dimerization of deoxyHb is very unlikely due to the low dimerization constant. Thus the more hydrophobic the surface, the more deoxyHb adsorbs. Figure 5 shows clearly the correlation between adsorbed amount and contact angle.
- (d) *The more hydrophobic the surface, the more adsorption of oxyHb.* As mentioned previously, surface-induced dimerization may occur when oxyHb contacts the hydrophilic surface¹⁸. The dimer of oxyHb is more hydrophobic. A hydrophilic surface minimizes the hydrophobic interaction and thus may decrease the adsorption of oxyHb dimer (Figure 1). When oxyHb contacts more hydrophobic surfaces, the hydrophobic interaction apparently increases and the adsorption of oxyHb would increase accordingly;
- (e) *DeoxyHb adsorbs faster than oxyHb onto hydrophobic surfaces.* This is probably because the hydrophobic interaction is the major driving force for Hb adsorption and deoxyHb is more hydrophobic than oxyHb;
- (f) *There may be no major difference in the rate of either deoxy or oxyHb adsorption onto hydrophilic surfaces.* As mentioned before, hydrophilic surface-induced dimerization may occur for oxyHb and the oxyHb dimer is hydrophobic. DeoxyHb is also hydrophobic; therefore, a similar rate and mechanism may be expected when these two forms of Hb adsorb onto hydrophilic surfaces. The slow rate of adsorption probably relates to the lack of strong hydrophobic interactions.

A summary of Hb adsorption in terms of its rate and mechanism is shown in Table 3.

The possible binding sites for Hb adsorption are hypothesized as the contact clefts of α_1 , β_2 , and α_2 , β_1 because:

- 1 The results suggest that hydrophobic interactions play a major role in Hb adsorption (Figure 5). The contact clefts of α_1 , β_2 , and α_2 , β_1 are nonpolar.
- 2 Some of the charged or polar amino acids around the clefts can form ionic interactions or hydrogen bonding when Hb contacts a hydrophilic surface. Hydrophilic surface-induced dimerization of oxyHb may occur if polar interactions with the surface are stronger than the hydrophobic interactions which stabilize the

oxyHb tetramer¹⁶. (DeoxyHb cannot dimerize because of the increased stability of the tetramer due to the 8 salt linkages). The dimers which may form *via* surface-induced dimerization would be $\alpha_1\beta_1$ and $\alpha_2\beta_2$, not $\alpha_1\beta_2$ nor $\alpha_2\beta_1$.

- 3 Upon oxygenation, the β chains rotate apart by about 7 Å, exposing many polar contacts between similar chains ($\alpha_1\beta_2$, $\alpha_1\beta_1$). In other words, the α_1 , β_2 , and α_2 , β_1 clefts are narrowed upon oxygenation⁵. Results in Figure 5 suggest the deoxyHb adsorbs more than oxyHb on all four surfaces studied, which may relate to the change in the binding sites upon oxygenation.
- 4 The binding site on Hb could be two clefts (e.g. α_1 , β_2 and α_2 , β_1) which should be large enough to bind 5 methyl groups. Hydrophobic chromatography studies have shown that 3 to 4 methyl groups are often required for effective binding to alkyl agarose columns. Since Hb has two hydrophobic binding sites, perhaps up to 8 surface methyl groups could be involved.

The criteria in 1–4 are satisfied by suggesting α_1 , β_2 and α_2 , β_1 clefts as the binding sites.

SUMMARY AND HYPOTHESES

The adsorption of deoxy and oxyHb onto four different surfaces (clean glass, NPS, PS, and PU) was studied by radiolabelling methods. The preliminary results are:

- DeoxyHb adsorbs more than oxyHb onto all four surfaces.
- Generally the more hydrophobic the surface, the more Hb adsorbs.
- The adsorbed amounts range from 0.1 to 0.6 $\mu\text{g}/\text{cm}^2$ for oxyHb and from 0.3 to 0.7 $\mu\text{g}/\text{cm}^2$ for deoxyHb ($\pm \sim 0.1 \mu\text{g}/\text{cm}^2$).
- The binding sites for Hb adsorption may be the clefts between α_1 , β_2 and α_2 , β_1 .
- The surface of deoxyHb was suggested as more hydrophobic than the surface of oxyHb.
- A hydrophilic surface-induced dimerization of oxyHb is hypothesized.

These results suggest the importance of changes in protein conformation and surface nature (oxy *versus* deoxyHb) on adsorption at solid/liquid surfaces.

Table 3 Summary of Hb adsorption rate (qualitative) and suggested mechanisms. As the data reported here are preliminary, this table suggests hypotheses, not conclusions.

Hb	Protein surface hydrophilicity	Hydrophilic surface-induced dimerization?	Initial adsorption onto	
			Hydrophilic surface	Hydrophobic surface
DeoxyHb	Hydrophobic	No	Slow	Fast
OxyHb	Hydrophilic for tetramer	Yes	Slow	Slow
	Hydrophobic for dimer			

ACKNOWLEDGEMENTS

The authors thank Dr Donald E. Gregonis, Dr Jiri Janata, Dr Dennis Coleman and Dr Lee Smith for their suggestions and discussions. The work was supported by NIH Grant HL 29209.

REFERENCES

- 1 Horbett, T.A., Weathersby, P.K. and Hoffman, A.S., The preferential adsorption of hemoglobin to polyethylene, *J. Bioeng.* 1977, **1**, 61-77
- 2 Pierce, J.M., Hb adsorption on alkyl agaroses, MS Thesis, University of Utah, Salt Lake City, 1981
- 3 Coleman, D.L., Lawson, J. and Kolff, W.J., Scanning electron microscopic evaluation of the surfaces of artificial hearts, *J. Art. Organs* 1978, **3**, 166-172
- 4 Otteman, R.D. and Williams, M.C., Material effects in shear-induced hemolysis, *Biomater., Med. Dev., Art. Organs* 1979, **7**, 359-391
- 5 Dickerson, R.E. and Geis, I., *Hemoglobin*, Benjamin Cummings, 1983
- 6 Stryer, L., *Biochemistry*, Freeman, San Francisco, 1975
- 7 Antonini, E. and Brunori, M., *Hb and Mb in Their Reactions with Ligand*, North-Holland Publishing Co., Amsterdam/London, 1971
- 8 Winterhalter, K.H. and Colosimo, K., Chromatographic isolation and characterization of isolated chains from hemoglobin, *Biochem.* 1971, **10**, 621-624
- 9 Perutz, M.F., Stereochemistry of cooperative effects in haemoglobin, *Nature* 1970, **228**, 726-734
- 10 Hallaway, B.E., Changes in conformation and function of hemoglobin and myoglobin induced by adsorption to silica, *Biochem. Biophys. Res. Comm.* 1979, **86**, 689-696
- 11 Jentoft, J.E. and Dearborn, D.G., ^{13}C NMR studies of ribonuclease A methylated with ^{13}C formaldehyde, *J. Biol. Chem.* 1979, **254**, 4539
- 12 Antonini, E., Rossi-Bernardi, L. and Chaircone, E., *Methods in Enzymology: 76, Hemoglobin*, Academic Press, 1981
- 13 Jentoft, J.E., Jentoft, N., Gerken, T.A. and Dearborn, D.G., ^{13}C NMR studies of ribonuclease A methylated with ^{13}C formaldehyde, *J. Biol. Chem.* 1979, **254**, 4366-4370
- 14 Laemmli, U.K., Cleavage of structural proteins during the assembly of the head of bacteriophage T4, *Nature* 1970, **227**, 680-685
- 15 Smith, L., Doyle, C., Gregonis, D.E. and Andrade, J.D., Surface oxidation of *Cis-trans* polybutadiene, *J. Appl. Polym. Sci.* 1982, **27**, 1269-1276
- 16 Clark, D.T. and Feast, W.J., Application of electron spectroscopy for chemical applications (ESCA) to studies of structure and bonding in polymeric systems, *J. Macromol. Sci. Rev.* 1975, **C12**, 191-286
- 17 Rossi, L., Fanelli, M.R. and Antonini, E., Properties of human hemoglobin immobilized on sepharose 4B, *Eur. J. Biochem* 1978, **92**, 253-259
- 18 Brietenback, M., *Hydrophobic Interaction Chromatography*, Pergamon, New York, 1975, p 687
- 19 Chen, J., Hemoglobin adsorption onto glass and polymers, MSc. Thesis, University of Utah, Salt Lake City, Utah, 1984

Surface Characteristics of Polysulfoalkyl Methacrylates

W. Y. CHEN¹ AND J. D. ANDRADE²

Departments of Bioengineering and Materials Science and Engineering, College of Engineering,
The University of Utah, Salt Lake City, Utah 84112

Received February 12, 1985; accepted May 31, 1985

Coated hydroxyethyl methacrylate-sodium sulfoalkyl methacrylate copolymer films were surface characterized. The contact angle hysteresis increases and the receding angle decreases with increasing alkyl side-chain length, while the advancing angle decreases with hydration time. It was found that the buoyancy slopes of the advancing (r_a) and receding (r_r) process determined by the Wilhelmy plate method were not parallel. The ratio of r_a to r_r was greater than 1, and increases with the alkyl side-chain length and the hydration time, contrary to that of polyhydroxyethyl methacrylate, where r_a/r_r was less than 1. The slope ratio would be suppressed in solution with added salt, revealing that the reorientation and expansion of the polymer chain in water is being suppressed. X-ray photoelectron spectroscopy (XPS) analysis of the surface of these copolymers showed a striking enrichment of the sulfonate groups in the surface. The zeta potential was between -40 and -50 mV as measured by the streaming potential method. During dehydration, along with a decrease in sulfur and sodium concentration in the surface, the carbon 1s peak at the high binding energy decreased and the alkyl carbon main peak increased. The surface tension of aqueous solutions of sulfoalkyl methacrylate monomers and homopolymers decreases with increasing alkyl side-chain length, which may contribute to the decrease in water-polymer film interfacial tension and thus the increase in the slope ratio. © 1986 Academic Press, Inc.

INTRODUCTION

Polysulfoalkyl methacrylates are recently synthesized polymers with promising blood compatibility properties (1, 2). These polymers contain long alkyl side chains and negatively charged sulfonate groups at the end of the side chains. Such structures are expected to show significant surface activity and perhaps unique interfacial properties.

Contact angle hysteresis is a measure of surface wettability, roughness, heterogeneity, deformation, and surface mobility (3, 4). The close relationship with surface functional groups has been known for a long time (5). Holly and Refojo, in studying the wetting properties of soft hydrogel contact lenses based on poly(hydroxyethyl methacrylate) concluded that the surfaces orient in air with the

hydrophobic methacrylate backbone exposed, while the hydroxyl-containing pendant groups orient toward the water phase (6). Kessaissia *et al.* grafted alkyl chains of different lengths onto silica and reported that the contact angle for water increases with increasing carbon chain length (7). Holly used sessile water droplets as a probe of the surface charge density of polymer electrets and found 3- to 6-degree decreases in water contact angle with increasing surface charge density in various polymer electrets (8). Charged methacrylic acid-methyl methacrylate and trimethylaminoethyl methacrylate copolymers and polysulfoalkyl methacrylates were studied in our laboratory, and the influence of surface charge and side-chain length on contact angles and contact angle hysteresis were reported (8-10).

The combined effect of the surface charge and the side-chain length has not been studied. We here report contact angle studies on a series of sodium sulfoalkyl methacrylate polymers

¹ Permanent address: Polymer Division, Department of Chemistry, Peking University, Beijing, China.

² To whom reprint requests should be addressed.

by the dynamic Wilhelmy plate method (3). Evidence of the side-chain mobility was further verified through the analysis of X-ray photoelectron spectra and streaming potential measurements (11).

MATERIALS AND METHODS

Hydroxyethyl methacrylate (HEMA) (Aldrich, 97%); sodium sulfodecyl methacrylate, $\text{CH}_2=\text{C}(\text{CH}_3)\text{COO}(\text{CH}_2)_{10}\text{SO}_3\text{Na}$ [SSDMA]; sodium sulfooctyl methacrylate, $\text{CH}_2=\text{C}(\text{CH}_3)\text{COO}(\text{CH}_2)_8\text{SO}_3\text{Na}$ [SSOMA]; and sodium sulfohexyl methacrylate, $\text{CH}_2=\text{C}(\text{CH}_3)\text{COO}(\text{CH}_2)_6\text{SO}_3\text{Na}$ [SSHMA] with purity greater than 99% were prepared in the Polymer Division of the Chemistry Department of Peking University (China). Sodium sulfoethyl methacrylate [SSEMA] was prepared from sulfoethyl methacrylate (Poly-sciences, 95%) through neutralization and purification. Other reagents were methylene bisacrylamide [MBAAM] (99+%, Aldrich), ammonium persulfate [APS] (Baker analyzed reagent) and dimethyl sulfoxide [DMSO] (EM Science).

Polymerization was carried out at 60° or 70°C under nitrogen and vacuum (after nitrogen purging) with 0.1% APS as initiator.

Crosslinked polymer coatings were prepared first by prepolymerizing the monomers in water or in DMSO solution (15% concentration) under nitrogen with 0.1–0.2% APS for 0.5–1.5 h. The prepolymer solutions were then diluted to the required concentration and filtered through a 0.5- μm membrane filter (type FHLPO 4700, Millipore Corp.).

Glass slides (Bev-1-edge, 3×1 in., 0.9–1.0 mm) or microscope coverslips (Corning type 2940, No. 1 $\frac{1}{2}$, 24×50 mm, 0.16–0.19 mm) were cleaned with chromic acid at 80°C for 20 min, followed by rinsing successively with distilled water and alcohol and finally dried over freon vapor. They were coated by dipping into the prepolymer solution at a speed of 2.5 cm/min.

Films coated on the glass slides or glass coverslips were further polymerized and cross-

linked by means of remaining pendant unsaturated groups at 65°C under nitrogen and vacuum for 16 h to 2 days. The films were stable over 5 days hydration in water.

Glass samples ($0.1 \times 1 \times 1$ cm) used for XPS analysis were cleaned and coated with prepolymer solution on one side, then mildly dried and crosslinked as above.

The Wilhelmy plate method was used to measure the contact angles of the polymer surfaces and the surface tension of water and aqueous solutions (3). In each case the glass slides were immersed into or drawn out of the double-distilled water or 0.1 M NaCl solution at the speed of 40 mm/min. Cleanliness of the glass was examined by the water contact angle measurement.

Zeta potential of the charged polymer surface was obtained from streaming potential measurements as described by Van Wagenen and Andrade (11). The plate separation was 130 μm . Streaming potentials (ΔE) were taken at driving pressures (ΔP) of 40, 60, and 80 mm Hg in both flow directions. At least 5 sets of readings were taken for each sample, then the data were fitted by linear regression with the slope yielding $\Delta E/\Delta P$. The correlation coefficient was always better than 0.990 and often better than 0.999, indicating an excellent straight-line fit to the streaming potential data.

X-ray photoelectron spectra (XPS) were obtained on a Hewlett-Packard 5950B using monochromatic $\text{Al K}_{\alpha 1,2}$ radiation at 1487 eV with 800-W power at the anode. An electron flood gun operated at 0.3 mA and 6.0 eV. The spectra were charge referenced to the C-1s alkyl binding energy at 284.6 eV. The surface characterization results indicate that the films are uniform.

RESULTS AND DISCUSSION

The mole ratio of all HEMA–SSRMA (R = ethyl, hexyl, octyl, or decyl) copolymers was 90:10. When the crosslinking agent MBAAM was used at 1 to 5% mole ratio, no detectable nitrogen was found in the surface by XPS wide-scan analysis. One net charge every 10

TABLE I
Contact Angles of SSRMA Copolymer Surfaces^a

Sample 90:10:5 (mol)	Contact angles after hydration for:					
	3 h			24 h		
	θ_a	θ_r	$\Delta\theta$	θ_a	θ_r	$\Delta\theta$
A. PolyHEMA-SSHMA-MBAAM	70.8	42.5	28.3	51.4	21.9	29.5
PolyHEMA-SSOMA-MBAAM	70.9	36.5	34.4	59.0	19.3	39.7
PolyHEMA-SSDMA-MBAAM	72.1	32.8	39.4	59.9	17.4	42.5
B. PolyHEMA-SSHMA-MBAAM	70.0	41.3	28.7	56.1	26.4	29.8
PolyHEMA-SSOMA-MBAAM	74.0	34.5	39.5	59.7	22.7	37.0
PolyHEMA-SSDMA-MBAAM	74.2	27.2	47.0	61.9	17.0	44.9

^a Prepared by dipping in DMSO solution: A, 3% DMSO solution; B, 1% DMSO solution.

structural units is enough for full expansion of the polymer backbone. The HEMA-SSRMA copolymers are useful model compounds with which to study the effect of charge on the side-chain orientation.

For copolymers with 5% crosslinker, similar to those used in the blood compatibility tests (2), there was no significant difference in contact angles, especially for the samples prepared from 3% solutions in dimethylsulfoxide (DMSO) (Table I). Samples prepared from 1% prepolymer solutions were also studied. The contact angle hysteresis increase and the receding angle decrease with increasing side-chain length were contrary to our expectation because the decyl polymer was considered to be the more hydrophobic component. Such phenomena were more evident with thinner films coated from prepolymer solutions of 1% concentration.

The degree of crosslinking influenced the mobility of the polymer chain, as shown in Fig. 1. The material without added crosslinker has the highest contact angle hysteresis. The variation of contact angle could be due to the migration of the alkyl side chains, although this would be contrary to work reported (6, 9).

Copolymers of lower degree of crosslinking (1%) were prepared and coated onto the glass coverslips from 1% solution by dipping. For these samples, the advancing angle decreased

with hydration time, but the receding angles remained nearly the same. Besides, to our surprise, the contact angle hysteresis loops were hardly repeatable and the buoyancy slopes of the advancing and the receding process were no longer parallel to each other.

Figure 2 shows a typical graph of contact angle loops by the Wilhelmy method (12), where the coated glass coverslip is immersed into (advancing process), then drawn out (receding process) of the water. The process is repeated to obtain the successive second or third loops, which should coincide with each other. Ordinarily, the advancing line is parallel to the receding line.

Figure 3 presents the hysteresis loops for poly(HEMA-SSHMA-MBAAM). Samples

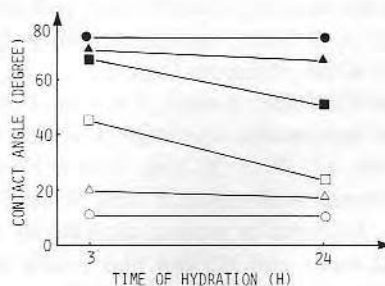


FIG. 1. Effect of degree of crosslinking and hydration time on HEMA-SSHMA copolymer film contact angles. Solid, advancing angles; hollow, receding angles. Circle, without crosslinking agent; triangle, 1% crosslinker; square, 5% crosslinker.

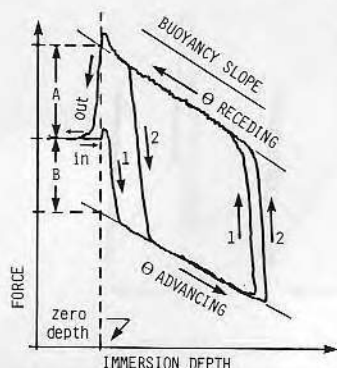


FIG. 2. Typical Wilhelmy plate wetting curve of a polybutadiene sample. The buoyancy slope parallels both advancing and receding contact angles. The sample was taken through two successive dipping cycles to demonstrate reproducibility. Displacement A is used to compute the receding angle, while displacement B is used to compute the advancing angle. Curves are measured at the point of zero depth of immersion so the buoyancy effect can be neglected (from Ref. 12).

with 5% crosslinker had reproducible surface properties after 24-h hydration. The samples prepared by dipping with prepolymer solution of 1% concentration produced hysteresis loops which did not coincide even after being hydrated for more than 54 h. Such behavior may be due to expansion of the polymer backbone and migration of the side chain to the interface.

Although the content of SSRMA in the copolymers is only 10%, the copolymers are polyelectrolytes. We hydrated the samples in 0.1 M NaCl solution and measured the contact angles with 0.1 M NaCl solution, the surface tension of which is nearly the same as pure water. As expected, the loops soon coincide, but advancing and receding slopes still differed as shown in Fig. 4. The deviation increases with increase in side-chain length and with hydration time. If we plot the ratio of the advancing to receding slope versus the number of carbon atoms in the side chains (Fig. 5), the slope ratio is greatest in water, and least in salt solutions. For the sulfodecyl methacrylate copolymer, after hydration for 100 h, the slope ratio in water is as high as 2.8, while in 0.1 M NaCl it is 1.6. The suppression effect of added salt to the slope deviation for this sulfodecyl

copolymer is shown in Fig. 6. After 24-h hydration in water, 0.1 M NaCl and 1.0 M NaCl solutions, the slope ratios are 2.0, 1.4, and 1.2, respectively, and approaches 1 in 1 M NaCl. This is a typical behavior for polyelectrolytes in solution. The addition of salt suppresses tendency for the counterion in the film surface to diffuse into the water, quenches the thickness of the electrical double layer which causes lessening of the net charge in the polymer backbone, and results in depression of the chain expansion and the side-chain orientation, that is, the contraction of the polymer chain in the salt solution makes itself behave as "normal."

X-ray photoelectron spectroscopy of the surface of these copolymers revealed a striking enrichment of the sulfonate groups in the surface (Table II). The amount of the charged groups was about 6 to 8 times in excess as compared with calculated bulk values. After being hydrated for 4 h, then dried again under vacuum for 2 days, the presence of S and Na in the surface decreased but was still 3 to 4 times in excess of the calculated.

The zeta potentials of these copolymer surfaces coincided with the XPS data, although the differences were small.

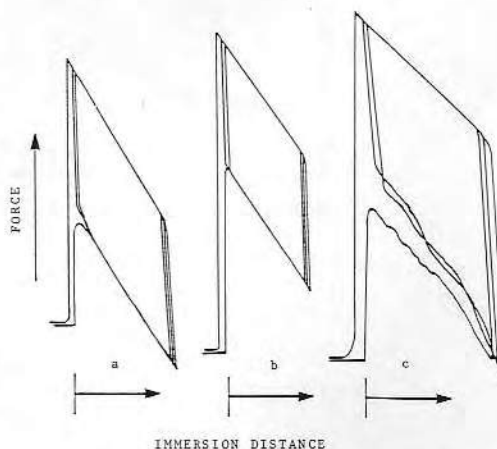


FIG. 3. Contact angle loops of polyHEMA-SSHMA-MBAAM. (a) 5% crosslinker, coated with 3% solution, hydrated 3 h; (b) 5% crosslinker, coated with 1% solution, hydrated 24 h; (c) 1% crosslinker, coated with 1% solution, hydrated 54 h.

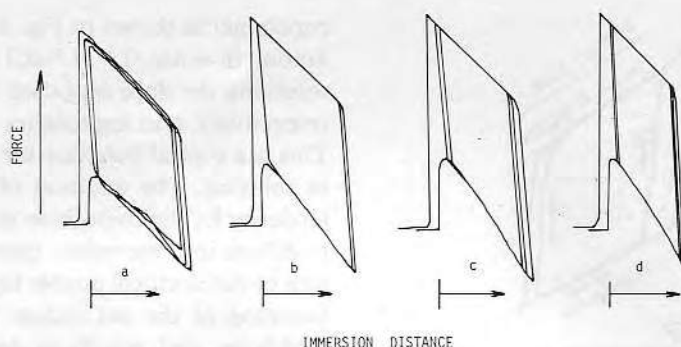


FIG. 4. Contact angle loops of polyHEMA-SSDMA-MBAAM films after being hydrated in 0.1 M NaCl for 0 (a), 44 (b), 24 (c), and 100 (d) h.

The enrichment of SO_3Na^+ groups in the surface seemed strange, because it was believed that polar sites tend to bury in the aqueous phase within the gel when the surface was exposed to air. Ratner *et al.* (13), reported that the amount of HEMA was significantly decreased in the surface upon dehydration, while the surface abundance of the hydrophobic ethyl methacrylate component was not affected by drying. Furthermore, Thomas and

co-workers demonstrated by XPS that sodium and sulfonic groups of ion exchange resin made of crosslinked sodium polystyrene sulfonate were not exposed to the resin-air interface but were buried in the bulk of the resin in the dry state.

But this is not always the case. In our experiments, SO_3^- and Na^+ were always enriched in the surface, especially when the coated films were cast from DMSO solution. Most proba-

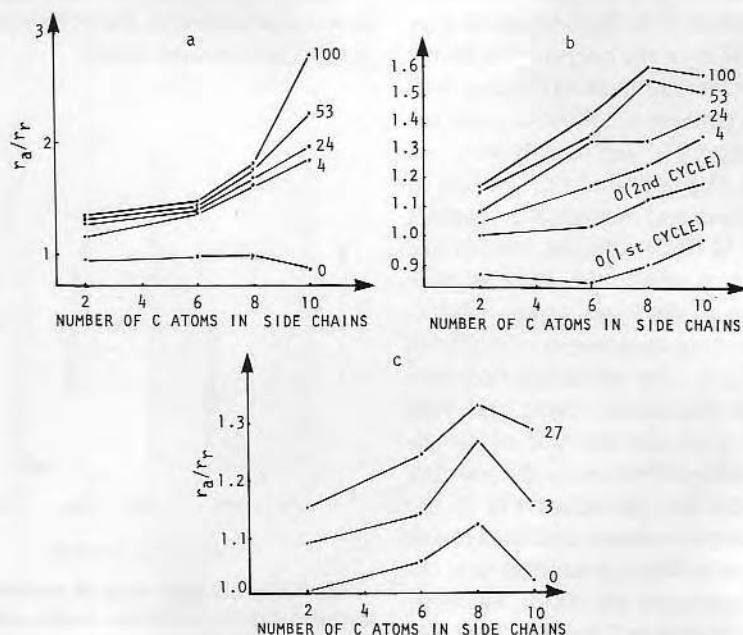


FIG. 5. Ratio of advancing slope (r_a) to receding slope (r_r) versus the side chain length. Numbers in the graph denote the time of hydration (a) in water, (b) in 0.1 M NaCl, (c) in 1.0 M NaCl.

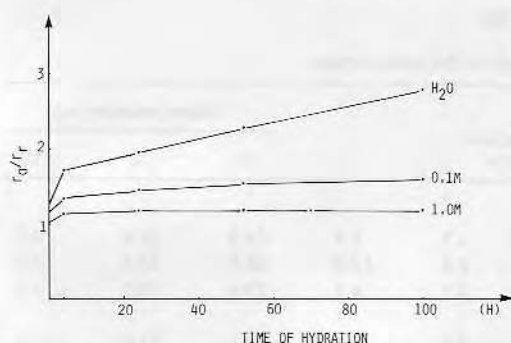


FIG. 6. Suppression effect of added salt to the slope ratio for polyHEMA-SSDMA-MBAAM (1% crosslinker).

bly it is due to the very strong solvation power of DMSO for the cations used, as Na^+ and for large anions ($-\text{SO}_3^-$) (14), thus carrying them to the surface.

In some cases the sulfonate group was more enriched, as high as 13 times the bulk value, or went down to nearly the bulk level, depending upon the treatment. One of the causes might be the time of gentle heating before applying the vacuum, which may cause a restriction of orientation. However, in any case the

carbon 1s peak for ester carbon never disappeared.

XPS carbon 1s spectra show three peaks: a main aliphatic peak at 284.6 eV (C1), the carbon adjacent to hydroxy or to the $-\text{OC}=\text{O}$ and $-\text{SO}_3^-$ groups appeared as a shoulder of the main peak (C2), and the carbon in the ester ($-\text{COO}-$) group which appeared as a separate peak at higher binding energy (289 eV). The theoretical and the found values of these three carbon components obtained through a peak-fit procedure are listed in Table III. When the side chain oriented toward the inner bulk, along with a decrease in S and Na in the surface, the C1s peak at the high binding energy decreased, and the alkyl carbon main peak increased. In any case the alkyl carbon content is concentrated in the surface, higher than the bulk value, which is in accordance with the enrichment of the S and Na elements in the surface.

Therefore, it could be assumed that when films of polysulfoalkyl methacrylates contact water, the alkylsulfonic groups might orient into water as if made a layer of pseudoaqueous solution and more or less concentrated at the

TABLE II
Surface Composition by XPS and Surface Charge of SSRMA Copolymers

Sample 90:10:1 (mol)	Elemental ratio C:O:S:Na				Zeta potential (, mV)	
					5 min ^a	4 h ^a
PolyHEMA-SSDMA-MBAAM						
Calculated	100.0	46.9	1.5	1.5	-47.3	-49.01
Found ^b	100.0	43.0	8.8	12.0		
Hydrated ^c	100.0	30.0	4.5	4.8		
PolyHEMA-SSHMA-MBAAM						
Calculated	100.0	49.8	1.6	1.6		
Found ^b	100.0	50.0	12.0	19.0	-49.07	-50.30
Hydrated ^c	100.0	41.0	4.4	6.10		
PolyHEMA-SSEMA-MBAAM						
Calculated	100.0	53.2	1.7	1.7		
Found ^b	100.0	57.0	8.4	8.7	-40.54	-44.50
Hydrated ^c	100.0	64.0	13.0	14.0		

^a Time of hydration before measurement.

^b Dried sample.

^c Sample surface was hydrated with deionized water for 4 h, then dried under vacuum for 2 days.

TABLE III
Carbon Component Analysis of Polymer Surface

Sample 90:10:1 (mol)			Elemental ratio C:O:S:Na			Carbon component (%) ^a		
						C1	C2	C3
PolyHEMA–SSDMA–MBAAM								
Calculated	100.0	46.9	1.5	1.5	55.9	29.4	14.7	
Found	100.0	43.0	8.8	12.0	68.8	23.3	7.9	
Hydrated	100.0	30.0	4.5	4.8	73.6	19.2	7.2	
PolyHEMA–SSHMA–MBAAM								
Calculated	100.0	49.8	1.6	1.6	53.1	31.3	15.6	
Found	100.0	50.0	12.0	19.0	68.1	21.1	10.9	
Hydrated	100.0	41.0	4.4	6.1	68.2	21.8	10.2	
PolyHEMA–SSEMA–MBAAM								
Calculated	100.0	53.2	1.7	1.7	50.0	33.3	16.7	
Found	100.0	57.0	8.4	8.7	51.2	35.3	13.5	
Hydrated	100.0	64.0	13.0	14.0	58.8	33.5	7.6	

surface, thereby decreasing the interfacial tension. From this consideration, we can now integrate some apparently contradictory statements. For example, it is true that surfaces with more hydrophobic component (as with longer alkyl chains) give higher contact angles, but in solution, compounds with long alkyl chains are more surface active than those containing short ones (15), thus lowering the surface tension. This effect may be enhanced in the presence of ionic groups as in charged surfactants. From a study of alkyl sulfo(methyl) propionates, Chebereva et al. concluded that when the hydrocarbon radical is extended by one methylene group, the surface activity of the sulfo(methyl) propionates increases by a factor of 2.1 (16). According to our experiments, the surface tension of the water solutions of SSRMA monomers or homopolymers evidently decreases with the increasing alkyl chain length as listed in Table IV. Since the homopolymers were of high molecular weight (10^5 – 10^6) (17), being random coils in water solution, with a lot of active groups entrapped inside the coils, the lowering of surface tension is not as great as that in monomer solutions.

In the Wilhelmy plate method of contact angle measurement, when the plate coated with SSRMA copolymer penetrates the aqueous solution or water, an interface is

formed with a pseudo surfactant layer (Fig. 7). As the plate proceeds continuously downward, a local accumulation of the Na^+ and the SO_3^- occurs, making the pseudointerfacial solution more concentrated, thus gradually lowering the interfacial tension, together with the effect of local lowering of surface tension, leading to gradually decreasing contact angles; therefore, a downward inclined slope is obtained.

TABLE IV
Surface Tension of SSRMA Monomer and Homopolymer Solutions

Solution	Surface tension (mN/m)
H ₂ O	72.9
0.001 M ^a PolySSHMA	72.7
0.01 M ^a PolySSHMA	72.1
0.001 M ^a PolySSDMA	72.0
0.01 M ^a PolySSDMA	69.1
H ₂ O	72.7
0.001 M SSEMA	72.2
0.01 M SSEMA	72.1
0.001 M SSHMA	71.7
0.01 M SSHMA	68.6
0.001 M SSDMA	61.1
0.01 M SSDMA	47.1

^a Mole concentration of segments.

Actually, buoyancy lines are parallel to each other only for certain compounds. The deviation occurs when there is strong interfacial activity, either positive or negative. For polyHEMA, the peculiar contact angle plots we obtained were just like that in literature (18) as shown in Fig. 8. If we draw a central line through the zigzag sawtoothlike advancing line, the slope is evidently lower than that of the receding angle line, which perhaps is due to the interaction between the polyHEMA surface and the water. The apparently contradictory properties of polyHEMA, such as hydrophobicity, swellability, and the possibility of reorientation of hydroxy groups toward water, contribute to the peculiar advancing line. The study of such surface mobility is difficult and such effects can be readily observed by the dynamic Wilhelmy plate method.

Hoffman reported the increase in contact angle of a polycation with increasing salt content and increasing binding force with counterions (19). If we take the midpoint of the

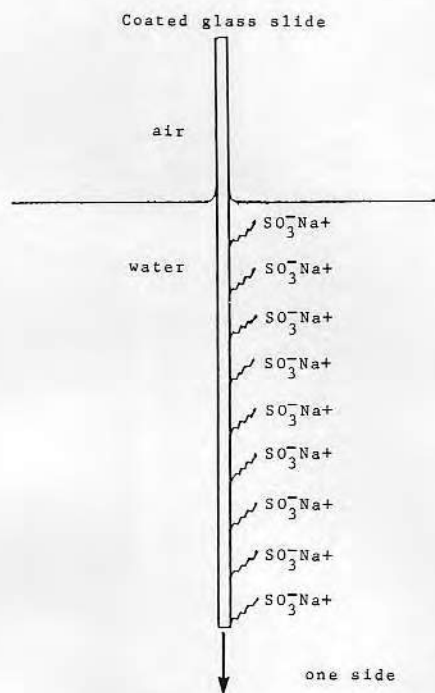


FIG. 7. A hypothetical sketch of pseudo surfactant layer in Wilhelmy plate method of contact angle measurement.

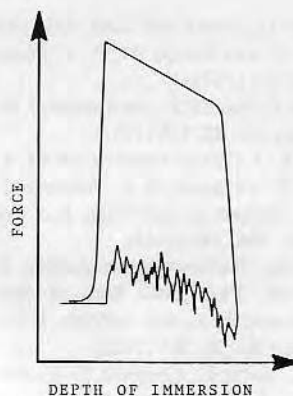


FIG. 8. Wilhelmy plate measurement of polyHEMA surface (reprinted with permission from Ref. 15).

advancing contact angle line of SSRMA copolymer surface, and draw a parallel line to the receding line, the advancing angle obtained also slightly increases with increasing salt content. But more important is the dynamic factor. Perhaps the diffusion of Na^+ into water is easier for polymers with longer side chains, which further supports the lowering of contact angles.

Clearly the interfacial dynamic of polyelectrolyte gels is a challenging and complex subject which requires more work and novel theoretical and mechanistic approaches. Such work is greatly needed and highly relevant to a wide range of biomedical and aqueous phenomena and applications.

ACKNOWLEDGMENTS

The authors hereby express their thanks to Mr. B. Z. Xu for the preparation of the sulfoalkyl methacrylate monomers, Mr. Paul Dryden for his generous help in the XPS laboratory, and Mr. Jim Warenski for aid with the streaming potential measurements.

REFERENCES

1. Chen, W. Y., Zu, B. Z., and Feng, X. D., *J. Polym. Sci.: Polym. Chem. Ed.* **20**, 547 (1982).
2. Chen, W. Y., Sung, D. H., Xu, B. Z., Zhang, G. L., Feng, X. D., Zhu, Y., and Chen, S. H., *Chinese J. Biomed Eng.* **1**, 1 (1982).
3. Johnson, R. E., and Dettre, R., *Surf. Colloid Sci.* **2**, 85 (1969).
4. Adam, N. K., "Physics and Chemistry of Surfaces," Dover, New York, 1968.

5. Langmuir, I., *Science*, No. 2266, 493 (1938).
6. Holly, F. J., and Refojo, M. F., *J. Biomed. Mater. Res.* **9**, 315 (1975).
7. Kessaissia, Z., Papirer, E., and Donnet, J. B., *J. Colloid Interface Sci.* **82**, 526 (1981).
8. Holly, F. J., *J. Colloid Interface Sci.* **61**, 435 (1977).
9. Hogt, A. H., Gregonis, D. E., Andrade, J. D., Kim, S. W., Dankert, J., and Feijen, J., *J. Colloid Interface Sci.* **106**, 289 (1985).
10. King, R. N., "Surface Characterization of Synthetic Polymers," Ph.D. thesis, Univ. of Utah, 1980.
11. Van Wagenen, R. A., and Andrade, J. D., *J. Colloid Interface Sci.* **76**, 305 (1980).
12. Smith, L., Doyle, C., Gregonis, D. E., and Andrade, J. D., *J. Appl. Polym. Sci.* **26**, 1272 (1982).
13. Ratner, B. D., Weathersby, P. K., and Hoffman, A. S., *J. Appl. Polym. Sci.* **22**, 643 (1978).
14. Martin, D., Weise, A., and Niclas, H. J., *Angew. Chem. Int. Ed.* **6**, 318 (1967).
15. Shiomi, T., *J. Colloid Interface Sci.* **99**, 586 (1984).
16. Chebereva, A. A., Kharkov, S. N., and Krutkov, Y. P., *J. Appl. Chem.* **56**, 352 (1983) (transl. from *Zhurnal Prikladnoi Khimii*).
17. Chen, Z. S., Chen, W. Y., Go, H. Q., and Piao, C. H., *Gaofenzi Tongxun (Polym. Commun.)*, 1983, (6) 463 (Ch.) (CA 101:91843v).
18. Gregonis, D. E., Hsu, R., Buerger, D. E., Smith, L. M., and Andrade, J. D., in "Macromolecular Solutions," (R. B. Seymour and G. A. Stahl, Eds.), p. 127. Pergamon, Elmsford, N. Y., 1982.
19. Hoffman, A. S., Gomes-Casseres, R., and Parfitt, G. D., in "Addition and Condensation Polymerization Processes," Adv. Chem. Ser., No. 91, p. 542, Amer. Chem. Soc., Washington, D. C., 1969.

THERMAL MODULATION REQUIREMENTS FOR REGENERATION OF IMMUNOLOGICALLY-ACTIVE SURFACES

Yi-Tung Chen¹, D. Christensen², J. Andrade², and R. Boehm^{1,3}
College of Engineering
University of Utah
Salt Lake City, UT 84112

Introduction

This is a study of methods to reversibly regulate and control the binding constant of surface-immobilized antibodies (Ab) and/or Ab fragments by changing the local temperature, thereby affecting the binding thermodynamics and equilibria. Specific chemical assay in complex mixtures generally depends on the use of specific, high affinity binding agents, such as antibodies, membrane receptors, enzymes, lectins, chelates, etc. Generally the greater the binding constant, the greater the ultimate sensitivity of the assay. Such assays are one-shot measurements. In the case of an immunoassay, one takes a sample, mixes the reagents, makes a reading, and then discards everything (Collins, 1985).

There is considerable interest and activity in developing specific chemical sensors, i.e. detectors which respond to changes in concentration of a specific chemical -- either continuously or at least semi-continuously (Andrade et al., 1985). Clearly we desire a high binding constant for maximal sensitivity, but we may also require a fast response time to permit continuous or semi-continuous measurements. Some means of decreasing the binding constant between measurements is therefore desirable. Ideally we would like to be able to zero the sensor between each measurement and yet make the measurement often enough to have a near-continuous readout (Andrade et al., 1985). Finally, we prefer a sensor with the maximum possible dynamic range. These characteristics are generally mutually exclusive, unless we can regulate the binding constant (Andrade et al., 1986).

The very high binding constants, which provide these agents with their exquisite sensitivity, usually mean that the dissociation rate of the complex is very slow (Pecht, 1982). Therefore, such systems are in reality dosimeters rather than true sensors or function as sensors with very slow time response. In order to reuse such a device, there must be a way to weaken the bond to permit the complex to dissociate in a reasonable time (Andrade et al., 1986; De Feijter et al., 1978).

The standard means to dissociate Ag-Ab complexes is to induce a significant conformational change in Ag, Ab, or both by drastic changes in the local solution environment, such as pH 2-3, pH 11, high concentration of chaotropic salts, high concentrations of agents which diminish hydrophobic interactions, temperature, etc. (Pecht, 1982; Goding, 1983; Walters, 1985). Unfortunately, such treatments often lead to irreversible conformational changes which destroy the specific binding properties (Goding, 1983). In addition, it is difficult to deliver acid, base, etc., on command to a remote sensor site. A different approach is to use low affinity antibodies, thus sacrificing sensitivity, or to use special monoclonal antibodies whose binding site structure makes them very susceptible to moderate changes in local pH (Hill, 1984).

There is a need for a method which can remove specifically bound ligand from a sensor surface without the use of often damaging eluting agents. The high affinities of antibodies can lead to almost irreversible binding of ligands. In vivo, the protein-ligand complex is usually broken down by proteolysis. In applications of

immunoassays and affinity chromatography, it is usually necessary to dissociate the protein-ligand complex without denaturation of the protein. Thus, the dissociation of the protein-ligand complex is a fundamental problem in both basic and applied research. It would be desirable to be able to modulate the affinity of the protein in a predictable and reversible manner.

A key element of the paper is the focus on the thermal dissociation to regulate and control ligand-receptor binding externally. It is clear that the dissociation rate constant can be increased by a factor of 10 if the interfacial temperature could be changed from 20 to 40°C, decreasing the response time from around 500 seconds to nearly 50 seconds. By raising the temperature to 60°C, the response time would be down to about 7 seconds.

The heating required to achieve the necessary thermal environment is related to typical conduction, convection, and radiation processes. In here, an aqueous solution (typically a buffered salt solution) is in contact with a surface. A fluid layer adjoining the surface and approximately 2000 Å thick must be transiently heated. Heating duty of this surface should be on the order of 20-30°C above an ambient fluid temperature which might range between 0-70°C. This process is complicated by the fact that there may be other operations (for example, some that require ultraviolet radiation to be incident on the layer simultaneously with the heating) to be performed simultaneously with the heating. We are considering three heating processes for the thermal modulation. They are an electrically-heated method, a direct radiatively-heated method, and an evanescent-wave-heating method.

Theory

Electrically heated method

One method of heating is to liberate the energy at an adjoining surface. For systems where a conducting surface, or at least a conducting film on the surface, can be used, then the simplest approach to fluid layer heating may be to use Joulean heating. Careful control of applied voltage vs. time will result in the ability to generate virtually any kind of thermal environment in the adjoining surface.

For short times, the temperature within the boundary layer of the fluid is given by a semi-infinite solution of the heat conduction equation. Two aspects must be present. First, the fluid must have heat sink capability (either a relatively thick layer of fluid or a slightly flowing fluid), and, second, the fluid must not convect significantly. The latter can be accomplished by placing the heated surface on top of the fluid and keeping any flow to very small velocities. The semi-infinite solution is given by, for example, Incropera and DeWitt (1985).

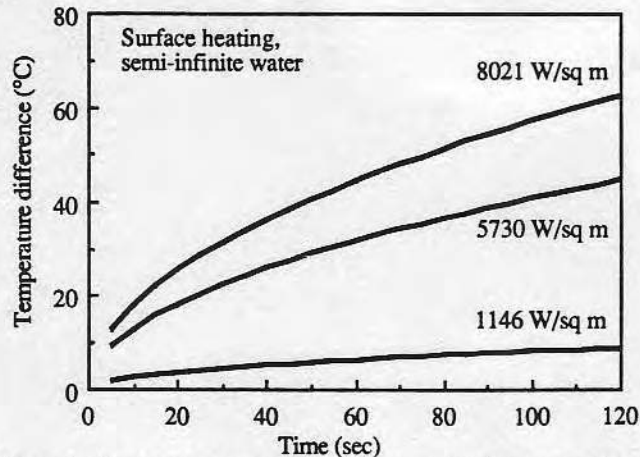


Figure 1. The temperature response at an semi-infinte water interface due to various surface fluxes.

Studies of this situation also serve as a base case for the other two heating modes discussed here. Fluid interface temperatures are shown in Figure 1 assuming an insulated interface and water properties. In the first phase of the work, electrically-conducting

¹Department of Mechanical Engineering

²Department of Bioengineering

³Fellow of ASME

coatings were applied to the containing surface that allowed Joulean heating of the adjacent fluid. This is discussed further below.

Radiatively heated method

This approach includes a number of methods that can be lumped together for discussion purposes. Included are: indirect methods where the adjoining surface is heated by thermal radiation absorption in the surface material or a coating; and direct methods where a fluid absorbs the radiation directly within the volume.

For the first method to be successful, the surface must be opaque to radiation with a coating that has a known radiative absorptivity. The second (direct absorption) method offers critical distinctions from the first. First, the surface can be an uncoated dielectric, such as typical optical waveguide materials. Now, however, the fluid molecules have to be selective absorbers of thermal radiation. Water and many of the organic-based materials demonstrate infrared band absorption. Care must be taken to find pertinent monochromatic sources that can be absorbed by the fluid molecules, but be not too far into the infrared to be cut-off by the dielectric surface material.

The laser radiation is assumed to be normally incident on a nonabsorbing containing plate and the adjacent fluid. To analyze this situation the radiation absorption is modeled using Beer's Law, with the incident intensity used in Beer's Law modified to include the effect of scattering in the media (if present). The temperature distribution in the fluid and containing plate is found as a function of wavelength using a finite difference conduction formulation. The light distribution may be modeled by using Beer's Law, with the incident intensity used in Beer's Law which can be modified to include the effect of scattering in the media. Scattering was not included in the present analysis.

Results for the temperature response estimates for radiatively heated water are shown Figure 2 for a single wavelength of radiation. The fluxes shown are the values used in the one-dimensional analysis.

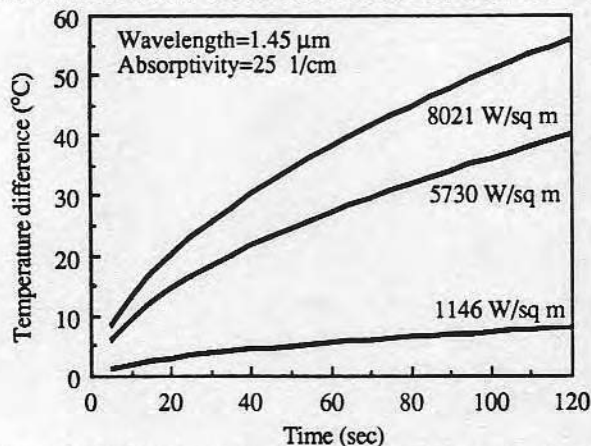


Figure 2. Surface temperature response at a quartz-water interface to a monochromatic beam of radiation at 1.45 μm for various incident fluxes. The water is assumed to be semi-infinite.

We were interested in exploring the complete near infrared region to see the effect of water absorptivity on the resulting surface heating. One representation of the results found in this analysis is given as Figure 3. This shows the net temperature rise of the surface for various monochromatic fluxes after heating for 50 seconds.

Evanescent wave heated method

Finally, evanescent wave heating is considered. Here the optical application method considers a beam of collimated monochromatic light impinging at the prism-air interface at an angle of incidence. The prism has a different refractive index than the surrounding medium. At low incidence angles, the beam will be refracted and transmitted into the low refractive index medium. The incident and reflected beams interfere to produce a standing wave at the interface. In the case of an interface between dielectric and an absorbing media, the standing wave has a finite electrical field amplitude right at the interface and decays exponentially in the

absorbing medium. It can be shown that the evanescent wave technique will yield power requirements that fall between the volume absorption method and the surface absorption method already described.

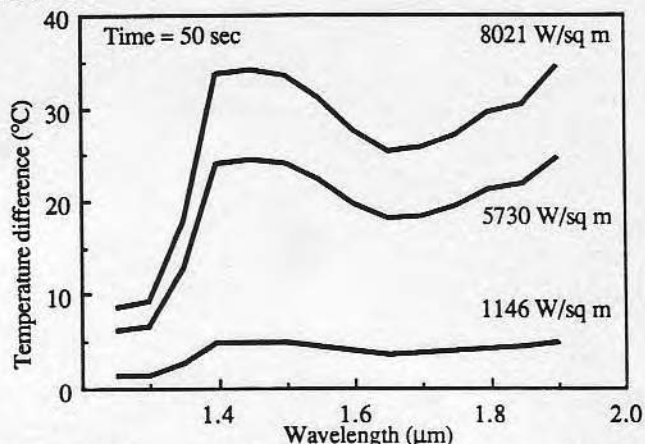


Figure 3. Temperature elevation at a quartz-water interface due to heating by various monochromatic sources for 50 seconds.

Experimental work

We have begun the experimental evaluation of several aspects of the thermal regeneration of immunologically-active surfaces. For the initial phases of the work, an electrically-heated surface was used. This surface was prepared by coating a quartz wall of a small flow chamber with a thin (500Å thick) film of titanium. The titanium was electrically insulated from the fluid with a thin (2000Å thick) silicon nitride film. 2000Å thick gold strips were used to bus the current to each side of the heater element. Temperatures on the active surface of the flow chamber were determined with narrow, thin (500Å thick) films of platinum, also electrically insulated from the fluid by the use of an overcoating of silicon nitride film. The platinum strips were used to infer the temperatures at the fluid-heater interface. Space limitations do not allow further discussion of the experiments.

References

- J. D. Andrade, R. A. VanWagenen, D. E. Gregonis, K. Newby, and J-N Lin, 1985, "Remote Fiber-Optic Biosensors Based on Evanescent-Excited Fluoro-Immunoassay: Concept and Progress," IEEE Trans. Elect. Dev., 1175-1179.
- J. D. Andrade, J-N Lin, J. Herron, and M. Reichert, and J. Kopecek, 1986, "Fiber Optic Immunodetectors: Sensors or Dosimeters?," SPIE 718, p. 280.
- W. P. Collins, ed., 1985, "Alternative Immunoassays," Wiley.
- J. A. De Feijter, J. Benjamins, and F. A. Veer, 1978, "Ellipsometry as a Tool to Study the Adsorption Behavior of Synthetic and Biopolymers at the Air-Water Interface," Biopolymers, Vol. 17, p. 1759.
- J. W. Goding, 1983, "Monoclonal Antibodies," Academic Press, pp.199-203.
- C. L. Hill, 1984, "Switch Immunoaffinity Chromatography with Monoclonal Antibodies," Biotechniques, Vol.14.
- F. Incropera and D. DeWitt, 1985, "Introduction to Heat Transfer," J. Wiley, p. 202-205.
- I. Pecht, 1982, "Dynamic Aspects of Antibody Function," in M. Sela, ed., The Antigens, Vol.6, Academic Press, P.1.
- R. R. Walters, 1985, "Affinity Chromatography," Anal. Chem. 57, 1099A; I. Parikh and P. Cuatrecasas, 1985, "Affinity Chromatography," Chem. Eng. News.

Acknowledgement

The partial support of the U. S. Army Research Laboratories through DAAL03-87-K0134 is appreciated.

BIOHEAT TRANSFER — APPLICATIONS IN HYPERTHERMIA, EMERGING HORIZONS IN INSTRUMENTATION AND MODELING

presented at
THE WINTER ANNUAL MEETING OF
THE AMERICAN SOCIETY OF MECHANICAL ENGINEERS
SAN FRANCISCO, CALIFORNIA
DECEMBER 10-15, 1989

co-sponsored by
THE HEAT TRANSFER DIVISION AND
THE BIOENGINEERING DIVISION, ASME

edited by
R. B. ROEMER
UNIVERSITY OF ARIZONA
J. J. McGRATH
MICHIGAN STATE UNIVERSITY
H. F. BOWMAN
MASSACHUSETTS INSTITUTE OF TECHNOLOGY

THE AMERICAN SOCIETY OF MECHANICAL ENGINEERS
United Engineering Center • 345 East 47th Street • New York, N.Y. 10017

Nature of Water in Synthetic Hydrogels

III. Dilatometry, Specific Conductivity, and Dielectric Relaxation of Poly(2,3-dihydroxypropyl methacrylate)

SUNHEE CHOI AND MU SHIK JHON¹

Department of Chemical Science, Korea Advanced Institute of Science, Seoul, Korea

AND

JOSEPH D. ANDRADE

University of Utah, Department of Materials Science and Engineering, Salt Lake City, Utah 84112

Received August 14, 1975; accepted August 26, 1976

The hypothesis that three classes of water exist in hydrogels, namely, X water (bulk water-like), Z water (bound water-like) and Y water (intermediate water), has been verified, and the dynamic aspects of those waters have been studied in poly(2,3-dihydroxypropyl methacrylate) (PDHPMA) hydrogels. Bulk gel conductivity data for PDHPMA gel was obtained. The activation energy for specific conduction was obtained from the specific conductivity curve at various temperatures. A plot of the activation energy vs volume percent of water in the gels clearly indicated three different zones, showing three classes of water in the gels. These results were confirmed by thermal expansion measurements. The high-water-content gels (60%) showed an extremely sharp volume change at 0°C, indicating the presence of normal bulk water. Lower-water-content gels (20%) showed no anomalous change in thermal expansion, indicating that the water is bound. The medium-water-content gels exhibited intermediate behavior. A semiquantitative analysis of the three classes of water is presented. The third method used was dielectric relaxation. At low frequencies the dielectric constant of PDHPMA gels is much higher than that of water. The dielectric constant decreases continuously as the frequency increases, tending to level off at about 10^8 Hz. The higher the concentration of polymer in the gel, the lower the dielectric constant. Results are most reasonably explained by assuming the more structured phase of water for the low dielectric constant.

INTRODUCTION

The nature of water has long been of great interest and has been extensively studied. Questions of water structure, water of hydration, and similar problems are of biological significance, e.g., the structure of water in living cells, the role of hydrated water around protein molecules, etc. (1-3). There has also been great interest in the hydration of macromolecular species and the state of water molecules in hydrophilic polymer systems. The interactions between water and synthetic

polymers have been widely reviewed recently by Molyneux (4).

Hydrogels are promising materials for biomedical applications (5). Many of the physical, physiological, and interfacial properties of such gels may be related to the organization of water within and on the surface of the hydrogels (6). So, the study of the nature of water in synthetic hydrogels is very important both for pure scientific interest and for the development of biomedical materials.

There is substantial evidence that a fraction of water in hydrogels may be significantly different from normal or bulk water. Jhon and

¹ To whom correspondence should be addressed.

Andrade (6) have hypothesized that hydrogels may contain three classes of water; X water (bulk water-like), Z water (bound water-like), and Y water (intermediate forms). Others have proposed similar hypotheses (7-9). This hypothesis is supported by experiments (10-12) carried out in natural systems, such as agar and starch. High-resolution NMR (12, 13) and infrared spectroscopic (13, 14) studies also demonstrate the presence of three types of water. Lee *et al.* (15, 16) have verified the hypothesis using dilatometry, specific conductivity, differential scanning calorimetry (DSC), and proton pulse NMR studies of poly(2-hydroxyethyl methacrylate) (PHEMA) gels.

The object of this research is to check further the validity of the X, Y, Z hypothesis and to study the dynamic aspects of X, Y, and Z water. Specific conductivity and thermal expansion have been measured from -15°C to room temperature for poly(2,3-dihydroxypropyl methacrylate) (PDHPMA) gels of various water contents to test the hypothesis.

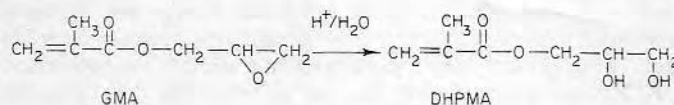
In addition, to obtain new information on the structure of water in hydrogels, dielectric relaxation studies were carried out at 15°C .

DHPMA is more hydrophilic than most other methacrylate monomers because it has two hydroxyl groups. Hydrophilicity of the gel may be very important in determining the biocompatibility of gels. It is hypothesized that blood compatibility may be improved as the interfacial free energy between the surface of the gel and blood plasma decreases (17), which may be dependent on water organization at the gel/solution interface (17).

EXPERIMENTAL

A. Preparation of DHPMA Monomer

The synthesis of DHPMA has been generally described by Refojo (18). DHPMA is prepared by hydrolyzing glycidyl methacrylate. Glycidyl methacrylate (GMA) is commercially available. The hydrolysis reaction is



B. Sample Polymerization

The monomer was dissolved in distilled water. About 0.6% by weight (with respect to monomer) of tetraethylene glycol dimethacrylate (TEGDMA) was added. The polymerization was initiated by an aqueous redox system of $(\text{NH}_4)_2\text{S}_2\text{O}_8$ and $\text{Na}_2\text{S}_2\text{O}_5$ at room temperature. Gelation of the monomer mixtures occurred within a few hours; after standing at room temperature overnight, they were cured at elevated temperature (60°C) for an hour.

The gels thus contained the amount of water present in the original monomer solution. They were not equilibrated with water.

C. Specific Conductivity

Specific conductivity was measured with a conductivity bridge (Yellow Springs Instru-

ment Co., Model 31) using a 1-kHz ac signal. The use of alternating current avoids polarization of the electrode in the conduction cell. Platinum disks (99.98%) were used for electrodes. The polymer sample (0.2-cm thickness) was placed between two electrode plates. They were contacted with silver conductive paint (GC Electronics, Rockford, Ill.) to minimize contact resistance.

D. Dilatometric Measurements

The volume change of the gels was determined by means of thermal expansion measurements over the temperature range of room temperature to -15°C using a dilatometer filled with sample and mercury. The apparent specific volume change, $\Delta\Phi_g$, of the gel was calculated by the equation

$$\Delta\Phi_g = [S(h - h_0) - \Phi_{\text{Hg}} \cdot V_{\text{Hg}}^{\circ} \cdot d_{\text{Hg}}^{\circ}] / M_s, [1]$$

where S is the cross-sectional area of the capillary; h and h_0 are the heights of the mercury column at the temperature $t^\circ\text{C}$ and the reference temperature, respectively; Φ_{Hg} is the specific volume of mercury at $t^\circ\text{C}$; V_{Hg}° is the volume of mercury in the dilatometer at the reference temperature; d_{Hg}° is the density of mercury at the reference temperature; and M_s is the mass of the sample.

E. Dielectric Relaxation

The dielectric constant, ϵ , of a medium may be defined as the ratio of a field strength in a vacuum to that in the medium for the same distribution of charge (19). It may also be defined, and is generally measured, as the ratio of the capacitance, C , of a condenser filled with the material in question to the capacitance, C_0 , of the empty condenser; that is $\epsilon = C/C_0$.

The monomer mixture was poured into a special coaxial cell and polymerized in the cell in order to obtain good contact between sample and electrodes. A standard replacement-bridge method, with an RF vector impedance meter (Hewlett Packard, Model 4815 A), was used. The interest region for bound water in gels occurs approximately at 10^5 to 10^7 Hz (20), but we explored the region of 10^6 to 10^8 Hz for all gels. All data were taken at about 15°C .

RESULTS AND DISCUSSION

A. Specific Conductivity

The specific conductivities for various water contents of gels over the temperature range of 20 to -10°C were determined. Plots of specific conductivity (κ) vs temperature for PDHPMA gels of different water contents are presented in Fig. 1. $\log \kappa$ is linearly proportional to $1/T$ for temperatures higher than the transition temperature. A sharp discontinuous change in the $\log \kappa$ vs the $1/T$ curve near 0°C indicates that the high-water-content gels have significant amounts of "normal" or X water. As the water content becomes lower, the change at the transition point becomes smaller. The

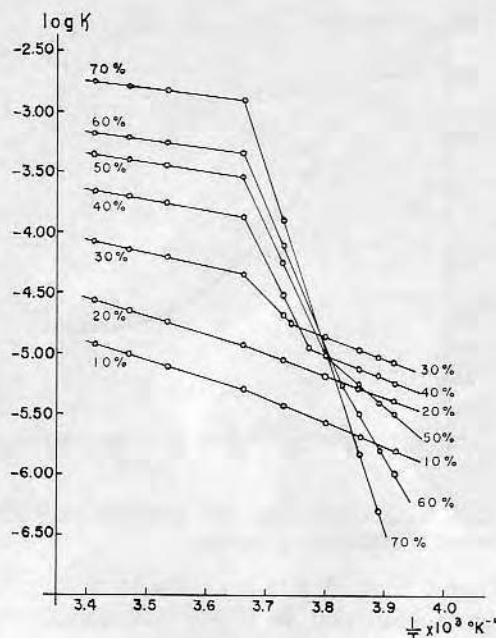


FIG. 1. Specific conductivity vs reciprocal temperature for PDHPMA hydrogels as a function of water content.

20% water gel does not show a sharp drop in specific conductivity at 0°C . This fact indicates that as the water content decreases, the amount of normal water decreases.

The apparent activation energy for specific conduction for each different gel (Fig. 2) could be obtained from the slope of the straight lines in Fig. 1, on the basis of the equation (21)

$$\log \kappa = \text{const} - (\Delta E_a / 2.303RT). \quad [2]$$

One can analyze Fig. 2 in terms of three classes of activation energies which may correspond to the activation energy of "normal" water (X water), that of "bound" water (Z water), and that of Y water. The activation energy, 2.8 kcal/mole for gels of 60 to 70% water content in Fig. 2 is near the value of the activation energy for proton transport in aqueous solutions, 2.5 to 2.8 kcal/mole (22). The activation energy of conduction for ice doped with ionic impurities is in the range of 6.8 and 7.8 kcal/mole (23), which is the same order as the activation energy for gels of 10 to 20% water content, 7.0 to 6.8 kcal/mole. These facts

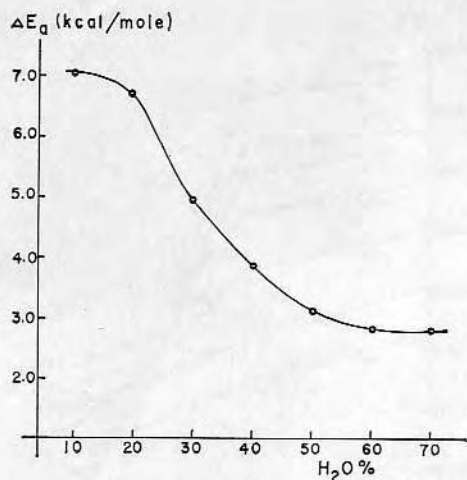


FIG. 2. Activation energy for conductivity vs water content of PDHPMA hydrogels.

suggest that in the low-water-content gels, the conductivity is largely determined by bound water with nonfreezing behavior while in the high-water-content gels, it is largely determined by nonbound water with normal freezing properties.

B. Dilatometric Measurements

The specific volume change of the gel, $\Delta\Phi_g$, was obtained from the dilatometric measure-

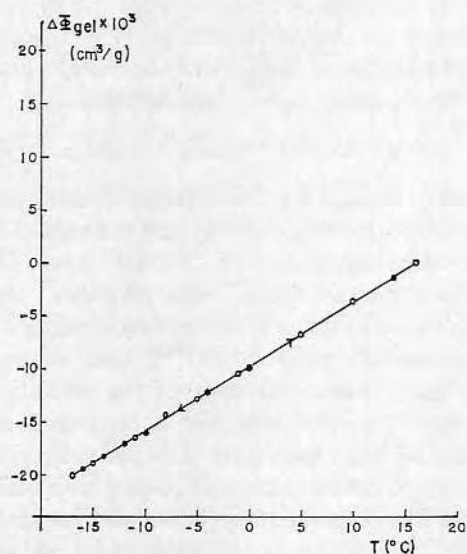


FIG. 3. The specific volume change vs temperature for a 20% water PDHPMA gel.

Journal of Colloid and Interface Science, Vol. 61, No. 1, August 1977

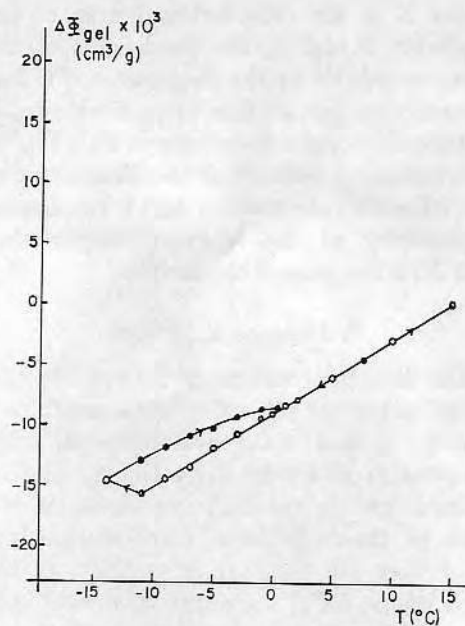


FIG. 4. The specific volume change vs temperature for a 25% water PDHPMA gel.

ments by Eq. [1]. The results are presented in Figs. 3 to 7. The gel with 20% water content shows a straight line having neither hysteresis

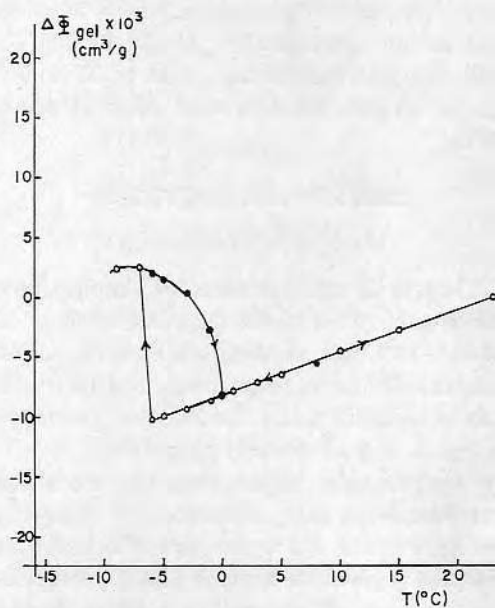


FIG. 5. The specific volume change vs temperature for a 30% water PDHPMA gel.

in thermal expansion nor an anomalous change in the specific volume around 0°C. The 25% water gel shows a slight hysteresis, the heating path discontinuously joining the cooling path in the vicinity of 0°C (Fig. 3). The hysteresis increases as the water content of the hydrogel increases (Figs. 4 to 7). The hysteresis is most pronounced in the high-water-content hydrogel (60% water).

Since no anomalous change was detected for gels with lower water contents, the water in such gels is considered to show no transition in this temperature range. Most of the water in such lower-water-content gels is presumed to be Z water (bound water). Therefore, Z water may have no transition over the range from -15 to 0°C.

Judging from the extremely sharp change in the specific volume for higher-water-content gels, the transition temperature of X water may be 0°C, for X water is presumed to be the main component of the higher-water-content gels.

The gradual decrease in the specific volume with an increase in temperature over the range

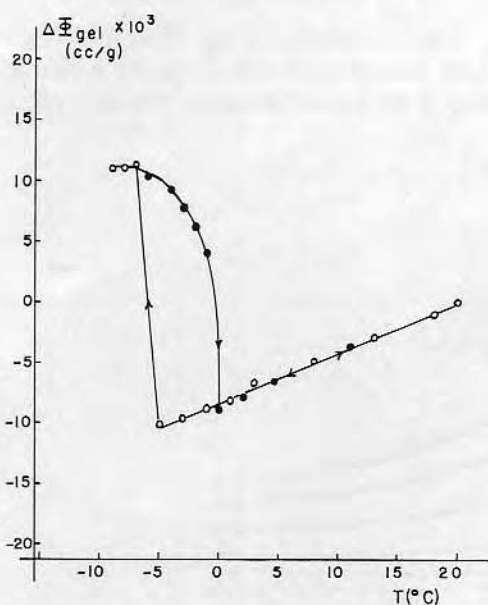


FIG. 6. The specific volume change vs temperature for a 40% water PDHPMA gel.

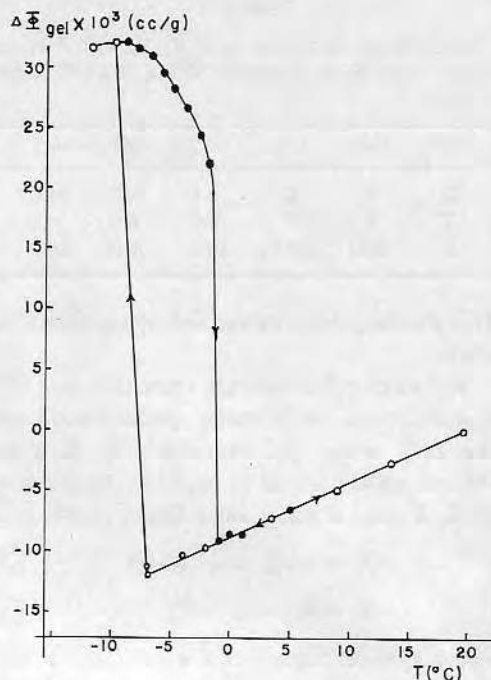


FIG. 7. The specific volume change vs temperature for a 60% water PDHPMA gel.

from -15 to 0°C is considered to indicate that the transition temperatures, perhaps for Y water, should be distributed over this temperature range.

These results lead us to conclude that (i) the transition temperature of X water may be 0°C, (ii) that of Y water may be distributed over the range from -15 to 0°C, and (iii) Z water may have no transition temperature in the range from -15 to 0°C. The above conclusions agree with the specific conductivity results.

Hysteresis phenomena similar to those shown in Figs. 3 to 7 can be found in the literature. Aizawa and Suzuki (10) and Lee *et al.* (15) obtained such data for agarose gels and PHEMA gels, respectively. The degree of hysteresis of PDHPMA gels is greater than that of PHEMA of the same water content. From this fact we may presume that the PDHPMA gel has a higher percentage of X water (normal water) than PHEMA gel.

TABLE I

Approximate Contribution of X, Y, and Z Water to the Total Water Contents (W) of PDHPMA gels (vol%)

W	20%	25%	30%	40%	60%
X	0	0	4.1	14.0	34.0
Y	0	0	5.9	6.0	6.0
Z	20.0	20.0	20.0	20.0	20.0

This presumption was verified by the following work.

The assumption that the transition near 0°C is mainly due to X water (bulk water) and the 20% water gel contains only Z water (bound water) led us to calculate the amount of X, Y, and Z water from Eqs. [3] and [4]:

$$X = (\Delta\Phi_g / \Delta\Phi_w) \times 100; \quad [3]$$

$$Y = W - X - Z, \quad [4]$$

where X = percentage of X water (bulk water) in the gel; $\Delta\Phi_w$ = volume change of ice to water at 0°C , $91.1 \times 10^{-3} \text{ cm}^3/\text{g}$; Y = percentage of Y water in the gel; W = total percentage of water in the gel; and Z = percentage of Z water (bound water) in the gel. The amount of normal water in the gel is obtained using Eq. [3] with $\Delta\Phi_g$ values taken from Figs. 5, 6, and 7, and the $\Delta\Phi_w$ value from Ref. (21). Also, the amount of Y water is

obtained using Eq. [4], assuming that up to 20% of the gel is Z water. The results are shown in Table I.

As seen in Table I, the amount of Y water appears to reach a near-constant value for gels of 30 to 60% water content. There is apparently no bulk or normal water in the gel until the maximum interfacial water content is reached; after that point, all additional water in the gel behaves as bulk or X water. The percentage of X water in PDHPMA gel is higher than that in PHEMA gel (15) with the same total water contents in the gels.

This observation is consistent with our model since PDHPMA gels are more hydrophilic than PHEMA gels (15, 18). However, the observed Z water percentage is the same for both gels. We studied 20, 25, and 30% water content PDHPMA gels, while Lee *et al.* (15) studied only 20 and 30% water PHEMA gels. We would expect that in PHEMA gels, the Z water percentage would be a little higher than 20% if more extensive experiments are performed. Such experiments are now in progress.

C. Dielectric Relaxation

The relationship of the dielectric constant with concentration and frequency is shown in Fig. 8 for PDHPMA gels. Toward very low

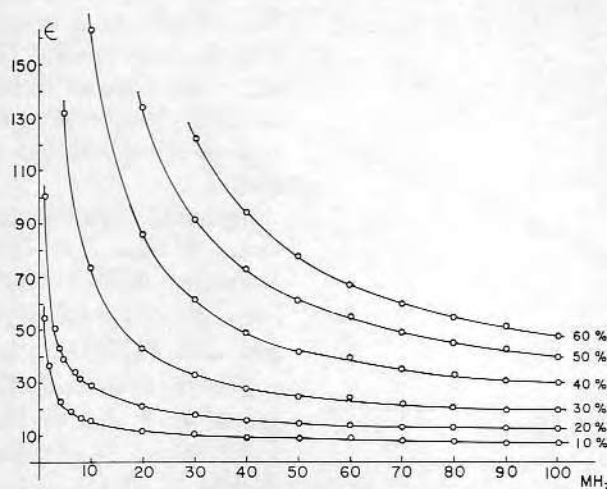


Fig. 8. Dielectric constant as a function of frequency and water content for PDHPMA hydrogels.

frequencies, ϵ values rise continuously and more sharply. Toward high frequencies, the curve of ϵ tends to level out. At the frequencies used, ϵ of water is about 80. It is apparent that the ϵ values of all gels are higher than the ϵ value of water at low frequencies; only at high frequencies do the values become lower than the ϵ of water, particularly in the gels of higher polymer concentration. The ϵ values of the gels do not follow a curve parallel to that of water, ice, or theoretically bound water (24).

Although the use of relaxation techniques (for example, NMR and dielectric) seems to offer the most promising prospects for the future studies of the role of water in polymers and many groups (25-28) use the relaxation technique to interpret the nature of bound water, the general theory about the relaxation of water interacting with other molecules has not been available up to now. While the data we have obtained are insufficient to discuss deeply the dielectric behavior of water in hydrogels, a few comments can be made. It seems that water molecules bound to the gel are polarized in an electric field acting as conductors, perhaps as in ice. With increasing order in the water lattice, the low-frequency dielectric constant increases, as is evident from the fact that ice has a higher dielectric constant than water, and the fact that the dielectric constant of ice increases rapidly with decreasing temperature (29). Furthermore, as the electric field alternates, there is probably electrical transfer through an oscillation of the electron cloud and/or the protons between the molecules (30). The conductivity behavior of polarized water can be thought to contribute considerably to the high dielectric increment at low frequencies. As the frequency increases, the mobility of the protons in the lattice-ordered water decreases (31), because they cannot follow the cyclic change. So, a sharp decrease of dielectric constant occurs. Unlike the situation in rigid ice, there is no sharp drop in dielectric constant of gels, however, because the protons and electron cloud in many of the water molecules still retain a certain mobility, which is greater the lower the concentration

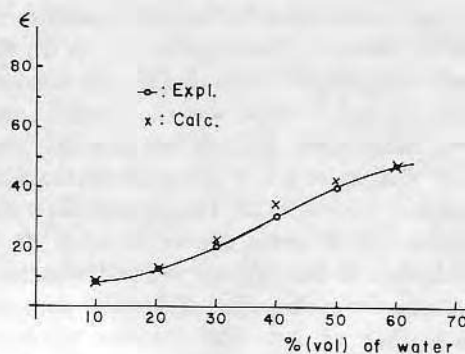


FIG. 9. Dielectric constant as a function of water content for PDHPMA hydrogels at the frequency of 100 MHz.

of polymer. So the lower the concentration of polymer, the broader the dielectric dispersion curve obtained. The varying degrees of lattice order also contribute to the broad distribution of dielectric dispersion.

At frequencies above the dielectric dispersion region, the gels give a decrement in the dielectric constant. This behavior is to be expected, since the lattice-ordered structure should have a lower dielectric constant than water at frequencies above the dispersion region.

The results are most reasonably explained by assuming a more solid structure of water the lower the dielectric constant at the high-frequency region. The concentration dependence of ϵ for the gel samples at 100 MHz is depicted in Fig. 9. In this frequency region, the following equation for the dielectric constant has been established.

$$\epsilon = \epsilon_X \cdot f_X + \epsilon_Y \cdot f_Y + \epsilon_Z \cdot f_Z + \epsilon_P \cdot f_P, \quad [5]$$

where $\epsilon_X, \epsilon_Y, \epsilon_Z$ = dielectric constants of X water, Y water, and Z water, respectively, ϵ_P = dielectric constant of pure polymer; f_X, f_Y, f_Z = mole fractions of X, Y, and Z water; and f_P = mole fraction of pure polymer. The dielectric constant of pure polymer is about 3, and the values of ϵ_X, ϵ_Y , and ϵ_Z are chosen so as to give the best fit to the experimental data (Fig. 9) when the above equation is used. The resulting values of ϵ_X, ϵ_Y , and ϵ_Z at 100 MHz are 75, 35, and 17, respectively.

The agreement between theoretical and experimental values is illustrated in Fig. 9. On the basis of calculated values of dielectric constant of X, Y, and Z water, one can deduce structural information. Because the dielectric constant of X water ($\epsilon_X = 75$) is almost the same as that of normal water. The very low dielectric constant of Z water ($\epsilon_Z = 17$) leads us to think that it has a very ordered structure, although the orderedness of Z water does not reach that of ice. The medium value of dielectric constant of Y water ($\epsilon_Y = 35$) indicates that it has intermediate structure between normal water and lattice-ordered water. In other words, its structure is more ordered than X water and less ordered than Z water.

ACKNOWLEDGMENT

This work was supported in part by the Euisok Research Foundation and by the National Institutes of Health, under Grant HL 16921-01.

REFERENCES

1. DROST-HANSEN, W., in "Chemistry of the Cell Interface" (H. D. Brown, Ed.), Part B. Academic Press, New York, 1971.
2. TAIT, M. J., AND FRANKS, F., *Nature* **230**, 91 (1971).
3. SAUNDERS, J. F., AND FLYMS, J. E., *Ann. N. Y. Acad. Sci.* **125**, 251 (1965).
4. MOLYNEUX, P., in "Water: A Comprehensive Treatise" (F. Franks, Ed.), Vol. 4, Chap. 7. Plenum, New York, 1974.
5. ANDRADE, J. D., Ed., "Hydrogels for Medical and Related Application," American Chemical Society, Washington, D.C. (1976).
6. JHON, M. S., AND ANDRADE, J. D., *J. Biomed. Mater. Res.* **7**, 509 (1973).
7. KRISHNAMURTHY, S., MCINTYRE, D., AND SANTEE, D., *J. Polym. Sci. Phys.* **11**, 427 (1973).
8. HORNE, R. A., DAY, A. F., YOUNG, R. P., AND YU, N. T., *Electrochem. Acta* **13**, 397 (1963).
9. DROST-HANSEN, W., *Ind. Eng. Chem.* **61**, 10 (1969).
10. AIZAWA, M., AND SUZUKI, S., *Bull. Chem. Soc. Japan* **44**, 2967 (1971).
11. MIZUGUCHI, J., TAKAHASHI, M., AND AIZAWA, M., *Nippon Kagaku Zasshi* **91**, 723 (1970).
12. AIZAWA, M., MIZUGUCHI, J., SUZUKI, S., HAYASHI, S., SUZUKI, T., MITOMO, N., AND TOYAMA, H., *Bull. Chem. Soc. Japan* **45**, 3031 (1972).
13. HAZELWOOD, C. F., NICHOLS, B. L., AND CHAMBERLAIN, N. F., *Nature* **222**, 747 (1969).
14. HANSEN, J. R., AND YELLIN, W., in "Water Structure at the Water-Polymer Interface" (H. H. G. Jellinek, Ed.), p. 19. Plenum, New York, 1972.
15. LEE, H. B., JHON, M. S., AND ANDRADE, J. D., *J. Colloid Interface Sci.* **51**, 225 (1975).
16. LEE, H. B., ANDRADE, J. D., AND JHON, M. S., *Polym. Prepr. Amer. Chem. Soc. Div. Polym. Chem.* **15**, 706 (1974).
17. ANDRADE, J. D., LEE, H. B., JHON, M. S., KIM, S. W., AND HIBBS, J. B., JR., *Trans. Amer. Soc. Artif. Intern. Organs* **19**, 1 (1973).
18. REFOJO, M. F., *J. Appl. Polym. Sci.* **9**, 3161 (1965).
19. SMYTH, C. P., "Dielectric Behavior and Structure: Dielectric Constant and Loss, Dipole Moment and Structure." McGraw-Hill, New York, 1955.
20. JACOBSON, B., *J. Amer. Chem. Soc.* **77**, 2919 (1955).
21. GLASSTONE, S., LAIDLER, K. J., AND EYRING, H., "The Theory of Rate Processes." McGraw-Hill, New York, 1941.
22. BOCKRIS, J. O., AND REDDY, A. K., "Modern Electrochemistry," Vol. 1. Plenum, New York, 1970.
23. GROSS, G. W., *Ann. N. Y. Acad. Sci.* **125**, 380 (1966).
24. SCHWAN, H. P., *Ann. N. Y. Acad. Sci.* **125**, 344 (1966).
25. WOESSNER, D. E., SNOWDEN, B. S., JR., AND MEYER, G. H., *J. Colloid Interface Sci.* **34**, 43 (1970).
26. WOESSNER, D. E., AND SNOWDEN, B. S., *J. Colloid Interface Sci.* **34**, 290 (1970).
27. PACKER, K. J., REES, C., AND TOMLINSON, D. J., *Advan. Mol. Relaxation Processes* **3**, 119 (1972).
28. DERBYSHIRE, W., AND PARSONS, J. L., *J. Magn. Resonance* **6**, 344 (1972).
29. AUTY, R. P., AND COLE, R. H., *J. Chem. Phys.* **20**, 1309 (1952).
30. LATIMER, M. W., *Chem. Rev.*, **44**, 59 (1949).
31. MASUZAWA, M., AND STERLING, C., *Biopolymers* **6**, 1453 (1968).

D. Christensen*[†], J. Andrade[†], J. Wang[†], J. Ives[†], and D. Yoshida*

*Dept. of Electrical Engineering and [†]Dept. of Bioengineering
University of Utah, Salt Lake City, Utah 84112 USA

ABSTRACT

An important consideration in the analysis of optical waveguide sensors (such as the fiberoptic fluorescent immunosensor) is the amount of total emitted fluorescence from the surface-bound proteins which is trapped and guided by the waveguiding structure of the sensor. In this paper we use a new Finite-Difference Time-Domain (FDTD) numerical technique to analyze the percentage of total fluorescence from surface dipoles which is coupled into the guided mode via the mode's evanescent tail.

1. INTRODUCTION

Guided wave devices are gaining increased attention in the fields of sensing, telecommunications, and optical processing. Of interest to our group is the use of optical waveguides for the evanescent detection of antigen concentrations on specially prepared surfaces of optical sensors--i.e., optical immunosensors.¹ In this application, the antigens to be measured are typically given fluorescence capability (either by being directly fluorescently labeled themselves, or by displacing predeposited labeled antigens through competitive binding). The fluorescently labeled antigens which attach to specific antibodies bound to the surface of the waveguide are excited via evanescent coupling of energy from a guided laser beam, whereupon they fluoresce, and in turn a portion of this fluorescence is coupled back into the waveguide through the waveguide mode's evanescent tail for remote detection. The limited depth of penetration of the evanescent energy into the sensing medium (typically less than 0.5 μ m) greatly increases the sensor's sensitivity to surface-bound antigens compared to emitters in the bulk solution.

A key question in comparing the optical efficiency of this type of sensor to more conventional bulk measurements is the amount of total emitted fluorescence which is collected and guided by the waveguide modes. Simple ray theory cannot be used here since it predicts no coupling between sources located outside the waveguide and the guided rays. More exact electromagnetic theory must be employed. Marcuse has recently dealt with a related question of the coupling efficiency of dipole sources distributed throughout the cladding layer into the core of a round fiber.²

2. FDTD MODEL

We have applied a newly developed technique, the Finite-Difference Time-Domain (FDTD) method, to this problem.³ In essence, this method numerically solves Maxwell's equations as a function of both space and time for regions of varying dielectric constants. Included in the two-dimensional model are a glass substrate region, a waveguide region, an outside bulk (solution) region, and varying configurations of fluorescent sources on the surface of the waveguide. Figure 1 shows a cross-section of the waveguide model analyzed here.

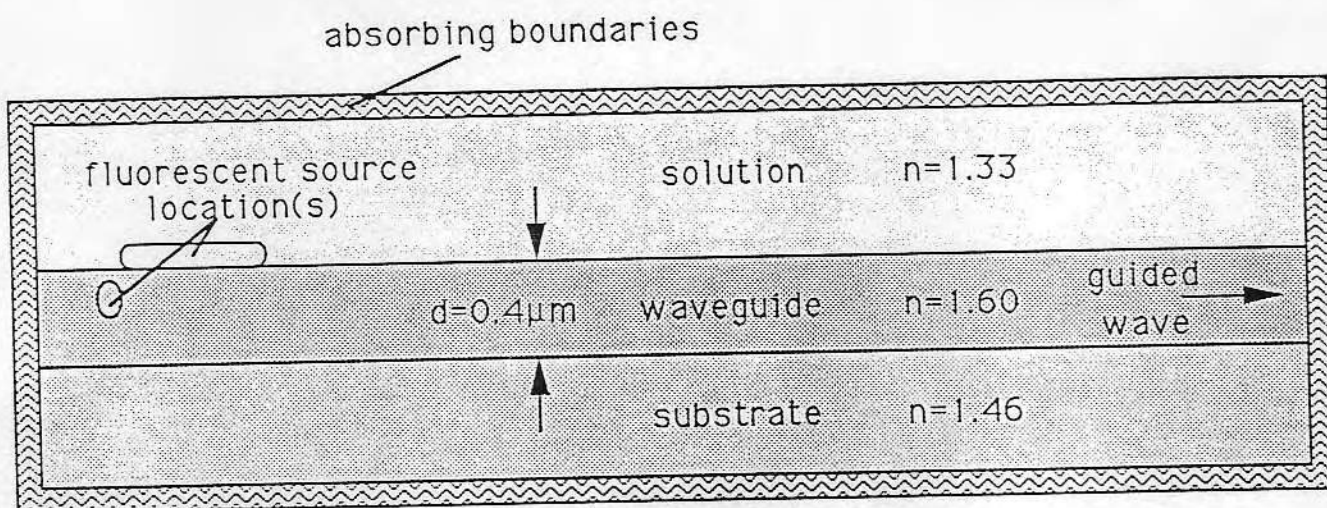


Fig. 1. Cross-section of the model used for FDTD analysis of power coupled from various fluorescent sources into the guided mode of the waveguide.

A fluorescence wavelength near 488 nm is assumed, and the waveguide thickness is chosen to be $0.4\mu\text{m}$, corresponding to a single-mode guide. For the indices of refraction shown in Fig. 1 for the waveguide and its cladding layers, the normalized frequency parameter V is calculated to be $V=3.377$, assuring that only the lowest order TM_0 mode will be guided by the waveguide, and higher order modes will be cutoff.⁴ This simplifies interpretation of the resulting radiation patterns.

In the FDTD method, the grid containing the model must be terminated on its outer boundaries by some means to avoid reflections from these boundaries. To simulate a model which effectively stretches to infinity, artificial "absorbing" boundary conditions are added to the outer perimeter of the grid. We used first order absorbing boundary conditions to achieve this effect (see Fig. 1).

3. FLUORESCENT SOURCE CONFIGURATIONS AND RESULTS

The fluorescent sources are treated as electric dipoles. We analyzed a series of different configurations of sources to examine the power coupling efficiency of each. A measure of this coupling efficiency may be made by calculating the amount of power carried in one direction along the waveguide by the guided mode (P_g) and also the total amount of power radiated in all directions by the source dipoles (P_s). The powers are determined from the FDTD results by numerically integrating the normal components of the Poynting vector along appropriate surfaces: within the waveguide at one end to determine P_g , and around the entire perimeter of the grid to determine P_s . The integration surface inside the waveguide is taken sufficiently far from the location of the sources to assure that the mode carries only truly guided power P_g , and that leaky mode power is dissipated.

The measure of coupling efficiency is determined by the percentage of total radiated power which is guided in one direction by the mode. That is:

$$\% \text{ guided} = P_g/P_s$$

Figure 2 shows the various source configurations analyzed and the resulting percentage of guided power for each.

4. DISCUSSION AND CONCLUSIONS

As seen in Fig. 2, the first configuration (Configuration #1) models a dipole source (E_x) embedded in the waveguide core itself. As expected, the percentage of power coupled into the guided mode is large (21.6%) since the source is in an ideal location where the strength of the vertical electric field of the mode is high. If the power trapped in the mode propagating in the reverse direction were added, the percentage of guided power would be even larger, approximately twice that listed.

Configuration #2 more directly applies to the question of evanescent coupling of surface sources into the guide. As shown in Figure 2, the percent coupling is still appreciable (6.4%) for an outside source polarized perpendicular to the guide (E_x). For electric dipole sources oriented in the direction parallel to the guide (E_y in Configuration #3) however, the coupling is very weak (0.7%) since the

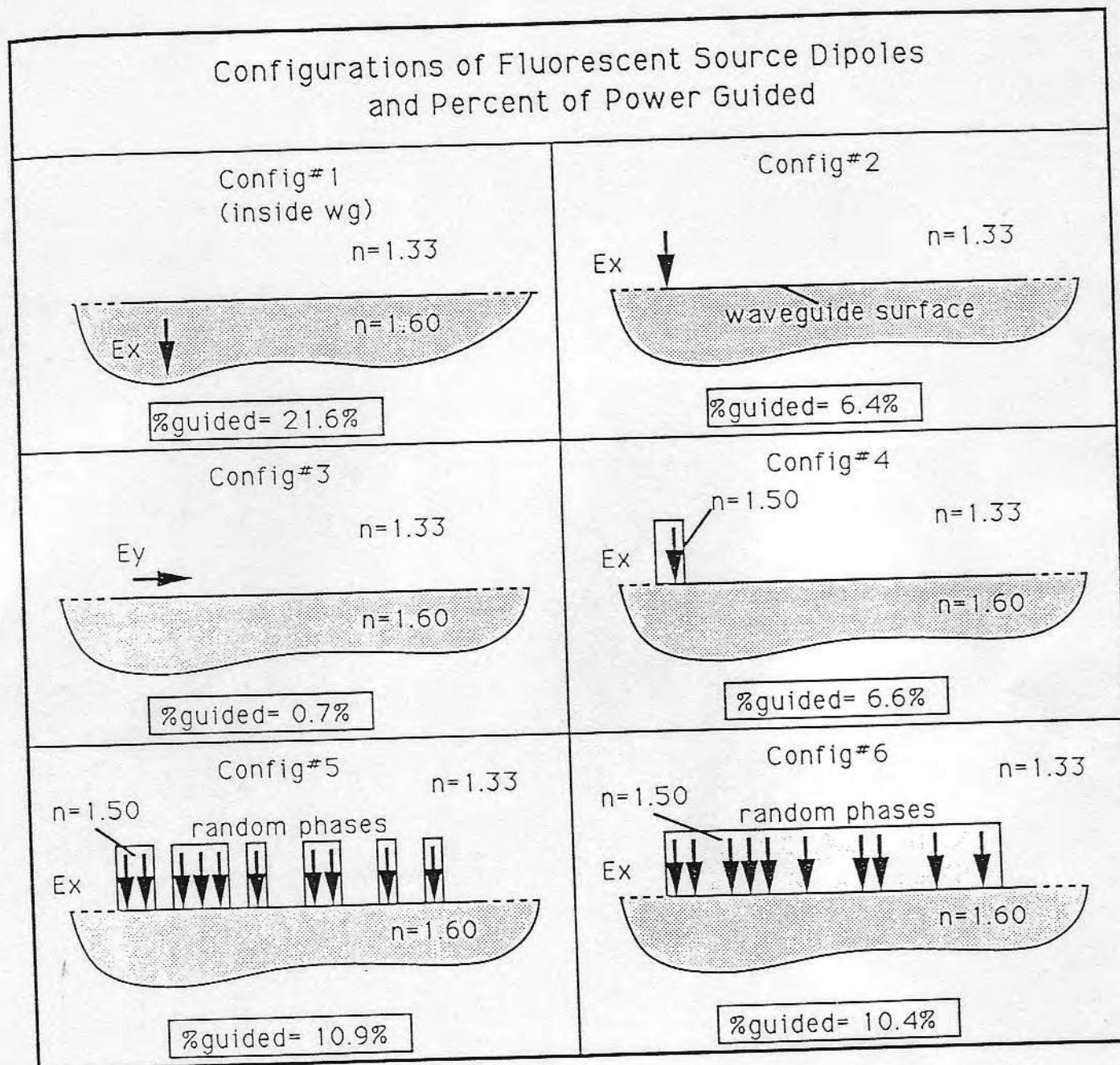


Fig. 2. Various source configurations analyzed and the resulting percentage of guided power for each.

guided TM_0 mode has only a very small component of its electric field in that direction. Configuration #4 shows that surrounding the source dipole with an intermediate index of refraction ($n=1.50$), as might be an appropriate model of proteins, has little effect on the coupling efficiency.

Multiple sources are treated in Configurations #5 and #6. Ten dipoles are spaced irregularly along the surface of the guide. Their phases are randomized by the computer in order to model largely incoherent fluorescent emission. The percentage of guided power increases slightly, probably due to a small amount of inadvertent coherence between the sources. Comparison of the two configurations shows that whether the medium immediately surrounding the sources is continuous or broken has a small influence on the percentage of power coupled into the guide.

In conclusion, these results show that a measurable amount of fluorescent emission from surface sources may be detected by an optical waveguide. Using an average of the results from Configuration #2 and Configuration #3 to approximate the random orientation that is usually found in fluorescent molecules, it can be seen that approximately 3.5% of the total emitted power is expected to be coupled into a waveguide in the form of a guided mode.

5. REFERENCES

1. A. Voller, A. Barlett, and D. Bidwell, eds., *Immunoassay for the 80's*, University Park Press, Baltimore, 1981.
2. D. Marcuse, "Launching Light into Fiber Cores from Sources Located in the Cladding," *J. of Lightwave Technology*, vol. 6, p. 1273, August 1988.
3. A. Taflov and M.E. Brodwin, "Numerical Solution of Steady-State Electromagnetic Scattering Problems Using the Time-Dependent Maxwell's Equations," *IEEE Trans. on MTT*, vol. MTT-23, pp. 623-630, August 1975.
4. D. Marcuse, *Theory of Dielectric Optical Waveguides*, Academic Press, New York, 1974.

Immunochemical detection by specific antibody to thrombin of prothrombin conformational changes upon adsorption to artificial surfaces

Hanson Y. K. Chuang*

Department of Pathology, University of Utah School of Medicine,
Veterans Administration Medical Center, Salt Lake City, Utah 84148

Joseph D. Andrade

Department of Bioengineering, University of Utah School of Engineering,
Salt Lake City, Utah 84112

Polyclonal antihuman α -thrombin antibodies produced in rabbits reacted minimally ($<0.05\%$) in solution with human prothrombin. However, when prothrombin was adsorbed to artificial surfaces such as polyvinyl chloride (PVC), the cross-reactivity of surface-bound prothrombin with antibody IgG to thrombin ($>95\%$ purity) was shown to be significantly enhanced. On PVC, the molar ratios of antibody IgG to thrombin/prothrombin approached the same level as that of antibody IgG to thrombin/thrombin when thrombin was adsorbed to the same material. The

analyses of antigen-antibodies interaction, in solution with a direct binding assay by immune precipitation at high-speed centrifugation (160,000 g, 30 min), and on solid-phase PVC, were accomplished by use of double-labeling technique, i.e., ^{131}I -thrombin (or ^{131}I -prothrombin) and ^{125}I -antibody IgG to thrombin. The results appear to suggest that prothrombin adsorption to PVC has resulted in some molecular conformational changes so that immunologically the adsorbed prothrombin resembles that of adsorbed thrombin on the same PVC surface.

INTRODUCTION

The study of antibody combining site is a sensitive probe of the structure and conformation of a macromolecule against which the antibody is directed. The relative degree of interaction of a monospecific antibody with different antigens is quantitatively related to the degree of structural similarity between them. Using these conformation specific antibodies, it is possible to study the conformational states or changes of a particular antigenic domain(s) on a protein.¹

Even though prothrombin is the zymogen or precursor of α -thrombin, the antibody to thrombin produced in rabbits by use of either diisopropylfluorophosphate-thrombin² or *N*- α -*p*-tosyl-L-lysine chloromethyl ketone-thrombin as antigen³ has been shown to exhibit a high degree of specificity for thrombin. Both Majerus's group and we have demonstrated by competitive

*To whom correspondence should be addressed.

binding radioimmunoassays that differences of at least three orders of magnitude exist between thrombin and prothrombin in reactions with antibody to thrombin. This small degree of prothrombin cross-reactivity has not been interpreted as being due to thrombin contamination in prothrombin preparations since the slopes for the displacement of ^{125}I -thrombin by thrombin and prothrombin are different.² During the development of an in situ immunoradiometric assay for thrombin adsorbed to artificial surfaces such as Cuprophane or PVC,^{3,4} we observed increased cross reactivity of prothrombin with ^{125}I -antibody IgG to thrombin. Furthermore, a recent study⁵ indicates that prothrombin, when adsorbed to Cuprophane, promotes the adhesion of granulocytes to the surface, an effect coinciding with that of surface-adsorbed thrombin and IgG. However, surface-adsorbed prothrombin does not show amidolytic and esteric activity by specific thrombin assays.⁵ We attempted here to use monospecific antibody IgG to thrombin as a tool to probe the prothrombin conformational changes during prothrombin adsorption to several different types of artificial surfaces. A more quantitative interaction between prothrombin and antibody to thrombin in solution and on artificial surfaces (PVC) is presented by using the double-labeling technique, i.e., ^{131}I -antigen and ^{125}I -antibody.

MATERIALS AND METHODS

1. Thrombin and prothrombin

Human α -thrombin was a gift from Dr. John Fenton II of New York State Department of Health, Albany, NY. Specific activity of the particular preparation used throughout this study was 2606 NIH U/mg. It contained α -thrombin, 89%; β -thrombin, 11%; and no γ -thrombin. The details of the preparation of thrombin and the analyses of the purity of the preparations have been published elsewhere.⁶ Prothrombin was purified from prothrombin complex concentrate (or factor IX complex), donated by Dr. Milan Wickerhauser of the American Red Cross National Fractionation Center, Washington, D.C., as described previously.⁵ The specific activity of prothrombin purified from that product was 1100 NIH U/mg and was shown as one protein band on SDS PAGE and gradient (2.5–27%) gel electrophoresis.⁵

2. Artificial surfaces

PVC discs (4 mm in diameter) were used throughout most of the study. Other materials such as Cuprophane (4 mm discs), glass (5 mm discs), or polystyrene (microtiter dishes) were also used for some comparative studies. The surface characterization and other properties of these materials have been described elsewhere.^{4,5,7–9}

3. Antibody to thrombin production and purification

The details of the preparation of antibody to thrombin with *N*- α -*p*-tosyl-L-lysine chloromethyl ketone (TLCK) inactivated human α -thrombin (α -thrombin, 100%, sp act 2100 NIH U/mg) by a modified method of Shuman and Majerus,² and the purification of antibody IgG to thrombin by immunoabsorption on thrombin-Sepharose have been published.³

4. Radiolabeling of proteins

Prothrombin, thrombin, or antibody IgG to thrombin was labeled with either ¹³¹I or ¹²⁵I by the modified chloramine T method of Tollefson et al.¹⁰ The labeling did not seem to alter the enzymic activities of prothrombin⁵ (on activation) and thrombin⁹ or the immunogenic property of antibody IgG to thrombin.³

5. Radioimmunoassay (RIA): competitive binding assay

For a competitive binding assay of thrombin or prothrombin, ¹²⁵I-thrombin (6–12 ng) was incubated with rabbit antibody IgG to thrombin (>95% purity, 112 ng) in phosphate-buffered saline (PBS, pH 7.4) containing BSA (0.1%) and benzamidine (1 mM) in the absence (controls) and presence of various concentrations of thrombin (0.5–15 ng) or prothrombin (200–10,000 ng) for 20 h at 4°C in 250 μ l microtubes (Airfuge, Beckman Instrument Co., Palo Alto, CA) precoated with BSA (1% in PBS). Goat antirabbit IgG (IgG fractions, 100 μ g, Cappel Laboratories, West Chester, PA) was added and incubated further for 6 h at 22°C. The immune precipitate was obtained by centrifugation at 60,000 *g* for 15 min (Airfuge) and washed once with PBS. The immune precipitate was counted in a gamma counter (Gamma 8000, Beckman Instrument Co., Palo Alto, CA).

6. Immunoradiometric assay (IRA): direct binding assay

Solid phase IRA

Thrombin adsorption,³ or prothrombin adsorption⁵ to artificial surfaces such as PVC and the subsequent reaction with ¹²⁵I-antibody IgG to thrombin has been described previously.³ Briefly, surfaces precoated with proteins were treated first with glutaraldehyde (1% in 0.1 M phosphate, pH 7.0) for 1 h at 22°C. After thorough rinsing, the surfaces were treated with lysine (0.1 M in PBS) for 30 min to block remaining free aldehyde groups. The surfaces were incubated with ¹²⁵I-antibody IgG to thrombin (10 μ g/ml) in PBS containing Tween 20 (0.1%) at 22°C for 4 h or 4°C for 20 h. The materials

were rinsed with PBS containing Tween 20 and BSA and the radioactivity was measured by gamma counting.

During the course of the development of IRA of thrombin we have found that the crosslinking of thrombin with glutaraldehyde is necessary so that thrombin can be stabilized on materials without desorption or exchange with other proteins in subsequent solutions.^{3,4} Crosslinking of other proteins, e.g., albumin, fibrinogen, IgG⁴ or mixture of other vitamin K-dependent factors VII, IX, X (not published), adsorbed on materials at much higher concentrations than thrombin did not seem to increase the nonspecific uptake of ¹²⁵I-antibody IgG to thrombin significantly. Furthermore, Tween 20 and BSA are found also to be absolutely needed in the assay mixtures so that the nonspecific uptake of ¹²⁵I-antibody IgG by materials (e.g., PVC) in the controls can be reduced from as high as 50% to <10% of the same material treated with thrombin (tests) (data not shown). The presence of these agents did not seem to affect the specific antigen and antibody conjugation in the reaction mixture as shown also in the case of fibrinogen-anti-fibrinogen reaction.⁸

IRA by centrifugation

Various amounts of ¹²⁵I-antibody IgG to thrombin (8–1,000 ng) were mixed and incubated with a fixed amount of thrombin (6 ng) or prothrombin (12 ng), or various amounts of thrombin (6–100 ng) or prothrombin (12–2000 ng) were mixed and incubated with a fixed amount of ¹²⁵I-antibody IgG to thrombin (100 ng) at 4°C for 20 h. Immune precipitate was obtained by centrifugation at 160,000 g for 30 min (Airfuge) and washed once with PBS. The radioactivity was counted in a gamma counter.

It was found that the presence of Tween 20 (0.1%) did not seem to affect the antigen and antibody conjugation in solution (data not shown).

RESULTS

To show the high specific interaction of thrombin with antibody IgG to thrombin produced in rabbits and the low cross-reactivity of prothrombin with the same antibody, we have performed two types of assays, namely, the competitive binding assay (RIA) and the direct binding assay (IRA). Figure 1 shows the results of competitive binding assay using ¹²⁵I-thrombin as a marker and a second antibody (goat antirabbit IgG) to facilitate immunoprecipitation. Prothrombin did not seem to compete strongly with thrombin for antibody IgG to thrombin, indicating that cross-reactivity was minimal. Roughly, a 2000-fold concentration (on a weight basis) of prothrombin was needed to compete with thrombin for antibody binding. Furthermore, other vitamin K-dependent factors such as factor VII, IX, and X were found not to be reactive with antibody IgG to thrombin by the same competitive binding assay (data not shown).

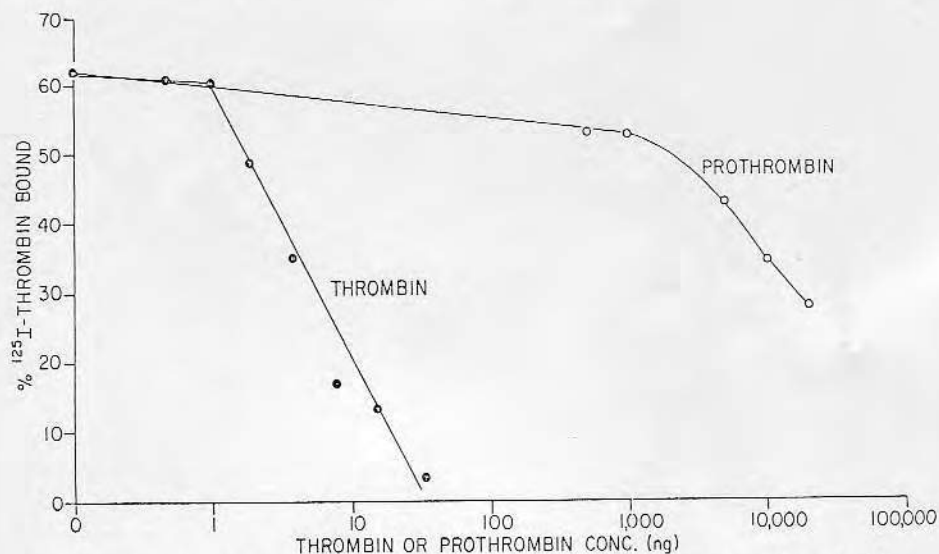


Figure 1. Radioimmunoassay of thrombin and prothrombin with antibody IgG to thrombin. ^{125}I -thrombin (7.8 ng) was incubated with rabbit antibody IgG (112 ng) in PBS containing BSA (0.1%) and benzamidine (1 mM) in the absence (controls) and presence of various concentrations of unlabeled thrombin (●) or prothrombin (○) for 20 h at 4°C. Goat antirabbit IgG (100 μg) was added and incubated further for 6 h at 22°C. The immunoprecipitate was obtained by centrifugation at 60,000 g (Airfuge, Beckman Instrument Co.) for 15 min and washed once with PBS. The immunoprecipitate was counted in a gamma counter. Results are representative of five determinations.

The results of direct immunoprecipitation of either thrombin or prothrombin with ^{125}I -antibody IgG to thrombin by sedimentation in an Airfuge (160,000 g, 30 min) are shown in Figures 2 and 3. It can be seen in Figure 2 that with fixed concentration of thrombin (6 ng) the amount of ^{125}I -antibody IgG to thrombin in the immunoprecipitate increased with increasing concentration of ^{125}I -antibody IgG to thrombin in the bulk solution. On the contrary, essentially no immunoprecipitate was formed when prothrombin (12 ng) was used under identical conditions since the amount of ^{125}I -antibody IgG to thrombin in the immunoprecipitate did not seem to increase with increasing concentrations of the antibody (same as the controls without thrombin or prothrombin). Similarly, the results in Figure 3 show the increased immune precipitation of antibody IgG to thrombin with increasing concentration of thrombin but not with prothrombin. Furthermore, direct analysis of antigen and antibody in the immunoprecipitate by the double-labeling method, as shown in Table I, indicated that very little antibody IgG to thrombin was found in the immunoprecipitate with prothrombin in contrast to that with thrombin. The antibody-antigen ratios ranged from 3.2 to 13.4 for thrombin and only 0.1–0.8 for prothrombin.

However, when prothrombin was adsorbed to artificial surfaces such as glass, Cuprophane, PVC, or polystyrene, the reactivity of prothrombin with antibody IgG to thrombin seemed to be greatly increased. The results are

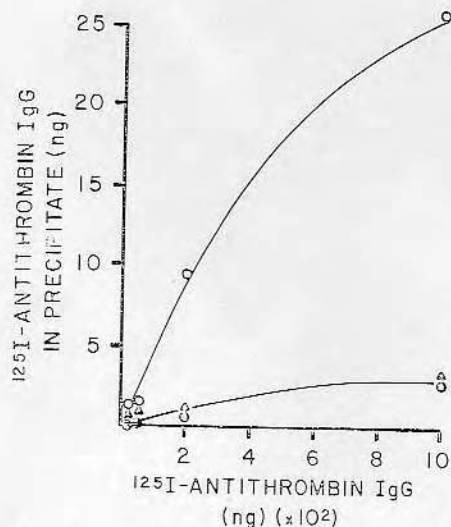


Figure 2. Immunoradiometric assay of thrombin and prothrombin with varying concentrations of antibody IgG to thrombin. Thrombin (6 ng) (○), prothrombin (12 ng) (Δ), or none (controls) (●), was incubated with various concentrations of ^{125}I -antibody IgG (8–1000 ng) in PBS containing BSA (0.1%) and benzamidine (1 mM) for 20 h at 4°C. The immunoprecipitate was collected by centrifugation at 160,000 g (Airfuge) for 30 min and washed once with PBS. The immunoprecipitate was counted in a gamma counter. Results are representative of two determinations.

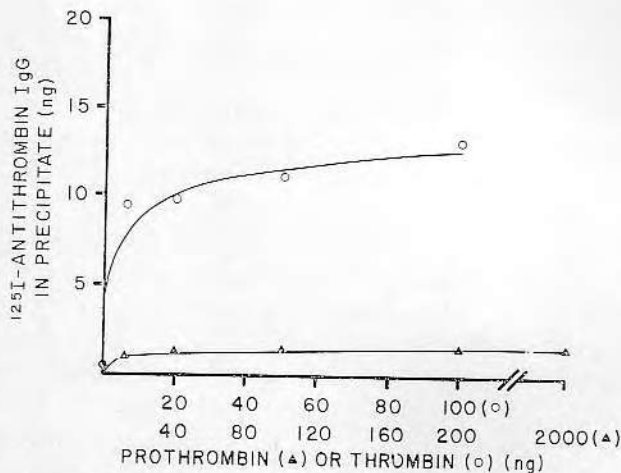


Figure 3. Immunoradiometric assay of thrombin and prothrombin at varying concentrations of thrombin or prothrombin. ^{125}I -antibody IgG to thrombin (100 ng) was incubated with various concentrations of thrombin (6–100 ng) (○), or prothrombin (12–2000 ng) (Δ), or none (●) in PBS containing BSA (0.1%) and benzamidine (1 mM) for 20 h at 4°C. The immunoprecipitate was collected by centrifugation at 160,000 g for 30 min and washed once with PBS. The immunoprecipitate was counted in a gamma counter. Results are representative of two determinations.

TABLE I
Direct Binding Assay of ^{131}I -Thrombin or ^{131}I -prothrombin with ^{125}I -antibody IgG to Thrombin in Solution at Various Antibody IgG to Thrombin Concentrations

Thrombin or prothrombin in immunoprecipitate (ng)	Antibody IgG to thrombin in immunoprecipitate (ng)	Antibody-antigen ratio
Thrombin	0.08	4.7
	0.3	6.2
	2.4	33.3
	3.6	80.4
	3.1	121.1
Prothrombin	0.4	0.1
	0.4	0.2
	0.9	0.5
	4.3	3.1
	3.9	7.0

Note. ^{131}I -thrombin (6 ng) or ^{131}I -prothrombin (12 ng) was incubated with ^{125}I -antibody IgG to thrombin (from 8 to 5000 ng) for 20 h and immunoprecipitate was sedimented at 160,000g (Airfuge, Beckman Instrument Inc.) for 30 min. The immunoprecipitate was washed once with phosphate-buffered saline and recentrifuged. The ^{131}I -thrombin (or prothrombin) and ^{125}I -antibody IgG to thrombin in the formed precipitate was measured by differential counting in a gamma counter. Molecular weights for prothrombin (72,000), thrombin (36,000), and antibody IgG (160,000) to thrombin were used to calculate the antibody-antigen molar ratios in the conjugates. Data are representative of two determinations.

TABLE II
Uptake of ^{125}I -Antibody IgG to Thrombin by Materials Pretreated with Thrombin or Prothrombin

Materials	Pretreatment (concentration)	^{125}I -antibody IgG (ng)
Glass	None	18.4
	Albumin (30 $\mu\text{g}/\text{ml}$)	8.3
	Thrombin (10 $\mu\text{g}/\text{ml}$)	112.3
	Prothrombin (30 $\mu\text{g}/\text{ml}$)	58.9
Cuprophane	None	0.1
	Albumin (1 mg/ml)	0.3
	Thrombin (10 $\mu\text{g}/\text{ml}$)	25.8
	Prothrombin (30 $\mu\text{g}/\text{ml}$)	29.3
PVC	None	4.0
	Albumin (1 mg/ml)	6.1
	Thrombin (10 $\mu\text{g}/\text{ml}$)	135.0
	Prothrombin (20 $\mu\text{g}/\text{ml}$)	125.5
Polystyrene	None	2.8
	Albumin (1 mg/ml)	4.0
	Thrombin (10 $\mu\text{g}/\text{ml}$)	63.7
	Prothrombin (20 $\mu\text{g}/\text{ml}$)	49.6

Note. Materials were pretreated with protein or Tyrode's buffer for 1 h at 22°C. After thoroughly rinsing, the protein adsorbed to test discs or polystyrene microtiter dishes was crosslinked with glutaraldehyde for 1 h. After removal of free glutaraldehyde, the discs were incubated with ^{125}I -antithrombin IgG (10 $\mu\text{g}/\text{ml}$) for 20 h at 22°C. The residual radioactivity on discs or dishes was measured by gamma counting and the uptake of ^{125}I -antibody IgG to thrombin was expressed as nanograms bound to the surface. Data are representative of three experiments.

shown in Table II. The amount of ^{125}I -antibody IgG to thrombin on surfaces precoated with either thrombin or prothrombin varied over a wide range depending on the type of the materials. The most remarkable results were that antibody IgG to thrombin did bind to a much higher degree not only to prothrombin (studies on glass) but also to a level as much as to the surfaces precoated with thrombin (such as Cuprophane, PVC, polystyrene). A more quantitative analysis of direct binding between thrombin or prothrombin adsorbed on PVC with antibody IgG by use of double-labeling technique are shown in Table III. Variations of both thrombin or prothrombin concentration on PVC surfaces were always accompanied by a proportional uptake of antibody IgG to thrombin. Furthermore, the antibody-antigen ratios remained similar to that on surfaces pretreated with either thrombin (1.2–2.1) or prothrombin (1.2–1.8).

Further experiments were performed to rule out that the observed interactions between prothrombin and antibody IgG to thrombin on PVC are not due to (1) an isotopic labeling effect on either prothrombin, thrombin, or antibody IgG, (2) artificial intramolecular and intermolecular crosslinking of prothrombin (or thrombin) itself, or prothrombin with material (such as PVC). The results in Table IV show that both unlabeled thrombin and prothrombin adsorbed on PVC react indifferently with unlabeled antibody IgG to thrombin since the subsequent reaction with ^{125}I -antibody IgG to thrombin was almost totally blocked. In addition, about the same blocking effect of antibody IgG to thrombin was observed for both thrombin (89%) and prothrombin (88%) precoated PVC. On the other hand, Table V shows that even though the crosslinking with glutaraldehyde stabilized the protein molecules

TABLE III
Direct Binding Assay of ^{131}I -Thrombin or ^{131}I -Prothrombin
Adsorbed on PVC with ^{125}I -Antibody IgG to Thrombin

Thrombin or prothrombin adsorbed on PVC (ng)		Uptake of antibody IgG in immunoprecipitate (ng)	Antibody-antigen ratio
Thrombin	5.7	52.6	2.1
	10.4	85.6	1.9
	13.5	104.8	1.7
	23.9	143.2	1.3
	27.9	153.4	1.2
Prothrombin	8.9	36.3	1.8
	13.2	52.4	1.6
	29.8	86.6	1.3
	39.0	111.5	1.3
	52.3	140.7	1.2

Note. PVC discs (4 mm in diameter) were precoated with either ^{131}I -thrombin or ^{131}I -prothrombin. Immunoradioassays were performed with ^{125}I -antibody IgG to thrombin (5000 ng) and incubation was 4 h at 22°C. Adsorbed thrombin or prothrombin and antibody IgG concentrations were estimated by differential counting in a gamma counter. Molecular weights of prothrombin (72,000), thrombin (36,000), and antibody IgG (160,000) were used to calculate the antibody-antigen molar ratio on PVC surfaces. Data are representative of three determinations.

on the surface, it reduced the antigenic binding sites of both thrombin and prothrombin for antibody IgG to thrombin concomitantly since the antibody-antigen ratios were reduced for both thrombin (from 1.9 to 1.0) and prothrombin (from 1.7 to 1.0). However, the antibody-antigen ratio for thrombin and prothrombin absorbed to PVC remained remarkably similar whether or not surface adsorbed antigen was crosslinked (1.0 for crosslinked prothrombin and thrombin; 1.7, 1.9 for noncrosslinked prothrombin and thrombin, respectively).

DISCUSSION

It is known that antibodies are directed to structural domains of macromolecules. It can therefore be assumed that thrombin-specific antibodies should not cross-react with prothrombin if their molecular conformations are different even though prothrombin is the precursor or zymogen of thrombin. Our studies with a polyclonal antibody to thrombin preparation produced in rabbits by conventional technique seem to suggest that this is the case. This is supported by (1) a competitive binding radioimmunoassay of ^{125}I -thrombin to purified antibody IgG to thrombin (Figure 1), (2) the direct binding analysis of antigen precipitation with varying concentrations of labeled antibody IgG to thrombin (Figure 2) or varying concentrations of thrombin or prothrombin (Figure 3), and (3) the direct analysis of antigen and antibody in formed immune precipitate by use of double-labeling method. A slight but insignificant cross-reactivity (0.05%) of prothrombin with antibody IgG to thrombin did exist in solution (Figure 1).

On the other hand, the surface-adsorbed prothrombin exhibited a much higher degree of cross-reactivity to antibody IgG to thrombin (Table II) than prothrombin in free solution (Table I). The surface-adsorbed prothrombin also seemed to react differently with antibody IgG to thrombin on different materials (Table II), indicating that prothrombin might adsorb in a different form on different materials. Further analyses of antibody IgG to thrombin/prothrombin and antibody IgG to thrombin/thrombin on PVC by

TABLE IV
Blocking Effects of Unlabeled Antithrombin IgG in the Reaction of ^{125}I -Antibody IgG to Thrombin with Thrombin or Prothrombin Adsorbed on PVC

PVC pretreated with	% Blocking of ^{125}I -antibody IgG conjugation by prior exposure of adsorbed antigen to unlabeled antibody IgG
Thrombin	89
Prothrombin	88

Note. PVC discs were pretreated with either thrombin (10 $\mu\text{g}/\text{ml}$) or prothrombin (20 $\mu\text{g}/\text{ml}$) and divided into two different sets of three discs each. One set was incubated with Tyrode's buffer (control) and one set with unlabeled antithrombin IgG (10 $\mu\text{g}/\text{ml}$) for 20 h at 22°C; subsequently each set was incubated with ^{125}I -antibody IgG to thrombin for an additional 20 h at 22°C. The uptake of ^{125}I -antibody IgG for each set was determined and % blocking calculated. Data are averages of two determinations.

TABLE V
Effect of Stabilization of Thrombin or Prothrombin on PVC by
Glutaraldehyde Crosslinking and the Subsequent Uptake of Antibody IgG to Thrombin

PVC pretreated with	Crosslinking	¹³¹ I-thrombin or prothrombin (ng)	¹²⁵ I-antibody IgG (ng)	Antibody-antigen ratio
None (control)	+	—	1.1	—
	—	—	1.1	—
Thrombin	+	27.4	125.8	1.0
	—	9.6	81.1	1.9
Prothrombin	+	41.8	92.3	1.0
	—	20.9	78.1	1.7

Note. PVC discs were pretreated with ¹³¹I-thrombin (10 µg/ml) or ¹³¹I-prothrombin (20 µg/ml). The discs were divided into two sets: one set was treated with 1% glutaraldehyde in phosphate buffer (pH 7.4) for 1 h and the other set was untreated. Both sets of discs were incubated with ¹²⁵I-antibody IgG to thrombin (10 µg/ml) in phosphate-buffered saline (pH 7.4) with 0.1% Tween 20 and 1 mg/ml BSA, for 4 h. The radioactivity on the discs was measured by differential counting in a gamma counter. Molecular weights of prothrombin (72,000), thrombin (36,000), and antibody IgG (160,000) were used to calculate the antibody-antigen molar ratio. Data are from one experiment with triplicate for each test. The variation of triplicate determinations is <10%.

a double-labeling method (Table II) showed clearly that the antibody IgG to thrombin/prothrombin ratios (1.2–1.8) had markedly increased (from 0.1–0.8, Table I), closed to the ratios of antibody IgG to thrombin/thrombin (1.2–2.1). The marked decrease of antibody IgG to thrombin/thrombin in solution from 3.2–13.4 (Table I) to 1.2–2.1 (Table II) on PVC might suggest that either (1) some antigenic domains on thrombin were lost due to the direct interaction (binding) of these sites with PVC, (2) a steric effect prevented the interactions of antibody IgG to thrombin with surface-adsorbed thrombin, (3) thrombin might reduce its antigenic binding sites due to its own conformational changes induced by adsorption, or (4) all of the above. Our results with polyclonal antibody at this stage failed to differentiate between these possibilities. Monoclonal antibodies specific only to one antigenic domain for thrombin or prothrombin are required to elucidate such mechanism. This is currently under investigation.

The results in Table IV and Table V seemed to rule out possible artifacts of interaction of PVC adsorbed prothrombin with antibody IgG to thrombin due to structural modification of prothrombin and antibodies by radio-labeling or by crosslinking glutaraldehyde. Even though crosslinking of prothrombin on PVC showed some stabilization of prothrombin on the surface and substantial reduction of antibody IgG to thrombin uptake (Table V), these effects seemed common also to thrombin (Table V) and other plasma proteins such as fibrinogen⁸ adsorbed to materials.

The data from this study appear to demonstrate that adsorption of prothrombin to artificial surfaces such as PVC had induced some conformational changes of the macromolecule that resembled antigenically the domain(s) of adsorbed thrombin. It is not known whether these changes have any biologic significance. Our earlier data showed that prothrombin adsorbed to Cuprophane did not directly produce thrombin clotting or amidolytic activity; on the other hand it enhanced the adhesion of granulocytes as surface-adsorbed thrombin did.⁵

Structural and conformational changes of proteins adsorbed on artificial surfaces have been studied by several groups of investigators with various techniques (see review by Morrissey¹¹). Kochwa et al.,¹² using potentiation titration technique, and Nyilas et al.,¹³ using microcalorimetric method, have demonstrated the substantial conformational changes of γ -globulin upon adsorption to artificial surfaces. These changes were also affected by the concentration of protein on the surfaces.¹⁴ On the other hand, Morrissey et al.,¹⁵ using infrared bound fraction measurements, and Smith et al.,¹⁶ using in situ ellipsometry, showed that the conformation of adsorbed albumin and prothrombin were not drastically changed upon adsorption. Most recently, Andrade et al.,¹⁷ using total internal reflection fluorescent spectroscopy to study the effects of protein adsorption on conformation and activity, have shown that there were some conformational changes and denaturation of human plasma fibronectin on adsorption to hydrophobic quartz and there was a blue shift of 9 nm on adsorption of bovine serum albumin to hydrophobic quartz. Our results with immunochemical tech-

niques using an IgG antibody to thrombin, specific to its biologic degradation product thrombin, demonstrated that some prothrombin conformational changes had occurred during prothrombin adsorption to several artificial surfaces such as glass, Cuprophane, PVC, and polystyrene. Our techniques, however, failed to detect any degree of prothrombin molecular changes. Monoclonal antibodies specific to either prothrombin or thrombin may be useful in pinpointing the exact domain(s) involved in such changes. More importantly, it should be investigated further whether these changes will elicit any previously unknown biologic activities of prothrombin, such as of antigenicity, effects on platelet or granulocyte functions.

In solid phase immunoassays, it is generally assumed that antigens adsorbed to a surface such as polystyrene microtiter dishes, will react with specific antibody in a manner similar to that antigen-antibody reaction in solutions such as occur in immune precipitation. However, our evidence and others¹⁸ seem to point out that data obtained from solid phase immunoassays should be interpreted with caution since adsorption of a nonantigen to a polymer surface could render it immunoreactive to previously unreactive antibodies.

The author is grateful to Dr. John Fenton II, New York State Department of Health, Albany, NY, for providing highly purified human α -thrombin, to Dr. Milan Wickerhauser, American Red Cross Fractionation Center, Washington D.C., for the gift of prothrombin complex concentrate. We appreciate also the skillful technical assistance of Thomas Sharpton, Joel Hardy, and Dr. Niyam Sharma (for thrombin antibody preparation), the critical review of Dr. Ernst Eichwald, and the secretarial assistance of Eleanor Hart and Mary Lee Warren. This study was supported in part by Grants HL-25807, HL-25808, NHLBI, National Institutes of Health.

References

1. B. Furie, R. A. Blanchard, D. J. Robinson, M. M. Tai, and B. C. Furie, "Conformation-Specific Antibodies: Approach to the Study of Vitamin K-Dependent Blood Coagulation Proteins," in *Methods in Enzymology*, J. J. Langone, H. V. Vunakis (eds.), Academic, New York, 1982, pp. 60-82.
2. M. A. Shuman and P. W. Majerus, "The Measurement of Thrombin in Clotting Blood by Radioimmunoassay," *J. Clin. Invest.*, **58**, 1249-1254 (1976).
3. H. Chuang, N. Sharma, S. Mohammad, and R. Mason, "Adsorption of Thrombin onto Artificial Surfaces and Its Detection by an Immunoradiometric Assay," *Proc. 2nd meeting of ISAO*, 226-232 (1979).
4. H. Y. K. Chuang, S. F. Mohammad, N. C. Sharma, and R. G. Mason, "Interaction of Human α -Thrombin with Artificial Surfaces and Reactivity of Adsorbed α -Thrombin," *J. Biomed. Mater. Res.*, **14**, 467-476 (1980).
5. H. Y. K. Chuang and S. P. Mitra, "Adsorption and Reactivity of Human Prothrombin to Artificial Surfaces," *J. Biomed. Mater. Res.*, **18**, 695-705 (1984).
6. J. W. Fenton II, M. J. Fasco, A. B. Stackrow, D. L. Aronson, A. M. Young, and J. S. Finlayson, "Human Thrombin: Production, Evaluation, and Properties of α -Thrombin," *J. Biol. Chem.*, **252**, 3587-3596 (1977).

7. H. Y. K. Chuang, W. F. King, and R. G. Mason, "Interaction of Plasma Proteins with Artificial Surfaces: Protein Adsorption Isotherms," *J. Lab. Clin. Med.*, **92**, 483-496 (1978).
8. H. Y. K. Chuang, "In situ Immunoradiometric Assay of Fibrinogen Adsorbed to Artificial Surfaces," *J. Biomed. Mater. Res.*, **18**, 547-559 (1984).
9. H. Y. K. Chuang, P. E. Crowther, S. F. Mohammad, and R. G. Mason, "Interactions of Thrombin and Antithrombin III with Artificial Surfaces," *Thromb. Res.*, **14**, 273-282 (1979).
10. D. M. Tollefson, J. R. Fengler, and P. W. Majerus, "The Binding of Thrombin to the Surface of Human Platelets," *J. Biol. Chem.*, **249**, 2646-2651 (1974).
11. B. W. Morrissey, "The Adsorption and Conformation of Plasma Proteins: A Physical Approach," *Ann. N.Y. Acad. Sci.*, **283**, 50-64 (1977).
12. S. Kochwa, M. Brownell, R. E. Rosenfield, and L. R. Wasserman, "Adsorption of Proteins by Polystyrene Particles. I. Molecular Unfolding and Acquired Immunogenicity of IgG," *J. Immunol.*, **99**, 981-986 (1967).
13. E. Nyilas, T. H. Chin, and G. A. Herzlinger, "Thermodynamics of Native Protein/Foreign Surface Interactions. I. Calorimetry of the Human γ -Globulin/Glass System," *Trans. Amer. Soc. Artif. Intern. Organs*, **20**, 480-490 (1974).
14. B. W. Morrissey and C. A. Fenstermaker, "Conformation of Adsorbed γ -Globulin and β -lactoglobulin. Effect of Surface Concentration," *Trans. Amer. Soc. Artif. Intern. Organs*, **22**, 278-283 (1976).
15. B. W. Morrissey and R. R. Stromberg, "The Conformation of Adsorbed Blood Proteins by Infrared Bound Fraction Measurements," *J. Colloid. Interface Sci.*, **46**, 152-164 (1974).
16. L. E. Smith, C. A. Fenstermaker, and R. R. Stromberg, "Adsorption of Blood Proteins from Solution," *ACS Polymer Preprints*, **11**, 557-563 (1970).
17. J. D. Andrade, V. L. Hlady, and R. A. Van Wagenen, "Effects of Plasma Protein Adsorption on Protein Conformation and Activity," *Pure Appl. Chem.*, **56**, 1345-1350 (1984).
18. F. Grinnell and M. K. Feld, "Fibronectin Adsorption on Hydrophilic and Hydrophobic Surfaces Detected by Antibody Binding and Analyzed During Cell Adhesion in Serum Containing Medium," *J. Biol. Chem.*, **257**, 4888-4893 (1982).

Received February, 1985

Accepted March, 1985

- [8] P. G. Laing, A. B. Ferguson, and E. S. Hodge, *J. Biomed. Mater. Res.*, **1**, 135 (1967).
- [9] J. E. Turner, W. H. Lawrence, and J. Autian, *J. Biomed. Mater. Res.*, **7**, 39 (1973).
- [10] B. S. Oppenheimer, E. T. Oppenheimer, A. P. Stout, and I. Danishefsky, *Science*, **118**, 305 (1953).
- [11] B. S. Oppenheimer, E. T. Oppenheimer, I. Danishefsky, A. P. Stout, and F. R. Eirich, *Cancer Res.*, **15**, 333 (1955).
- [12] B. S. Oppenheimer, E. T. Oppenheimer, A. P. Stout, M. Willhite, and I. Danishefsky, *Cancer*, **11**, 204 (1958).
- [13] B. S. Oppenheimer, E. T. Oppenheimer, A. P. Stout, I. Danishefsky, and M. Willhite, *Acta Union Int. Cancer*, **15**, 659 (1959).
- [14] N. T. Stinson, *Brit. J. Exper. Pathol.*, **45**, 21 (1964).
- [15] E. J. Kaminski and R. J. Oglesby, Certain aspects of implant shape in experimental testing of biological materials, I, in *Research in Dental and Medical Materials*, Plenum Press, 1969, pp. 113-119.
- [16] A. C. Shuttleworth and R. H. Smythe, *Clinical Veterinary Surgery*, Vol. III, Charles C. Thomas, Illinois, 1960.
- [17] M. Westhues and R. Fritsch, *Animal Anaesthesia*, J. B. Lippincott, Philadelphia, 1965.
- [18] L. G. Luna, *Manual of Histologic Staining Methods of the Armed Forces Institute of Pathology*, 3rd ed., McGraw-Hill, New York, 1968.
- [19] J. J. Klawitter, Research techniques in biomaterials evaluations, Clemson University's 3rd Annu. Symp.-Workshop Biomater., 1971.
- [20] J. H. Luft, *J. Biophys. Biochem. Cytol.*, **9**, 409 (1961).
- [21] C. F. A. Culling, *Handbook of Histopathological Techniques*, 2nd ed., Butterworth and Company, Ltd., 1963.
- [22] T. N. Salthouse and D. A. Wiligan, *J. Biomed. Mater. Res.*, **6**, 105 (1972).
- [23] R. Ross and E. P. Benditt, *J. Cell Biol.*, **27**, 83 (1965).
- [24] A. W. Rogers, *Techniques of Autoradiography*, Elsevier Publishing Co., London and New York, 1967.
- [25] W. R. Sewell, J. Wiland and B. N. Crauer, *Surg. Gynecol. Obstet.*, **100**, 483 (1955).
- [26] J. D. Andrade, *Med. Instrument.*, **7**, 110 (1973).
- [27] R. I. Leininger, *CRC Critical Rev. Bioeng.*, **1** (3), 333 (1972).
- [28] D. A. Gough and J. D. Andrade, *Science*, **180**, 380 (1973).
- [29] W. F. Walker, *A Study of the Cat*, Saunders, Philadelphia, 1967, p. 65.

The Foreign Body Reaction—An Experimental Protocol

D. L. COLEMAN, R. N. KING and J. D. ANDRADE, *Division of Materials Science and Engineering, Institute for Biomedical Engineering, and the Department of Pathology, University of Utah, Salt Lake City, Utah 84112*

Summary

A comprehensive protocol is presented for the in vivo evaluation of soft tissue foreign body reactions to surgical implants. A number of methods of evaluation and quantitation of the tissue reaction to implants are presented and discussed. A strong plea is made for semi-quantitation of tissue reactions, rather than relying on subjective, qualitative methods.

INTRODUCTION

The biocompatibility of materials for implantation has been inadequately evaluated in the past. Homsy [1] claimed in 1970 that gross tissue reaction adjacent to the implant had usually been the only basis for rejecting a material for implantation. "The absence of systematic preclinical procedures for rational selection of prosthetic materials must be counted incongruous and intolerable for this era" [1].

The importance of finding methods to quantitate tissue reactions cannot be overemphasized. Protocols for qualitative evaluation do exist. The U. S. Pharmacopeia [3] and the American Society for Testing and Materials (ASTM) [2] have developed protocols and tentative standards based largely on subjective observation. Quantitative methods for evaluating tissue reactions also exist and will be discussed. The adoption of quantitative methods for objective evaluation of tissue reactions to various materials is imperative. Hopefully, such data would lead to understanding and to more advantageous use of artificial materials in medicine.

The value of quantitative methods of evaluation has been demonstrated in the wound healing and inflammation literature. Since the foreign body reaction is also an inflammatory reaction [4], quantitation should be feasible.

It is important to have a firm understanding of the events and variables involved in acute and chronic inflammation before attempting

to elucidate the mechanisms of tissue reactions to implants [4]. Such factors must be considered before designing properly controlled experiments.

The purpose of this paper is to offer the reader a detailed experimental protocol for testing and evaluating implant materials in soft tissue. We are hopeful that the information provided will act as the basis for establishing uniformity in methods used in the field of implantation research. We encourage others to refine, improve, and clarify this protocol while building a data base that can be used to increase our understanding of the *in vivo* reactions to implant materials.

IN VIVO TESTING PROTOCOL

Background

A protocol for the test and evaluation of biomaterials must allow maximum control over variables which can affect the reaction. As some amount of surgical trauma is necessary for implanting any material, all of the factors which affect general inflammation and wound healing must be considered and controlled if valid conclusions are to be drawn [4].

Concern for the lack of uniformity in methods used to test tissue reactions is becoming increasingly more apparent. Wood [5] feels that some of the contributing factors to varying results is due to the variation in the species of the test animals, variation in the tissues used for implant sites, inconsistency in the size and shape of the specimens implanted, and variation in the methods used for implantation. Another variable that should be added to this list is the inconsistency in evaluating results [3], [6], [9].

The basic criteria that should be met by any implantation study are: 1) the elimination and/or standardization of variables which might affect the tissue reaction to the material; 2) adequate controls to eliminate the variability of tissue reaction due to unusual or unique individuals in the test population; 3) test animals should be relatively inexpensive and easily cared for; 4) implantation sites should be easily accessible surgically, should provide a homogeneous environment for the implant, and should be as mechanically inactive as possible (unless mechanical trauma is being studied); 5) proper sterile and pyrogen-free technique should be used during implantation; 6) experimental design should be such that results are reproducible within experimental limits; and 7) ideally, the results should be quantitative rather than purely qualitative.

Choice of Experimental Animal

Past implantation studies have involved a large variety of animals. Experimental implant hosts have ranged from monkeys, dogs, pigs, and one human volunteer in a study of Ocumpaugh and Lee [6], to rabbits [5], [7]–[9], rats and guinea pigs [10]–[14], and many others.

Certainly each animal species has its own distinct advantages and disadvantages for implantation studies. For the purpose of general *in vivo* screening of implant materials, rabbits (6–9 lb) offer many advantages over other species. Rabbits are easily handled, inexpensive to buy, house, and feed, and they are large enough to tolerate several implants with no cross reaction between samples and no physical impairment to the animal.

Size and Shape of the Implant

As stated previously, the size and shape of the implant can greatly influence the severity of the tissue reaction [4]. It is difficult to suggest the optimal size and shape for standard screening of materials, but certain precautions should be taken to avoid sharp edges, acute angles, scratches, and other avoidable surface defects. The size of the implant should be small enough that it is easily accommodated by the tissue, yet large enough that it can be easily handled and located for histological examination.

Wood et al. [5], and Kaminski et al. [15] compared the disk-shaped implant with the rod-shaped implant at various sites of implantation. The tissue reaction to the disk was more uniform and easier to grade than the rod implants. Rod-shaped implants demonstrated a "clubbing" phenomenon when implanted in muscle while disk-shaped implants revealed small local areas of corrosion products. The disk-shaped implant measuring 1 to 1.5 mm in thickness and 10 mm in diameter, as described by Wood, is a convenient size and shape for implantation in rabbits. This is the standard specimen utilized in our laboratory for soft tissue foreign body reaction studies.

Sites of Implantation

Implant sites have varied as greatly as the species of animals used for tissue reaction. Common soft tissue sites for *in vivo* testing are the masseter muscle, the thigh muscle, brain tissue, subcutaneous tissue, and the paravertebral muscle [7]. Hard tissue sites include the anterior calvarium, mandible, and the femur [7]. Although the paravertebral muscle (Fig. 1) has the disadvantage of being mechanically active, as any muscle, it has the advantage of being large enough to host at least

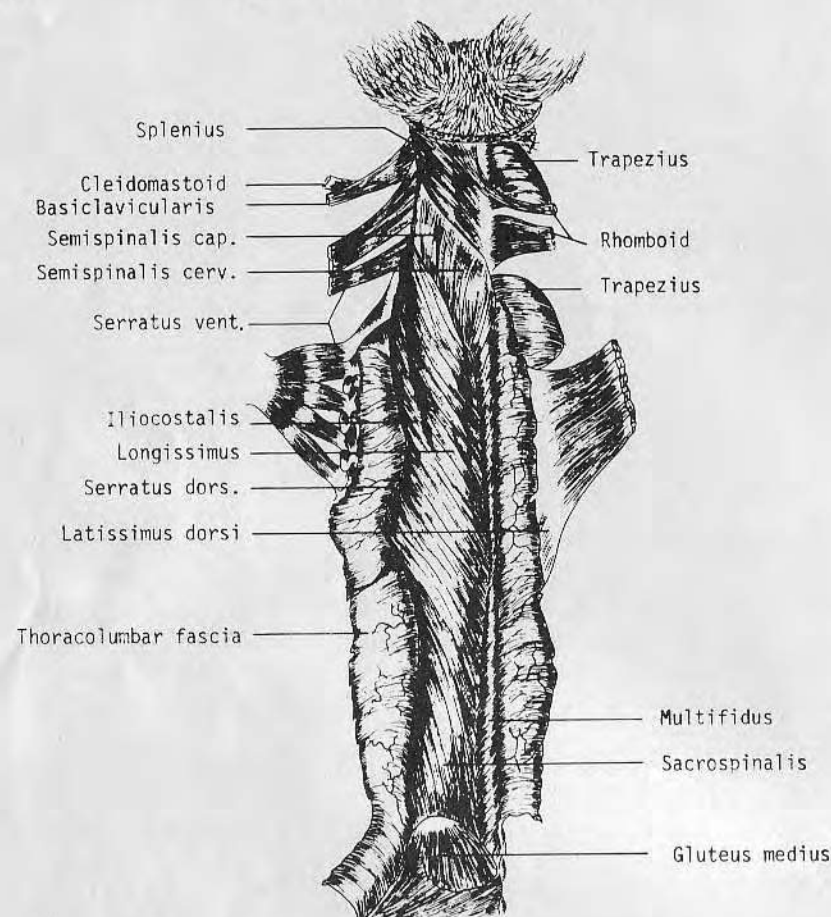


Fig. 1. Dorsal view of the musculature of the rabbit. The sacrospinalis muscle (paravertebral) is a long, broad muscle ideal for implantation studies. (Redrawn from [29]).

three implants per muscle, the implant environment is homogeneous and it is easily accessible surgically, unlike brain tissue. The most important concern when selecting an implant site is that all implants are subjected to identical environments and uncontrolled variables are limited. This is easier to accomplish with the paravertebral muscle as the implant site.

Method of Implantation

There are two basic methods for implanting materials for testing: 1) injection of the implant through a large bore needle [3], and 2) surgically

creating a wound to house the implant. The injection technique limits the size and shape of the implant to a strip or cylinder with a small enough diameter to fit into a large bore needle. The U. S. Pharmacopeia XVIII describes such a technique and details the implant specifications for the injection method [3].

Surgical implantation is more involved, not only in equipment and expense, but also in time and surgical skill. Probably the most difficult aspects of the surgery are learning to be efficient at maintaining sterility and administration of suitable anesthetics. Sterile technique is easily mastered with a little reading [16] and much practice, but it is essential to be completely familiar with the limitations, actions, and effects of the various anesthetic agents available [17]. Intravenous administration of veterinary grade sodium pentobarbital has been very successful in this laboratory for rabbits. Inhalants can also be used successfully but many are flammable and/or explosive in nature and must be used with caution.

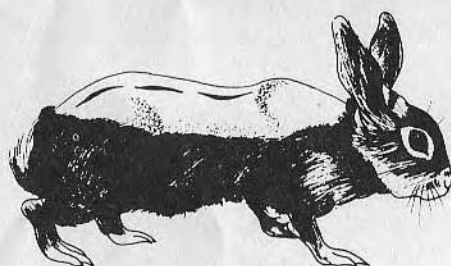
Prior to the administration of the anesthetic, an appropriate area of skin should have the hair or fur removed by means of clippers. For implantation into the paravertebral muscle, hair should be removed from the nape of the neck to the posterior region of the sacrum with a lateral width of 3 to 4 in. on each side of the spine [Fig. 2(a)]. After the animal has been anesthetized, the exposed skin could be cleaned with surgical soap followed by a bactericidal concentration of benzalkonium chloride, tinted tincture 1:750 (or equivalent bactericide), to sterilize the skin.

Following the skin cleaning, the operative area should be isolated with sterile drapes to aid in maintaining sterility of the operative field. Proper surgical methods should be used for maintaining hemostasis and for dissecting and exposing the paravertebral muscle. Using blunt dissection, [Fig. 3(a) and 3(b)], a "pocket" is made in the muscle such that the muscle fibers are separated longitudinally, i.e., parallel to the spine. The implant is inserted into the pocket [Fig. 3(c)] by means of a hemostat with silicon rubber tubing protecting the ends of the instrument. This will minimize implant defects due to abrasion by the rough metallic instrument. The wound is then closed in layers by the apposition of cut surfaces, using a nonabsorbable, "nonreactive" suture. Absorbable suture causes a more severe reaction around it and may lead to false interpretation of results. Teflon coated polyester, size 4-0 or 5-0 has been adequate for implant studies in this laboratory, but other non-absorbable suture materials are available that will serve the purpose just as well.

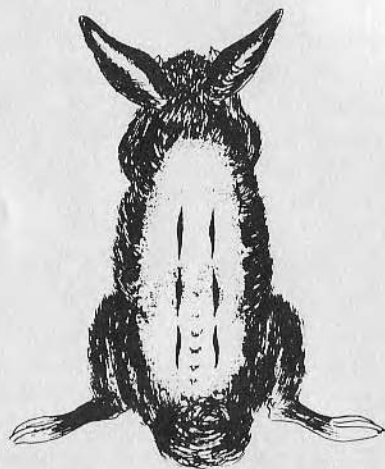
Each animal should be given antibiotics following surgery, preferably a wide spectrum antibiotic such as penicillin-streptomycin combination. The antibiotic treatment should be continued for five days to prevent

wound and other infection. The skin suture should be removed at seven days.

Additional measures to prevent infection, such as wound dressings, are usually unnecessary but should be used if there is a high incidence of infection among the test population. Test animals with infected wounds should immediately be removed from the study and must not be considered in the evaluation of test materials. A daily weight check of the animals will give some indication of their general health and also allows examination of the wound site for infection on a regular basis.

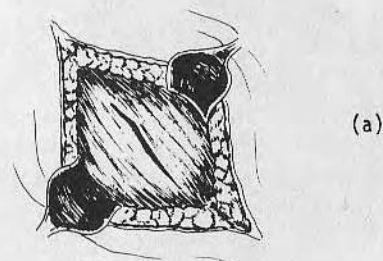


(a)

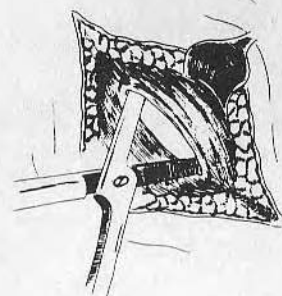


(b)

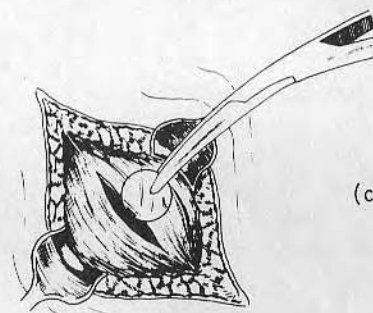
Fig. 2. The relative position of implants in the paravertebral muscle of rabbits; (a) side view, (b) dorsal view.



(a)



(b)



(c)

Fig. 3. Surgical implantation involves exposing the paravertebral muscle (a); and creating a "pocket" in the muscle using blunt dissection (b). The disk-shaped implant is then inserted into the "pocket" (c).

Test Program and Tissue Preparation

Each animal should receive six implant sites [Fig. 2(b)] as follows: a negative control (U.S.P. Negative Control Plastic Reference Standard [3]), a sham site (surgical procedure with no implant), and four implant sites for test materials. Each test material should be implanted in a minimum of three animals for each survival group. Additional animals are recommended for some statistical significance.

The selection of implant harvesting time is somewhat variable. The ASTM "Recommended Practice for Assessing Compatibility of Polymeric Implant Materials—Effect of Implant on Tissue" [2], suggests starting with eight survival groups of 3 days, 7 days, 2, 4, 12, 26, 52, and 104 weeks. However, for practical screening applications, survival times should be classified into short term survival and long term survival. Short term implants should include survival groups of 1 week, 2 weeks, 6 weeks, and 8 weeks. If the material demonstrates an absence of chronic inflammation after 8 weeks of implantation it should then be subjected to long term implantation studies. Ten to twelve animals should be implanted with the acceptable material with a maximal survival period of two years or until gross lesions can be seen in the implant site.

Studies by Turner et al. [9] suggest that the tissue reaction to most implant material reaches a maximum at seven days but the duration of the response varies with the material being tested.

Samples should be harvested by sacrificing the animal with an overdose of anesthetic or by other humane means. A mid-line incision is then made from the nape of the neck to the posterior sacrum. The skin is reflected back exposing all implant sites. Any gross changes in the muscles should be noted at this time, e.g., necrosis, redness, pus or abscess formation, etc. Leaving the implant in situ, a large block of muscle surrounding the implant is dissected out and placed in a covered container with 4×4 sponges saturated with isotonic saline. Muscle samples should be left in the container for about 10 min to allow the contractile properties to become quiescent. Extraneous muscle is then trimmed leaving the implant surrounded with approximately 1/8 in. of tissue on all surfaces. This block of tissue is then fixed in 10% buffered formalin, or some other appropriate fixative [18].

After the tissue has been properly fixed and dehydrated through absolute alcohol the sample is then embedded in an embedding medium that is as hard or harder than the implant material [19], [20]. Hopefully, this will allow the implant to remain in situ during sectioning. The samples are sectioned using a low speed diamond saw, as described by Klawitter [19], to a thickness of about 50 to 60 μ . The thin sections are fixed to a microscope slide and appropriately stained [18], [21] for histopathological examination.

METHODS OF EVALUATION

In the past, tissue reactions to various materials have been described in subjective terms which are often nebulous, difficult to compare with the work of others, and often lack any form of standardization. A quan-

titative method of evaluation would be an extremely valuable tool in allowing materials to be classified on a universal level with at least some degree of standardization.

There have been few attempts to quantitate foreign body reactions [42]. Salthouse [22] evaluated tissue reactions by using specific histochemical methods to detect various enzymes present in the implant site; he was able to determine the relative area of enzyme concentration. Frozen sections of tissue were treated histochemically for the detection of succinic dehydrogenase, acid phosphatase, amino peptidase, and adenosine triphosphatase. The reactive zones were measured to determine the area of enzyme activity. They found that giant cells and areas of severe tissue destruction exhibited marked increases in aminopeptidase; acid phosphatase increase was associated with the original trauma of implantation, but was also found in greater amounts in areas of tissue destruction involving cell lysis. Macrophages appeared to be the main contributors of the acid phosphatase. The ATPase activity was confined to the vascular endothelium in vessels in the area of the tissue reaction.

Ross and Benditt [23] studied wound healing and collagen formation by means of injected L-proline-3,4- H^3 as a tracer. They determined the concentration of free amino acid in the blood after the labeled proline was injected intraperitoneally. Quantitative analysis of collagen formation was accomplished by means of electron microscope autoradiography. The use of autoradiography, both light and electron microscopic techniques [24], should be adapted to the study of foreign body reactions. Autoradiography has the advantage over other forms of tracer experiments, i.e., scintillation counting, in vitro labeling, etc., in that quantitative measurements of silver grains can be made without compromising histopathological examination [24].

As applied to implantation studies, 3H -proline injected intraperitoneally at a dose of 20 microcuries/gm body weight [23] will be incorporated into the newly synthesized collagen surrounding the implant. Variations of the administration time of the isotopically labeled amino acid could yield additional valuable information. Quantitative results could be used to evaluate the effects of mechanical trauma, geometry, and chemical toxicity as related to the implant material.

Another method which might prove of value is differential counting of the number of inflammatory cells per high powered field. This method simply elaborates the system of Sewell et al. [25] devised in 1955 in which the number of different types of cells and their concentrations were assigned an arbitrary value. The summation of the various factors measured offered a means of grading tissue reactions from very slight (0 to 16 points) to extensive (>112 points) with six grades in between. It

seems logical to assume that the number of inflammatory cells participating in the reaction is directly related to the severity of the response. If the number of inflammatory cells per high power field (HPF) (we use $400\times$ and a wide field eyepiece) were counted and averaged around the implant, then an estimate of the relative number of cells involved in the reaction could be obtained. Since the number of cells would be expected to vary among individuals, it would be necessary to subtract the average number of inflammatory cells found in the sham control samples. By using a micrometer grid the percent viable tissue vs. necrotic or connective tissue can also be estimated.

This method could be used in conjunction with the autoradiographic technique to evaluate factors that contribute to the tissue response to an implanted material. It might also be used to analyze the importance of each type of cell participating in the tissue reaction, i.e., eosinophils, neutrophils, lymphocytes, giant cells, etc.

Certainly, gross and microscopic observation should not be abandoned but should be used to confirm and complement more quantitative methods. Evidence of degenerative changes or neoplasia should be confirmed by visual examination of the tissue surrounding the implant.

The above methods may be too cumbersome for routine evaluation of some materials. Tissue culture techniques (see [27] for review) may be more practical for some purposes. The real value of quantitative in vivo methods is in detailed studies of the factors affecting tissue-implant reactions. Such questions as, to what extent does mechanical trauma contribute to the reaction; what is the most tolerable structural unit size for an implant; how much of the reaction is contributed by surface morphology? Such questions remain to be answered.

In providing a criteria for the acceptance or rejection of a material for in vivo use it must be remembered that the conditions of the implantation may be more important in determining the tissue reaction than the material per se. Therefore, it is absolutely necessary that all procedural and observed data be reported before final judgment is made.

DISCUSSION

Many of the materials available for implant medicine do not exhibit gross tissue reactions. Even for new materials or modifications of established materials, the methods discussed in this paper may prove too cumbersome and detailed for routine evaluation and screening. The detailed and specific nature of the foreign body reaction may be relatively insignificant for some implant applications. Indeed in some applications a certain degree of reaction may be desirable.

There are a number of applications wherein subtle changes in the tissue reaction may seriously affect the functioning of the device, such as electrodes for stimulations and for detection of physiologic events, particularly biochemical sensors [28], biochemically active surfaces and devices can be compromised by tissue reactions, including drug delivery systems, enzymatically active surfaces or membranes, surfaces for the binding of toxic agents, etc.

The nature of the interactions which occur at the interface between implant materials and their living host are still largely unknown or misunderstood (see [26] for a review). Detailed studies of the tissue reaction to implant materials, assuming such materials are very well characterized, especially with respect to their surface properties, should provide the data base which will aid us in understanding the nature of the phenomena which take place when a "foreign" object is placed in contact with living tissues. Once we begin to understand these reactions, then we will be able to engineer them for special applications, such as minimum or maximum implant-host tissue fixation.

CONCLUSIONS

A selected portion of the tissue reaction literature was reviewed to establish the need and basis for a foreign body reaction experimental protocol. A complete, detailed protocol was presented, including animal selection, sample configuration, surgery, sample harvesting, and fixation. A discussion of semi-quantitative means of evaluating the samples was also presented.

We thank Dr. Harold Dunn, Mrs. Traute Diem, Mr. David Malm, Mr. Douglas Parish, and Mr. Bob Wright for helpful discussions and assistance. Mr. Manuel Arevalo produced the figures. Mr. Robert N. King gratefully acknowledges the Corning Glass Works Educational Assistance Program. Portions of this work have been supported by the National Science Foundation Grant GK 29382 and by Public Health Service Grant RR07092.

References

- [1] C. A. Homsy, *J. Biomed. Mater. Res.*, **4**, 341 (1970).
- [2] American Society for Testing and Materials (ASTM), Committee F-4.
- [3] U. S. Pharmacopeia, XVIII, 926-929.
- [4] D. L. Coleman, R. N. King, and J. D. Andrade, *J. Biomed. Mater. Res.*, in press.
- [5] N. K. Wood, E. J. Kaminski, and R. J. Oglesby, *J. Biomed. Mater. Res.*, **4**, 1 (1970).
- [6] D. E. Ocumpaugh and H. L. Lee, Foreign body reactions to plastic implants, in *Biomedical Polymers*, A. Rembaum and M. Shen, Eds., Marcel Dekker, New York, 1971, pp. 101-118.
- [7] E. J. Kaminski, R. J. Oglesby, N. K. Wood, and J. Sandrick, *J. Biomed. Mater. Res.*, **2**, 81 (1968).

The Foreign Body Reaction: A Chronic Inflammatory Response

D. L. COLEMAN,* R. N. KING, and J. D. ANDRADE,† *Division of Materials Science and Engineering, Institute for Biomedical Engineering, and Department of Pathology, University of Utah, Salt Lake City, Utah 84112*

Summary

A brief discussion is presented of some of the problems and artifacts inherent in the testing of soft tissue reactions to artificial implants. The process of inflammation and wound healing is presented. The various factors affecting the foreign body reaction (chemical, mechanical, geometrical, and others) are discussed. The cellular components of the foreign body reaction are described and the sequential cellular changes that may occur as a result of implanting an artificial device are examined. The foreign body reaction should be considered as a chronic inflammatory response.

INTRODUCTION

The importance of tissue reactions to implant materials is becoming increasingly more apparent as new materials and new devices become available. An in depth understanding of foreign body and inflammatory reactions is a necessary prerequisite to solving the biological problems that presently exist with some artificial implants.

A brief review of the process of inflammation and wound healing will be given before describing the classical foreign body reaction. Soft tissue reactions to materials^{1,2} will be analyzed in terms of possible factors which might influence the foreign body reaction, or more properly, the "foreign implant reaction," and in terms of the sequential events that constitute the tissue's reaction to an implant.

* This represents part of the work done by D. L. Coleman as the thesis requirement for an M.S. degree from the Department of Pathology, University of Utah, Salt Lake City, Utah 84112.

† To whom correspondence and reprint requests should be addressed.

At this point in time, many investigators have considered the foreign body reaction as a distinct mechanism completely unrelated to the course of events which take place in normal wound healing. Acute and chronic inflammatory responses are usually mentioned only in passing, if at all.³ It must be kept in mind that inflammation is a dynamic process, and this process is broken down into stages only for convenience. The stimulus necessary to initiate an inflammatory response can vary greatly, but it is the continued presence or absence of the stimulus that dictates the eventual classification of the inflammatory response. In the case of the foreign body reaction there are many stimuli acting at the same time to maintain the inflammatory response. Attempts by the organism to neutralize or eliminate inflammatory stimuli can lead to eventual problems with an implanted device.

INFLAMMATION

Although inflammation is a complex dynamic process, it can be simply defined as the reaction of tissues to injury.⁴ The ultimate goal of inflammation is to facilitate healing; i.e., repair or regeneration of the injured tissue. Inflammation aids healing by destroying or neutralizing the injurious agent, or if this is not possible, by restricting the effects of the injurious agent to the smallest possible zone. The inflammatory process also facilitates repair by removing debris from the injured area and providing a fluid medium for the migration of repair cells into the area.⁵

Acute inflammation is short lived and results in rapid healing of the injury. Such is the case with most surgical wounds inflicted under sterile conditions. The acute inflammatory response (Fig. 1) is characterized microscopically by the infiltration into the injured tissue of polymorphonuclear leukocytes which remove cellular debris from the wound area prior to the appearance of fibroblasts. Although acute inflammation is usually not the predominant feature of tissue reactions to implant materials it must be kept in mind that an acute response is initially present in all implantation studies due to the fact that surgical trauma is a necessary condition for implantation.

When the injurious agent is present for a long period of time the inflammatory process is then classified as chronic; tissue destruction

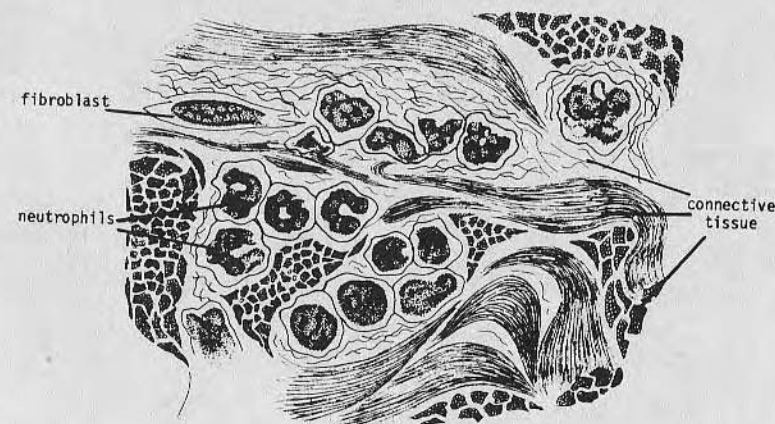


Fig. 1. Schematic drawing of an acute inflammatory response. The injured tissue is infiltrated by neutrophils which remove cellular debris from the wound area prior to the appearance of fibroblasts (repair cells). Note the random appearance.

and edema may be minimal or nonexistent⁴ in contrast to acute inflammation. At the cellular level chronic inflammation (Fig. 2) is characterized by large numbers of macrophages and lymphocytes which outnumber polymorphonuclear leukocytes in the exudate. Chronic inflammation is unique in that the proliferative changes of healing are active at the same time that the mild inflammatory response is going on.⁴

One specific type of chronic inflammation is the classical foreign body reaction. Pathologists have generally used this term to describe tissue reactions to foreign bodies; e.g., splinters, bullets, trichina infestations, etc. Usually these objects are not sterile so that the inflammatory response is complicated by infection. Infection involves the presence of pathogenic bacteria in the wound. However, bacteria are not a prerequisite for an inflammatory response.

The most prominent cell in a foreign body reaction is the macrophage, although some granulocytes and monocytes are also present. The macrophage generally attempts to phagocytize the material, but usually the foreign body is much larger than the macrophage and is not easily degraded. Some of the macrophages then merge their cytoplasm to become multinucleate giant cells (Fig. 3) or poly-

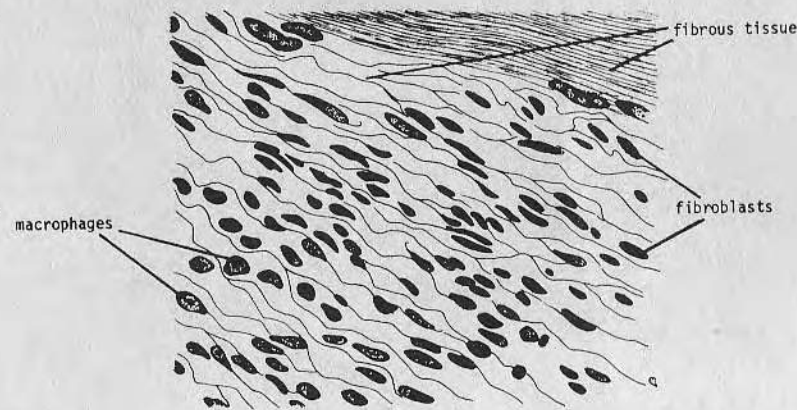


Fig. 2. Schematic representation of chronic inflammation. Large numbers of macrophages and lymphocytes are characteristic of chronic inflammation, although neutrophils are occasionally seen. This drawing also demonstrates an orientation of cells and fibrous tissue, as often observed in a chronic response to an implant. This orientation is usually parallel to the surface of the implant.

karyocytes.⁶ Polykaryocytes do not form in all foreign body reactions and the concept that giant cells form in an attempt to phagocytize larger materials may be an erroneous one. Giant cells can vary in size from 40 to 100 μ in diameter and can contain from 10 to 200 nuclei.⁵ If the foreign body is too large to be phagocytized and removed, granulation tissue, consisting of fibroblasts and angioblasts in a matrix of collagen, begins to form about the mass of phagocytes and encapsulates the foreign body in a tight, dense membrane of connective tissue. This tends to isolate the implant from the rest of the body tissues. With time this localized lesion can undergo caseation (cheese-like) necrosis, calcification, liquifaction and hyperplasia.¹¹

After fibrous encapsulation has occurred the lesion is generally referred to as a granuloma. A foreign body granuloma (Fig. 4) is thus composed of the foreign body surrounded by giant cells with a zone of macrophages, lymphocytes, and granulocytes around the giant cells, and finally, an encapsulating membrane of fibrous tissue.

It is the inflammatory process that eventually initiates and facilitates the end result of wound healing. Tissue injury, no matter how minute, disrupts tissue continuity (both structure and composi-

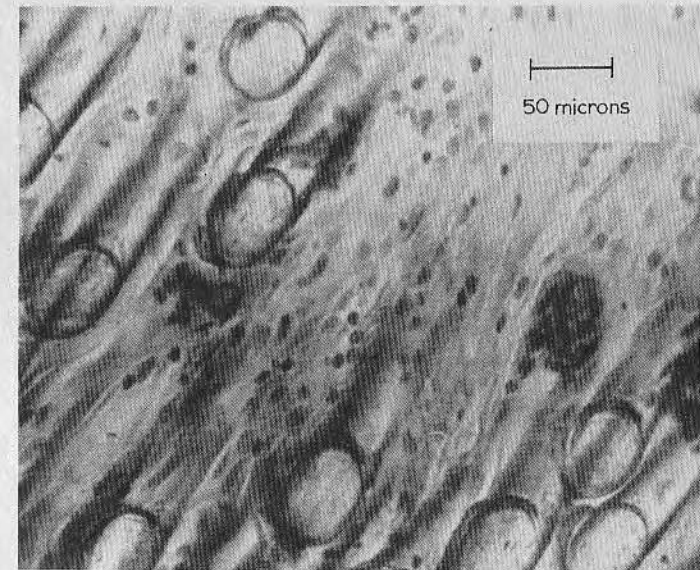


Fig. 3. Photomicrograph of multinucleate giant cells surrounding polyester fibers implanted in rabbit muscle. Giant cells can vary in size from 40 to 100 μ in diameter and can contain from 10 to 200 nuclei.

tion) and often causes a loss of function in the injured area. Ideally, restoration of injured tissue should be such that the new tissue is identical to the tissue before the injury. However, complete regeneration, restoration of continuity and function, is usually the exception rather than the rule. Generally, as cells become more specialized they lose their ability to proliferate, and their regenerative potential is poor. Healing of specialized tissue involves repair by fibrous tissue substitution (scar tissue); i.e., tissue continuity is restored but the original function of the injured tissue may be partially or completely lost.

There are many factors, besides degree of specialization, that may influence wound healing. Florey describes these factors in more detail⁸ than can be covered in this review. All of these variables should be reviewed when designing an implantation protocol. Briefly, some of the more important factors which directly affect wound healing are: 1) position of the wound in the body, 2) interference of blood supply to the surrounding tissue, 3) apposition and

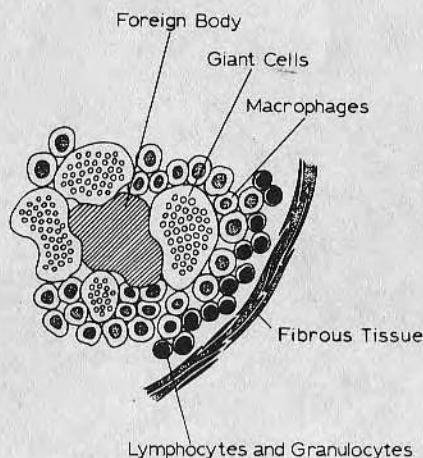


Fig. 4. A diagrammatic representation of a foreign body granuloma. The major component of this reaction is the macrophage, but giant cells may also surround the foreign body. Encapsulation by fibrous tissue aids in localizing the lesion, thus isolating it from normal tissue. (Redrawn from reference 5).

immobilization of cut surfaces, and 4) general health and nutritional status of the experimental animals. Factors which contribute to the severity of the tissue reaction to implants will be considered later in this paper.

To summarize the process of fibrogenesis and tissue repair, it is beneficial to examine the events in terms of time-dependent changes (Fig. 5). Gould has outlined⁹ the following five phase process for incisions and excised wounds.

Phase I—Days 0-2 Post-Operative. Acute (nonproliferative) inflammation. Vasodilatation, edema, neutrophil, and mononuclear cell accumulations extravascularly. Death and dissolution of previously injured cells and extracellular fibers.

Phase II—Days 2-3 Post-Operative. "Activation" and possible "transformation" of extravascular mononucleocytes and/or fibroblasts, all of which are involved in the phagocytosis of damaged tissue components.

Phase III—Days 3-6 Post-Operative. Mitosis of extravascular cells and growth of new blood vessels within the edematous tissue in or bounding the wound space.

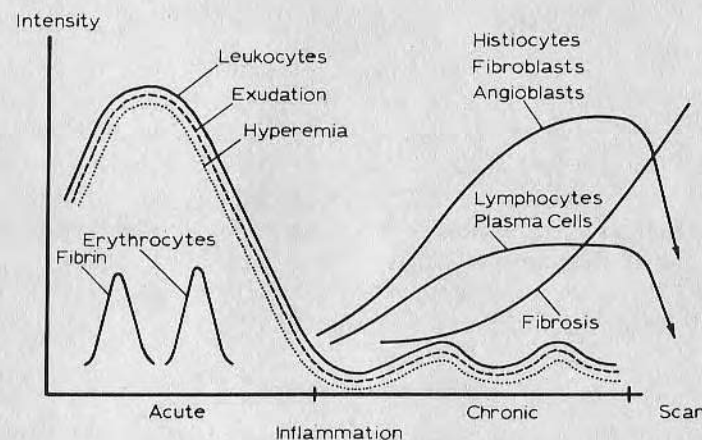


Fig. 5. Schematic representation of the course of events in acute and chronic inflammation (Redrawn from reference 31).

Phase IV—Day 4 or 5 Post-Operative. Extracellular collagen deposition (random at first); ingrowth of granulations into the wound space and to the surface blood clot.

Phase V—Day 6 Post-Operative and Thereafter. Remodeling of intact tissue abutting the site of repair; union of old and new collagen fibrils.

This general scheme is applicable to most soft tissue wounds. The expansion of this scheme to include events in a chronic foreign body reaction is difficult in terms of a time sequence. It must be remembered that the foreign body reaction represents a continuum of mild to severe chronic reactions. At about Phase III or IV the neutrophil population decreases and increased numbers of macrophages and lymphocytes appear in the wound area. As the events of Phase IV and V are taking place, the macrophages continue their attempt to phagocytize the foreign body. Giant cells appear on the scene and both macrophages and giant cells persist in the area as long as the foreign body remains.¹⁰ Evidence for the longevity of these cells is demonstrated by their presence in tattoos. Macrophages ingest the carbon particles and remain in the area for an indefinite length of time as seen by the continued presence of the tattoo. Calcification of the fibrous capsule, hyperplasia, caseation necrosis, and liquefaction can all result from the chronic lesion.

SOFT TISSUE REACTION TO IMPLANTS

Evaluation of the foreign body reaction to "inert" materials is usually very difficult because many of the variables involved in the reaction are difficult to control. Not only must investigators contend with the factors discussed above for wound healing; i.e., site of the wound, interference of the blood supply, apposition of cut surfaces, and general health of the animals, but also variables characteristic of the implant itself. If the implant produces noxious stimuli, chemical or physical, a chronic state of inflammation will exist as long as the stimulus is present.

Chemical Factors

Unfortunately, most implants are not truly inert. "Inert" implants can be the source of many chemical irritants. The stimulus can be due to ions evolved during the corrosion of implanted metals. It can be due to monomer or catalyst residues in polymers leaching into the tissues as well as plasticizers, antioxidants, and other additives. It may also be the result of impurities or filler material in the polymer, mold-release agents, machining oils, etc. Virtually any chemical or material that can make its way to the tissue-implant interface may result in some degree of chemical stimulus to the tissue.

Laing et al.¹¹ differentiated four basic reactions, based on capsule thickness, to a large variety of metals in rabbit muscle. Fibrous membrane thickness ranged from 0.002 to 0.008 mm in their Group I and from 0.1 mm to several millimeters in their Group IV.¹¹ The fibrous membrane thickness was correlated with the degree of implant corrosion. The capsule thickness varied from 2 to 8 μ for a mild reaction to in excess of 1000 μ for a very severe response. Not only did they find a correlation between membrane thickness and ion concentration, but also between thickness and ion toxicity. More recent investigations concluded that no correlation of membrane thickness with toxic products could be established.^{3,7,12} A possible explanation is that the method of Laing et al.¹¹ involved implants of variable size, shape, and surface roughness which could account for the results in their study. Some of the materials tested varied in membrane thickness from a Group II reaction to a Group IV reaction for the same metal. It is indeed possible that toxic corrosion products will affect the tissue reaction, but it is also ex-

pected that the type and number of cells participating in the reaction would vary as well as the membrane thickness.^{7,12}

Homsy¹³ has shown that cytotoxic material from many polymers and metals can be quantitated by using *in vitro* tissue culture techniques. Test materials were placed in a "pseudo-extracellular fluid" containing physiological concentrations of NaHCO_3 , K_2HPO_4 , NaCl , KCl for 62 hr at a temperature of 115°C. Following the exposure period the physiological fluid was analyzed by infrared spectrophotometry for low molecular weight degradation products. The electrolyte solution was then used to prepare the nutrient medium for tissue culture of new-born mouse heart. The tissue culture response generally correlated with the amount of extracted material detected in the pseudo-extracellular fluid.

Nontoxic chemical interactions of the implant and physiological substances can also play an important role in determining the success of implant materials. Such interactions can lead to changes in the surface properties and also mechanical function of an implant. This may be the case with the absorption of lipid by silicone rubber in heart valve prostheses.¹³ A similar phenomenon may take place during the *in vivo* degradation of polyvinyl alcohol (Ivalon) sponge implants. Chen et al.¹⁴ noted increased deposits of adipose tissue as the implantation time of the Ivalon sponge increased. Further investigation into the effects of nontoxic chemical interactions may be of great value in explaining why some implant materials fail in one part of the body but are tolerable if implanted in another site.

Denaturation of proteins as a result of an implanted material may evoke an immunologic response which could contribute to the inflammatory response. Evidence for immunogenicity of various materials has been elaborated by Stern et al.¹⁵ by exposing plasma from individual rabbits to large surface areas of various test materials. The plasma was then repeatedly injected into the original animal. Antibody determinations were made by several *in vitro* tests. Stern's method may be useful as a means of characterizing materials for implantation.

Mechanical Factors

Movement of an implant with respect to adjacent or surrounding tissue will produce cellular irritation, thus provoking a tissue response. The effects of prolonged mechanical movement of an object in con-

tact with tissue should be obvious to anyone who has worn a shirt with an over-starched collar. Mechanical trauma must be considered as a contributing factor to the foreign body reaction in most implant studies.

It is not difficult to visualize movement, to a greater or lesser degree, in almost any part of the body; muscles contract and relax, skin and subcutaneous tissue are very pliable, joints bend and rotate, and bulk fluid movements take place in many compartments of the body. Animal implant studies have the added variable of mechanical trauma due to the host biting or scratching the wound or due to rubbing the wound against the cage.

It is interesting to note that in a study comparing several different sites of implantation, the anterior calvarium, mandible, and the paravertebral and thigh muscles, the conclusion was that muscle showed the greatest reaction,¹² probably due to the extension and contraction movement invariably present in muscle. However, it was also concluded that the thigh and paravertebral muscles showed no difference in tissue reactions to implants even though one would expect the two muscles to have different degrees of mechanical activity.¹²

Geometrical Factors

The foreign body reaction is also dependent on the size and shape of the implant with respect to the cells and surrounding tissue. Less severe tissue reactions have been observed with powder forms as compared to solid structures of the same material.^{3,16-18}

Davila^{19,20} suggests that larger implants impair the nutrient supply of surrounding tissue. Studies of tumor production by implanted polymers suggest similar causes.^{18,21} Thin fibers, 30 to 50 μ in diameter, of most materials are well tolerated in tissue and have only a thin fibrous capsule, a good blood supply and good cellularity.²⁰ Davila has shown²⁰ for a variety of inert materials that the diameter of the fiber has a greater influence on the foreign body reaction than the type of material. Davila's work establishes an explanation for the success of velours, felts, weaves, knits, and other textile structures in implant applications.

Oppenheimer et al.^{22,23} have shown that in certain cases the presence of the implant is the primary factor inducing a severe reaction; the presence of the implant exerts an influence for a mini-

mum of six months, after which the wall of fibrous tissue encapsulating the implant becomes the essential irritating structure. They also noted that with textiles and also with plastic films perforated with holes, the material was ingrown with connective tissue fibers penetrating between textile threads or through the perforations in the plastic film. A gross "pocket" of fibrous encapsulation was not seen with these materials.

It should be noted that studies of human implants have revealed no malignant tumor production due to long term polymeric implants.^{18,24,25} Such studies indicate that the rat and his relatives are poor models for studying solid state carcinogenesis in man. S. C. Woodward states that: "the Oppenheimer effect is meaningless in terms of neoplasm induction in man and primates. Useful materials should not be excluded from human use on the basis of a positive Oppenheimer test."²⁶

Other Factors

The very presence of an interface between the implant and the surrounding tissue serves to permit a variety of phenomena which may be important in the foreign body reaction. Some of these factors have been speculatively discussed by Kordan.²⁷

The presence of an implant grossly changes the local dielectric environment, thus affecting local intermolecular interactions. The possibility exists that cells very near to or touching an implant will have their membrane potential altered due to the lack of physiological ions at the implant interface.²⁸ Surface defects and local crystallinity or lattice orientations on the implant surface can affect the tissue reaction as can residual surface charge or dipole orientations.²⁸ Interfacial free energy is an important consideration.²⁸

Cellular interactions at the implant interface and the need for restoration of tissue continuity appear to play a very important role in the tolerability of artificial materials implanted in biological systems. At present, these phenomena are poorly understood and deserve more intensive investigation.

DISCUSSION AND CONCLUSIONS

Although there are many materials available for implant medicine that exhibit an "insignificant" tissue reaction, there are a number of

applications wherein subtle changes in the tissue reaction may seriously affect the functioning of the device. Electrodes for stimulation and for detection of physiologic events (particularly biochemical sensors or enzyme electrodes)²⁹, biochemically active surfaces and devices (including drug delivery systems), enzymatically active surfaces or membranes, etc., can be seriously compromised by "mild" tissue reactions.

The nature of the interactions which occur at the interface between implant materials and their living host are still largely unknown and often misunderstood (see reference 28 for a review). It is important to have a basic understanding of inflammation and wound healing before detailed studies of the tissue reaction to implants can be properly evaluated. Such studies should provide the data base which will aid us in understanding the nature of the phenomena which take place when a "foreign" object is placed in contact with living tissues. Once we begin to understand these reactions, then we will be able to engineer them for special applications, such as minimum or maximum implant-host tissue adhesion and fixation.

We have presented a brief review of wound healing and inflammatory reactions in soft tissues. The foreign body reaction has been examined. We have also discussed the factors which may be inherent in and the cause of foreign body reactions to implanted materials.

Methods for the evaluation of tissue reactions on a quantitative level must become available if mechanisms are to be determined and meaningful events and components of the tissue reaction are to be understood. Such protocols are becoming available.³⁰

The authors wish to thank Dr. Harold Dunn, Mrs. Traute Diem, Mr. David Malm, Mr. Douglas Parrish, and Mr. Bob Wright for helpful discussion and assistance. Mr. Manuel Arevalo produced the figures. Mr. Robert N. King gratefully acknowledges the Corning Glass Works Educational Assistance Program. This work has been supported by the U.S. Atomic Energy Commission, Division of Applied Technology, Contract AT(11-1)-2147, and PHS Grant RR07092.

References

1. K. Little, *The Interaction of Polymers and Tissues*, in press.
2. R. I. Leininger, CRC Critical Rev. in *Bioengineering*, **1**, 333 (1972).
3. N. K. Wood, E. J. Kaminski, and R. J. Oglesby, *J. Biomed. Mater. Res.*, **4**, 1 (1970).

4. T. M. Perry, *Pathology*, Little Brown and Company, Boston, 1961.
5. H. C. Hopps, *Principles of Pathology*, Appleton-Century-Crofts, New York, 1964.
6. B. Roizman, *Cold Spring Harb. Symp. Quant. Biol.*, **27**, 327 (1972).
7. J. E. Turner, W. H. Lawrence, and J. Autian, *J. Biomed. Mater. Res.*, **7**, 39 (1973).
8. Sir H. W. Florey, *General Pathology*, Saunders, New York, 1970, pp. 510-516.
9. B. S. Gould, *Treatise on Collagen*, Vol. 2, Part B, Academic Press, New York, 1968, pp. 359-363.
10. S. R. Haythorn, *Arch. Path.*, **7**, 651 (1929).
11. P. G. Laing, A. B. Ferguson, and E. S. Hodge, *J. Biomed. Mater. Res.*, **1**, 135 (1967).
12. E. J. Kaminski, R. H. Oglesby, N. K. Wood, and J. Sandrick, *J. Biomed. Mater. Res.*, **2**, 81 (1968).
13. C. A. Homsy, *J. Biomed. Mater. Res.*, **4**, 341 (1970).
14. R. W. Chen, A. W. Musser, and R. W. Postlethwait, *Surgery*, **66**, 899 (1969).
15. I. J. Stern, A. A. Kapsalis, B. L. DeLuca, and W. Pieczynski, *Nature*, **238**, 151 (1972).
16. K. Little and J. Parkerhouse, *Lancet*, **ii**, 857 (1962).
17. K. Little, *Biomed. Eng.*, **3**, 414 (1968).
18. B. S. Oppenheimer, E. T. Oppenheimer, A. P. Stout, and I. Danishefsky, *Science*, **118**, 305 (1953).
19. J. C. Davila, *Ann. Thorac. Surg.*, **2**, 126 (1966).
20. J. C. Davila, E. V. Lautsch, and T. E. Palmer, *Ann. N.Y. Acad. Sci.*, **146**, 138 (1968).
21. N. T. Stinson, *Brit. J. Exper. Path.*, **45**, 21 (1964).
22. B. S. Oppenheimer, E. T. Oppenheimer, A. P. Stout, M. Willhite, and I. Danishefsky, *Cancer*, **11**, 204 (1958).
23. B. S. Oppenheimer, E. T. Oppenheimer, A. P. Stout, I. Danishefsky, and M. Willhite, *Estrait de Acta Union Int Contre Le Cancer*, **15**, 659 (1959).
24. F. B. Johnson, *Plastics in Surgical Implants*, Amer. Soc. Testing and Materials (ASTM), Special Technical Publication No. 386, 1965.
25. L. R. Rubin, B. E. Bromberg, and R. H. Walden, *Surg. Gyn. Obstet.*, **132**, 603 (1971).
26. S. C. Woodward, personal communication, 1972.
27. H. A. Kordan, *J. Theoret. Biol.*, **17**, 1 (1967).
28. J. D. Andrade, *Medical Instrumentation*, **7**, 110 (1973).
29. D. A. Gough and J. D. Andrade, *Science*, **180**, 380 (1973).
30. D. L. Coleman, R. N. King, and J. D. Andrade, *J. Biomed. Mater. Res. Symp.*, in press (1974).
31. W. Sandritter and W. B. Wartman, *Color Atlas and Textbook of Tissue and Cellular Pathology*, Yearbook Medical Publishers, Inc., Chicago, 1969, p. 20.

Received March 15, 1973

Revised June 25, 1973

PLATELET RETENTION BY ALBUMINATED GLASS AND POLYSTYRENE BEADS

by

D. L. Coleman, A. I. Atwood, and J. D. Andrade

Department of Materials Science and Engineering

University of Utah

Salt Lake City, Utah 84112

(Received in final form September 8, 1976)

Summary

Ex vivo platelet retention by albuminated glass and polystyrene beads has been evaluated as a function of flow rate, bead surface area, blood exposure time and albumin treatment. The stability of the albumin coatings as well as scanning electron microscopy of the various surfaces before and after blood exposure has also been included. Results indicate that platelet retention is sensitive to changes in the above parameters and that albumin pretreatment of different substrates can decrease platelet retention. This decrease is substrate dependent in that platelet retention is different for the albuminated glass and polystyrene substrates. Chemical analysis of the substrate materials by X-ray photoelectron spectroscopy (XPS) as well as bulk chemical analysis is also reported.

The interaction of native blood proteins with a foreign surface is becoming recognized as an important process in the eventual success or failure of materials required to interface with blood (1-4). The interaction of cellular blood components with various materials has been the subject of a great deal of investigation, not only in terms of mechanisms (5-8), but also as a tool to evaluate general blood tolerability of various materials which must contact blood (9-12). Blood proteins that are known to adsorb and play a role in the eventual adhesion of cells, mainly platelets, include fibrinogen, γ -globulin and albumin. Kim et. al. (7) have demonstrated that polymers which preferentially adsorb greater amounts of albumin over fibrinogen or γ -globulin adhere fewer platelets. In fact, the general biocompatible nature of albuminated surfaces has been shown to be of value in extracorporeal systems including charcoal hemoperfusion (13-15) and membrane oxygenators (16, 17).

To evaluate further the effectiveness and initial stability of adsorbed albumin and glutaraldehyde crosslinked albumin coatings of a more permanent nature, a modified ex vivo platelet retention test was used in our studies. The original platelet retention test described by Hellem (18) has been modified by many investigators (19, 20) to become a popular diagnostic aid in von Willebrand's disease. The importance of controlled blood flow rate, bead surface area, hematocrit, temperature, and anticoagulants have been examined using human blood (18, 19). This study is directed towards defining test parameters using the rabbit as an experimental model to evaluate the blood tolerability of materials

prior to and after surface modification by different albumin treatments. The stability of albumin adsorbed to glass and polystyrene beads is also examined over a 24 hour period. Scanning electron microscopy of the bead surfaces before and after the platelet retention test is used as a check on the retention data.

Methods and Materials

A. Test Chambers. Glass beads, 1.00 - 1.05 mm diameter (B. Braun Melsunger Apparatebau) were extracted in a Soxhlet apparatus with 95% ethanol for 48 hours followed by distilled water extraction. The beads were oven dried for 24 hours at 60°C and stored dry as stock test material. A sample of the stock beads was evaluated for chemical composition (Emhart Corp., Hartford, Conn.) and found to contain the following:

	%
Silica (SiO ₂)	56.9
Baria (BaO)	0.66
Alumina plus Iron Oxides (R ₂ O ₃)	1.27
Soda (Na ₂ O)	3.95
Potassia (K ₂ O)	9.90
Lead Oxide (PbO)	26.53
Boron Oxide (B ₂ O ₃)	0.83
Total	100.00

Polystyrene beads, 1.00 mm diameter (Sinclair-Koppers Co.), were extracted in a Soxhlet apparatus using petroleum ether for 24 hours followed by vacuum drying.

The beads were examined by X-ray photoelectron spectroscopy (XPS) (21) using a du Pont 650B source. The surface of the polystyrene beads was highly oxidized, which is typical for many commercial hydrocarbon polymers. The glass beads exhibited the expected silicon and oxygen photoelectron lines. No lead lines were observed indicating that the lead is not present in detectable concentrations at the surface but is present in the subsurface and bulk regions of the sample.

Test chambers were made from 9.5 cm lengths of ¼" i.d. polyvinyl chloride tubing (Tygon S-50-HL, Norton Plastics). Nylon screen, mesh size approximately 100, was used to contain the packed beads. Columns were packed with about four grams of glass beads or 1.2 grams of polystyrene beads.

B. Adsorbed Albumin. The columns were packed with stock glass beads, primed with 1% w albumin in normal saline and allowed to stand at least one hour at room temperature. Several types of commercially available albumins (Sigma Chemical) were used: 1) Rabbit Albumin, Fraction V (RAFV); 2) Rabbit Albumin, Crystalline (RAC); 3) Bovine Albumin, Fraction V (BAFV); and 4) Bovine Albumin, Crystalline (BAC).

Polystyrene beads were only adsorbed with crystalline type rabbit albumin using the same procedure as for glass beads.

C. Crosslinked Albumin. To 200 ml of acetate buffer, pH 4.9, one gram of RAC was dissolved. Stock glass beads were added and allowed to stand for 15-20 minutes with mild agitation. Two milliliters of 25% glutaraldehyde (Sigma Chemical) were added to the albumin solution. The mixture was placed on a shaker and allowed to react for one hour at 37°C. The albumin solution was decanted and the beads rinsed in phosphate buffered saline (PBS), pH 7.0; three changes of 15 minutes each. The beads were then stored in PBS until use. Columns with glutaraldehyde treated albumin were primed at least one hour before use with 1% w RAC

in normal saline. This step was necessary to quench any reactive aldehyde remaining from the original crosslinking procedure (16).

D. Pump Circuit. The extracorporeal circuit was designed as a low prime (6.5 ml) controlled flow system (Figure 1). An intravenous infusion pump (Extracorporeal[®], Model RL 175) was used to remove blood at a constant flow rate. The arterial cannula was made from polyethylene tubing, 1.40 mm i.d.. Circuit tubing was Silastic[®] (Dow Corning), 2.64 mm i.d..

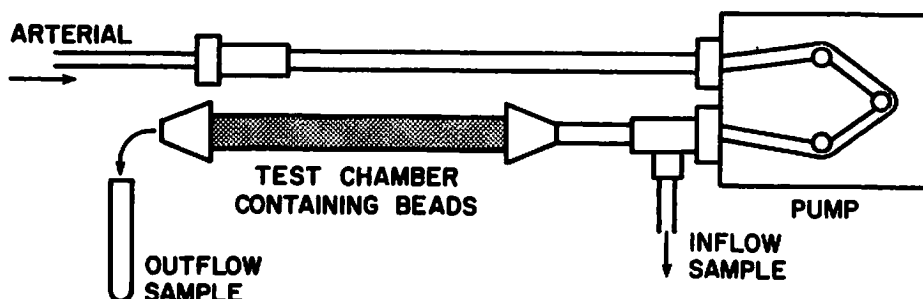


FIG. 1

A schematic representation of the low prime, controlled flow, ex vivo circuit used to evaluate platelet retention of albuminated glass beads.

Experimental Procedure

A. In Vitro Testing. Glass beads coated with I^{125} Human Albumin as described in B and C of the 'Materials and Methods' section, and polystyrene beads coated as described in part B were extracted in either PBS, pH 7.4, or citrated human plasma, pH 7.0-7.3 for periods up to 24 hours at 37°C. The radioactivity on the beads was monitored as a function of extraction time. The total amount of albumin per bead was calculated from the radioactivity values.

These experiments were necessary not only to insure the presence of albumin on the beads during the platelet retention test, but also to evaluate the longer term stability of albumin coatings.

B. Ex Vivo Testing. New Zealand White Rabbits of both sexes, weighing from 3.2 to 4.5 Kg were used in this study. Animals were anesthetized with pentobarbital sodium, 30 mg/Kg given intravenously. The left carotid artery was surgically isolated and just prior to cannulation the animal was given sodium heparin (Upjohn, beef lung) 400 units/Kg i.v.. The pump circuit was primed with physiologic saline (0.9% NaCl) to avoid a blood/air interface. After cannulation of the artery the infusion pump was started at a flow rate of 10 ml/min. and the saline prime was flushed out of the system by the animal's blood. An afferent blood sample was collected for eight seconds (1.3 ml), the tubing clamp on the end of the test chamber was removed to allow blood to flow through the chamber and efferent blood was collected. The blood transit time from afferent to efferent was 30 seconds. Blood samples were collected in tubes containing 7.5 mg disodium EDTA. Platelet counts were performed with the aid of an automatic cell counter (Technicon Autocounter).

C. Scanning Electron Microscope (SEM) Studies. Bead samples before and after blood exposure were rinsed with phosphate buffered saline (PBS), pH 7.3. The samples were then fixed in 37°C 3% glutaraldehyde (Polysciences, E.M. grade) for 30 to 60 minutes. The beads were rinsed with distilled water and postfixed in 1% osmium tetroxide (Polysciences), and dehydrated through absolute ethanol.

Samples with glass as the substrate material were dried by using the liquid CO₂ critical point drying (CPD) method described by Porter et. al. (22). Samples evaluated using polystyrene as the substrate material were air dried out of 100% ethanol because the CPD method caused the beads to swell.

Results

A. In Vitro Stability. Preliminary in vitro studies indicate that for purposes of the short term platelet retention studies, both adsorbed and crosslinked albumin coatings were stable. However, longer extraction in plasma, up to 24 hours, suggests that the original adsorbed albumin on glass is virtually gone and that glutaraldehyde crosslinked albumin on glass is much more resistant to extraction in plasma (Table 1). It is interesting to note that polystyrene beads adsorbed with albumin and extracted in the same manner do not adsorb as much albumin per bead, yet maintain very close to the original adsorbed concentration throughout the 24 hour extraction period.

Extraction in PBS offers some insight into what might happen if albuminated samples were stored wet for any length of time. Desorption is evident after 24 hours and depending on the material, may be quite dramatic. In the case of adsorbed albumin on glass the albumin decreases by 86%, and adsorbed albumin on polystyrene is reduced by about 50% after a 24 hour extraction in PBS. Others have reported (23, 24) that desorption and exchange of adsorbed albumin is characteristic of many substrate materials.

TABLE 1

A Summary of Albumin Stability of Substrate Materials Extracted for a 24 Hour Period.

Substrate and Surface Treatment	µg Albumin per Bead, Pre-Extraction	Extraction Medium	µg Albumin per Bead, Post-Extraction	% Drop
Glass Adsorbed Albumin	0.186 ± .051	PBS*	0.023 ± .001	86.3 ± 4.6
		Plasma**	0.003 ± .001	97.2 ± 0.4
Glass Glutaraldehyde Crosslinked Albumin	0.279 ± .063	PBS**	0.183 ± .081	40.0 ± 11.7
		Plasma**	0.156 ± .017	44.5 ± 9.4
Polystyrene Adsorbed Albumin	0.02 ± .004	PBS*	0.013 ± .002	49.6 ± 12.0
		Plasma**	0.004 ± .001	81.1 ± 2.7

*Phosphate Buffered Saline 0.01 M pH 7.4

**Citrated Human Plasma pH 7.0 - 7.3

B. Blood Flow Rate Studies. The platelet retention of untreated glass beads (UGB), glutaraldehyde crosslinked rabbit albumin-crystalline (GARAC) and empty chambers (EC) was evaluated as a function of blood flow rate. Flow rates were precalibrated to deliver 1.0, 3.0, 5.0 and 10 ml/min.. The first 1.3 ml of undiluted blood was collected for platelet counting.

Results suggest, as expected, that as the flow rate decreases the platelet retention increases (Table 2). More importantly, it appears that the reliability of the test diminishes as the flow rate decreases below 5 ml/min, i.e. the

standard deviation greatly increases as the flow rate is reduced from 10 ml/min. to 1.0 ml.min.

C. Surface Area Studies. The importance of variation in the surface area of the test materials was evaluated for UGB and GARAC beads. The surface area of the beads was estimated by weighing several beads to get the mean weight per bead. The mean surface area of each bead size was calculated from the equation for the surface area of a sphere, $A = 4\pi r^2$. The total weight of the beads contained in a 7.5 cm cartridge was then used to give an approximation of the total surface area per cartridge. Bead sizes used in this study were 0.25 - 0.20 mm diameter, 0.45 - 0.50 mm diameter, and 1.00 - 1.05 mm diameter giving calculated surface areas of 260 cm², 120 cm², and 60 cm², respectively. Microscopic observations confirmed the bead sizes.

It was not surprising to see that platelet retention rapidly increases as surface area increases (Table 2). However, it is interesting to note that the glutaraldehyde crosslinked albumin beads consistently retained fewer platelets than did UGB at each surface area tested.

TABLE 2
A Summary of Data Showing the Effects of Flow Rate and Surface Area on Platelet Retention by Glass Beads.

Surface Treatment	*% Platelet Retention (± S.D.)						
	Flow Rate (ml/min.)				Surface Area (cm ²)		
	1	3	5	10	60	120	260
Untreated Glass Beads	66.3 ±10.9	52.9 ±13.3	36.2 ±8.1	23.7 ±6.7	23.7 ±6.7	58.7 ±5.3	78.4 ±6.7
Glutaraldehyde Crosslinked Albumin on Glass Beads	32.8 ±14.1	36.3 ±19.1	12.5 ±8.5	1.0 ±6.4	1.0 ±6.4	23.4 ±4.3	49.6 ±11.0
Empty Chambers	2.0 ±8.0	14.7 ±10.3	1.3 ±6.5	0.7 ±3.8	-	-	-

*Based on the first 1.3 ml of blood to pass through the column.

D. Time Dependent Studies. Using the conditions described in the experimental procedure section above, serial 1.3 ml blood samples were collected on the outflow side of the test cartridge. As seen in Figure 2, there is a dramatic difference in platelet retention of UGB and GARAC beads with time. This difference was evaluated with the Student "T" test and found to be significant ($P < .001$) at all time intervals. The data comparing UGB with ARAC revealed that adsorbed albumin only showed a significant decrease in platelet retention at the first time interval tested. Platelet retention of ARAC samples increased in the same fashion as UGB. However, unlike UGB the standard error of the mean (S.E.) increased with time in the adsorbed albumin samples.

The change in platelet retention of adsorbed albumin (ARAC) as a result of glutaraldehyde crosslinking is striking. Even the very first blood sample shows a significant ($P < .05$) difference in the platelet retention suggesting a positive effect of albumin crosslinking or at least the use of glutaraldehyde to crosslink.

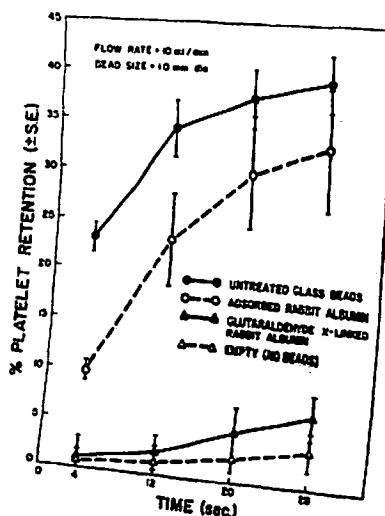


FIG. 2

Platelet retention (\pm Standard Error) as a function of time for UGB, ARAC, GARAC, and EC. The GARAC is significantly different ($P < .001$) in platelet retention than UGB and ARAC.

Polystyrene beads proved to be worse than the glass beads in terms of platelet retention. Attempts to passivate the surface with adsorbed albumin were successful and comparable with the glass surface. It can be seen from Figures 2 and 3 that the platelet retention of ARAC on polystyrene remained much lower than that seen for ARAC on glass beads.

To determine if the tubing used to make the cartridges had a significant effect on platelet retention, empty chambers (EC) were used as controls. The mean percent platelet retention for an EC ranged from 1 to 4 percent depending on the time interval sampled. Comparing the results of GARAC to EC suggests that the tubing played a significant role in platelet removal (Figure 2).

Exposure of the glass beads to just glutaraldehyde (no albumin) followed by a rinse prior to platelet retention evaluation did not significantly change the results from that of untreated glass beads (unpublished data).

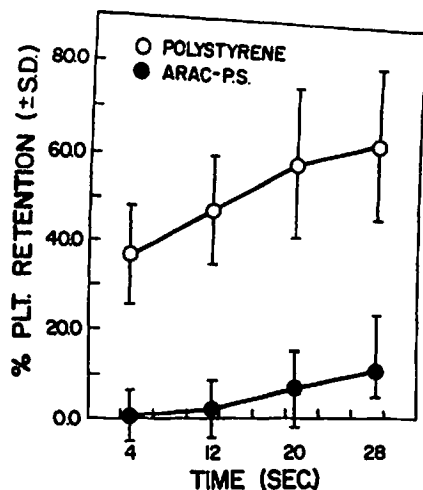


FIG. 3

Polystyrene control beads have a somewhat elevated platelet retention compared to glass beads but the passivating effect of adsorbed albumin on polystyrene (ARAC-P.S.) is more prolonged than on glass.

E. Albumin Treatment Studies. Various commercial grades of albumin, rabbit and bovine, were adsorbed on the glass beads. Test conditions included a bead surface area of about 60 cm² and a flow rate of 10 ml/min.

In a comparison between adsorbed bovine and adsorbed rabbit albumin evaluated with rabbit blood there is a significant difference ($P < .01$) in platelet retention only at the first time interval sampled. The superiority of rabbit albumin in retaining fewer platelets is quickly negated in the following samples. Variation in surface treatments with the resultant changes in platelet retention are summarized in Figure 4. It is interesting to note that even though there is a difference in the platelet retention of rabbit and bovine albumins of the crystalline type the same is not true of fraction V rabbit and bovine albumins.

The superior behavior of GARAC was conspicuous throughout all experiments. Adsorbed albumin, although showing a decrease in the initial platelet retention over UGB, was not as impressive as the glutaraldehyde treated albumin samples in reducing platelet retention.

The point should be made that not only can the type, i.e. species, fraction, purity, etc., of albumin influence the platelet-material interaction, but also the substrates' influence on the albumin layer, i.e. adhesive strength, molecule orientation, etc., can be important. This phenomenon is evident from a comparison of the polystyrene and glass retention experiments.

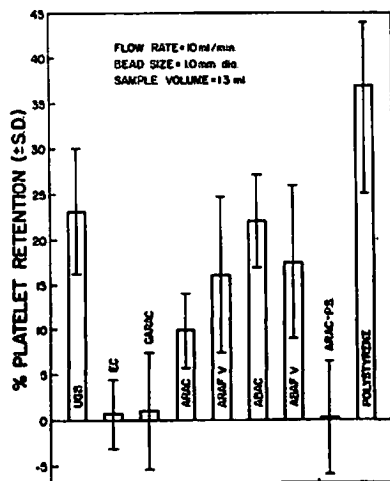


FIG. 4

A summary of the platelet retention data as a function of variation in albumin surface treatments (±S.D.).

F. SEM Evaluation. In order to check the reliability of the retention results scanning electron microscopic evaluation of the beads before and after perfusion was done. The spherical shape and size of the beads was also confirmed by this method.

The control glass beads were reasonably smooth in appearance (Figure 5a), although imperfections and a definite surface texture could be seen. After exposure to blood the bead surface was well populated with platelets (Figure 5b). Albumin adsorbed on glass did not visibly change the surface. However, after blood exposure the albuminated beads were generally free of adhered platelets. Glutaraldehyde crosslinked albumin on glass did reveal a rougher surface than the control beads (Figure 6a). After blood exposure the surface was strikingly

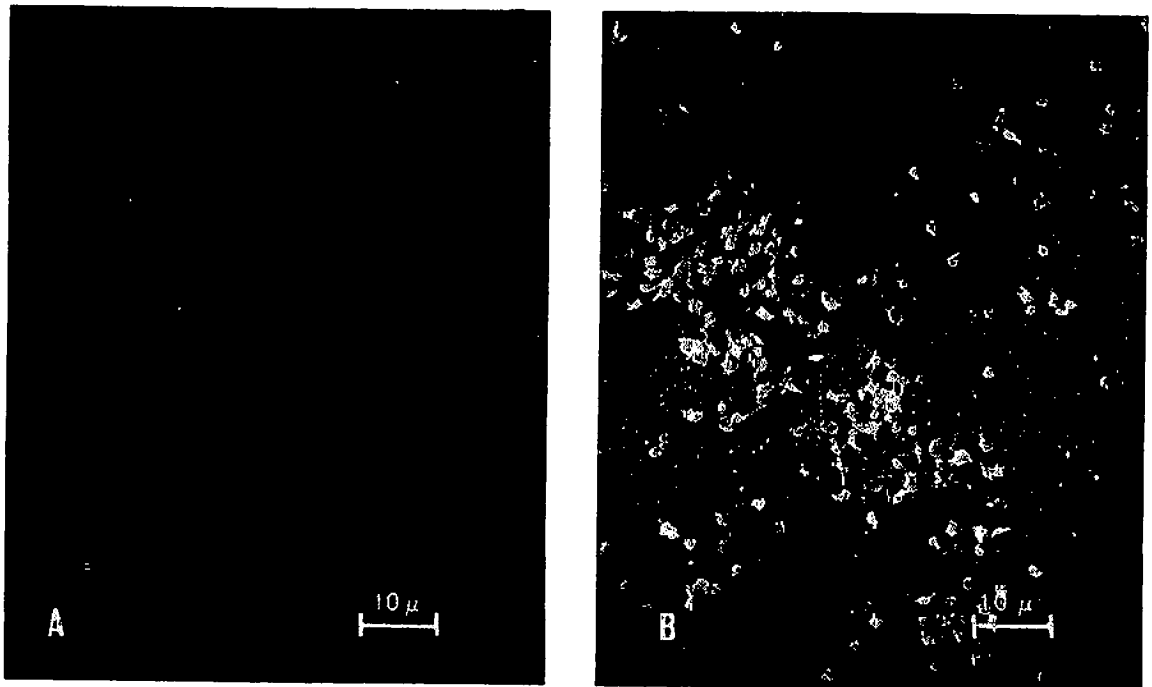


FIG. 5

Scanning electron micrograph of the surface of untreated glass beads before blood exposure (A) and after 30 sec. of blood flowing at 10 ml per minute (B). After exposure to blood numerous adhered platelets and platelet aggregates are deposited on a sublayer of protein-like material. Cracking of this sublayer is a preparation artifact. (1000x)

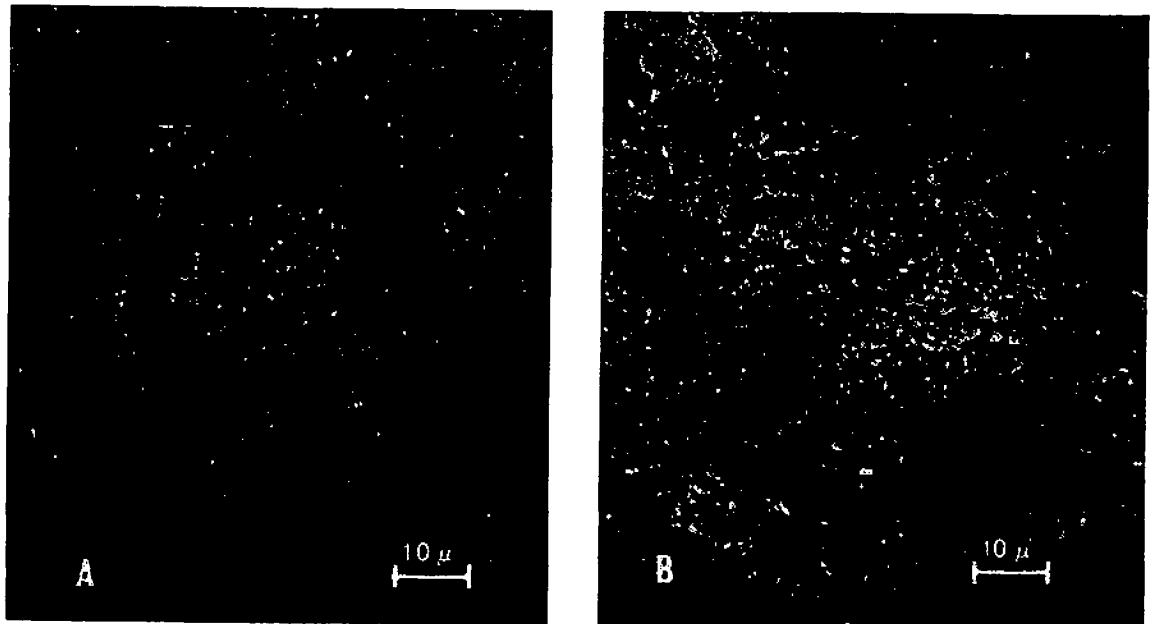


FIG. 6

The surface of crosslinked albumin on glass beads prior to blood contact (A) is somewhat rougher than the control glass beads (Fig. 5A). After blood exposure (B) the surface appears eroded but adhered platelets are strikingly absent. (1000x)

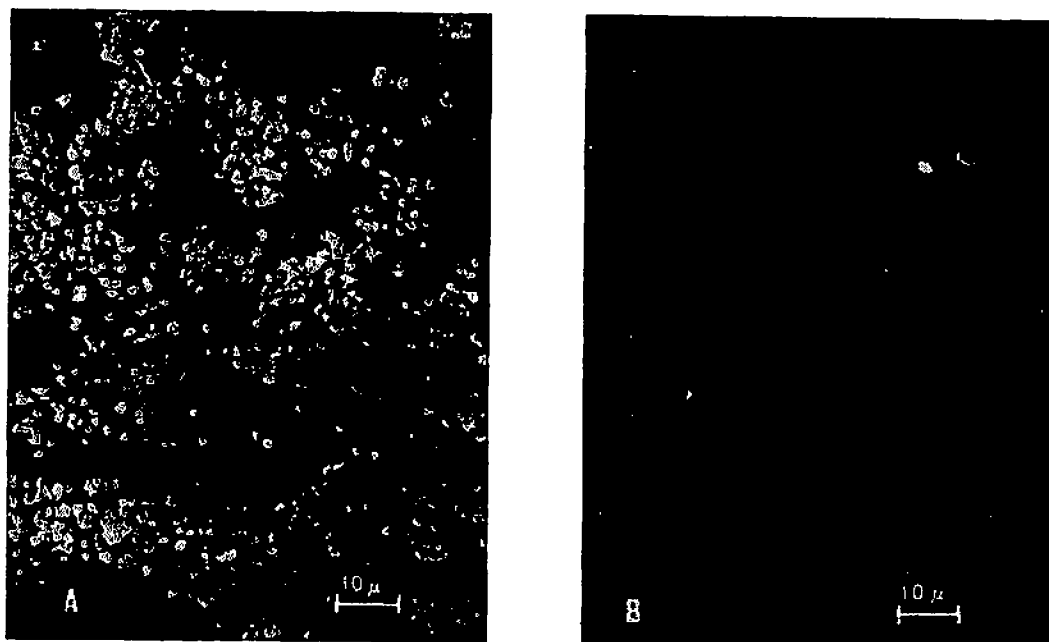


FIG. 7

Scanning electron micrographs demonstrate the striking difference between blood exposed control polystyrene (A) which is heavily populated with adhered platelets and albumin adsorbed polystyrene beads (B) which are consistently free of platelets. (1000x)

free of adhered platelets (Figure 6b). The polystyrene showed similar results to that of glass except the difference in the blood exposed control polystyrene (Figure 7a) and the adsorbed albumin beads (Figure 7b) was even more dramatic. This data compares favorably with that reported by Chang (15).

Discussion

The use of the standard glass bead platelet retention test first described by Hellem(18) and later revised by Salzman (10) and others (19) has proven to be a useful tool in the evaluation of platelet interactions with materials. Evans and Mustard (6) have examined the effect of the surface on adhesion and the release reaction of platelets using glass beads as a substrate for adsorbing various proteins. Their methods were not sensitive enough to show striking differences between uncoated and albumin coated beads. Mustard et. al. (25) also studied the influence of plasma proteins adsorbed to polystyrene on platelet interaction. Conclusions from these studies indicated that fibrinogen and gamma globulin coated surfaces aid both platelet adhesion and release of platelet factors. Albumin coated surfaces were less thrombogenic.

The ex vivo platelet retention test described in this study has proven to be moderately sensitive in that differentiation of two surfaces treated by adsorbing albumin in the same way can be identified as such by this method. However, we have also demonstrated that the results of this test can be greatly affected by changes in flow rate, surface area, individual variation among the test population, and the nature, quality and purity of the albumin coating.

Negative platelet retention, i.e. more platelets coming out than going in, although theoretically impossible over a long time interval, is observed in some experimental situations. Goldsmith, et. al. (26) have shown that red blood cells

do accumulate at the air-blood interface as noted by the increase in the first few drops coming out of the column. This phenomenon was not observed with platelets in whole blood but only platelets in platelet rich plasma. The system utilized in this study eliminated the air-blood interface by priming the columns with normal saline prior to blood exposure. However, accumulation of cells at the saline-blood interface may occur. It is also reasonable to expect that initially platelets might be delayed in many different ways by the bead column accounting for observed bursts of platelets on the outflow side. Since this phenomenon was more consistently associated with albumin coated materials and not uncoated glass or polystyrene and usually affiliated with the first one or two milliliters of blood collected it may be that platelets can interact with surfaces in several ways. In the case of glass and polystyrene this interaction may be irreversible, that is adhesion occurs, but in prealbuminated surfaces platelets may interact with beads and are delayed on the surface until the shear from the blood flow washes them into the bulk and out of the column giving an apparent negative retention. Platelets could only adhere when small areas of the albumin coating desorbed or exchanged with native blood proteins such as fibrinogen and gamma globulin. Substrate materials having a greater affinity for adsorbed protein allowing little exchange of albumin with bulk protein would be more likely to maintain a negative or low ($< 5\%$) platelet retention.

Evaluation of platelet retention based on a theoretical model put forth by Robertson and Chang (27) suggests that retention is independent of both hemodynamic factors and column geometry. Evaluation of data from the present study using the method of Robertson et. al. revealed that platelet retention in this system does not follow their equations. Assumptions made in the derivation of their analysis simply do not hold in our study. They assume desorption of platelets to be negligible, that platelets adhere only as individuals not as aggregates, and that only a platelet monolayer is formed on the glass beads. Such assumptions are inconsistent with our experimental observations. Other investigators who have examined platelet retention as a function of time (20, 28-30) have reported that platelet retention increases with time in normal subjects. This is just the opposite of the findings of Robertson and Chang (27).

The albumin stability studies offer some insight into the potential usefulness of albuminated surfaces. The continued presence of pre-adsorbed albumin is not only dependent on the extraction media and albumin treatment, but also on the substrate material. In Table 1 it can be seen that although glass initially adsorbs almost 6 times more albumin than does polystyrene, the amount remaining after 24 hours of extraction in PBS is about twice that of polystyrene. Extraction in plasma is much more severe, as might be expected. The amount of adsorbed albumin remaining on glass and polystyrene is about the same when extracted in plasma. However, the crosslinked albumin is extracted at about the same rate in both PBS and plasma. The amount of albumin on the beads after crosslinking is much greater than either adsorbed albumin on glass or polystyrene.

Long term stability of immobilized proteins is important in areas other than blood compatibility including enzyme electrodes (31), detoxification (13, 15), hepatic assist, and others (16, 17). Efforts to understand and control protein surface chemistry are necessary before the potential of proteinated surfaces is functionally realized.

In terms of blood compatible protein surfaces there is some evidence to suggest that other macromolecules might be better than albumin (33). However, in terms of a model protein system for surface alteration albumin offers one major advantage in that it is one of the most well characterized and easily handled proteins available (34). The observation that platelet retention appears to correlate with the stability of the protein is currently under more intensive investigation. Platelet retention as a function of extraction time should provide

some idea of the sensitivity of the retention test and may also aid in defining storage and handling of albuminated surfaces.

Conclusions

Albumin is a useful tool in passivating normally thrombogenic surfaces which may contact blood. The ex vivo platelet retention test has been shown to be of value in characterizing different albuminated surfaces. The degree of retention has also been shown to be a function of flow rate, surface area, substrate nature, albumin source and purity, and exposure time. The tenacity of albumin for a surface is substrate dependent and for the two surfaces evaluated in this study the ex vivo platelet retention test has been discriminating.

Continued efforts to evaluate long term stability and correlate it with platelet retention are necessary to define storage and handling conditions. Future efforts to define sterilization procedures and possible effects of chronic exposure of blood to albuminated surfaces should be undertaken. The ex vivo platelet retention test should be expanded to include measurement of the platelet release reaction, sublethal damage to red cells, and changes in normal platelet aggregability resulting from the interaction of blood with different surfaces.

Various methods of immobilizing albumin on surfaces and the chemistry involved should be explored in greater detail. Crosslinking with glutaraldehyde decreases platelet retention but the mechanism of this observation remains speculative at present. It is felt that efforts to completely characterize albuminated surfaces to serve as a model system for other coatings of biological origin (proteins, carbohydrates, lipids, etc.) will lead to useful technology and applications in the medical arena.

References

1. R. E. Baier and R. C. Dutton, J. Biomed. Mater. Res. **3** 191 (1969).
2. W. J. Dillman and I. F. Miller, J. Colloid. Sci. **44** 221 (1973).
3. B. W. Morrissey in Behavior of Blood and its Components at Interfaces, L. Vroman and E. Leonard, Eds., Ann. N. Y. Acad. Sci. (1977) in press.
4. R. G. Lee, C. Adamson and S. W. Kim, Thromb. Res. **4** 485 (1974).
5. S. W. Kim, R. G. Lee, H. Oster, D. L. Coleman, J. D. Andrade, D. J. Lentz and D. Olsen, Trans. Amer. Soc. Artif. Int. Organs **20** 449 (1974).
6. G. Evans and J. F. Mustard, Surgery **64** 273 (1968).
7. C. S. P. Jenkins, M. A. Packham, M. A. Guccione and J. F. Mustard, J. Lab. and Clin. Med. **81** 280 (1973).
8. E. W. Salzman, J. Lindon, D. Brier and E. W. Merrill in Behavior of Blood and its Components at Interfaces, L. Vroman and E. Leonard, Eds., Ann. N. Y. Acad. Sci. (1977) in press.
9. R. M. Lindsay, C. R. M. Prentice, D. Ferguson, W. M. Muir and G. P. McNicol, Brit. J. Haemat. **24** 377 (1973).
10. D. J. Lyman, K. G. Klein, J. L. Brash and B. K. Fritzinger, Throm et. Diathesis Haemorrh. **23** 120 (1970).
11. W. H. Zucker, B. A. Shinoda and R. G. Mason, Amer. J. Path. **75** 139 (1974).
12. J. L. Brash and S. J. Whicher, Strathclyde Bioengineering Seminar, Preprints, Aug. 1976.
13. J. D. Andrade, D. L. Coleman, S. W. Kim and D. J. Lentz in Artificial Liver Support, R. S. Williams and I. M. Murray-Lyon, Eds., (pp. 84-93), Pittman Medical Publishers, (1975).
14. T. M. S. Chang and N. Malave, Trans. Amer. Soc. Artif. Int. Organs **16** 141 (1970).
15. T. M. S. Chang, Canad. J. Physiol. Pharmacol. **52** 275 (1974).
16. G. Broun, D. Tran-Minh, D. Thomas, D. Domurado and E. Selegny, Trans. Amer. Soc. Artif. Int. Organs **17** 341 (1971).

17. A. J. Landé, L. Edwards, J. H. Bloch, R. G. Carlson, V. Subramanian, R. S. Ascheim, S. Scheidt, S. Fillmore, T. Killip and C. W. Lillehei, Trans. Amer. Soc. Artif. Int. Organs **16** 352 (1970).
18. A. J. Hellem, Scandinav. J. Clin. Lab. Invest. **12** Suppl. 51 (1960).
19. J. R. O'Brien, J. Clin. Path. **14** 140 (1961).
20. E. W. Salzman, J. Lab. Clin. Med. **62** 724 (1963).
21. T. A. Carlson, Photoelectron and Auger Spectroscopy, Plenum Press (1975).
22. K. R. Porter, D. Kelley and P. M. Andrews in Proceedings of the Fifth Annual Stereoscan Colloquium, (pp. 1-19) Kent Cambridge Scientific, Inc., Chicago (1972).
23. G. K. Limber, C. H. Glenn and R. G. Mason, Thromb. Res. **5** 735 (1974).
24. J. L. Brash, S. Uniyal and Q. Samak, Trans. Amer. Soc. Artif. Int. Organs **20** 69 (1974).
25. J. F. Mustard, M. F. Glynn, E. E. Neshizawa and M. A. Packham, Fed. Proc. **26** 106 (1967).
26. H. L. Goldsmith, P. L. Rifkin and M. B. Zucker, Microvasc. Res. **9** 304 (1975).
27. C. R. Robertson and H. N. Chang, Ann. Biomed. Engng. **2** 361 (1974).
28. E. J. W. Bowie, C. A. Owen, J. H. Thompson and P. Didisheim, Amer. J. Clin. Path. **52** 69 (1969).
29. J. R. O'Brien and J. B. Heywood, J. Clin. Path. **20** 56 (1967).
30. B. N. Bouma, J. J. Sixma, S. deGraaf, Y. Wiegerinck, J. A. van Mourik and I. A. Mochtar, Brit. J. Haemat. **25** 645 (1973).
31. D. A. Gough and J. D. Andrade, Science **180** 380 (1975).
32. B. F. Scharschmidt, P. H. Plotz, P. D. Berk, J. G. Waggoner and J. Vergalla, J. Clin. Invest. **53** 786 (1974).
33. R. G. Mason, W. H. Zucker, B. A. Shinoda, H. Y. Chuang, H. S. Kingdon and H. G. Clark, Lab. Invest. **31** 143 (1974).
34. J. Janatová, J. Med. **5** 149 (1974).

ACKNOWLEDGEMENTS

This work was supported in part by U.S. ERDA Contract AT(11-1)2147 and more recently by NIH Grant HL18519-01. The assistance of K. Klauber and R. Ruff is gratefully acknowledged. We thank Dr. S. W. Kim for stimulating discussions.

Scanning Electron Microscopic Evaluation of the Surfaces of Artificial Hearts

Dennis Coleman, John Lawson and Willem J. Kolff

ABSTRACT

This report summarizes the surface changes seen in artificial hearts implanted in calves for periods up to four months. Fabrication defects as well as degradation resulting from wear are identified. SEM evaluation of the blood contacting surface as well as the surface of the diaphragm associated with the drive mechanism has revealed potential problems with current heart designs and methods of fabrication. Materials evaluation of implanted hearts is crucial for a clinically useful system to evolve.

artificial hearts, fabrication defects, degradation, SEM (Scanning Electron Microscope), blood contacting surface

INTRODUCTION

Calves with artificial hearts are now beginning to survive for several months: Kolff and associates, six months, several three months;¹ Nosé, five months;² Bücherl, four months; Pierce, two months;³ Akutsu, one month⁴ and Atsumi, two months (goats).⁵ This suggests that human trials may be warranted in the near future. With increased survival times, more emphasis is placed on the mechanical properties of materials and it is important to gain as much information as possible on the wear and possible degradation of artificial heart materials, especially the flexing diaphragms. Such degradation and/or wear may be the result of micro defects resulting from fabrication procedures, absorption of physiological constituents such as lipids by the material, calcium

deposition, abrasion, etc. Use of the scanning electron microscope for this purpose is reported herein.

While not inclusive of all the evaluation required or indicated, the SEM evaluation does supply information at a level in which other testing and evaluation may be indicated. Early detection of the beginning of wear problems and their subsequent correction will improve the reliability of future artificial hearts for implantation in humans.

Pathological evaluation of implant materials, not only in the classical sense of studying tissues affected by implant materials but also studying the nature of the implant, must be done before cause and effect relationships are clearly defined. By studying the "intima" of artificial hearts with the SEM, we hope to recognize the beginning of wear, factors that induce thrombus formation and other conditions which may cause device failure.

Improvements in the design of artificial hearts have provided satisfactory results with various non-fibril surfaces,⁶ mostly polyurethane, Avcothane® and even Silastic®. Yet complete freedom from thromboembolism has not been achieved. It should be remembered that the design of the artificial heart and the use of artificial valves may lead to thromboembolism for which the ventricle material is not the cause.⁷

MATERIALS AND METHODS

This study provides qualitative information, by means of scanning electron microscopy, on artificial heart diaphragms from two heart designs (Jarvik III and ERDA) made from three materials, Biomer® (Ethicon Inc., Somerville, N. J.), Avcothane® (Avco Medical Products, Everett, Mass.) and Silastic® (Dow Corning, Midland, Mich.) with a polyester fibril surface. Implant times ranged from 69 hours up to 122 days (Table).

All hearts for scanning microscopy were treated at autopsy by rinsing the inside of the right ventricle with physiological saline. The heart was disassembled while in saline and the pumping diaphragm removed. Sections of the diaphragm which contact blood were placed in 2% phosphate buffered glutaraldehyde, pH 7.2, for preservation of any blood elements which

From the Division of Artificial Organs, Department of Surgery, College of Medicine, the Institute for Biomedical Engineering, College of Engineering, University of Utah, Salt Lake City, Utah, 84112.

Supported in part by the NIH via the National Heart and Lung Institute, Grant #5-PO1-HL-13738-07, ERDA Contract #EY-76-S-0202155-A001 and by the Development Fund of the Division of Artificial Organs to which contributions have been made by many including: Ethicon, the Sandoz Foundation, Benjamin Matthews, Lawrence Harvey and the Skaggs Foundation.

The work reported in this paper is the result of the combined efforts of many people. A special thanks to Dr. Joseph Andrade, Mr. Lee Smith, Mr. James McRea, Mr. Thomas Kessler and Ms. Connie Schumann.

TABLE
CALVES EVALUATED

Calf	Heart		Survival time	Anticoagulant Therapy
	Design	Material		
ERDA 23	ERDA	Silastic® with fibrils	69 hours	no
Burk	Jarvik III	Biomer®	94 days	no
James Bond	Jarvik III	Biomer®	46 days	yes
NASA-Tu	Jarvik III	Avcothane®	64 days	yes
Mohammad	Jarvik III	Biomer®	10 days	no
ERDA 17	ERDA	Avcothane®	11 days	no
AOPA	Jarvik III	Avcothane®	122 days	yes

might have been present. Other components of the diaphragm, the polyester mesh and the air contacting portion, were not exposed to any fluids and were stored dry for mounting on SEM stubs. The blood exposed surfaces were dehydrated with absolute ethanol and critical point dried with liquid carbon dioxide.⁸ The samples were mounted on stubs and coated with carbon and gold by vapor deposition. Samples for SEM were selected from areas of the diaphragm suspected, from macroscopic examination, to have imperfections. If such areas were not evident, samples were then selected at random.

Air driven hearts have a pumping diaphragm that consists of three separate layers: one layer of polyurethane facing the blood, a layer of polyester mesh and a layer of polyurethane facing the air chamber (Fig. 1). Both sides of the blood contacting and air contacting portions of the diaphragm were examined as well as the reinforcing mesh.

ERDA (Energy Research and Development Administration) hearts are driven by a mechanical pusher-cup over which a rolling diaphragm is draped.⁹ The majority of ERDA hearts are fabricated from silicone rubber since fabrication is easier and, as yet, long survivals are not expected from this type of heart. Polyester fibrils have occasionally been used to cover the surface of the Silastic® hearts.

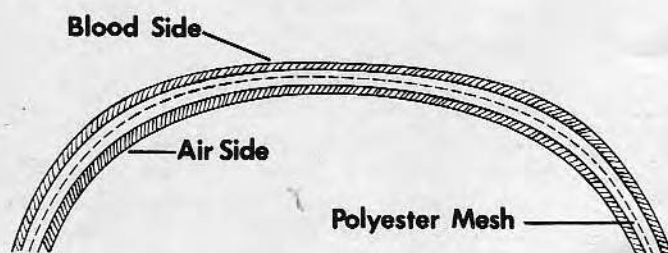


FIG. 1. A diagrammatic cross section of the pumping diaphragm of the Jarvik III artificial heart design. This type of design is used with polyurethane materials and is air driven.

RESULTS

Silastic

Polyester fibril-coated Silastic® hearts have not been successful in this laboratory, though others have utilized fibril surfaces successfully.¹⁰ The fibrils have come off the surface and have been seen in histologic sections of kidney, lung, brain and other vital organs.¹¹ Direct observation of the pumping diaphragm of ERDA 23 (Fig. 2) reveals areas devoid of fibrils with only the imprint of the fibril left in the surface. ERDA 23 lived only 69 hours and was not treated with anticoagulants. Histopathology demonstrated multiple small infarcts in the liver and kidneys, although no gross emboli were seen. Fibrils are no longer used by this group to coat heart surfaces.

The pusher-cup side of the ERDA 23 diaphragm was filled with sperm oil as a coolant. These chambers were initially overpressurized when filled with

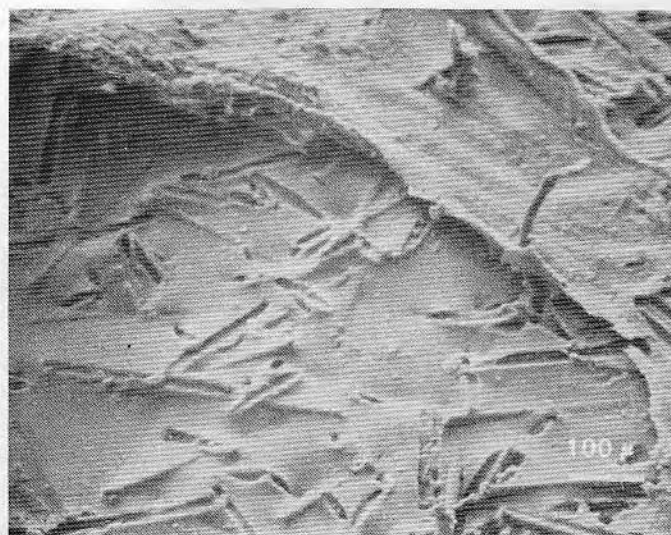


FIG. 2. The blood contacting surface, as seen by SEM, of a polyester fibril-coated silicone rubber heart which was implanted for 69 hours (ERDA 23). Note the loss of fibrils from the surface. Anticoagulant therapy was not used. Magnification 100X.

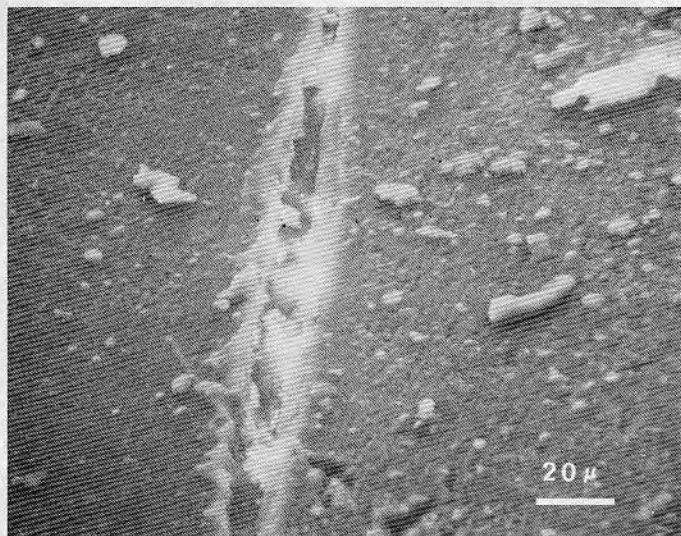


FIG. 3. A fracture in the diaphragm (ERDA 23) on the pusher-cup side resulted from overpressurizing the heart while filling with a coolant (sperm oil). The crack had not completely penetrated the diaphragm. Magnification 500X.

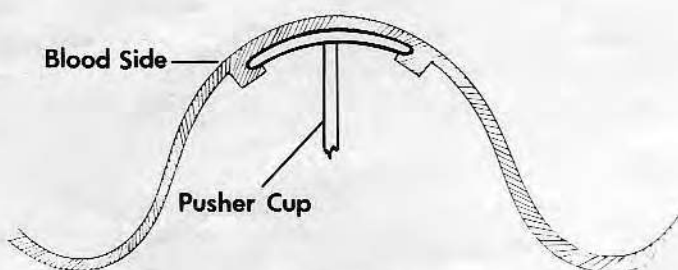


FIG. 4. A cross section of the diaphragm used in the ERDA designed heart. Silicone rubber or polyurethane is used for construction purposes. This heart is mechanically driven by a pusher-cup.

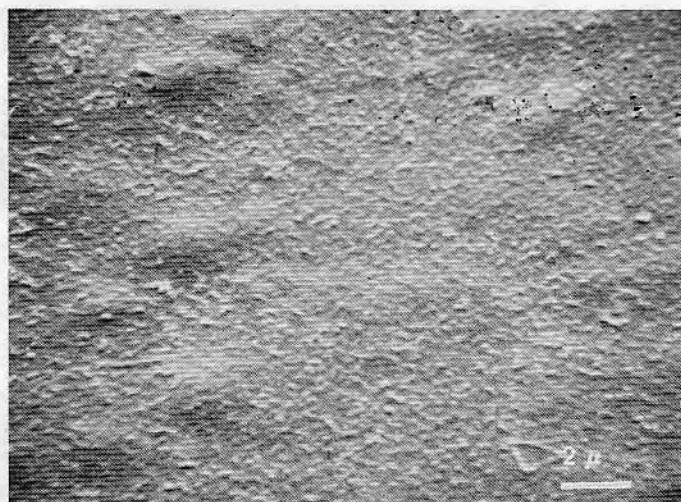


FIG. 5. A SEM of the blood contacting surface of a Biomer® heart after 94 days implantation (Burk). Anticoagulant therapy was not used, yet the surface is remarkably thrombus free. The surface appears to have adsorbed a fine layer from the blood. Magnification 4800X.

oil and the stress of this technical error is seen in Fig. 3. A fracture, which does not completely penetrate, in the Silastic® diaphragm is observed where the ridge holding the diaphragm to the pusher-cup joins the diaphragm (Fig. 4).

Polyurethane

In this laboratory, the greatest success has been with polyurethane (Biomer®) and a blend of polyurethane and Silastic® (Avcothane®-51 elastomer).

Blood contacting surface

The first long-term survivor was a calf named Burk, which lived 94 days with a Biomer®, air driven, Jarvik III type of heart. The diaphragm from the right ventricle was remarkably free of formed blood elements and fibrin deposition even though no anti-coagulants were used (Fig. 5). There was, however, some indication of an adsorbed film, possibly protein, on the surface of this diaphragm. There were a few infarcts in the kidneys and there was thrombus formation on the rings of the heart valve.

A Biomer® Jarvik III type heart was implanted in a calf named James Bond which survived 46 days and was treated with warfarin, dipyridamole and aspirin.¹² Unlike Burk, numerous surface defects were observed on the diaphragm (Fig. 6) along with well organized thrombi. Although thrombus formation is occasionally associated with surface irregularities (Fig. 7), it is also likely that these defects act as emboli generators. Since thrombus-free areas are populated with surface defects, such defects appear to be the result of microbubbles trapped in the polymer surface during fabrication of the heart.

Like James Bond's, the artificial heart of the calf named NASA-Tu (Fig. 8) revealed areas of organized fibrin deposition on the diaphragm surface even though a warfarin, dipyridamole and aspirin regimen¹² was used. This heart was fabricated from Avcothane® and the calf survived 64 days with the Jarvik III type heart. Surface defects were not seen on the sections chosen for microscopic evaluation.

Mohammad survived only ten days with a Jarvik III Biomer® heart. Like James Bond's, this heart showed a pitted surface with thrombi frequently adherent to the surface defects. This animal was not treated with anticoagulants and had multiple small infarctions at autopsy.

In contrast to the Jarvik III design, the two ERDA type Avcothane® hearts subjected to SEM evaluation demonstrated fibrin and thrombus deposition especially where the diaphragm flexes. ERDA 17 survived eleven days with no anticoagulant therapy.

AOPA represented the summum bonum of what had been attained at the time of this study: more than four months survival. In contrast to Burk (three

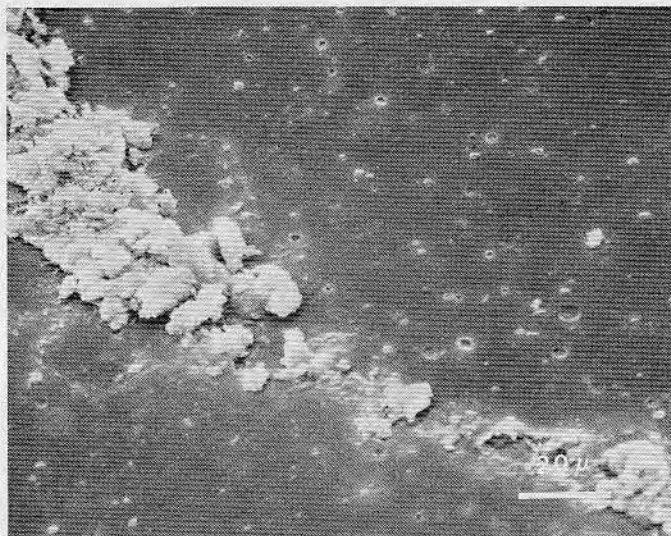


FIG. 6. The blood exposed side of a Biomer® heart which pumped 46 days in James Bond. Anticoagulant therapy was used. Numerous surface defects can be seen in an area where thrombus formation is evident. Magnification 600X.

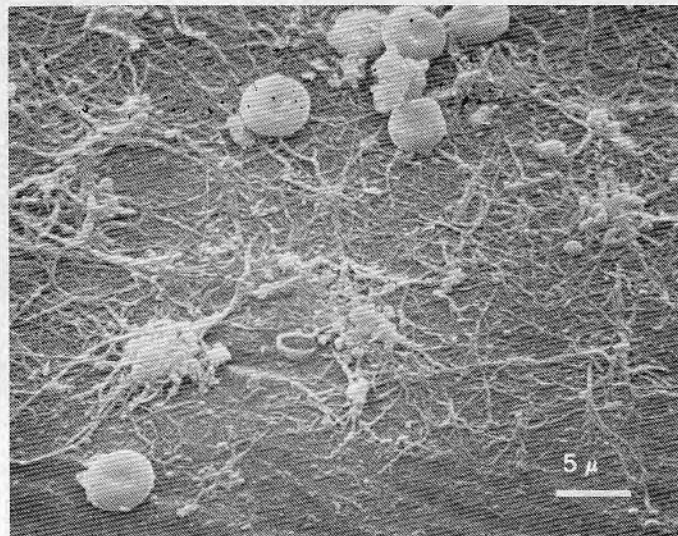


FIG. 8. An Avcothane® heart surviving 64 days (NASA-Tu) also revealed areas of fibrin deposition even though anticoagulant therapy was initiated. Magnification 2000X.

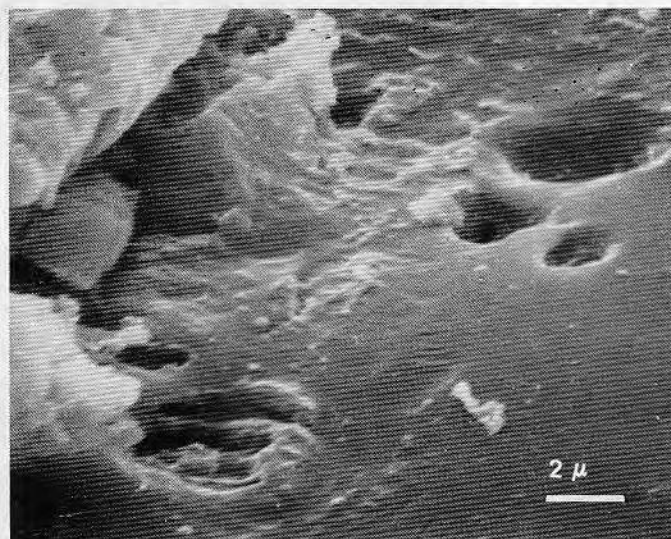


FIG. 7. At a higher magnification, the thrombus in Figure 6 is clearly seen to be associated with surface irregularities. Magnification 5000X.

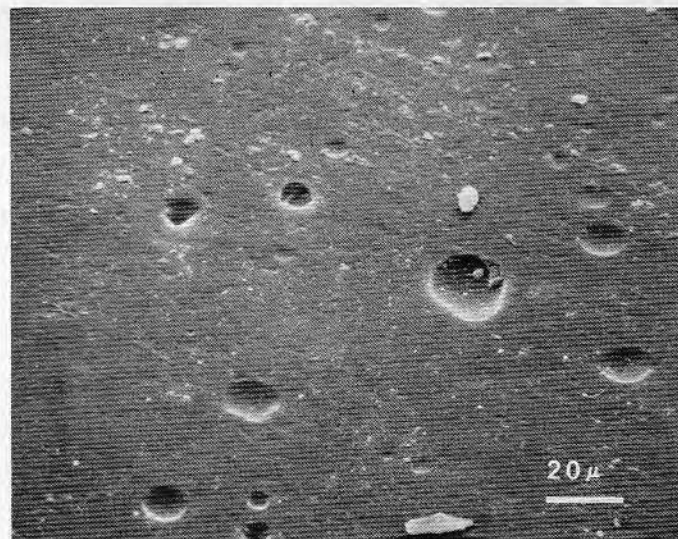


FIG. 9. Surface defects in this Avcothane® heart which pumped 122 days (AOPA) are surprisingly free of thrombus and formed blood elements. Anticoagulant therapy was used in this animal. Magnification 500X.

months), warfarin, dipyridamole and aspirin¹² were used to chronically anticoagulate the animal. AOPA had a Jarvik III type of artificial heart made of Avcothane®. A new surgical technique¹³ developed to eliminate synthetic heart valves allowed retention of the animal's aortic and pulmonary artery valves. After 122 days, the diaphragm from this heart was free of formed blood elements even though many surface defects ranging in size from 2 to 20 microns could be seen (Fig. 9). A sample taken from the center of the

diaphragm revealed a thin protein-like layer (Fig. 10). At postmortem, AOPA showed emboli only in the lungs with no evidence of multiple small emboli. There was no coagulopathy which indicates that there was no large consumption of clotting factors.

Diaphragm facing the mesh

Wear resulting from rubbing of the polyurethane against the polyester mesh appears to be a potential problem with the Jarvik III type of heart, even though this heart has performed well for over a year

on mock circulation testing. This problem is dramatically demonstrated in Fig. 11, a scanning electron micrograph of the diaphragm of Burk which pumped for 94 days. Samples from unpumped hearts are extremely smooth at the same magnification (4500X).

This type of wear contributed to failure of the restraining polyester mesh in James Bond (46 days). Wear particles penetrated the strands of the mesh ultimately leading to fracture of the fibers making up the strand (Fig. 12). The uniformly abraded surface seen in Fig. 11 has frequently been seen in other hearts constructed of Biomer®.

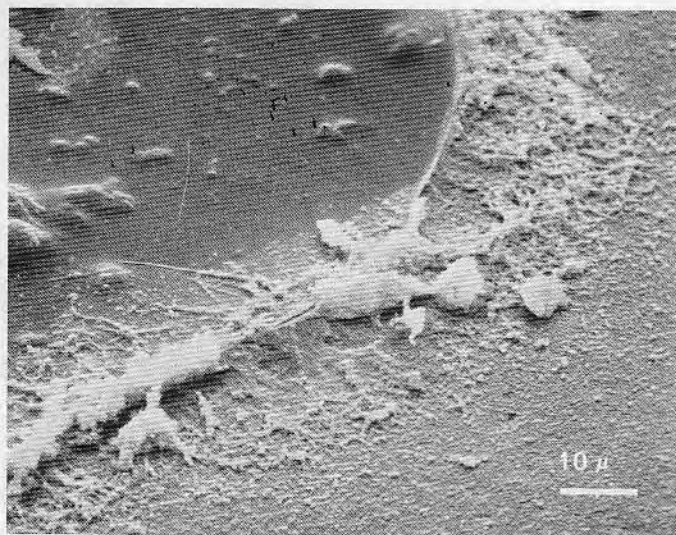


FIG. 10. A sample taken from the center of the diaphragm shown in Figure 9 revealed a thin protein-like layer adsorbed to the surface. Magnification 1000X.

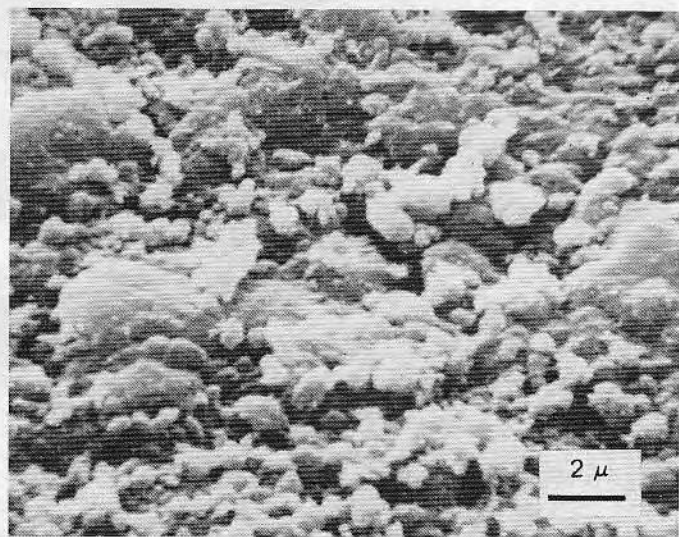


FIG. 11. The polyester mesh used in the Jarvik III design has abraded the pumping diaphragm of a Biomer® heart implanted for 94 days (Burk). Magnification 4500X.

Avcothane® hearts do not show the same kind of abrasion as the Biomer® hearts. Wear effects of the mesh on Avcothane® appear to be the result of knots in the mesh (Fig. 13) taken from NASA-Tu (64 days). However, this effect was not seen in the heart from AOPA which pumped for 122 days (Fig. 14).

The ERDA design avoids the problem of abrasive wear seen in the Jarvik III type of heart. Fabrication defects have been observed (Fig. 15) in the pusher-cup side of several ERDA diaphragms. The potential hazard for diaphragm failure from such defects remains to be clarified.

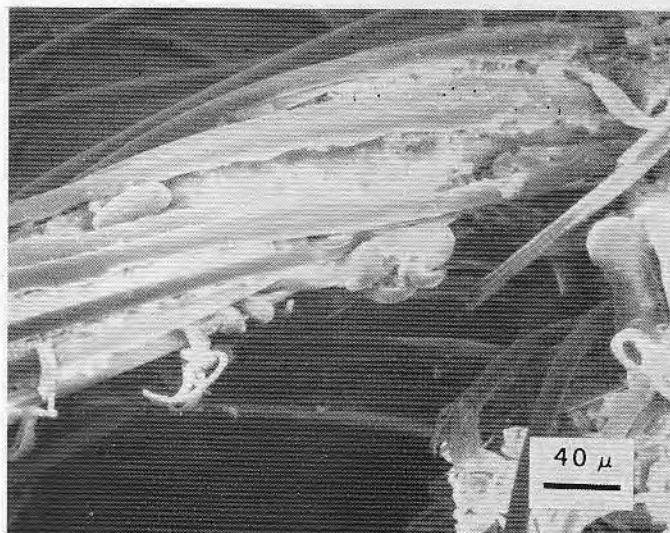


FIG. 12. Failure of the polyester mesh as a result of penetration of polyurethane wear particles is evident in this sample after 46 days of pumping (James Bond). Magnification 220X.

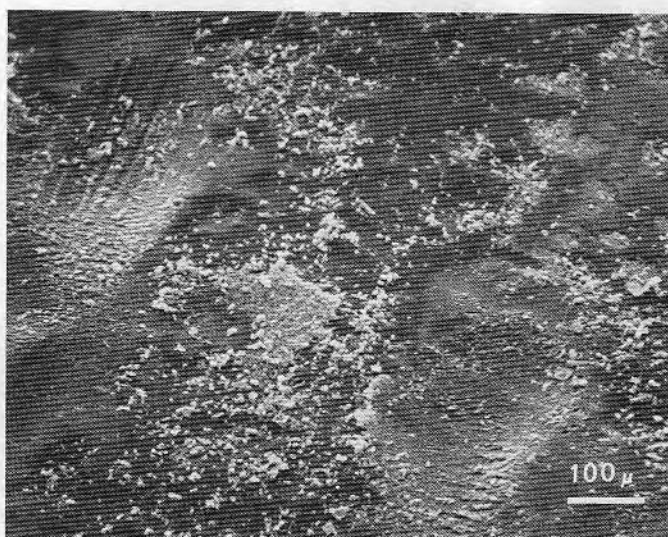


FIG. 13. Wear effects on Avcothane®, even after 64 days (NASA-Tu), do not appear to be as generalized as with Biomer® (Fig. 12). Wear is apparent where the knots in the polyester mesh contacted the surface. Magnification 100X.

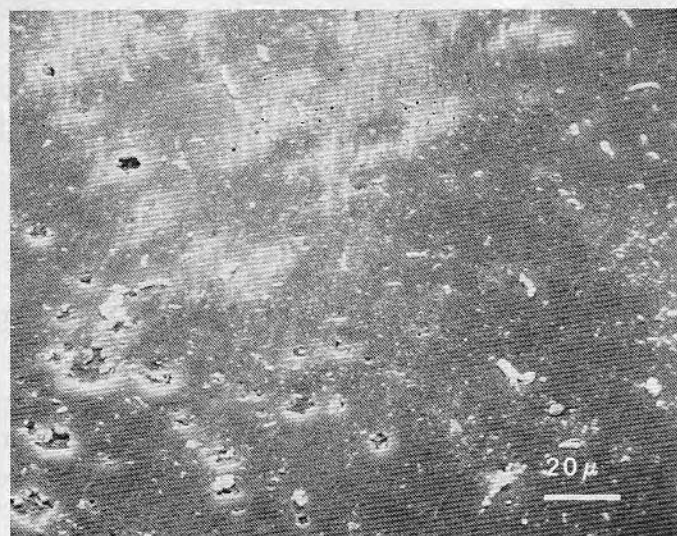


FIG. 14. Minimal wear was observed in an Avcothane® heart surviving 122 days (AOPA). Magnification 500X.

CONCLUSIONS

There is enough evidence that the polyester mesh causes damage to the polyurethane diaphragms to come to the conclusion that the mesh should be avoided in the future. Small surface defects created during fabrication are not always avoidable. As a rule, our blood facing surface is air dried during fabrication, whereas the surface of the membrane away from the blood is cured against the mold and may, therefore, have imprints of irregularities on the mold. Small irregularities on the blood side diaphragm can sometimes be seen in areas where blood elements have been adherent, which indicates that either some adherent thrombus has come off or that it has been bare all the time. One would hope that the amount of thrombus formed on these surfaces would be so small that it could be routinely processed by the body. It is significant that Burk, who lived three months without anticoagulants, revealed only minor signs of thromboembolism and AOPA, who lived 122 days, showed less than Burk. Moreover, there were no overt changes in platelet count, platelet adhesion, total fibrinogen, prothrombin time and partial thromboplastin time which could not be accounted for by the anticoagulant therapy. Fibrin degradation products, as measured by the protamine sulfate dilution method, returned to normal two weeks post-implantation.

Fibril-coated hearts have consistently released fibril emboli which have been discovered in the vital organs of the animals. For this reason, non-fibril surfaces are preferred and have been more successful in this laboratory. SEM evaluation of hearts to date has not revealed any consistent discernable differ-

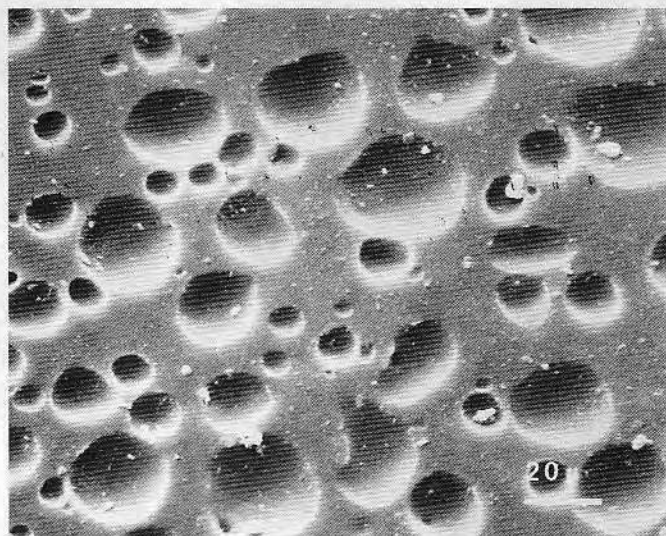


FIG. 15. Fabrication defects on the pusher-cup side of the ERDA type of heart are frequently seen (ERDA-17). Potential problems from such defects remain to be clarified. Magnification 500X.

ence in the blood contacting surface of Avcothane® or Biomer® hearts, nor has it been possible to clearly distinguish between animals treated with anticoagulants or left untreated in terms of microscopic deposits on the surface of the diaphragm.

The hearts from animals that had survived for a long time do not show more significant changes than those from animals that died early in the experiment. Anticoagulation is usually not started until 48 hours after surgery for fear that hemorrhages may occur in the chest. It is during the first hours following surgery, when the heparin is neutralized, that one might expect the thrombotic process to begin. For this reason, we are looking for any method that will give relief from the initial thrombus formation seen in the first days following implantation of the artificial heart. It may be that the heparin binding method of Schmer,¹⁴ which allows release of heparin for several weeks, has something to offer the artificial heart system.

Another possibility is the use of glutaraldehyde crosslinked albumin^{15,16} to treat the inside of the artificial heart cavities. It is unlikely that the albumin will remain for extended periods of time, but it might offer protection during the first days of pumping.

An artificial heart which has been implanted and pumping for some period of time is a valuable source of information relating to interface-induced thrombosis and coagulation, lipid or other sorption, wear or degradation of the material and changes in the physical and mechanical properties of the heart material. Continued efforts to provide feedback information to designers, fabricators and surgeons must improve artificial hearts for future human use.

References

1. LAWSON, J. H., OLSEN, D. B., KOLFF, W. J., LIU, W. S., HERSHGOLD, E. J., VAN KAMPEN, K. A three month survival of a calf with an artificial heart. *J Lab Clin Med*, 87:848, 1976.
2. TSUSHIMA, N., KASAI, S., KOSHINO, I., JACOBS, G., MORINAGA, N., WASHIZU, T., KIRALY, R., NOSE, Y. 145 days survival of calf with total artificial heart. *ASAIO Abst*, 6:91, 1977.
3. LANDIS, D. L., PIERCE, W. S., ROSENBERG, G. R., DONACHY, J. H., BRIGHTON, J. A. Long term *in vivo* automatic electronic control of the artificial heart. *ASAIO Abst*, 6:48, 1977.
4. HONDA, T., KITO, Y., GIBSON, W. H., COCKRELL, J. V., AKUTSU, T. Circulatory pathophysiologic manifestations in two long surviving calves with total artificial hearts. *Cardiovasc Dis*, 2:285, 1975.
5. ATSUMI, K., FUJIMASA, I., IMACHI, K., NISHISAKA, T., OHMACHI, H., IWAI, N., KOUNO, A. Pathophysiological analysis on the long survivals with total artificial heart replacement. *ASAIO Abst*, 6:5, 1977.
6. LAWSON, J. H., OLSEN, D. B., HERSHGOLD, E., KOLFF, J., HADFIELD, C., KOLFF, W. J. A comparison of polyurethane and Silastic® artificial hearts in 10 long survival experiments in calves. *Trans Am Soc Artif Intern Organs*, 21:368, 1975.
7. KOLFF, W. J., STELLWAG, F. Blood at artificial organ surfaces: progress to date as stepping-stones for the future. *Ann NY Acad Sci*, 283:443, 1977.
8. PORTER, K. R., KELLY, D., ANDREWS, P. M. The preparation of cultured cells and soft tissue for SEM. *Proc Fifth Ann Stereoscan Coll*, Kent Cambridge Scientific Company, Morton Grove, Illinois, p. 1, 1972.
9. SMITH, L., BACKMAN, K., SANDQUIST, G., KOLFF, W. J., SCHATTEN, K., KESSLER, T. Development on the implantation of a total nuclear powered artificial heart system. *Trans Am Soc Artif Intern Organs*, 20:732, 1974.
10. LAFARGE, C. G., POIRIER, V., BORNHORST, W., BERNHARD, W. F. An implantable power system for chronic left ventricular bypass. *Trans Am Soc Artif Intern Organs*, 20:725, 1974.
11. OLSEN, D., VAN KAMPEN, K., VOLDER, J., KOLFF, W. J. Pulmonary hepatic and renal pathology associated with an artificial heart. *Trans Am Soc Artif Intern Organs* 19:578, 1973.
12. MANSFIELD, P. B., WECHZAK, A. R., SAUVAGE, L. R. Preventing thrombus on artificial vascular surfaces: true endothelial cell linings. *Trans Am Soc Artif Intern Organs*, 21:264, 1975.
13. OLSEN, D. B., KOLFF, J., LAWSON, J., STELLWAG, F., CECCARELLI, V., FUKUMASU, H., KOLFF, W. J. Saving the aortic and pulmonary artery valves with total heart replacement. *Trans Am Soc Artif Intern Organs*, 22:418, 1976.
14. SCHMER, G. The biological activity of covalently immobilized heparin. *Trans Am Soc Artif Intern Organs*, 18:321, 1972.
15. GUIDOIN, R. G., AWAD, J., BRASSARD, A. Blood compatibility of silicone rubber chemically coated with cross-linked albumin. *Biomater Med Dev Artif Organs*, 4:205, 1976.
16. COLEMAN, D. L., ATWOOD, A. I., ANDRADE, J. D. Platelet retention by albuminated glass and polystyrene beads. *J Bioeng*, 1:33, 1976.

CALCIFICATION OF NONTEXTURED IMPLANTABLE BLOOD PUMPS

D. L. Coleman, D. Lim, T. Kessler, and J. D. Andrade

Improvements in surgical techniques, implant design and fabrication, and the materials used to construct blood pumps have greatly contributed to the increased longevity of animals implanted with total artificial hearts¹. However, with this increase in survival time, new problems and unanswered questions have become apparent. Degradative changes in the bulk and surface properties of long-term mechanically active polymers have been suggested² to account for diminished function or complete failure of the device.

Calcification of the pumping diaphragm has been reported by numerous groups including Nosé et al³, Kolff et al⁴, Pierce et al⁵, Norman et al⁶, Lian Levy⁷, and Hennig et al⁸. Since calcification has not been reported in adult goats implanted for long periods⁹ but has been seen in calves³⁻⁸, there has been some speculation that species and/or age is a predisposing factor¹⁰.

This report reviews the evidence accumulated from total artificial hearts implanted in 33 calves and 2 sheep surviving from 30 days to 268 days. Observations made in this study support the hypothesis that surface defects serve as a nidus for mineralization and that this process is accelerated by, but not totally dependent on, mechanical stress or shear stress.

MATERIALS AND METHODS

Total Artificial Hearts. Two heart designs, the Jarvik 5¹¹ and Jarvik 7¹, were fabricated from either Avcothane 51[®] or Biomer[®] and implanted in calves for variable time periods up to 268 days. Upon termination of the experiment the ventricles were rinsed with normal saline and either the right or left ventricle submitted for more extensive examination¹². A summary of these experiments is given in Table I.

The amount or severity of mineralization was qualitatively graded from 0 to 5 according to the following criteria: 0, no calcium detected at the SEM level 1000 X magnification; \pm , rare (one plaque/10 fields examined); 1+, "sandpaper" appearance under the stereomicroscope using Alizarin red S; 2+, localized areas < 1 cm² and < 2 mm thick; 3+, patchy areas > 2 mm thick covering < 25% of the surface area of the diaphragm; 4+, patchy areas > 2 mm thick covering < 50% of the pumping diaphragm; 5+, > 50% of the blood contacting area calcified.

TABLE I. SUMMARY OF THE HEARTS SUBMITTED FOR AUTOPSY

Heart Design	Material		Anticoagulant Therapy*					% with Detectable Calcification
	Biomer	Avcothane 51	None	PCA	CA	PA	C	
Jarvik 5 (# of Animals)	19	7	9	11	1	2	3	77% (20/26)
Jarvik 7 (# of Animals)	7 ⁺	2	2	2	2	1	2	78% (7/9)
Median Survival Time (days)	75.5	86	74	64	124	142	111	
Range (days)	35-268	40-210	36-210	35-184	35-221	63-268	35-217	
Detectable Calcification (Percent)	77	67	82	54	100	100	60	
Calcification Grade [#] (mean \pm SD)	1.1 \pm 1.15	1.0 \pm 1.09	1.1 \pm 0.74	0.7 \pm 0.83	0.8 \pm 0.29	3.0 \pm 1.7	1.0 \pm 1.22	

*Persantine, Coumadin, Aspirin

⁺2 Sheep

[#]See text for description.

Anticoagulation. Various combinations of Persantine (dipyridamole), Coumadin, and aspirin were administered in daily doses, 200 mg, 5-10 mg, and 10 grains, respectively. Eleven animals, 9 calves and 2 sheep, did not receive any anticoagulants. Thirteen calves were given a daily dose of Persantine, Coumadin and aspirin; Coumadin and aspirin were given to 3 calves; Persantine and aspirin were given to 3 animals; and Coumadin

From the Division of Artificial Organs, Departments of Bioengineering and Pharmaceutics, University of Utah, Salt Lake City, Utah.
Supported by NIH Grant HL 13738.

alone was administered to 5 calves. A summary of the median survival times for each anticoagulation therapy is given in Table I.

Microscopic Analysis. The entire pumping diaphragm and housing was examined under a stereomicroscope to aid in identifying possible area of early calcification. These areas were stained with von Kossa's stain or Alizarin red S to identify calcium deposits¹³. Some of the diaphragms were embedded in epoxy and cross sections cut with a low speed diamond saw as previously described¹⁴. The cross sections were examined by optical and scanning electron microscopy coupled with x-ray microanalysis.

Energy Dispersive Analysis of X-Rays (EDAX). Selected areas of the pumping diaphragm were critical point dried using CO₂ substitution¹⁵, and coated with carbon and chromium using a standard vapor deposition technique. Elemental maps for calcium were generated for visual identification of local calcium deposits. Identification of subsurface calcium deposits was accomplished by varying the accelerating voltage of the primary electron beam.

Chemical and Biochemical Analyses. Calcified deposits on most heart samples were not extensive enough for normal chemical and biochemical techniques. However, a 268 days animal (TH80 C12) did have severe calcification which allowed for a more extensive analysis.

A sample of this diaphragm was evaluated for osteocalcin levels by Dr. Jane Lian (Children's Hospital Medical Center, Boston, MA) using a radioimmunoassay technique¹⁶. This technique has also been reported by Price and Nishimoto¹⁷ to identify vitamin K-dependent protein of bone in bovine plasma.

Deposits from TH80 C12 were also sent to Galbraith Laboratories, Inc. (Knoxville, TN) for microanalyses to determine the atomic percent of nitrogen, phosphorus, sulfur, calcium and carbonate (CO₃).

Removal of the deposits in 10% w/v ethylenediaminetetra-acetic acid (EDTA) followed by 1% sodium dodecylsulfate (SDS) was not completely effective at removing all of the material. Treatment with 5% HCl and 1% trichloroacetic acid for 24 hrs was more effective at removing deposits from the pumping diaphragm.

Thin-layer chromatography of deposits extracted in chloroform:methanol (2:1) was performed using a solvent developing system of hexane:ether:acetic acid (85:15:1).

RESULTS

Gross Observations. It was apparent in reviewing the location of the mineralized areas that permanent set creases and fiber contaminants were associated with the heaviest mineral deposits. In the case of fiber-associated calcification, a small local thrombus was usually firmly attached to the fiber. Mineralization was clearly localized to fiber contaminants and associated with the thrombus. The solution to eliminating this type of calcification is obvious and will not be further discussed.

A second type of calcification was seen along creases. These deposits were not necessarily associated with thrombotic material, were heaviest along the crease, and frequently resulted in failure of the blood diaphragm due to a small hole or holes worn in the material. On closer macroscopic examination, especially near the margins of the mineral deposits, an apparent orientation of the deposits at right angles to the crease could be seen (Figure 1). Removal of these deposits with trichloroacetic acid reveal what appear to be small surface cracks at right angles to the crease (Figure 2).

A third type of calcium pattern consisted of a more general type of mineralization that was not easily detected without the aid of a microscope. Macroscopically, the deposits appeared as small plaques on the surface of the pumping diaphragm giving a "sandpaper" feel to the blood-contacting surface. Thrombus was generally not seen in areas where this type of mineralization was occurring.

Evaluation of the degree of calcification and the percent of animals with detectable calcium phosphate is summarized in Table I. It appears that Coumadin treated animals may have a slightly decreased amount of mineralization. However, increased numbers are required to confirm these data, and it is clear that calcification will eventually occur in these animals.

Microscopic and X-Ray Microanalysis. In the case of type 2 calcification removal of deposits with trichloroacetic acid did reveal microscopic cracks (Figure 2) in the diaphragm where deposits had been. Abrasive wear was also evident in areas of heavier deposits. Abrasive wear on the housing has been observed when diaphragm deposits had grown thick enough to contact the housing during systole.

Type 3 calcium deposition was usually a more general phenomenon. Cross sections of the diaphragm examined under the scanning electron microscope (SEM) suggests that deposits are associated with microbubble defects in the blood contacting surface. Figure 3 is a calcium x-ray map of a secondary image of a diaphragm cross section. A surface irregularity is associated with the calcium deposit. En face examination demonstrates microbubble defects in an area of numerous calcium plaques (Figure 4). Some of the plaques still have a small hole in the center suggesting that microbubbles acted as a nidus for the calcium phosphate deposition. This was also seen in a small area of a heart implanted in a sheep surviving 77 days (Figure 5A and 5B).

Until recently these deposits had not been seen on the housing of the ventricles even though microbubbles could be detected. However, a ventricle implanted 268 days in a calf did show this same pattern of deposition on

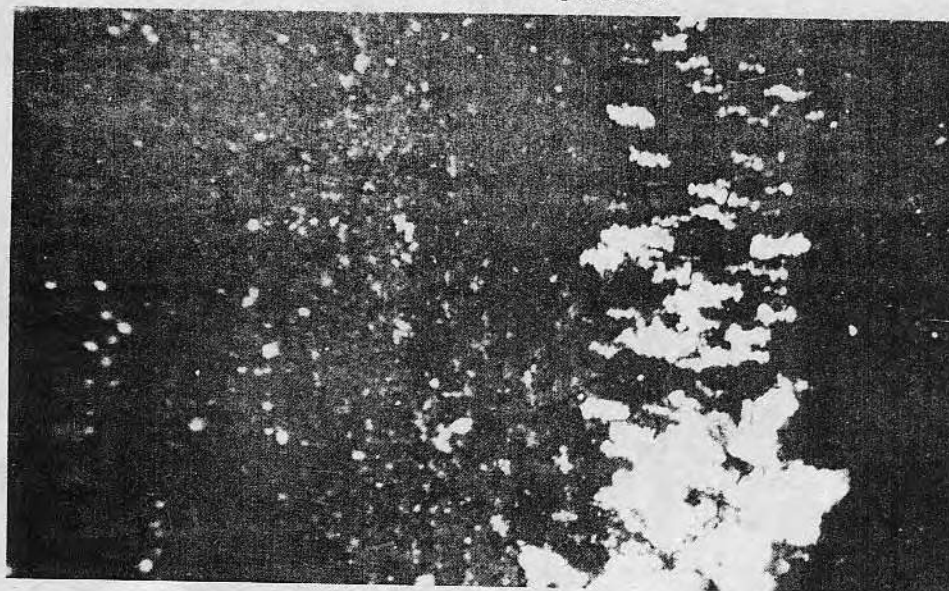


Figure 1. Calcified areas on a pumping diaphragm of a total artificial heart implanted for 104 days in a calf. Original magnification 15X.

Figure 2. After treatment with 10% trichloroacetic acid the calcium deposits have been removed from Figure 1 revealing small cracks underneath the deposits and numerous microbubble defects. Original magnification 500X.

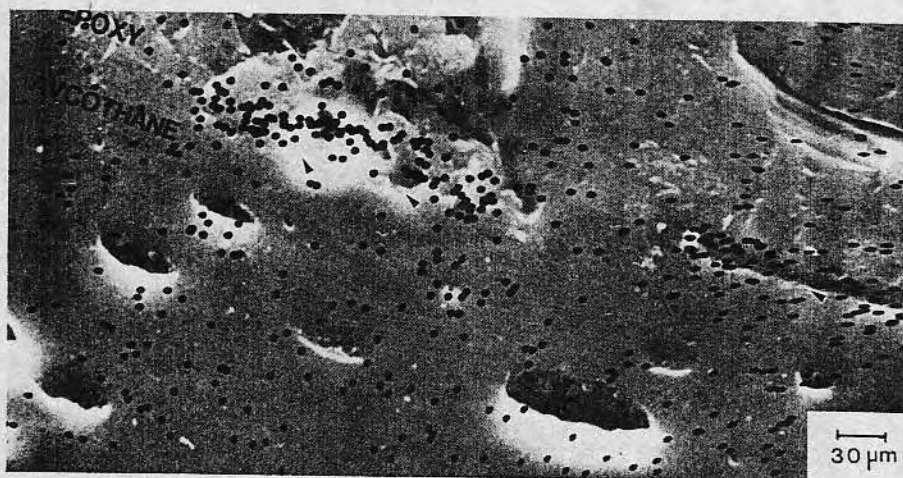
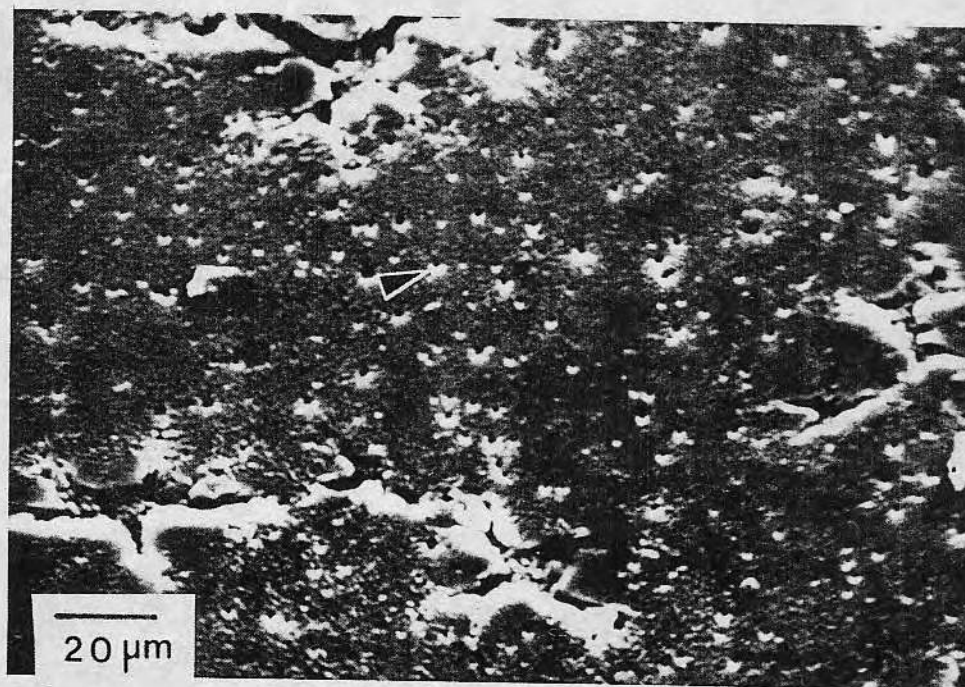


Figure 3. A calcium map of a cross section of a diaphragm implanted 184 days. Note surface irregularities associated with concentrated calcium areas (arrows).

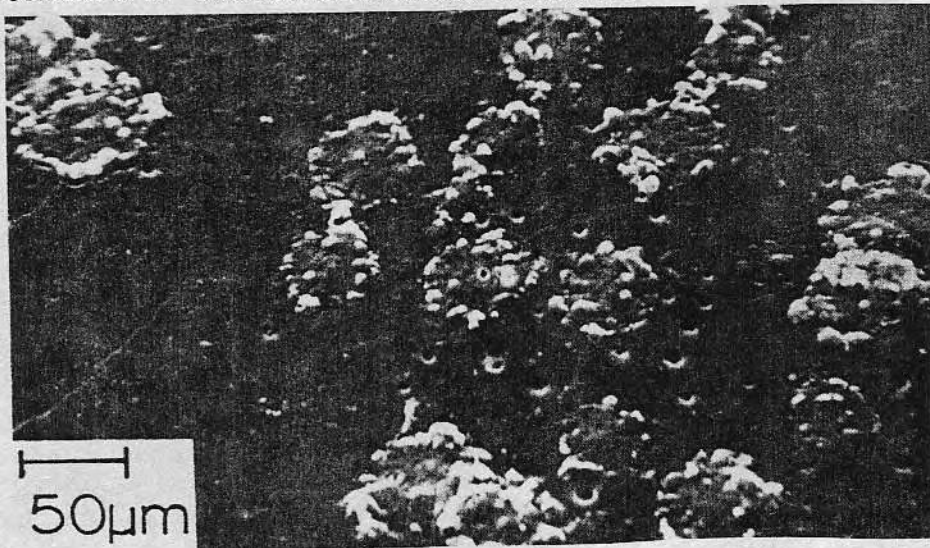


Figure 4. Microbubble defects are a common feature of type 3 calcium deposition. Occasionally a hole can still be seen in the center of a developing plaque (arrow).

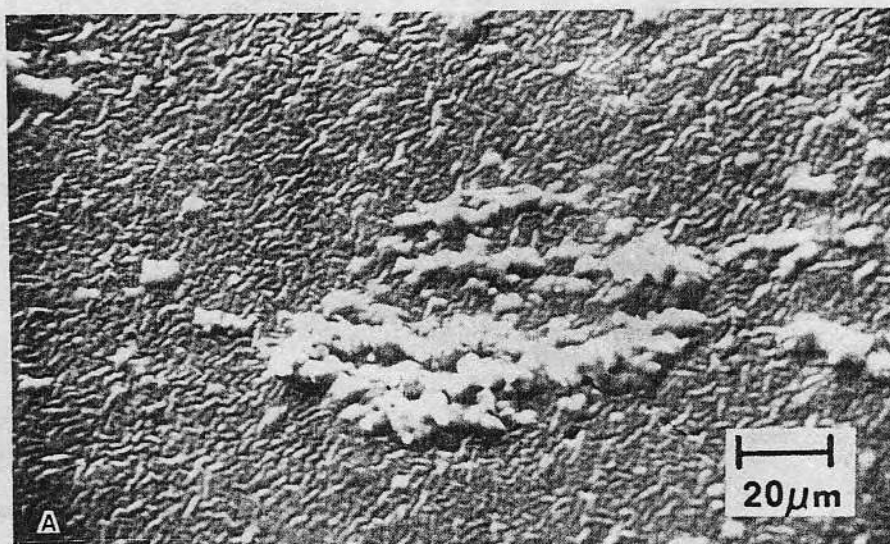


Figure 5. Type 3 calcification is also apparent on the pumping diaphragm of a heart implanted for 77 days in a sheep (A). A calcium EDAX map confirms the localization of the deposits (B).

the housing. Subsequent SEM/EDAX did demonstrate that the calcium accumulation could be detected subsurface in microbubble defects (Figure 6A). Reduction of the accelerating voltage of the primary electron beam from 20 KEV to 10 KEV gave the same chromium signal from the coating material but the calcium and phosphorus signals disappeared (Figures 6C and 6D), suggesting that the calcium is subsurface. An EDAX map for calcium of the same area clearly defines the subsurface deposit (Figure 6B).

Chemical Analysis. Deposits from the ventricle of a 268 days animal (TH80 C12) did contain osteocalcin levels of 195 ng/ml/0.25 cm² as determined by radioimmunoassay¹⁶. Circulating osteocalcin levels in control calves (7-9 mos) was 16-23 ng/ml¹⁶. The total weight percent of osteocalcin in the deposits is still being determined.

Elemental analysis of deposits analyzed by Galbraith Laboratories revealed a nitrogen content of 5.8%, phosphorus level of 9.27%, sulfur content of 0.41%, calcium content of 18.15% and a carbonate level of 0.74%. Assuming that all of the carbonate is in the form of calcium carbonate the resulting Ca/P ratio is 1.88. This suggests that hydroxyapatite is present in the deposits.

Results of the SDS electrophoresis have not been fully analyzed at this point but do demonstrate the presence of at least 6 different bands in both the SDS and EDTA extracted material. Additional analyses are continuing.

Samples of the SDS extracted material were further extracted in chloroform:methanol (2:1) containing 0.005% butylated hydroxy toluene as an antioxidant. The thin-layer chromatography results demonstrate the presence of cholesterol esters, cholesterol and possibly free fatty acids in the deposits.

DISCUSSION

Interest in the calcification of cardiovascular devices, especially blood pumps, continues to grow as various research centers increase the survival time of these devices. Ultimate failure of mechanically active portions of the pump will result if mineralization continues unchecked.

Causes or contributing factors in the calcification process have been discussed at a recent symposium¹⁰. Animal species and age have been implicated as an important factor in this process¹⁰ especially in the case of valve heterografts¹⁸. Adult sheep implanted with Biomer total artificial hearts for up to 77 days have revealed early signs of mineralization at the microscopic level. This suggests that the phenomenon is not unique to calves.

The anticoagulation regime, especially Coumadin, has been reported by Pierce¹⁰ to reduce the incidence and severity of mineralization by inhibition of the vitamin K-dependent protein, osteocalcin. Results reported here do suggest that Coumadin may reduce the incidence and severity of mineralization, but it is clear in our experience that long-term animals (> 100 days) given Coumadin consistently show evidence of calcification. Thus, Coumadin simply delays the onset or growth rate of calcium deposition.

The hypothesis that microbubble defects and surface cracks serve to accumulate calcium binding proteins or result in denaturation of trapped proteins creating an environment for calcification has not been totally demonstrated in this study. However, the facts presented here are consistent with this hypothesis in that mineral deposits are clearly seen subsurface in microbubble defects. Even though osteocalcin has been measured in large amounts (195 ng/ml/0.25 cm²) in areas of gross deposits, microscopic evidence of osteocalcin associated with the developing plaques and/or surface defects should be demonstrated. Future work in this area is under way.

Likewise, the role of lipids and lipoproteins in this process has not been satisfactorily demonstrated even though the deposits clearly contain these components.

Surface defects have been reported by Harasaki et al² and Hennig et al⁸ to be indirectly responsible for calcification by inducing thrombus which ultimately will calcify. Empirical observations in this study suggest that this process can occur without prior thrombus formation. In either case it is clear that mechanical or shear stresses accelerate the process. However, evidence presented in this study (Figure 6) does suggest that micro-defects will eventually calcify even on mechanically inactive portions of the pump.

CONCLUSIONS

Calcification is a problem that is not unique to calves. Adult sheep surviving up to 77 days also show early signs of calcification. Vitamin K-dependent osteocalcin is present in unusually large amounts in gross deposits but evidence for microscopic involvement should be generated. Anticoagulants to inhibit osteocalcin production may delay but do not prevent mineralization in long-term animals. Efforts to eliminate microbubble defects and prevent microfractures in the surface of blood contacting materials should prevent or substantially reduce calcification. In vitro studies are necessary to confirm this hypothesis and to explore variations in fabrication methods to solve this problem.

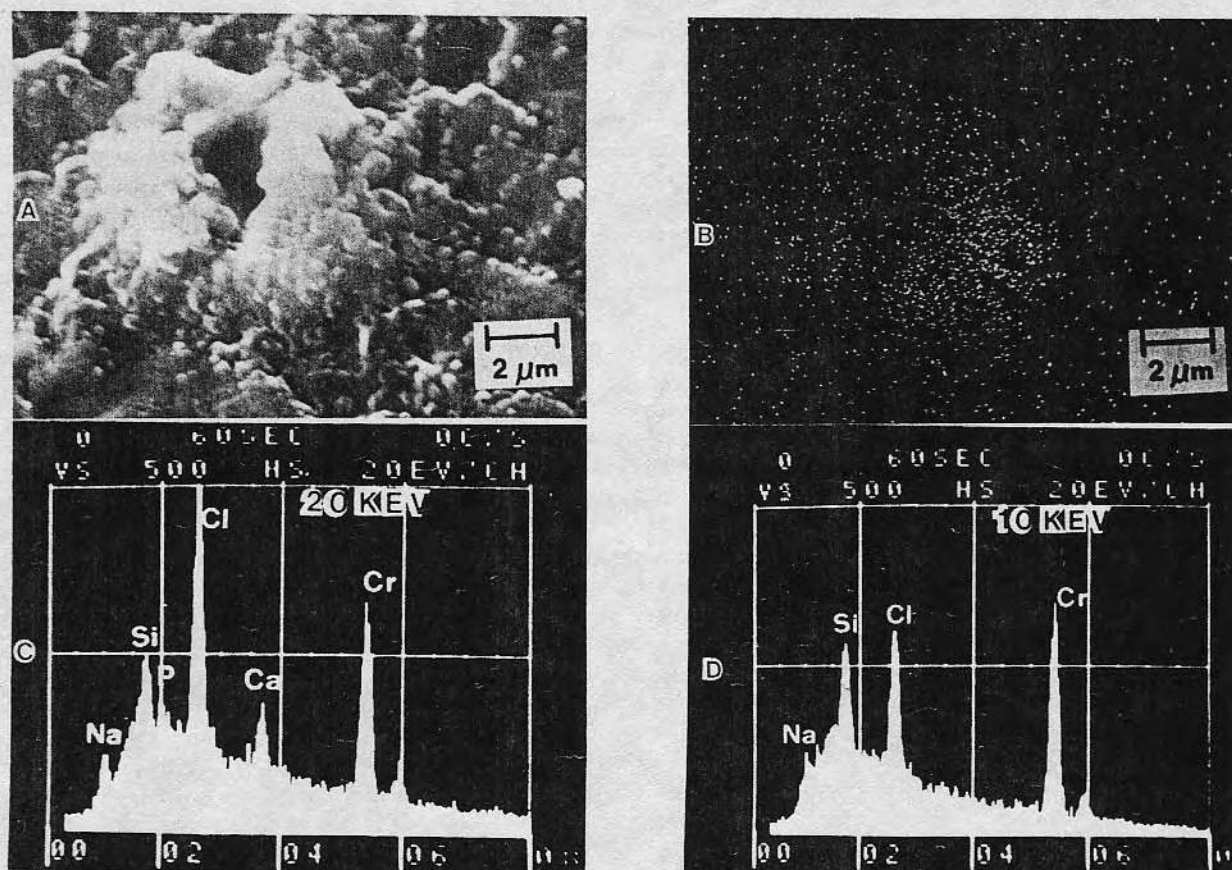


Figure 6. A microbubble defect seen on the housing of a heart implanted 268 days in a calf (A) contains subsurface calcium as determined by a calcium EDAX map (B). The subsurface nature of the deposit is verified by reducing the accelerating voltage from 20 KEV (C) to 10 KEV (D) and noting the disappearance of the calcium and phosphorus signal but the chromium signal remains constant.

ACKNOWLEDGMENTS

The authors are grateful to Dr. Jane Lian (Children's Hospital Medical Center, Boston, MA) for osteocalcin measurements and her helpful suggestions for analysis. The technical assistance of David Dong and Janice Blaylock is gratefully acknowledged.

REFERENCES

1. Jarvik RK. The total artificial heart. *Sci Am* 244:74, 1981.
2. Harasaki H, Gerrity R, Kiraly R, Jacobs G, Nosé Y. Calcification in blood pumps. *Trans Am Soc Artif Intern Organs* 25:305, 1979.
3. Nosé Y, Kiraly R, Harasaki H. Studies on prosthetic total heart replacement. *Contractors Conference Proceedings, Devices and Technology Branch, NIH, 1977, p 63.*
4. Kolff WJ, Olsen DB, Jarvik RK, Fukumasu H, Nielsen SD, Andrade JD, Smith LM, Lawson JH, Razzeca KJ, and Sandquist GM. Cardiac assist devices and artificial heart. *Contractors Conference Proceedings, Devices and Technology Branch, NIH, 1978, p 58.*
5. Pierce WS, Phillips WM, Landis DL, Donachy JH, Rosenberg G, Olsen EK, Shaikh BS, White WJ. Development and evaluation of an artificial heart. *Contractors Conference Proceedings, Devices and Technology Branch, NIH, 1979, p 99.*
6. Norman JC, Edelman SK, Fuqua JM, McGee MG, Poirier VL. Development and evaluation of a long-term, low profile intracorporeal (abdominal) left ventricular assist device. *Contractors Conference Proceedings, Devices and Technology Branch, NIH, 1979, p 109.*
7. Lian JB, Levy RJ. Blood-material interactions. *Contractors Conference Proceedings, Devices and Technology Branch, NIH, 1979, p 233.*
8. Hennig E, Keilbach H, Bohme-Schmokol D, Bucherl ES. Calcification of artificial heart valves and artificial hearts. (Abstract) *Am Soc Artif Intern Organs* 10:27, 1981.
9. Imachi K, Fujimasa I, Miyake H, Takido N, Nakajima M, Koumo A, Ono T, Atsumi K. Evaluation of polyurethane sac type blood pump after 232 and 288 days total artificial heart pumping without anticoagulant. (Abstract) *Am Soc Artif Intern Organs* 10:6, 1981.
10. Andrade JD. Moderator's summary of biomaterials discussion. *World Symp Hearts, Berlin, Germany, 1979.*
11. Kessler TR, Pons AB, Jarvik RK, Lawson JH, Razzeca KJ, Kolff WJ. Elimination of predilection sites for thrombus formation in the total artificial heart - before and after. *Trans Am Soc Artif Organs* 24:532, 1978.
12. Coleman D, Lawson J, Kolff WJ. Scanning electron microscopic evaluation of the surfaces of artificial hearts. *Artif Organs* 2:166, 1978.
13. Lillie RD, Fullmer HM. *Histopathologic Technique and Practical Histochemistry, Fourth Edition.* New York: McGraw Hill, 1976, p 790.
14. Klawitter JJ. Research techniques in biomaterials evaluations. *Clemson University's Third Annual Symp-Workshop Biomater, 1971.*
15. Porter KR, Kelly D, Andrews PM. The preparation of cultured cells and soft tissue for SEM. *Proc Fifth Annu Steroscan Coll, Kent Cambridge Scientific Company, Morton Grove, IL, 1972, p 1.*
16. Lian J. The role of γ -carboxyglutamic acid-containing proteins in mineralization. *Trans Am Soc Artif Intern Organs* 27:680, 1981.
17. Price PA and Nishimoto SK. Radioimmunoassay for the vitamin K-dependent protein of bone and its discovery in plasma. *Proc Natl Acad Sci* 77:2234, 1981.
18. Geha AS, Laks H, Stansel HC, Cornhill JF, Kilman JW, Buckley MJ, Roberts WC. Late failure of porcine valve heterografts in children. *J Thorac Cardiovasc Surg* 78:351, 1979.

DR. ATSUMI: We use adult goats, and no case of calcification in valves or pumps has been seen. I think it may depend on the age of the animal.

DR. COLEMAN: I don't know the age of the sheep that we used, perhaps Dr. Olsen can comment.

DR. OLSEN: They were 9 mos and one and a half years.

DR. COLEMAN: How old are your goats, Dr. Imachi?

DR. IMACHI: From one year to 2 or 3 yrs.

DR. COLEMAN: I think the fact that calcification does occur as a pathological process in adults and aging individuals, suggests that age is not the only factor involved in mineralization.

DR. IMACHI: In our laboratories we use a sac-type pump in which calcification has not occurred. Do you think that is closely related to calcification?

DR. COLEMAN: It may be. As I pointed out, stress can accelerate the process, but I don't completely understand why. Perhaps it causes denaturation of proteins adsorbed or trapped at the surface, but the fact that we have seen it on the housing does indicate that it is a potential problem on mechanically inactive parts of the pump. I think that the causal factors have to be worked out in an in vitro system, however.

DR. HARASAKI: You are using the SEM for classification of the severity of calcification. I am wondering if you can detect the calcification simply from the morphology on the surface.

DR. COLEMAN: The morphology is consistent but x-ray microanalysis is used to confirm composition of deposits. I should point out that we do stain with calcium specific stains to determine exactly where mineral deposits are located.

DR. HARASAKI: I saw in one of your SEM photomicrographs that the calcified deposits look very uniform about 50 μ m diameter, and very similar to flattened cells or their debris. Do you think there is any possibility that calcification occurs in dead cells or debris of cells?

DR. COLEMAN: That certainly is a possibility. I think the crystalline nature of hydroxyapatite is somewhat plate-like. However, the photograph you refer to is obviously several crystals that have grown out to form large plaque-like structures. If cells were involved in this process, I would expect to see them in various stages of the process relative to the survival time of the hearts we have evaluated and this has not been the case. However, I have no positive proof to rule out mummification of dead cells.

DR. W. KOLFF: I would like to thank my younger collaborators for their presentations, and I would like to say that if this process of calcification does persist in all older sheep and perhaps other species, we can fortunately take the heart out since we have quick connections and give it a new heart.

Blood-materials interactions: the minimum interfacial free energy and the optimum polar/apolar ratio hypotheses

D. L. Coleman,* D. E. Gregonis, and J. D. Andrade

Department of Pharmaceutics and Department of Bioengineering, University of Utah, Salt Lake City, Utah 84112

Numerous hypotheses exist to explain observed blood-materials interactions. It is the purpose of this article to test two popular hypotheses, namely, the minimum interfacial free energy hypothesis and the optimum polar/apolar ratio hypothesis. Methacrylate polymers and copolymers were characterized using the captive bubble underwater contact angle method; bulk water content was determined by gravimetric methods; streaming potential measurements were made; and surface roughness and possible particulate contamination were evaluated by reflected light microscopy. *In vitro* blood tests include whole blood clotting time measurements on polymer-coated tubes; centrifugal force platelet adhesion on polymer-coated coverslips; and a measure of

the partial thromboplastin time, Russell's viper venom time (Stypven time), and the prothrombin time of native whole blood exposed to polymer-coated microscope slides. Results suggest that platelet adhesion correlates in the opposite direction of whole blood clotting time and partial thromboplastin time, emphasizing the need for a multiparameter approach to blood-materials testing. Based on these tests the minimum interfacial free energy hypothesis is not supported. In fact, the data suggest the opposite to be true. It is apparent that platelet adhesion can be a misleading indicator of blood compatibility. Neither hypotheses can explain the apparent conflict between the platelet adhesion data and the coagulation time data.

INTRODUCTION

The basic premise of the minimal interfacial free energy hypothesis is that as the interfacial free energy approaches zero, the driving force for protein adsorption decreases. Thus, nonspecific protein adsorption should not occur and proteins at or near a low interfacial energy interface should not feel any greater effects from the surface than they do from the bulk solution. The concept of interfaces as they relate to biomaterials has been reviewed by Andrade et al.^{1,2}

The hypothesis that interfacial free energy (γ_{sw}) is responsible for blood-material interactions is attractive because it attempts to integrate the contribution of the solid phase (implant) and the liquid phase (blood) to the eventual physiological end results.³ Also, the interfacial free energy concept reflects

* To whom correspondence should be addressed.

changes in either the solid or liquid phase and should account for changes in the electrical nature of the substrate, as well as the hydrophobic or hydrophilic nature of the surfaces, surface entropy, etc. Unfortunately, the components that make up the γ_{sw} may change dramatically, yet the γ_{sw} can remain nearly the same, as the effects of contributing components may cancel each other out. Current methods of calculating γ_{sw} , based on contact angle determinations and several assumptions¹ only allow one to separate out, in a very crude fashion, the contribution of the polar and dispersion components of the solid and aqueous phases to the γ_{sw} .^{4,5} If the liquid phase is held constant in composition, as is generally the case with implants *in vivo* and for *in vitro* tests which utilize a constant liquid phase, then it is reasonable to assume that changes in the activation of the coagulation mechanism should correlate with changes in the solid surface phase.

Early efforts of Fowkes,⁶ Good and Elbing,⁷ Kaelble⁸ and others evolved the concept that materials have both a hydrophilic and hydrophobic character. This hypothesis has recently been applied by Nyilas et al.⁹ to blood-compatible materials. Nyilas et al. concluded that surface properties and hemodynamic characteristics are interrelated in thrombus induction and that thrombogenicity increases as the polar contribution to the surface free energy increases. Kaelble and Moacanin,⁵ using contact angle data generated by R. Baier, have provided an extensive list of the polar and dispersion energetics of biomaterials. They conclude from a comparison of the surface energetics with literature results of blood compatibility that a high dispersion force, low polarity surface will favor the adherence of a stable protein film while materials with a dispersion-free, highly polar surface will have a weak affinity for plasma proteins with the possible result of emboli generation.

The hypothesis that the hydrophilic and hydrophobic natures of a surface must be in balance has been suggested by Ratner et al.¹⁰ as a somewhat novel extension of the polar/dispersion argument of Nyilas⁹ and of Kaelble and Moacanin.⁵ The general premise of the hydrophilic-hydrophobic ratio hypothesis represented by Ratner et al.¹⁰ is that suitable proteins will be adsorbed and remain adherent if the polar and apolar surface character is properly balanced.

This study attempts to test these hypotheses using well-characterized materials and simple *in vitro* blood assays to probe activation of coagulation, platelet adhesion, and a rough measure of increased platelet factor 3 activity. Activation of extrinsic activation is monitored as a check on the blood handling methods.

MATERIALS AND METHODS

Materials preparation

Selection of materials specifically to test these hypotheses required that γ_{sw} be varied over a reasonably wide range without significantly changing chemical composition or polymer type and that ionic contributions to the γ_{sw} be minimal (the effect of surface charge is the subject of another study.)¹¹

Copolymers of hydroxyethyl methacrylate and methyl methacrylate allowed for a variation in water content from about 1 to 40% by weight, with the calculated γ_{sw} varying from essentially zero to about 20 erg/cm². Since water contents above 40% were unattainable in this methacrylate series without the addition of ionic species, agarose was therefore evaluated as an uncharged, high water content, low γ_{sw} surface. Glass, filler-free poly(dimethyl siloxane) (PDMSO)* and Avcothane-51 elastomer* were included as relevant control materials.

Details of the methacrylate polymerization conditions have been reported elsewhere.^{4,12,13} Briefly, these materials were prepared as soluble uncross-linked polymers by mixing the monomer or comonomers at 10:1 v/v solvent-to-monomer concentration and polymerizing at 60°C using azobis(methyl isobutyrate) to initiate the reaction. The polymers were precipitated in appropriate nonsolvents and dried to constant weight under vacuum.

Polymer solutions were made up in appropriate solvents as either a 10% w/v solution for coating test tubes or a 1% w/v solution for spin casting^{14,15} coverslips and microscope slides. The solutions were filtered through a 0.5 μ m or 1.0 μ m Fluoropore filter† and stored in particulate-free brown glass bottles.

Glass test tubes (12 × 75 mm), coverslips (circular, 25 mm diam), and microscope slides (1 × 3 in.) were used as support substrates for the test polymers. All glass was precleaned in hot chromic acid, rinsed four times in filtered distilled deionized water, rinsed two times in filtered absolute ethanol, and exposed to Freon THF vapor to accelerate drying. Polymers that did not adhere well to clean glass were cast on vapor silanized glass.¹⁶ All test substrates were extracted and hydrated overnight in distilled water and calcium-free Tyrode's buffer, respectively.

The filler-free PDMSO-coated samples were cured for 6 h at room temperature in a closed container with a small amount of distilled water in the bottom. After removal from this humid environment, they were placed in a 60°C nitrogen-purged oven for 4 h.

Agarose, 3 mg in 100 mL distilled water, was coated on test tubes by adding a small amount of the warm solution to the tube, tilting 90°, and rotating the tube until a gel formed. The tubes were then filled with calcium-free Tyrode's buffer and stored at 4°C overnight.

Avcothane-51* was heat cured at 60°C in a nitrogen-purged oven.

Materials characterization

Characterization of the test substrates was generally done on a quality control basis to insure that the polymers used for blood studies were within acceptable limits for our laboratory. Most of the characterization tests are included as either level I, II, or III tests in the NHLBI Task Force Report on Physicochemical Characterization of Biomaterials.¹⁷ The characterization protocol is schematically represented in Figure 1.

* Avco Medical Products, Inc., Everett, MA.

† Millipore Corporation, Bedford, MA.

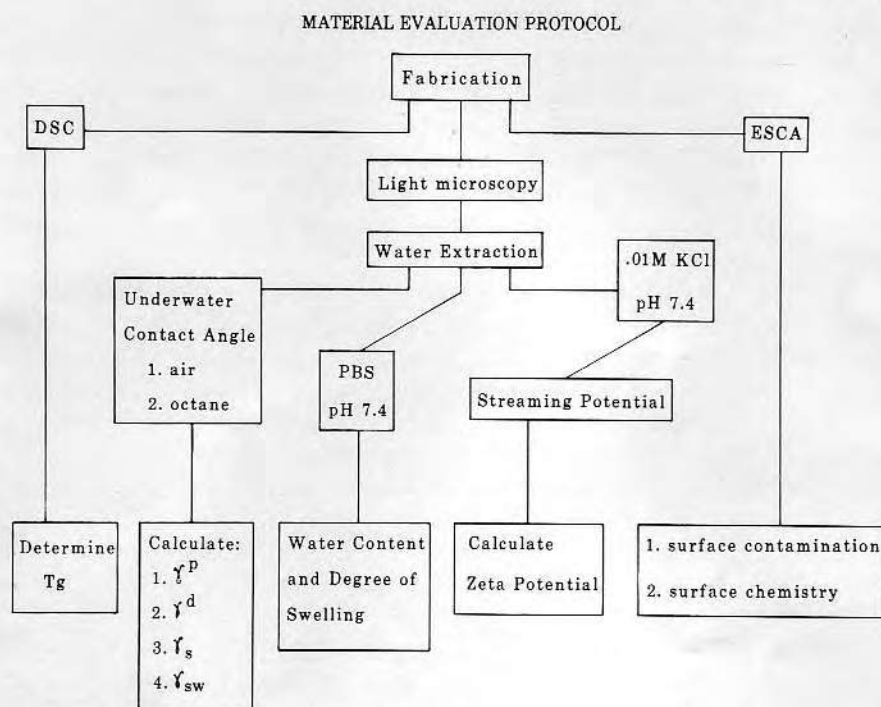


Figure 1. A schematic diagram of the materials evaluation protocol.

The use of differential scanning calorimetry (DSC) is not directly applicable to polymers containing significant amounts of water and is therefore not routinely reported for all of the polymers evaluated. Electron spectroscopy for chemical analysis (ESCA) was used in this particular study to screen for surface contamination.

The captive bubble underwater contact angle method^{4,18} was used to calculate surface energetics of fully hydrated surfaces. Bulk water content was determined on separate samples of bulk polymer and assumed to be the same for the thin film system.¹³ Surface roughness and possible particulate contamination were evaluated with reflected interference light microscopy. Streaming potential measurements were done on polymer thin films cast on microscope slides.¹⁹

Blood studies

Evaluation of blood-materials interactions consisted of primary static *in vitro* tests described in the *Guidelines for Blood-Materials Interactions*, issued by NHLBI.³⁹ These tests were selected for their simplicity and general usefulness in screening activation of the intrinsic coagulation system, extrinsic system, and platelet contribution to the overall interaction of blood with biomaterials.

Blood collection

Blood from rabbits was collected via cardiac puncture using an 18 g needle and a two-syringe technique. Calf blood was collected from the jugular vein using a 19 g butterfly catheter and a two-syringe technique. The blood was not anticoagulated prior to exposure to the test surfaces except in the case of platelet adhesion tests where 0.1M sodium citrate was added to the syringe at a ratio of 1 mL citrate to 9 mL blood.

Whole blood clotting time (WBCT)

This test is a modification of the standard Lee and White test.²⁰ Three tubes coated with the test polymer were hydrated overnight in calcium-free Tyrode's solution. Five different polymers and a glass control were tested with each blood collection. One milliliter of blood was added to each tube and incubated at 37°C. The first tube was tilted for each test material until a firm clot formed. The second and third tubes were tilted in a similar fashion, and the clotting time was recorded as the time required for the third tube to clot. Since there was a high correlation ($r = 0.91$) between the results of materials treated with calf and rabbit blood, the combined results are presented in this article.

The WBCT for each experiment has been normalized to the glass control WBCT. The mean clotting time for glass controls was 12.7 ± 1.59 (SD) min for the calf and 11.3 ± 1.67 min for the rabbit. These values are similar to reported normal human values (11.9 ± 1.77) using this technique.²¹

Platelet adhesion and morphology

The adhesion of platelets to artificial surfaces is thought to be an important indicator of blood compatibility.^{3,22-24} Although a variety of methods have been used to monitor platelet adhesion successfully, a modification²⁵ of the adhesion test described by George²⁶ was used in this work.

Citrated rabbit blood was centrifuged at 200 g for 10 min to prepare platelet-rich plasma (PRP). A 0.2 mL sample of PRP was removed, and platelet-poor plasma (PPP) prepared by recentrifuging the blood at 1400 g for 20 min. During this time the PRP was counted using Rees-Ecker platelet diluent.²⁷ Platelet counts from 11 animals were $(5.1-16.8) \times 10^6$ platelet/ μ L. Platelet-free plasma (PFP) was prepared by filtering PPP through a 0.45 μ m filter, and a platelet concentration of roughly 2000 platelet/ μ L was made by adding 1.0 μ L of PRP to 5.0 mL of PFP.

The adhesion cell and test conditions have been described by Mohammad et al.²⁵ Briefly, the dilute platelet suspension is added to the test chamber where the bottom coverslip has been coated with the polymer to be tested and the top coverslip is coated with poly(methyl methacrylate). The platelets are centrifuged to the bottom coverslip 1.0 min at 1000 g and the platelets are allowed a 5-min contact time. The test chambers are turned over and again centrifuged 1.0 min at 1000 g to remove nonadherent platelets from the test

surface. The percent of platelet adhesion is calculated by dividing the mean number of platelets on the test surface by the sum of the mean number of platelets attached to the PMMA and the test surface.

Since the polymer films were frequently damaged during the disassembly of the test chamber, the morphology studies required a modification of the centrifuge adhesion technique. Round (25 mm diam) coverslips coated with the test polymer were placed in a 35-mm petri dish (Falcon) and 0.8 mL of the dilute platelet suspension was allowed to cover the entire surface of the coverslip without running over the edge. The petri dishes were centrifuged for 1.0 min at 1000 *g* and allowed a 5-min contact time with the surface. The coverslips were rinsed two times with Tyrode's buffer and fixed with 2% electron microscopy grade glutaraldehyde for 30 min. This was followed by two rinses with distilled water and dehydration through absolute ethanol. The coverslips were critical point dried using liquid CO₂ as the transition fluid.²⁸

The coverslips were mounted on SEM stubs and coated with carbon and chromium. Samples were then examined by reflected light microscopy and scanning electron microscopy.

Elliptical cell test

Two glass microscope slides coated with the polymers to be tested were separated by an elliptically shaped gasket (2.0 mm thick) made of Estane* and coated with Avcothane-51 elastomer.[†] This type of cell has been described by Mason, Shermer, and Rodman.²⁹

The test cells were assembled using a clamping device to hold the microscope slides in firm contact with the gasket. Six test chambers were run with each blood collection. The chambers were primed with calcium-free Tyrode's solution until blood exposure. The volume of each cell was 2.5 mL.

Rabbit blood was collected as discussed above, and a timer was started as blood entered the syringe. A 2.5 mL blood sample was immediately citrated to act as a control sample. Each of the six test chambers were filled in random order, after which another 2.5 mL sample was citrated to serve as a control for possible activation due to the syringe during filling. The chambers were left undisturbed at room temperature for 15 minutes. Blood from each chamber was successively injected into tubes containing 0.28 mL citrate (9:1) and thoroughly mixed.

Platelet factor-3 determination

The citrated blood was centrifuged at 200 *g* for 10 min, and the PRP was collected for platelet factor-3 (PF-3) determinations. The method described by Spaet and Cintron³⁰ was modified to allow the test surface to be the activator rather than using kaolin or ovolecithin to activate platelets or supplement the

* B. F. Goodrich Chemical Co., Cleveland, OH.

† Avco Medical Products, Inc., Everett, MA.

Russell's viper venom (RVV) reaction. Therefore, platelets activated by the test material should be the main sources of PF-3 in this test system. The Russell's viper venom* was reconstituted with 2.0 mL isotonic saline to give a one-in-10,000 solution. The RVV was prewarmed to 37°C as was the calcium chloride solution (0.02M). All tests were completed using a Fibrometer† test system. A PRP sample (0.1 mL) was added to a Fibrometer cup, and 0.1 mL of prewarmed RVV was added and mixed. Exactly 30 s later, 0.1 mL of CaCl₂ was added at the same time, triggering the Fibrometer timing and mixing system. The test was repeated two or three times for each blood sample. The pretest control averaged 40.7 ± 3.22 s (\pm SEM, $n = 8$), and the post-test control averaged 35.6 ± 2.54 s (\pm SEM, $n = 8$) for the same animals. Therefore, some activation was occurring during the time the blood was in the syringe. Addition of celite shortened the time of the control PRP to 8–10 s, indicating that syringe activation was minimal. The RVV time for the test polymers is reported as a percent of the mean pre- and post-test control samples for each experiment. Glass could not be used as a control because it clotted in the test chamber in 10 min or less.

Intrinsic activation

After the PRP had been collected for PF-3 tests, the blood samples were centrifuged at 1400 g for 10 min (4°C) and the PPP was collected and stored on ice. The partial thromboplastin‡ time (PTT) was evaluated using the Fibrometer method with minor modifications.

A 0.1 mL volume was prewarmed in a fibrometer cup for 5 min, and a 0.1 mL sample of test plasma (4°C) was added to the prewarmed partial thromboplastin. Exactly 30 s later, 0.1 mL of prewarmed 0.02M CaCl₂ was added, activating the Fibrometer. Each test plasma was evaluated two or three times. The mean precontrol value was 149.3 ± 15.35 s (\pm SEM, $n = 11$), and the mean post-control PTT was 152 ± 15.65 s (\pm SEM, $n = 11$). Celite-activated plasma gave a PTT of 30–40 s, indicating that syringe activation of the intrinsic system was minimal.

The PTT was designed to test activation of the intrinsic system, and modifications for this study allowed the test surface to serve as the activator.²⁹ The PTT results are reported as the percent of the mean pre- and post-controls for each experiment.

Extrinsic activation

Activation of the extrinsic system was monitored by means of the one-stage prothrombin time (PT)²¹ using PPP obtained from experiments described above. Strictly speaking, this test could not be modified to examine activation

* Wellcome Reagents Ltd., Beckenham, England.

† Becton-Dickinson, Laboratories, Inc., Baltimore, MD.

‡ Ortho Diagnostics, Inc., Raritan, NJ.

TABLE I
Physical Characterization of Materials

Polymer mol %	% H ₂ O (<i>n</i> = 4)	Contact angle (degrees)				Surface energetics (erg/cm ²)				Zeta potential (mV) (<i>n</i> = 3)
		Air	(<i>n</i>)	Octane	(<i>n</i>)	γ_{sw}	γ^p	γ^d	γ^p/γ^d	
Agarose	96	0 ± 0 ^b	(3)	16 ± 3.4	(3)	0.1	48.6	23.6	2.42	-18.0 ± 1.3
HEMA	37 ± 0.4 ^a	18 ± 1.7	(5)	18 ± 1.4	(5)	0.1	48.6	20.1	2.42	-24.1 ± 0.7
75 HEMA										
25 MMA	31 ± 3.5	24 ± 1.4	(2)	33 ± 0.4	(2)	0.7	42.5	23.0	1.85	
50 HEMA										
50 MMA	21 ± 1.4	30 ± 0.6	(4)	43 ± 3.8	(3)	0.9	41.7	22.8	1.83	-28.7 ± 1.0
25 HEMA										
75 MMA	7 ± 0.6	42 ± 1.2	(2)	63 ± 2.8	(2)	7.1	30.3	32.0	0.95	
MMA	1 ± 0.3	62 ± 1.1	(4)	87 ± 1.4	(3)	19.2	17.6	35.4	0.50	-31.5 ± 1.8
PDMSO-FF	<1	84 ± 7.7	(5)	120 ^b	(2)	36.4	7.2	36.7	0.20	-49.6 ± 1.6
Avco-51	<1	53 ± 3.6	(3)	82 ± 4.2	(2)	19.5	41.8	20.1	0.48	-38.6 ± 1.8
B. Glass	^d	<10		<10		0.1	49.7	21.3	2.33	
S. Glass	^d	<10		<10		0.1	49.7	21.3	2.33	-52.3 ± 1.3 ^c -62.7 ^e

^a ± SEM.

^b Calculated from air values.

^c *P* = Proper bevel edge slides.

^d High surface content, low bulk content.

^e Gold seal, Becton-Dickinson.

of Factor VII by the test surface but was used as a check on the Russell's viper venom time, which should be the same as the prothrombin time when PF-3 is available in adequate amounts.²¹

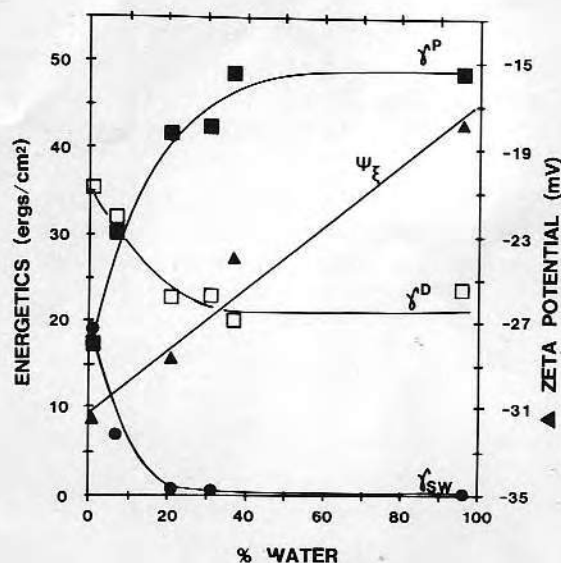


Figure 2. The water content appears to control not only surface energetics but is also important in the zeta potential of hydrogels containing up to 95% water by weight.

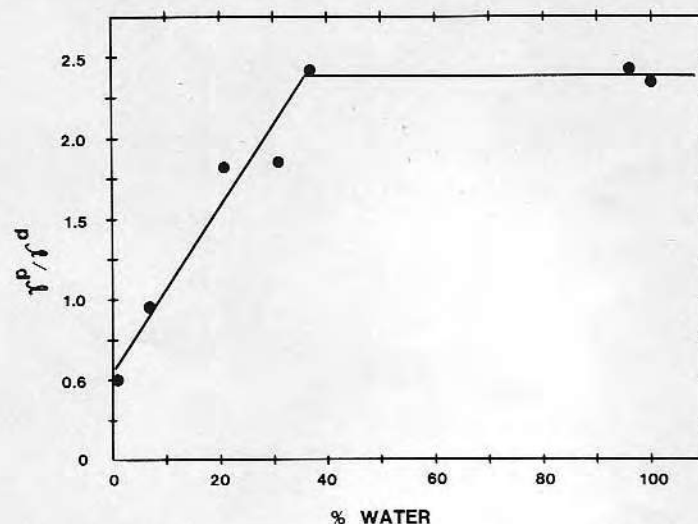


Figure 3. The γ^p/γ^d is greatly affected by water content up to 40%, but is relatively constant above that value.

RESULTS

Physical characterization

Table I summarizes the physical characterization data of the materials used in this study.

The interfacial free energy of hydrogel systems rapidly approaches zero as the water content is increased up to 20%.³¹ Therefore, it seems reasonable that for the hydrogel materials used in this study the water content should control the interfacial parameters including the zeta potential and γ_{sw} as well as the polar (γ_{sv}^p) and dispersion (γ_{sv}^d) components of the surface free energy (γ_{sv} =

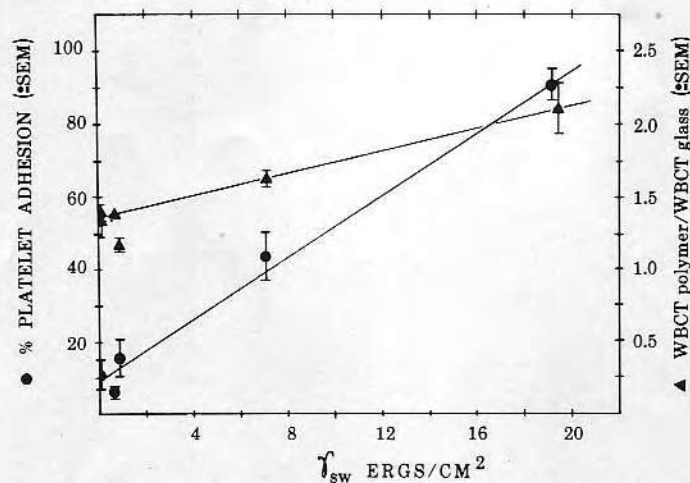


Figure 4. A linear correlation exists between γ_{sw} and WBCT ($r = 0.93$). A similar correlation is apparent for platelet adhesion ($r = 0.99$).

TABLE II
Summary of *In Vitro* Blood Data

Polymer (mole %)	WBCT (\pm SEM)		% Platelet adhesion (\pm SEM)		% Citrated control ^a (\pm SEM)		PT
	<i>n</i>	Min	Normalized	<i>n</i>	PTT	RVVT	
Agarose	11	14.1 (1.53)	1.62 (0.056)	6	ND ^c	ND	ND
HEMA	10	17.2 (0.64)	1.39 (0.057)	6	11.0 (4.14)	44.5 (15.78)	102.0 (4.44)
75 HEMA	10	17.2 (1.05)	1.38 (0.036)	5	6.0 (1.78)	78.8 (2.85)	103.6 (1.15)
25 MMA	10	14.4 (1.07)	1.17 (0.047)	5	15.6 (5.09)	69.6 (8.71)	107.9 (4.69)
50 HEMA	10	20.2 (0.79)	1.62 (0.055)	6	43.6 (6.55)	91.5 (4.40)	101.9 (3.07)
75 MMA	10	25.3 (2.82)	2.10 (0.176)	5	90.5 (4.24)	78.0 (3.25)	102.5 (2.43)
MMA	10	35.1 (4.34)	3.0 (0.372)	5	24.0 (4.26)	86.6 (2.84)	98.1 (1.18)
PDMSO-FF	10	34.5 (3.36)	2.93 (0.263)	5	30.4 (6.66)	80.2 (5.66)	101.4 (1.75)
Avco-51	43	12.0 (1.76)	1.00	8	7.1 (0.90)	ND	ND
B. Glass		ND	ND		ND	ND	ND
S. Glass					ND	ND	ND

^a 15 min exposure.

^b Clotted after 10 min.

^c No data.

$\gamma_{sv}^p + \gamma_{sv}^d$). This effect is graphically demonstrated in Figure 2. Examination of the γ^p/γ^d ratio as a function of water content (Fig. 3) suggests that a water content above 40% will not alter the ratio of the polar to dispersion forces as measured by the captive bubble technique.

It is interesting to note that although none of the hydrogel polymers and copolymers contained ionic groups, the calculated zeta potential became more electronegative as the water content decreased (Fig. 2).

Blood evaluation

The *in vitro* blood data are summarized in Table II. The whole blood clotting time data are mean values of both rabbit and calf experiments. The correlation coefficient for testing materials in the calf versus the rabbit was high enough ($r = 0.91$) to justify pooling the data. All other tests were done with rabbit blood.

The WBCT data expressed as a function of water content suggest that an increased water content activated the coagulation mechanism and at 20% water is essentially the same as glass (Fig. 4). This observation is confirmed by the PTT data. Platelet adhesion, however, decreases as the water content increases (Table II). The RVVT and PT tests appear to be less predictive, although the rapid decrease in the RVVT for HEMA relative to the control suggests that activation of the platelets increases even though platelet adhesion decreases (Fig. 5).

Platelet morphology, frequently considered an indicator of platelet release, does not vary in a strikingly different way among PHEMA, 50 HEMA/50 MMA copolymer, and PMMA [Figs. 6(A)–(C)], although more dendritic platelets seem to be associated with PMMA. This may be somewhat deceiving because a significant number of platelets are removed from the low adhesion surfaces

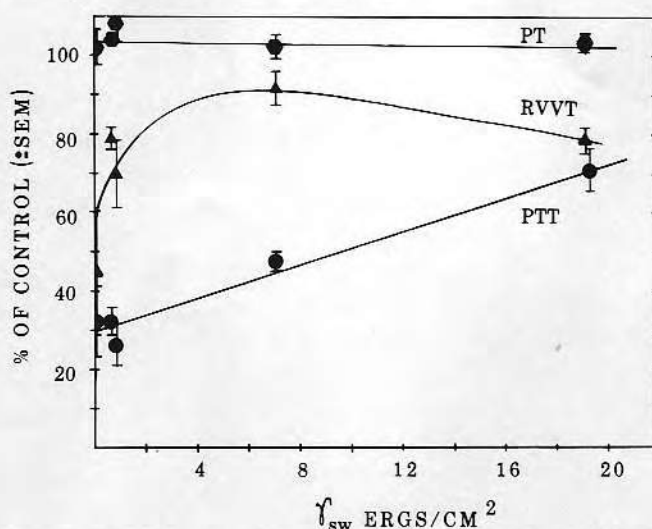


Figure 5. The PTT does correlate with γ_{sw} ($r = 0.98$), but RVVT and PT do not, $r = 0.42$ and -0.36 , respectively.

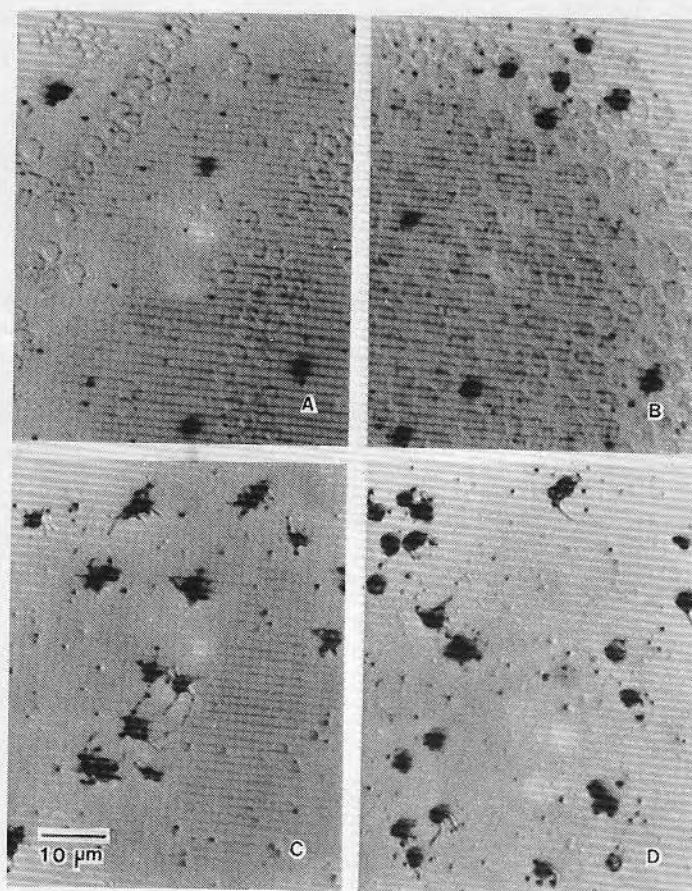


Figure 6. Platelet morphology on (A) HEMA, (B) 50 HEMA/50 MMA, (C) PMMA, and (D) glass after critical point drying. Some platelet loss does occur during processing. Reflected light microscopy ($\times 400$).

during fixation and critical point drying (CPD). Platelets adhered to glass [Fig. 6(D)] have increased pseudopod formation relative to HEMA but are not strikingly different from platelets adhered to PMMA. The CPD process does cause surface pitting in the gel materials. Further studies are necessary before any useful conclusions can be made about changes in platelet morphology versus platelet release. Rabbit platelets do not spread like human platelets, but it is well established that release can occur throughout the time course of spreading.³² Rabbit platelets on glass resemble the early polypodial stage described for human platelets adhering to glass.³²

DISCUSSION

It is quite obvious from the data in Table I that increasing water content has a profound effect on interfacial energetics. Somewhat surprising is that the charge measured by streaming potential at or near the interface of nonionic polymers of increasing water content are significantly different. Significance

($p < 0.01$) in this case is determined from the calculated critical value for the correlation coefficient reported in Figure 2 ($df = 2$).³³ Possible explanations include specific ion adsorption at the surface, water dipole orientation, or electron injection from the water into the polymer.³⁴ Williams³⁵ suggests that both positive and negative ions are repelled from an insulator interface with a dielectric constant lower than water, although there is considerable evidence for specific anion binding at such surfaces. Brown et al.³⁶ have reported zeta potentials for selected neutral hydrophobic polymers using 0.01 or 0.02M Tris-HCl at pH values ranging from 3.0 to 7.2. Specific ion adsorption is thought to be the primary cause of negative electrophoretic mobility seen with oil droplets and air bubbles³⁷ and is the likely cause of the streaming potential data reported in this study.

Blood interactions with this series of polymers are strikingly different, and the majority of the variation of WBCT, platelet adhesion, and PTT can be explained by changes in the γ_{sw} ($r^2 = 0.96, 0.99$, and 0.97 , respectively). Platelet adhesion data support the hypothesis that a decrease in γ_{sw} improves blood compatibility, but this assumes that increased platelet adhesion is indicative of poor blood compatibility. Closer examination of the data reveals that WBCT and PTT decreases as γ_{sw} decreases, indicating activation of the coagulation system. This apparent conflict is the reason why a multiparameter approach is important in assessing blood-material compatibility. For this series of methacrylates, platelet adhesion appears to be a desirable quality and correlates ($r = 0.94$) quite well with prolonged WBCT (Fig. 7). Activation of the intrinsic system (PTT) does correspond to the WBCT results ($r = 0.99$) as one would predict (Fig. 7).

Model copolymers used by Ratner et al.¹⁰ to test the hydrophilic/hydro-

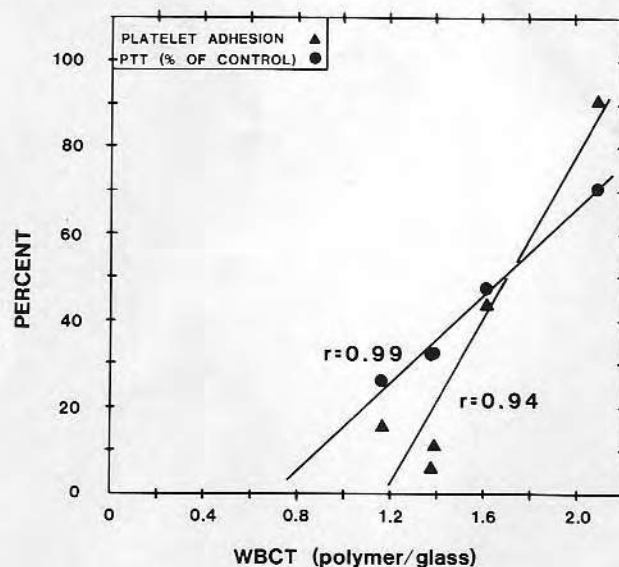


Figure 7. It is surprising that the percent of platelet adhesion correlates in a positive way with prolonged WBCT ($r = 0.94$). As expected, WBCT is prolonged when PTT is not activated by the material ($r = 0.99$).

phobic ratio hypothesis were hydroxyethyl methacrylate/ethyl methacrylate radiation grafted to silicone rubber tubing. The copolymer with the best blood compatibility, as determined by minimal platelet consumption, was HEMA/EMA (1:1). The measured contribution of the polar and dispersion components of these copolymers is not provided in this study, but assuming a HEMA/EMA copolymer system similar to the HEMA/MMA series in Table I and a water content of 14%, then from Figure 2 the polar contribution would be about 36 erg/cm² and the dispersion component would be around 27 erg/cm², giving a γ^p/γ^d ratio of about 1.3. Again, it is important to remind the reader that these values are calculated from underwater air and octane contact angles⁴ which give higher values for the polar contribution than the technique of Kaelble and Moacanin⁵ which are based on classical advancing contact angle data.

Data presented in Figures 8 and 9 suggest that the coagulation system is sensitive to changes in γ^p/γ^d . It is even tempting to suggest that platelets begin to sense changes in γ^p/γ^d around 1.3 to 1.4, since the RVTT is rapidly reduced as the ratio increases beyond these values.

In considering the results of all the *in vitro* tests in Table II reported as a function of γ^p/γ^d , it appears that a correlation does exist for WBCT ($r = -0.86$) and PTT ($r = -0.97$) to indicate that for this series of polymers, as the dispersion component begins to dominate the surface, blood compatibility improves.

The data presented in this study do not support the minimal interfacial free energy hypothesis as stated in the introduction, but suggests that the opposite situation may be true: increasing γ_{sw} of nonionic polymers may lead to improved blood compatibility. The explanation for this observation logically must reside in the nature of protein adsorption during initial blood or plasma contact. Exactly how γ_{sw} or the components of γ_{sw} control protein adsorption and conformation is still unknown.

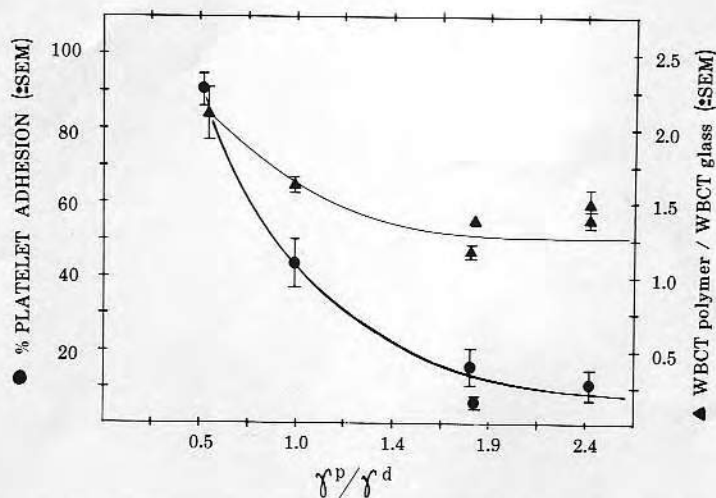


Figure 8. Platelet adhesion and WBCT decrease as the polar contribution of the material increases.

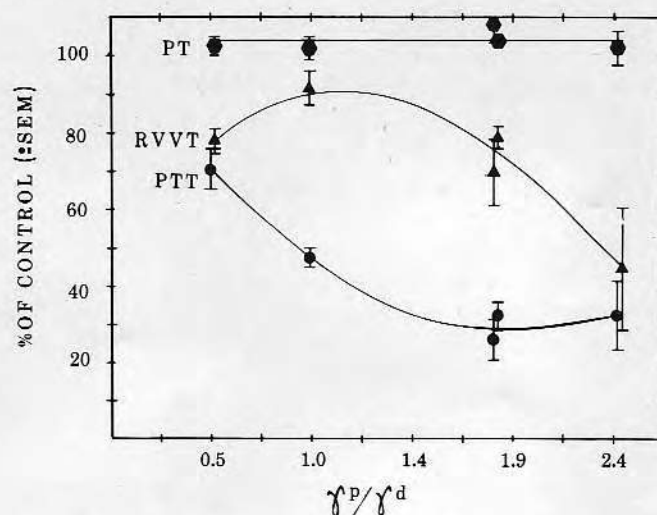


Figure 9. The intrinsic system (PTT) becomes more activated as γ^p/γ^d increases but platelet activation (RVVT) is not significantly affected until the polar contribution of the material is greater than about 1.4 times the dispersion component.

The original study by George²⁶ using centrifugal force to measure platelet adhesion also reported that platelet adhesion was low on poly(ethylene oxide)-coated glass, but the WBCT was not prolonged by this coating. Likewise, silane-treated glass had a prolonged WBCT and increased platelet adhesion, which supports the results reported here. Brash³⁸ noted that platelet adhesion and platelet release were roughly inversely related and that adhesion was higher on the low water content urethanes. It appears that a reassessment of the importance of platelet adhesion to blood compatibility is in order.

CONCLUSIONS

The data presented in this study clearly demonstrate the need for a multi-parameter evaluation of both the material properties and the biological interactions. Changes in any one material property can result in changes in all the physical properties of that material. This is demonstrated by the significant increase in the negative charge of nonionic hydrogel copolymers as the water content decreases.

Results of the *in vitro* blood studies presented in Table II do not support the minimal interfacial free energy hypothesis, but a strong correlation in the opposite direction does suggest that interfacial energetics are important. This misconception has resulted from the longstanding observation that platelets do not adhere to high water content materials. Platelet adhesion is not a good indicator of "hemocompatibility" and should not be used as the only test to screen polymers. A rather surprising and strong linear correlation ($r = 0.94$) between platelet adhesion and WBCT supports this conclusion.

The optimal polar/dispersion ratio hypothesis is consistent with the data

presented in this study but does not explain the platelet adhesion data. It appears that as the dispersion component begins to dominate the interface the general hemocompatibility (WBCT, PTT, and RVVT) improves.

Since γ_{sw} and γ^p/γ^d values are calculated from contact angle measurements, one would expect the blood tests to correlate with θ or $\cos \theta$. This is the case, but the linear correlation is best when the data are plotted as functions of the calculated γ_{sw} .

The authors extend their appreciation to Dr. Reginald G. Mason and Dr. Fazel Mohammad for their critical comments and technical suggestions. The technical assistance of Mr. Lyle Brostrom is gratefully acknowledged. This work was supported by NIH grants HL-16921 and HL-26469.

References

1. J. D. Andrade, "Interfacial Phenomena and Biomaterials," *Med. Instrum.*, **7**, 110-121 (1973).
2. J. D. Andrade, H. B. Lee, M. S. Johns, S. W. Kim, and J. B. Hibbs, Jr., "Water as a Biomaterial," *Trans. Am. Soc. Artif. Intern. Organs*, **19**, 1-7 (1973).
3. S. K. Chang, O. S. Hum, M. A. Moscarello, A. W. Neumann, W. Zingg, M. J. Leutheusser, and B. Reugsegger, "Platelet Adhesion to Solid Surfaces. The Effects of Plasma Proteins and Substrate Wettability," *Med. Progr. Technol.*, **5**, 57-66 (1977).
4. J. D. Andrade, R. N. King, D. E. Gregonis, and D. L. Coleman, "Surface Characterization of Poly(hydroxyethyl Methacrylate) and Related Polymers. I. Contact Angle Methods in Water," *J. Polym. Sci. Polym. Symp.*, **66**, 383-386 (1979).
5. D. H. Kaelble and J. Moacanin, "A Surface Energy Analysis of Bioadhesion," *Polymer*, **18**, 475-482 (1977).
6. F. M. Fowkes, "Attractive Forces at Interfaces," *Ind. Eng. Chem.*, **56**, 40-52 (1964).
7. R. J. Good and E. Elbing, "Generalization of Theory for Estimation of Interfacial Energies," *Ind. Eng. Chem.*, **62**, 54-78 (1970).
8. D. M. Kaelble, "Dispersion-Polar Surface Tension Properties of Organic Solids," *J. Adhesion*, **2**, 66-81 (1970).
9. E. Nyilas, W. A. Morton, D. M. Lederman, T-H. Chiu, and R. D. Cumming, "Interdependence of Hemodynamic and Surface Parameters in Thrombosis," *Trans. Am. Soc. Artif. Intern. Organs*, **21**, 55-69 (1975).
10. B. D. Ratner, A. S. Hoffman, S. R. Hanson, L. A. Harker, and J. D. Whiffen, "Blood Compatibility-Water Content Relationships for Radiation Grafted Hydrogels," *J. Polym. Sci. Polym. Symp.*, **66**, 363-375 (1979).
11. D. L. Coleman, D. E. Gregonis, and J. D. Andrade, "Blood-Materials Interactions: The Effect of Surface Charge," Manuscript in preparation (1982).
12. D. E. Gregonis, G. A. Russell, J. D. Andrade, and A. C. DeVisser, "Preparation and Properties of Stereoregular Poly(hydroxyethyl Methacrylate) Polymers and Hydrogels," *Polymer*, **19**, 1279-1284 (1978).
13. D. E. Gregonis, C. M. Chen, and J. D. Andrade, "The Chemistry of Some Selected Methacrylate Hydrogels," *Am. Chem. Soc. Symp.*, **31**, 88-104 (1976).
14. F. L. Givens, and W. J. Daughton, "On the Uniformity of Thin Films: A New Technique Applied to Polyamides," *J. Electrochem. Soc.*, **126**, 269-272 (1979).
15. J. H. Lai, "An Investigation of Spin Coating of Electron Resists," *Org. Coatings Plastics Chem., Prepr. Am. Chem. Soc.*, **40**, 181-187 (1979).

16. I. Haller, "Covalently Attached Organic Monolayers on Semiconductor Surfaces," *J. Am. Chem. Soc.*, **100**, 8050-8055 (1978).
17. K. H. Keller, Chairman, *NHLBI Task Force Report on Physicochemical Characterization of Biomaterials*, National Heart, Lung, and Blood Institute, Devices and Technology Branch, Bethesda, MD, April, 1979.
18. R. N. King, "Surface Characterization of Synthetic Polymers for Biomedical Applications," Ph.D. Dissertation, University of Utah, 1980.
19. R. A. VanWagenen and J. D. Andrade, "Flat Plate Streaming Potential Investigations: Hydrodynamics and Electrokinetic Equivalency," *J. Colloid. Interface Sci.*, **76**, 305-314 (1980).
20. R. I. Lee and P. D. White, "A Clinical Study of the Coagulation Time of Blood," *Am. J. Med. Sci.*, **145**, 495-503 (1913).
21. J. B. Miale, Ed. *Laboratory Medicine Hematology*, 4th ed., C. V. Mosby Co., St. Louis, 1972, pp. 1267-1295.
22. R. G. Mason, "The Interaction of Blood Hemostatic Elements with Artificial Surfaces," in *Progress in Hemostasis and Thrombosis*, Vol. 1, T. H. Spaet, Ed., Grune and Stratton, New York, 1972, pp. 141-164.
23. C. D. Forbes and C. R. M. Prentice, "Thrombus Formation and Artificial Surfaces," *Br. Med. Bull.*, **34**, 201-207 (1978).
24. P. Didisheim, J. Q. Stropp, J. H. Borowick, and E. F. Grabowski, "Species Differences in Platelet Adhesion to Biomaterials: Investigation by a New Two-Stage Technique," *ASAIO J.*, **2**, 124-132 (1979).
25. S. F. Mohammad, M. D. Hardison, C. H. Glenn, B. D. Morton, J. C. Bolan, and R. G. Mason, "Adhesion of Human Blood Platelets to Glass and Polymer Surfaces. I. Studies with Platelets in Plasma," *Haemostasis*, **3**, 257-270 (1974).
26. J. N. George, "Direct Assessment of Platelet Adhesion to Glass: A Study of the Forces of Interaction and the Effects of Plasma and Serum Factors, Platelet Function and Modification of the Glass Surface," *Blood*, **40**, 862-874 (1972).
27. O. W. Schalm, N. C. Jain, and E. J. Carroll, *Veterinary Hematology*, 3rd ed., Lea and Febiger, Philadelphia, 1975, pp. 69-70.
28. A. A. Bartlett and H. P. Burstyn, "A Review of the Physics of Critical Point Drying," in *Proceedings of the Eighth Annual SEM Symposium*, IIT Research Institute, Chicago, IL, 1975, pp. 305-316.
29. R. G. Mason, R. W. Shermer, and N. F. Rodman, "Reactions of Blood with Nonbiologic Surfaces," *Am. J. Pathol.*, **69**, 271-284 (1972).
30. T. H. Spaet and J. Cintron, "Studies on Platelet Factor-3 Availability," *Br. J. Haemat.*, **11**, 269-275 (1965).
31. R. N. King, J. D. Andrade, S. M. Ma, D. E. Gregonis, and L. R. Brostrom, "Interfacial Characterization of Hydrogel-Water Interfaces," in *Fundamentals of Interfacial Phenomena: Research Needs and Priorities*, J. Berg, Ed., Proc. of NSF Workshop, Seattle, Washington, 1979.
32. R. D. Allen, L. R. Zacharski, S. T. Widirstky, R. Rosenstein, L. M. Zaithlin, and D. R. Burgess, "Transformation and Motility of Human Platelets," *J. Cell Biol.*, **83**, 126-142 (1979).
33. R. R. Sokal and F. J. Rohlf, *Biometry*, W. H. Freeman and Company, San Francisco, 1969, p. 516.
34. F. M. Fowkes and F. H. Heilscher, "Electron Injection from Water into Hydrocarbons and Polymers," *Am. Chem. Soc., Org. Coatings Prepr.*, **42**, 169-174 (1980).
35. R. Williams, "Structure and Energy of the Interface Between an Insulator and an Electrolyte," *R.C.A. Rev.*, **36**, 542-550 (1975).
36. J. F. Brown, Jr., J. A. Bergerson, H. P. M. Fromageot, J. N. Groves, G. M. J. Gluscrzczuk, and W. J. Dodds, *Studies of Elastin as a Biomaterial*, NIH Rep. No. N01-HV-4-2981, 1977.
37. D. J. Shaw, *Electrophoresis*, Academic Press, New York, 1969, p. 4.

38. J. L. Brash and S. J. Whicker, "Interaction of Platelets with Surfaces: A Factorial Study of Adhesion and Associated Release of Serotonin," in *Artificial Organs*, R. M. Kenedi, Ed., University Park Press, Baltimore, MD, 1977, pp. 263-272.
39. R. G. Mason, Chairman, *NHLBI Guidelines for Blood-Material Interactions*, National Heart, Lung, and Blood Institute, Devices and Technology Branch, Bethesda, MD, May 1979.

Received December 1, 1981

Accepted March 11, 1982

foot page

CRANDALL, JANATOVA, AND ANDRADE

62. P. Bohlen, S. Stein, W. Dairman, and S. Udenfriend, Arch. Biochem. Biophys., 155, 213-220 (1973).
63. S. De Bernardo, M. Weigle, V. Toome, K. Manhart, W. Leimgruber, P. Bohlen, S. Stein, and S. Udenfriend, Arch. Biochem. Biophys., 163, 390-399 (1974).
64. W.L. Ragland, J.L. Pace, and D.L. Kemper, Anal. Biochem., 59, 24-33 (1974).
65. J.L. Pace, D.L. Kemper, and W.L. Ragland, Biochem. Biophys. Res. Commun., 57, 482-487 (1974).
66. Shu-i Tu and L. Grosso, Biochem. Biophys. Res. Commun., 72, 9-14 (1976).
67. R.F. Chen, Anal. Letters, 7(1), 65-77 (1974).
68. A. Van Der Scheer, J. Feijen, J.K. Elhorst, P.G. Krugers-Dagneaut, and C.A. Smolders, J. Colloid Interface Sci., 66, 136-145 (1978).
69. G.K. Koch, I. Heertje, and F. Van Stijn, Radiochimica Acta, 24, 215-219 (1977).

THE EFFECTS OF RADIOIODINATION AND FLUORESCENT LABELLING
ON ALBUMIN

R.E. Crandall, J. Janatova, J.D. Andrade

Department of Bioengineering

University of Utah

Salt Lake City, Utah 84112 U.S.A.

ABSTRACT

The preparation and characterization of fluorescamine -, fluorescein isothiocyanate (FITC) -, and radioiodine-labelled bovine serum albumin is critically evaluated. Electrophoretic mobility and ion-exchange chromatography, together with measures of degree of conjugation and sulfhydryl content, are used to assess the changes due to conjugation. Fluorescamine labelling results in drastic changes in chromatographic behavior and electrophoretic mobility. FITC labelling also results in significant changes in chromatographic and electrophoretic properties. Radioiodination leads to minor changes in chromatographic properties and oxidation of sulfhydryl groups, with little or no change in electrophoretic properties. All three labels have some degree of lability and show increased levels of free label with time, even after extensive initial purification. It is concluded that the two fluorescent labels and possibly the radioiodine labelling

method used here are unsuitable for certain studies of BSA, such as its adsorption at solid-liquid interfaces.

INTRODUCTION¹

The widespread practice of labelling proteins with radioiodine and/or fluorescent dyes warrants the need of definitive characterization to establish if there are significant changes in the physical properties and/or behavior of a protein due to conjugation. When interpreting the results of experiments performed with tracer proteins the following criteria should be considered:²⁻⁴

1. The labelled protein should behave *in vitro* or *in vivo* like native protein.
2. The labelling should be uniform and homogeneous (among all the protein subfractions).
3. The label should remain bound to the protein during the experiment.
4. Protein conjugates should be free of unreacted fluorescent materials, unbound radioisotopes, and degradation products.

Before using a protein conjugated with any label it must be established that the conjugate is identical in its behavior to the native molecule for the experiment or processes under study.

This paper describes the application of ion exchange gel chromatography on DEAE Sepharose CL-6B as a method of analysis to evaluate the character of bovine serum albumin conjugates. This method permits relatively fast analysis of small samples (< 100 mg) after the removal of unreacted label. Other methods, such as

Sephadex G-25 gel filtration, sulphhydryl content titration, polyacrylamide gel electrophoresis, agar gel immunoelectrophoresis, and cellophane membrane dialysis, provide supportive evidence of instability and change in properties induced by the tested tracer methodologies.

MATERIALS AND METHODS

Materials

The bovine serum albumin (BSA) used in these studies was lyophilized BSA, Fraction V, lot 283, from Miles Laboratories. The bovine mercaptalbumin (BMA) was prepared in our laboratory by the method of Janatova, et al.⁵ The BSA preparation contained 0.43 sulphhydryl group per molecule and about 10-11% dimer as determined by polyacrylamide gel electrophoresis (PAGE). The BMA preparation contained 0.9 sulphhydryl group per molecule directly after fractionation. After a brief exposure to air, the sulphhydryl group per molecule content dropped and stabilized at 0.83. 5,5'-dithiobis (2-nitrobenzoic acid) (lot 072677) was a product of the Aldrich Chemical Company. DEAE Sepharose CL-6B (lots 3102 and 5717), and Sephadex G25 coarse (lot 5115) were obtained from Pharmacia Fine Chemicals. Centriflo membrane cones CF25, and PM10 membranes were products of Amicon. Activated charcoal type 517 was produced by the Witco Company. Fluorescamine (lot 0002-02) was obtained from Hoffman-LaRoche, Inc., Nutley, New Jersey. Fluorescein isothiocyanate Isomer I (lot 56C-5017) was a product of Sigma Chemical Company. Lactoperoxidase immobilized on Sepharose beads was supplied by Worthington Biochemical Corporation.

General

Osmolarity measurements were performed on an osmometer (model 3L, Advanced Instruments, Inc.). Conductivity of buffers was measured using a General Radio conductivity bridge, model 1650-B.

Absorbance measurements were made on Hitachi Perkin Elmer 139, Gilford 240, and Beckman Acta II spectrophotometers using Beckman quartz 1.0 and 0.5 cm cells. A Corning Model 12 research pH meter and Corning glass electrode was used for pH monitoring of buffers. Color pHast pH indicator sticks from E. Merck Laboratories Inc. were used to estimate the pH of protein solutions.

Protein concentration was determined routinely by measuring absorption at 279 nm. An absorption coefficient ($A_{1\text{cm}}^{1\%}$ at 279 nm) of 6.67 was used for BSA. The molecular weight of albumin was taken as 66,500. A modification of the biuret reaction as described by Janatova⁶ was also performed occasionally and found to agree with the UV absorption method within $\pm 5\%$.

Sulfhydryl content was determined by spectrophotometric titration with 5,5'-dithiobis (2-nitrobenzoic acid) by the procedure of Ellman⁷ as modified by Janatova, et al.⁶ The method was performed in our laboratory using 0.06 M phosphate buffer, pH 7.00, in all reagent and protein solutions. The final pH of the protein reaction mixture was found to be 7.0. Protein samples were tested for sulfhydryl content within 24 h of elution or immediately after dissolving the starting materials. Typically, individual fractions or pools were concentrated by means of dry Sephadex G25 coarse centrifugation in order to fall within the required concentration range.

The methods used for protein desalting, and the concentrating of protein solution have been described.⁵

Fractionation Procedures

Gel Filtration on Sephadex G25: Gel filtration on Sephadex G25 coarse can be used for separation of BSA conjugates from free, unbound tracer molecules. Separation of conjugates and free label has been achieved when up to 100 mg of BSA in up to three ml has been fractionated on a 2.0 x 25 cm gel bed under the following conditions: six g of Sephadex G25 provided V_t of 30 ml in 0.04 M phosphate buffer, pH 7.0, with elution by gravity at about five ml/min; two ml per tube collected; V_e of BSA conjugates was 16 ml; V_e of fluorescent or iodinated molecules was 30 ml.

Analytical Chromatography on DEAE Sepharose CL-6B: All buffers used were prepared by mixing monobasic and dibasic phosphate solutions of particular molarities in ratios to obtain pH 7.0 (measured at room temperature). Each new batch was checked for osmolarity:

molarity	0.05	0.06	0.08	0.125
milliosmols	125	140	180	270
conductivity $\times 10^3$ (25°) $\Omega^{-1} \text{ cm}^{-1}$	6.21	7.14	9.09	13.42

All buffers contained 0.02% NaN_3 which had to be removed from some serum albumin (SA) fractions over Sephadex G25 prior to further study.

Various commercial SA samples of quantities 70 to 200 mg were dissolved in two to five ml 0.05 M phosphate buffer, pH 7.00 and fractionated at 25°C on DEAE Sepharose CL-6B using a Glenco column

(0.9 cm x 30 cm, V_t of 19 ml) prewashed with ≥ 60 ml 0.05 M phosphate buffer, pH 7.00. A freshly dissolved albumin solution was applied to the top of the DEAE Sepharose CL-6B, and the albumin was allowed to flow down the column by gravity. The protein was moved into the resin bed by several three ml additions of 0.05 M phosphate. Two phosphate solutions (240 ml of 0.06 M phosphate, pH 7.00, and 240 ml of 0.08 M phosphate, pH 7.00) were employed to obtain the first linear phosphate gradient ($4.063 \times 10^{-3} \Omega^{-1} \text{cm}^{-1}/\text{ml}$, 25°).

The column eluate was collected in three ml fractions by a Gilson Medical Electronics fraction collector using a constant flow rate of 25 ml/h provided by an Extracorporeal Medical Specialties, Inc., infusion pump model #RDO 74-110 (several runs were performed at 72 ml/h yielding no adverse effects on the resolution using this small analytical column).

After 110 fractions were collected, a second gradient was employed using 200 ml of 0.08 M phosphate pH 7.00, and 200 ml 0.125 M phosphate with 0.2 M NaCl pH 7.00 ($5.42 \times 10^{-2} \Omega^{-1} \text{cm}^{-1}/\text{ml}$, 25°). After 100 more fractions were collected, 0.125 M phosphate with 0.2 M NaCl pH 7.00 was passed down the column until all the protein had been eluted from the column⁵. In some instances buffers of greater ionic strength were used to elute tightly bound fractions from the column. The concentration of the eluate was estimated by absorbance measurements at 279 nm on every second or third tube.

After inspection of the absorbance profile of the eluate, sulfhydryl determination, polyacrylamide gel electrophoresis, and immunoelectrophoresis were performed on certain pooled fractions after concentration by dry Sephadex G25 or by centrifugation in

Centriflo membrane cones (CF25).

Electrophoresis

Polyacrylamide gel electrophoresis (PAGE) was performed using an Ortec pulsed power system⁵. Agar gel electrophoresis was performed on a Pol-E-Film precast agarose film (1% agarose, 5% sucrose in 0.075 M barbital buffer at pH 8.6) on a flexible backing at 90 volts (Pfizer Diagnostics). Rabbit antisera to bovine serum were obtained from Microbiological Associates (Lot #15016). The plates were stained as required in Amido Black 10B, 0.2 g% in 5% acetic acid.

Spectrofluorometry and Radioactivity

Fluorescence measurements and spectra were made with an Aminco-Bowman Spectrophotometer. For fluorescein isothiocyanate (FITC) an excitation wavelength of 490 nm and an emission wavelength of 520 nm gave maximum fluorescence. Optimum fluorescence for fluorescamine (FA) conjugates occurred at an excitation wavelength of 388 nm and emission wavelength of 470 nm. The FITC concentration and dye/protein ratios were calculated according to⁸. The radioactivity of radio-iodine labelled proteins was counted by a Beckman Gamma counter.

PREPARATION OF CONJUGATES

BSA-I¹²⁵

Bovine serum albumin was labelled by the solid state lactoperoxidase enzyme method⁹⁻¹¹. In our laboratory ~ 100 mg BSA or BMA in two ml acetate buffer, pH 4.0, $I = 0.025$, 37 m osmol, was reacted with 150 μl lactoperoxidase beads for 30 minutes while

stirring with a magnetic stirrer. The KI and H_2O_2 molarities of the reaction mixtures were varied to test the effect of iodine incorporation on the -SH content of MA.

The reaction was stopped by the addition of 0.02% NaN_3 (100 μ l/ml reaction mixture). The free I^{125} was removed by passing over four g of Sephadex G25 coarse and centrifuging; the process was repeated six times.

BSA-FA

Fluorescamine - BSA derivatives were prepared at + 4°C according to Brynda, et al.¹² Typically 2.0 mg fluorescamine, dissolved in ice cooled 7.0 ml acetone, was added to a ten ml solution of BSA (five mg/ml) in 0.1 M borate buffer pH 9.0 while mixing rapidly on a vortex mixer for two minutes. Acetone and non-fluorescent hydrolysis products of fluorescamine were eliminated by dialysis for 24 hours in 1000 ml 0.04 M phosphate buffer + 4°C using cellophane tubing. The final volume was adjusted to approximately five ml by adding dry Sephadex G25 coarse and centrifuging. The resulting ten mg/ml of BSA-FA could be used for chromatographic or electrophoretic analysis.

BSA-FITC

The procedure described by Goldman¹³ was used for the preparation of BSA-FITC conjugates. 150 mg of BSA or BMA was dissolved in or transferred into 5.0 ml 0.9% NaCl. 7.5 mg of FITC (50 μ g FITC/mg BSA) was dissolved in 0.6 ml 0.5 M carbonate bicarbonate buffer pH 9.6. These solutions were mixed (4°) and gently stirred with a magnetic stirrer for 24 hours at 4°. Unreacted FITC was removed from the reaction mixture by desalting over four g Sephadex

G25 four times and finally passing the mixture through a 1 x 40 cm Sephadex G25 column using 0.04 M phosphate as the eluant buffer.

Dialysis

Dialysis of BSA conjugates was accomplished in 0.04 M phosphate buffer pH 7.0 at 4°C using cellophane dialysis bags tied with three knots to insure no leakage. Dialysates were checked for protein leakage using a modification of the Biuret method⁶. The dialysate solution was stirred during dialysis with a magnetic stirrer.

RESULTS AND DISCUSSION

Fractionation of Commercial BSA-Fraction V on DEAE Sepharose CL-6B

A typical elution profile of BSA-Fraction V fractionated at pH 7.0 with linear gradients of increasing ionic strength is shown in Figure 1. The DEAE Sepharose CL-6B gel bed used repeatedly gave highly reproducible results. Whole fractionation as shown in Figure 1, is achieved under ten hours with good resolution of the fractions. A detailed description of the BSA fractions (and their significance) as isolated by DEAE Sepharose CL-6B chromatography is given by Janatova, et al.⁵

BSA-I¹²⁵

Studies utilizing albumin may be further complicated by iodination if the conjugated protein is different from that of the native molecule. The need for a mild iodination method as well as for unaltered products is apparent. The lactoperoxidase method was chosen because of its mild reaction conditions.¹⁴ What constitutes a change in protein behavior, and how deviant must that behavior be before results lose their validity, is dependent on the sensitivity of the property under study. For example, protein inter-

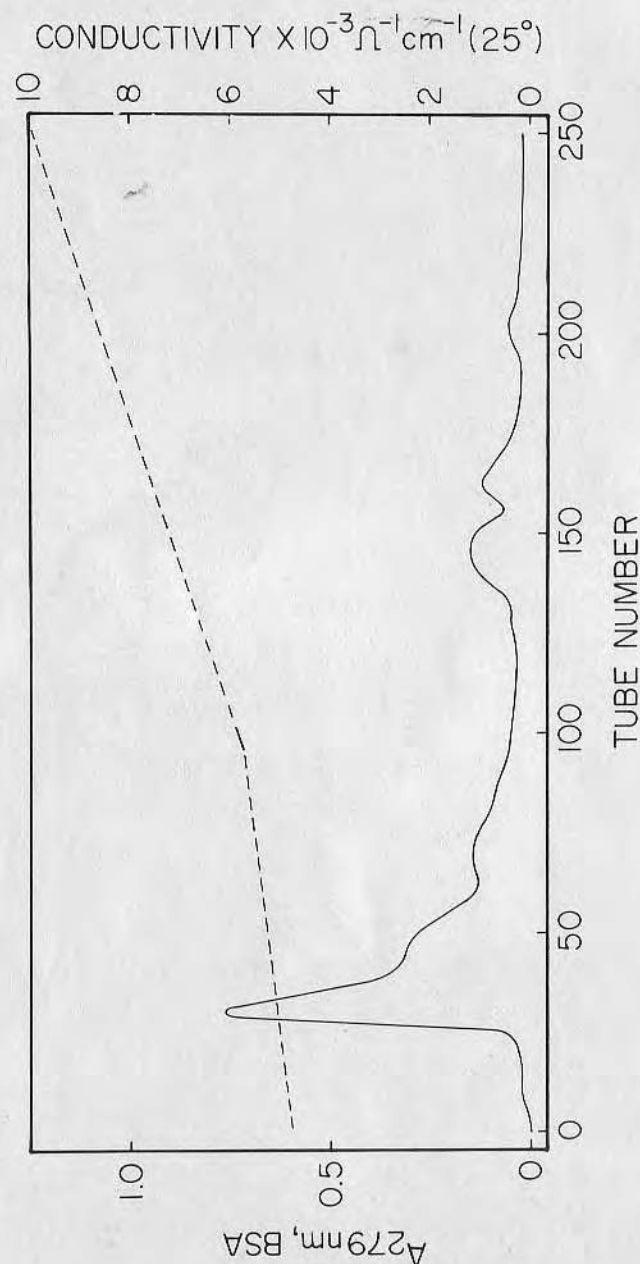


FIGURE 1

Analytical fractionation of bovine serum albumin, Fraction V, on DEAE Sepharose CL-6B, using 100 mg BSA in 2 ml 0.05 M phosphate, pH 7.0. A buffer gradient was used beginning with 0.06 M phosphate and ending with 0.125 M phosphate with 0.2 M NaCl, as indicated by the dotted lines. Each tube was 3 ml, see text for other details.

actions which are a function of charge may be affected by alteration of the total charge of the protein or its distribution. A method that could measure slight differences in ionic interactions may be a good means of monitoring subtle change in protein characteristics.

Fractionation of BSA-I¹²⁵ on DEAE Sepharose CL-6B

Fractionation of BSA-I¹²⁵ on the DEAE Sepharose CL-6B gel bed has yielded results which are highly reproducible. Changes in labelling conditions are reflected by changes in the elution profiles. The elution profile of BSA-I¹²⁵ is given in Figure 2, where KI was 8.0×10^{-6} M and H₂O₂ was 7.0×10^{-5} M, yielding mild iodination (2.0×10^{-3} M I⁻/1.0 M BSA). The latter non-mercaptalbumin fractions are in greater concentration as compared to unlabelled Fraction V (Figure 1). Note the larger Cpm/A²⁷⁹ ratios for the non-mercaptalbumin fractions B1, B2, C, and D. This suggests a greater iodine affinity of these albumin fractions. It has been well shown that proteins differ in their susceptibility to enzymatic iodinations¹⁵⁻¹⁷. The data in Figure 2 suggests this may also be true for the fractions of heterogeneous protein preparations.

Dialysis was chosen to characterize how the protein-I binding might result in fluctuations in the Cpm/A²⁷⁹ ratio (Figure 2). Desalted BSA-I¹²⁵ was first dialyzed in four 500 ml dialysates of 0.1 M PBS to remove loosely bound I⁻. Equilibration could be reached within about 48 hours. However, when subsequently dialyzed in 0.05 M KI in 0.1 M PBS at 4°, I¹²⁵ was rapidly exchanged for nonradioactive I¹²⁷ with an apparent first order rate constant. After 42

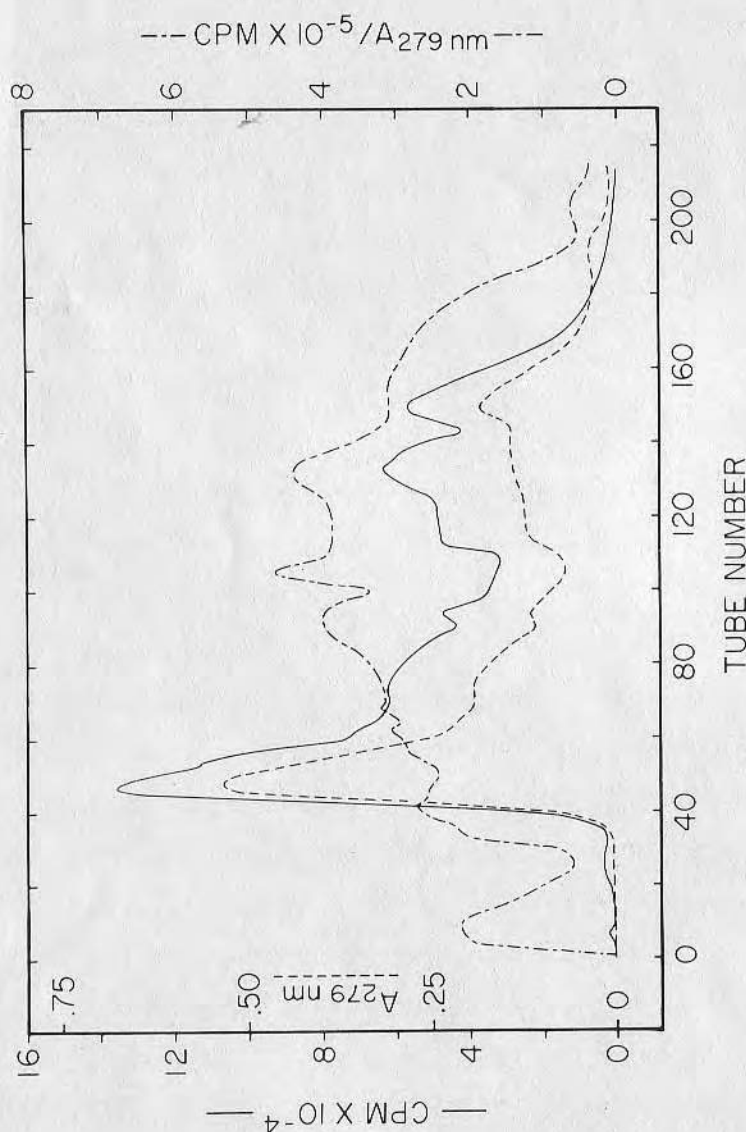


FIGURE 2. Analytical fractionation of I^{125} -Fr. V on DEAE Sepharose CL-6B using the same elution conditions and gradient as in Fig. 1. The lower dashed line is the absorbance at 279 nm (1 cm cell), representing protein concentration. The upper solid line is the radioactivity in $\text{cpm} \times 10^{-4}$. The dot-dash line is the ratio of $\text{cpm} \times 10^{-5}/A_{279}$, which is a measure of the level of radioiodine bound in each protein fraction. Note the increased labelling in the non-mercaptalbumin fractions (tubes 80-150) and their increased concentration relative to unlabelled material (Fig. 1). The monomer mercaptalbumin fraction (tubes 40-60) is shifted to the right relative to the unlabelled material (Fig. 1), indicating a change in the chromatographic behavior of the fraction.

days of dialysis over 50% of the activity had exchanged across the cellophane membrane. It was shown that at least 30% of this released I^{125} was probably originally strongly bound to BSA molecule. In the iodination of BSA without H_2O_2 or lactoperoxidase, BSA would only bind 20% as much I^{125} as compared to enzymatically-labelled BSA using lactoperoxidase. The dialyzed BSA- I^{125} conjugate was fractionated on DEAE Sepharose CL-6B. Again the Cpm/protein ratio approached its highest point with the non-mercaptalbumin fractions. A significant inflation of the non-mercaptalbumin populations was evident as well as broadening and shifting of the peaks. Sulfhydryl analysis of several pooled fractions showed little mercaptalbumin to be present. As the dialyses were performed under an Argon atmosphere in physiological buffer, the striking changes in fraction distribution may be attributed to the prolonged exposure to KI. One plausible explanation for this result is sulfhydryl oxidation.

Effect of Iodination Level on Sulfhydryl Content

When mercaptalbumin is labelled with increased levels of iodine, a corresponding drop in sulfhydryl content is noted. Thomas and Aune¹⁸ have discussed how lactoperoxidase can catalyze the peroxide-dependent oxidation of protein sulfhydryls in the presence of iodide. Sulfhydryls were oxidized to the sulphenyl iodide derivative. At NaI concentrations above one μM sulfhydryl oxidation is preferred to lactoperoxidase catalyzed iodination of tyrosine residues. At low I^- concentrations protein derivatives decompose to yield I^- and the oxidized derivative. The released I^- may

then be reoxidized and participate in the oxidation of another sulfhydryl. If peroxidase or H_2O_2 are in low concentration accomplished by dialysis, reoxidation of I^- is stopped and I^- is simply released without oxidation of more sulfhydryls.

This loss in sulfhydryl function caused by lactoperoxidase iodination casts serious doubt on its applicability for the study of albumin. Figure 2 demonstrates the alteration in chromatographic properties. As the mercaptalbumin fraction is a significant component of native BSA and is affected by the oxidation of its sulfhydryl group, the peroxidase-catalyzed side reaction precludes the acceptability of this method for the iodination of proteins which require unoxidized cysteinyl residues for natural activity¹⁹.

The effect of iodination level has been shown to effect biological clearance behavior²⁰, heterogeneity²¹, electrophoretic mobility²², metabolic behavior²³, coagulability of fibrinogen²⁴⁻²⁷, immunologic reactivity²⁸⁻³⁰, antigenicity³¹, and interchain disulfide bond reactivity³².

The enzymatic method for protein iodination has been shown to give better results, considering the above protein properties, than the iodine monochloride, chloramine -T, and electrolytic methods³³⁻⁴¹. When performed under the proper conditions, the peroxidase catalyzed halogenation may be more selective and reproducible than these other methods.

Nevertheless, for studies requiring absolute integrity of sulfhydryl groups several new methods have been introduced which may be void of such side reactions^{19, 41, 42}, though the chromatographic

behavior of the labelled BSA products must still be thoroughly examined.

Instability of BSA-I Conjugates

The instability of BSA- I^{125} conjugates and the release of free I^{125} into the test media can have serious ramifications⁴³⁻⁴⁵. The increased concentration of unbound iodine in bulk solution has been shown to alter the results of protein adsorption onto platinum surfaces^{43, 45}. Protein adsorption experiments on hydrogels (high water content polymers) have shown that the polymer may take up free I from bulk solution (S.W. Kim and U.R. Kim, personal communication). Typically, the unreacted free iodine has been removed by gel filtration and/or dialysis. Sephadex G-25 gel filtration by centrifugation^{46,47} removes greater than 99% of the free iodine (original activity).

Iodinated BSA has been fractionated on Sephadex G25 before and after Sephadex G25 separation and centrifugation. Only about 5% of the total activity in the reaction mixture is bound to the BSA.

After six runs of Sephadex G25 separation, BSA- I^{125} only had 2% free I^{125} (Figure 3a). This represents removal of 99.9% of the free I^{125} that was in the original reaction mixture. After 200 minutes (Figure 3b) incubation at 37°C, the activity due to free I^{125} was now 7.5%. Release of free iodine was measured up to 2640 minutes, at which time 19.2% of the activity was now unbound (Figure 3d). A mechanism is not offered as to which bonds are responsible for degradation and subsequent release of iodine but

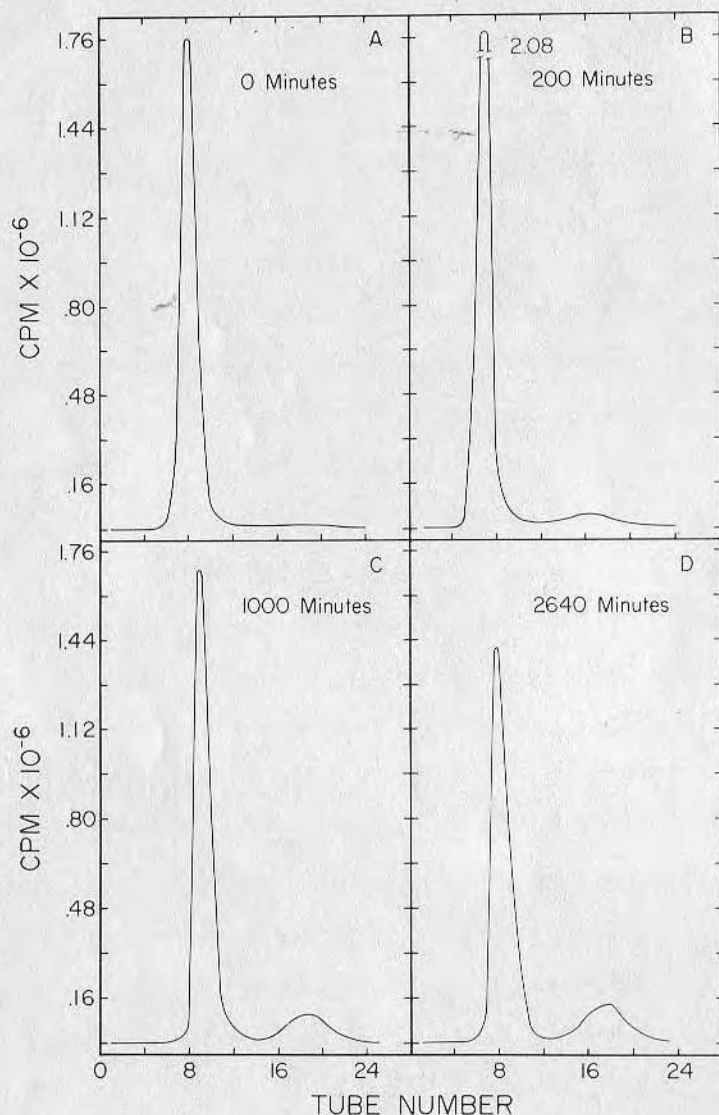


FIGURE 3

Separation of free iodine from iodinated-BSA by gel filtration on Sephadex G-25. a) Immediately after initial purification and removal of unbound iodine; no unbound iodine is present. b) After 200 minutes unbound iodine is 7%. c) After 1000 minutes unbound iodine is about 16%. d) After 2640 minutes (~ 44 hours), unbound iodine is up to nearly 20%. No free iodine was detected immediately after initial purification. This study demonstrates the lability of the protein-bound iodine with time, thus casting some doubt on long time studies (over one hour) with iodinated albumin unless the effect of free label is taken into account.

several possibilities may be suggested. Diffusion of loosely bound iodine, oxidation of sulfide bonds, and radioactive degradation of the I bond of tyrosine may all be involved in the process.

Agar Gel Electrophoresis

Iodinated BMA migrates identically to the control mercapt-albumin. Apparently, the heterogeneity of the labelled conjugate demonstrated by DEAE Sepharose CL-6B chromatography is not made evident in the electrophoretic properties shown by agar gel electrophoresis.

BSA-FITC

The study of fluorescent protein-dye conjugates has been undertaken by several investigators. Most of the work on FITC has focused on labelling techniques⁴⁸⁻⁵⁴ and fluorescence or absorption properties⁵⁵.

Landel² and Schiller, et al.³ concluded that FITC-labelled BSA retains its chromatographic, electrophoretic and immunological properties as well as its integrity in serum. Covalent, stable FITC bonds were reported. These studies suggested that low degrees of saturation yielded conjugates similar to native protein and suitable for investigations of capillary permeability and tissue distribution.

However, the use of FITC-BSA conjugates for tracer studies in protein adsorption onto solid surfaces may yield different results due to the change in charge character. The formation of an ϵ -fluorescein thiocarbamyl-lysyl bond upon conjugation yields a product with an isoelectric point at pH 4.80, whereas native

BSA has an isoelectric point at pH 4.92².

Our studies establish that there are significant changes in chromatographic behavior on DEAE Sepharose CL-6B as well as non-specificity upon conjugation, instability of the FITC bond, and increased heterogeneity of the FITC-labelled fractions.

Fractionation of BMA-FITC on DEAE Sepharose CL-6B

The elution profile of FITC-labelled mercaptalbumin fractionated on DEAE Sepharose CL-6B is shown in Figure 4. Purified BMA isolated from Cohn's Fraction V by the method of Janatova, et al.⁵ was labelled with FITC by the method described earlier. Untreated BMA is shown together with labelled BMA; the two samples were fractionated separately on an identical column. An elution shift would be expected, considering the formation of an ϵ -fluorescence thiocarbamyl-lysyl bond upon conjugation of BMA with FITC². However, the gross broadening and new heterogeneity of the BMA-FITC conjugate suggests a microheterogeneity of FITC labelling even within this highly purified mercaptalbumin. We attempted to completely fractionate FITC-labelled Fraction V by increasing the ionic strength in the elution gradients. Even with 0.125 M phosphate in 0.5 M NaCl, all of the conjugates could not be eluted. We also observed striking fluctuations in the FITC/protein molar ratio among the eluted fractions (not shown) by ratioing A_{279} and A_{496} .

Electrophoresis

The optimal pH for greatest incorporation of FITC in BSA is 9.5⁵³. Some investigators have reported FITC/protein ratios up to

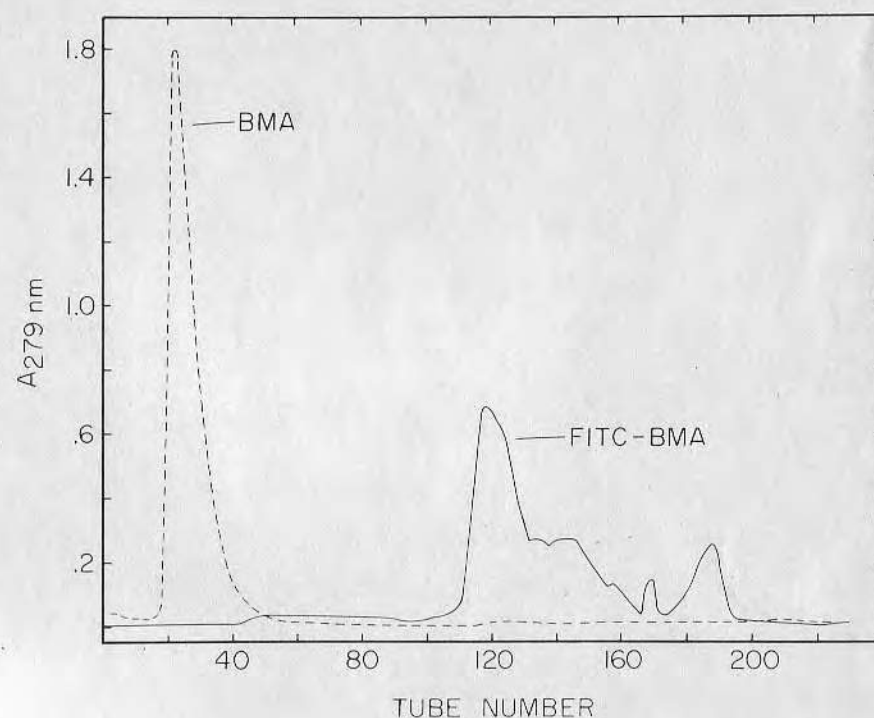


FIGURE 4

Effect of FITC-labelling on the chromatographic behavior of bovine mercaptalbumin, utilizing DEAE Sepharose CL-6B. The unlabelled BMA is the sharp peak on the far left. The FITC-labelled-BMA (after removing free FITC by G-25 treatment) is the series of fractions at the right. These were eluted by a 0.08 M-phosphate going to 0.125 M phosphate in 0.2 M NaCl gradient (tubes 92-160). Beyond Tube 160 0.125 M phosphate in 0.5 M NaCl was used to elute the remaining two peaks. Thus, FITC-BMA could not be eluted using normal gradients. Ionic solutions greater than about 0.1 M phosphate were needed and it was necessary to go to 0.125 M phosphate and 0.5 M NaCl to get all of the material off the column.

12. Conjugates of lower ratios can be made by varying pH, temperature, reaction time, or FITC concentration.

BMA labelled with FITC at pH 7.0 and pH 9.6 with all other parameters constant, was electrophoresed on agar gel plates. Both conjugates have greater electrophoretic mobilities and heterogeneity than untreated MA. The BMA labelled at pH 7.0 and 9.6 had dye:protein ratios of 2.16 and 2.37, respectively. The more highly conjugated material had a higher electrophoretic mobility and greater broadening.

Lablity

The stability of FITC-BSA conjugates has been a subject of investigation by several authors. Release of the FITC label during an in vivo or in vitro experiment could yield misleading results⁸. Storage of BMA-FITC conjugates for six months at + 4°C gave solutions with a high content of free FITC in the bulk solution. The greatest fluorescence observed was due to unbound FITC rather than conjugated FITC. Furthermore, even freshly prepared FITC-BMA purified four times by Sephadex G25 centrifugation shows already a significant amount of free FITC.

BSA-FA

The presence of free label in solution as shown with FITC¹² and I¹²⁵⁴⁵ has lead some investigators to study fluorescamine as a label for protein tracing. Fluorescamine labelling produces conjugates of a light blue fluorescence which can be detected with great sensitivity⁵⁷⁻⁶³. The free label in solution is non-fluorescent, thus minimizing many of the problems involved with other

conjugates; for example, small amounts of free label could be tolerated in many experiments.

The properties of fluorescamine-protein conjugates have been investigated, including electrophoretic mobility^{64, 65}, conformational integrity⁶⁶, and fluorescence properties⁶⁷.

Fluorescamine reacts with the ϵ -amino group of lysine and the N-terminal amino groups, generating a negative charge on the fluorophor⁶⁵. The resultant conjugate has a net charge change of -2 for every molecule of label.

Fractionation of Fluorescamine-Labelled BSA Fraction V on DEAE Sepharose CL-6B

The elution profile of BSA-FA on DEAE Sepharose CL-6B is not reproducible. In every case more than 50% of the conjugate applied to the column would not elute even under conditions of high ionic strength and a pH of 4.0. This strong affinity for the DEAE Sepharose CL-6B anion exchanger can be attributed to the ϵ -fluorescamine-lysyl bond upon conjugation of BSA with fluorescamine and the ionizable carboxyl group on each fluorescamine molecule.

Due to the great sensitivity of the anion exchange column to the electronegative character of the protein conjugates, great differences could be seen in elution patterns with only slight changes in labelling parameters. The dye/protein ratio could be varied by altering the pH, temperature, or amount of fluorescamine. Even at relatively low ratios great heterogeneity is evident. The mercaptalbumin fraction as well as the non-mercaptalbumin-fraction which could be eluted were shifted indicating more electronegative character.

Electrophoresis

Electrophoresis on agar plates, shown in Figure 5, demonstrates the great heterogeneity of the BSA-FA conjugates. Reaction conditions at pH 9 yielded the highest dye/protein ratio but also the greatest electronegativity and heterogeneity. When reacted at pH 7.0 the increase in electrophoretic mobility was smaller, however, the heterogeneity was still pronounced.

CONCLUSIONS

The conjugation of BSA with fluorescamine results in large changes in electrophoretic mobility and ion exchange properties, as measured by polyacrylamide gel electrophoresis (PAGE) and ion-exchange chromatography on DEAE Sepharose CL-6B. Such conjugates are clearly unsuitable for any studies dealing with the ionic character of the protein, including studies of albumin adsorption at solid-liquid interfaces.

The conjugation of BSA with fluorescein isothiocyanate at dye:protein ratios of roughly two results in significant changes in ion exchange chromatographic character. In addition, conjugation results in increased heterogeneity of the purified protein and the release of free FITC. Although these effects are not as drastic as with fluorescamine, they are significant enough to preclude any serious studies with FITC-BSA in which ionic character, chromatographic character, and/or adsorptive character is important.

The radioiodination of BSA by the lactoperoxidase-peroxide method results in no change in electrophoretic mobility as mea-



Figure 5. Agar gel electrophoresis of the various samples discussed in this paper. The far left column is a filtered serum as a reference followed by (left to right), FITC control, bovine mercaptalbumin, iodinated mercaptalbumin, FITC-albumin labelled at pH 7.0 and 9.6, respectively, and fluorescamine-mercaptalbumin labelled at 7.0 and 9.0, respectively. Note significant changes in electrophoretic mobility for the FITC- and fluorescamine-labelled BMA, particularly at higher levels of dye binding (pH 9.0, 9.6). Note no significant change in mobility for iodinated BMA.

sured by PAGE, as expected because the reaction should not produce any net charge change. However, the chromatographic properties are very sensitive to the iodination conditions. The apparent lability of the bond results in release of free label with time. Of particular concern with albumin is the decrease in the free sulfhydryl content due to the labelling procedure, a problem with all common methods for iodination.

The change in chromatographic properties of the protein, the sulfhydryl oxidation problem, and the problem of free label may preclude the use of radioiodinated albumin for certain studies, perhaps including the study of albumin adsorption at solid-liquid interfaces^{68,69}.

ACKNOWLEDGEMENTS

This work was supported by NIH Grant 18519. The technical assistance of Kathryn Irons and Lyle Brostrom is appreciated. Discussions with D.L. Coleman and D.E. Gregonis have been very helpful. We thank Gary Bates for the agar gel immunoelectrophoresis work.

REFERENCES AND NOTES

- Abbreviations used include: BSA, bovine serum albumin; BMA, bovine mercaptalbumin; PAGE, polyacrylamide gel electrophoresis; DEAE, diethyl aminoethyl; SA, serum albumin; FITC, fluorescein isothiocyanate; FA, fluorescamine (4-phenylspiro [furan-2(3H), 1'-phthalan] - -3,3'dione).
- A.M. Landel, *Anal. Biochem.*, **73**, 280-289 (1976).
- A.A. Schiller, R.W. Schayer, and E.L. Hess, *J. Gen. Physiol.*, **36**, 489-505 (1953).
- S. Margen and H. Tarver, *Advances in Tracer Methodology*, **2**, S. Rothchild, ed., Plenum Press, New York, 61-72 (1965).
- J. Janatova, R.E. Crandall, and J.D. Andrade, *Prep. Biochem.*, **10**, 405-430, (1980).
- J. Janatova, J.K. Fuller, and M.J. Hunter, *J. Biol. Chem.*, **243**, 3612-3622 (1968).
- G. Ellman, *Arch. Biochem. Biophys.*, **82**, 70-78 (1959).
- A. Jobbagy and K. Kiraly, *Biochim. Biophys. Acta*, **124**, 166-175 (1966).
- G.S. David and R.A. Reisfeld, *Biochemistry*, **13**, 1014-1021 (1974).
- G.S. David, *Biochem. Biophys. Res. Commun.*, **48**, 464-471 (1972).
- I. Schenkien, M. Levy, and J.W. Uhr, *Cell Immuno.*, **5**, 490-493 (1972).
- E. Brynda, J. Drobnik, J. Vacik, and J. Kalal, *J. Biomed. Mater. Res.*, **12**, 55-65 (1978).
- M. Goldman, *Fluorescent Antibody Materials*, Academic Press, New York and London, 101 (1968).
- M. Morrison and G.S. Bayse, *Biochemistry*, **9**, 2995-300 (1970).
- S.S. Sarimo and J. Tenovuo, *Biochem. J.*, **167**, 23-29 (1977).
- J. J. Marchalonis, *Biochem. J.*, **113**, 299-305 (1969).
- J. Gow and A.C. Wardlaw, *Biochem. Biophys. Res. Commun.*, **67**, 43-49 (1975).
- E.L. Thomas and T.M. Aune, *Biochemistry*, **16**, 3581-3586 (1977).
- C.E. Hayes and I.J. Goldstein, *Anal. Biochem.*, **67**, 580-584 (1975).
- S.S.L. Harwig, J.F. Harwig, R.E. Coleman, and M.J. Welch, *Thromb. Res.*, **6**, 375-386 (1975).
- U. Rosa, F. Pennisi, R. Bianchi, G. Federighi, and L. Donto, *Biochim. Biophys. Acta*, **133**, 486-498 (1967).
- C. Ambrosino, G.A. Scassellati, G. Papa, and U. Rosa, *J. Labeled Compounds*, **3**, 380-386 (1967).
- G. Federighi, R. Bianchi, C. Ambrosino, F. Pennisi, G. Scassellati, and U. Rosa, *J. Nucl. Biol. Med.*, **10**, 58-65 (1966).

24. A.S. McFarlane, *J. Clin. Invest.*, 42, 346-361 (1963).
25. B. Ly and P. Kierulf, *Thromb. Res.*, 6, 387-398 (1975).
26. F.A.G. Teulings and G.J. Biggs, *Clin. Chim. Acta*, 27, 57-64 (1970).
27. M.F. Scully, V.V. Kakkar, and J.G. Nievel, *Biochem. Soc. Trans.*, 2, 1333-1334 (1974).
28. H.N. Eisen and A.S. Keston, *J. Immunol.*, 63, 71-80 (1949).
29. C. Gandolfi, R. Malvano, and U. Rosa, *Biochim. Biophys. Acta*, 251, 254-261 (1971).
30. W.A. Hemmings and M. Redshaw, *Int. J. Appl. Radiat. Isotopes*, 26, 426-429 (1975).
31. M. Morrison, G.S. Bayse, and R.G. Webster, *Immunochem.*, 8, 289-297 (1971).
32. U. Rosa, A. Massaglia, F. Pennisi, I. Cozzani, and C.A. Rossi, *Biochem. J.*, 103, 407-412 (1967).
33. R.E. Coleman, K.R. Krohn, J.M. Metzger, M.J. Welch, R.H. Secker-Walker, *J. Lab. Clin. Med.*, 83, 977-982 (1974).
34. J.I. Thorell and B.G. Johansson, *Biochim. Biophys. Acta*, 251, 363-369 (1971).
35. N. Ardailou and M.J. Larrieu, *Thromb. Res.*, 5, 327-341 (1974).
36. K.A. Krohn and M.J. Welch, *Int. J. Appl. Radiat. Isotopes*, 25, 315-323 (1974).
37. V. Jovanovic, D. Nemoda, and K. Lwin, *Int. J. Appl. Radiat. Isotopes*, 23, 242-244 (1972).
38. J.M. Burrin, *Clin. Chim. Acta*, 70, 153-159 (1976).
39. S.-L. Karonen, P. Morsky, M. Siren, and U. Seuderling, *Anal. Biochem.*, 67, 1-10 (1975).
40. G.S. Sundaram, H.S. Sodhi, and R. Bhatnagar, *Clin. Chim. Acta*, 39, 115-123 (1972).
41. A.E. Bolton and W.M. Hunter, *Biochem. J.*, 133, 529-539 (1973).
42. F.T. Wood, M.M. Wu, and J.C. Gerhart, *Anal. Biochem.*, 69, 339-349 (1975).

43. W.H. Grant, L.E. Smith, and R.R. Stromberg, *J. Biomed. Mater. Res. Symposium*, 8, 33-38 (1977).
44. R.A. Caro, V.A. Ciscato, S.M.V. De Giacomini, S. Quiroga, and R. Radicella, *Int. J. Appl. Radiat. Isotopes*, 26, 527-532 (1975).
45. W.H. Grant, L.E. Smith, and R.R. Stromberg, *J. Biomed. Materials Res. Symp.*, 8, 33-38 (1977).
46. M. Franek and K.J. Hruska, *J. Chromatogr.*, 93, 471-474 (1974).
47. M. Ceska, P. Pihl, L. Holmqvist, and F. Grossmuller, *J. Chromatogr.*, 57, 145-147 (1971).
48. C.A. Gabel and B.M. Shapiro, *Anal. Biochem.*, 86, 396-406 (1978).
49. R.P. Tengerdy and C-A. Chang, *Anal. Biochem.*, 16, 377-383, (1966).
50. H. Rinderknecht, *Nature*, 193, 167-168 (1962).
51. R. McKinney, L. Thacker, and G.A. Hebert, *J. Dent. Res. Special Issue A*, 55, A38-A44 (1976).
52. R.M. McKinney, J.T. Spillane, and G.W. Pearce, *Anal. Biochem.*, 14, 421-428 (1966).
53. R.M. McKinney, J.T. Spillane, and G.W. Pearce, *J. Immunol.*, 93, 232-242 (1964).
54. A.F. Wells, C.E. Miller, and M.K. Nadel, *Appl. Microbiol.*, 14, 271-275 (1966).
55. R.F. Chen, *Arch. Biochem. Biophys.*, 133, 263-276 (1969).
56. R.W. Watkins, Ph.D. Dissertation, Stanford University (1976).
57. S. Stein, P. Bohlen, J. Stone, W. Dairman, and S. Udenfriend, *Arch. Biochem. Biophys.*, 155, 203-212 (1973).
58. S. Udenfriend, S. Stein, P. Bohlen, W. Dairman, W. Leimgruber, and M. Weigle, *Science*, 178, 871-872 (1972).
59. B. Klein and F. Standaert, *Clin. Chem.*, 22, 413-416 (1976).
60. M. Weigle, J.F. Blount, J.P. Teng, R.C. Czajkowski, and W. Leimgruber, *J. Amer. Chem. Soc.*, 94, 4052-4054 (1972).
61. U.E. Handschin and W. Ritschard, *Clin. Chem.*, 21, 18 (1975).